Solubility and partitioning of biomolecules. Experimental studies and modeling

Thesis for the degree of

Doctor Philosophiae

in Chemical and Biological Engineering

presented to the Faculty of Engineering

University of Porto

by

M.Sc. -Eng. Kamila Wysoczańska

Supervisor: Prof. Maria Eugénia Rebello de Almeida Macedo

Programa Doutoral em Engenheria Química e Biológica (PDEQB)
Laboratory of Separation and Reaction Engineering/Laboratory of Catalysis and Materials - Associate Laboratory

November, 2020

SOLUBILITY AND PARTITIONING OF BIOMOLECULES.

EXPERIMENTAL STUDIES AND MODELING

Faculdade de Engenharia da Universidade do Porto

Solubility and partitioning of biomolecules. Experimental studies and modeling

M.Sc. -Eng. Kamila Wysoczańska

Thesis submitted to Faculdade de Engenharia da Universidade do Porto

to obtain the degree of

Doctor Philosophiae in Chemical and Biological Engineering

President: Prof. Doutora Maria Arminda Costa Alves

Referee: Prof. Doutora Ana Isabel Nobre Martins Aguiar de Oliveira Ricardo

Referee: Prof. Doutora Ángeles Domínguez Santiago

Referee: Prof. Doutora Maria Eugénia Rebello de Almeida Macedo

Referee: Prof. Doutor Domingos Azavedo Gonçalves Barbosa

Referee: Doutora Elena Gómez Costas

November, 2020

To my family and friends

Abstract

Biomolecules such as amino acids or vitamins have experienced an increased interest in the industry and academia. However, the purification of these molecules is a challenging task given by their narrow chemical and thermal stability ranges. In the state-of-the-art methods, environmentally harmful solvents are still involved. Biodegradable Aqueous Two-Phase Systems (ATPS) are promising alternatives to conventional systems containing toxic components since they can prevent biomolecular activity loss by using water as a solvent. In contrast to classical ATPS, biodegradable ATPS consist of organic salt (and polymer) as phase formers.

From the thermodynamic point-of-view, the design and application of ATPS for the purification of biomolecules requires initial and solid knowledge on ATPS equilibria and the understanding of biomolecule behavior in water. Some of the biomolecules are poorly water-soluble and this can affect the reliability of experimental measurements. Therefore, in this thesis, the solubility enhancement by variation of different conditions, e.g. pH or addition of co-solutes, was studied. The selection of ATPS phase formers relied on two criteria: efficient formation of ATPS biphasic area and high partition coefficients. The efforts needed to obtain accurate experimental data were huge, and this was related to the number of required measurements. Thus, the experimental input was coupled with the predictive thermodynamic model contribution (electrolyte PC-SAFT). The biomolecules under investigation were dinitrophenyl amino acids (DNP-AA) and water-soluble vitamins.

Aqueous solubility data were measured as a function of pH and upon the addition of covitamins. The predictions are in excellent agreement with these data. The key to the success was to understand the speciation of the biomolecules in water depending on the pH/the presence of covitamins. ATPS were characterized using binodal curves and tie-lines. The partitioning of four DNP-AA and five water-soluble vitamins was carried out in biodegradable ATPS composed by polyethylene glycol (M_{PEG} = 4000 – 8000 g·mol^{-1}) and organic salt (Na_3Citrate, Na_2Tartrate, K_3Citrate, KNaTartrate) at T=298.15 K and p=1 bar. The highest partition coefficients were obtained in citrate-based ATPS, and Na^+-based ATPS were found to be better than K^+-based ATPS. The predictions have proven that, despite the high complexity of these ATPS, the designed strategies adopted in this work for the ePC-SAFT modeling can be successfully applied for predicting the partitioning in such multi-component systems. The experimental work and ePC-SAFT prediction results have also contributed to a better understanding of the phenomena that rule both the solubility in water and partitioning in ATPS.

Keywords: vitamins, DNP-AA, low-solubility, ATPS, ePC-SAFT, phase equilibria

Resumo

Biomoléculas como aminoácidos ou vitaminas têm sido alvo de um interesse crescente a nível industrial e académico. No entanto, a purificação destas moléculas constitui ainda um desafio, em parte devido às suas gamas de estabilidade química e térmica muito reduzidas. Nos métodos de ponta, estão ainda envolvidos solventes prejudiciais ao meio ambiente. Os sistemas bifásicos aquosos biodegradáveis (ATPS) são alternativas promissoras aos sistemas convencionais que contêm componentes tóxicos, pois podem impedir a perda de atividade biomolecular usando a água como solvente. Em contraste com ATPS clássicos, o ATPS biodegradável consiste em sal orgânico (e polímero) como base para o estabelecimento das fases.

Do ponto de vista termodinâmico, o desenvolvimento e a aplicação de ATPS para a purificação de biomoléculas requer o conhecimento inicial sobre os equilíbrios de ATPS e a compreensão do comportamento das biomoléculas em água. Algumas das biomoléculas são pouco solúveis em água e isso pode afetar a confiabilidade das medições experimentais. Com efeito, nesta tese, o aumento da solubilidade por variação de diferentes condições, pH ou adição de co-solutos, foi estudado. A seleção dos componentes para a formação de ATPS baseou-se em dois critérios: obtenção de maior área bifásica para os ATPS e elevados coeficiente de partição. O esforço necessário para obter dados experimentais de elevado rigor foi substancial, e esteve relacionado com o número de medições necessárias. Assim, a componente experimental foi associada à contribuição do modelo termodinâmico preditivo (eletrólito PC-SAFT). As biomoléculas sob investigação foram aminoácidos dinitrofenilados (DNP-AA) e vitaminas solúveis em água.

Os dados de solubilidade aquosa foram medidos em função do pH e da adição de covitaminas. As previsões apresentam excelente concordância com esses dados. A chave para este sucesso foi entender a especiação das biomoléculas na água, dependendo do pH / presença de covitaminas. Os ATPS foram caracterizados usando curvas binodais e linhas de equilíbrio. A partição de quatro DNP-AA e cinco vitaminas hidrossolúveis foi realizada em ATPS biodegradável composto por polietileno glicol (M_{PEG} = 4000 - 8000 g · mol^{-1}) e sal orgânico (Na_3Citrato, Na_2Tartrato, K_3Citrato, KNaTartrato) a T = 298,15 K e p = 1 bar. Os coeficientes de partição mais elevados foram obtidos no ATPS constituído por citrato, e o ATPS à base de Na^+ permite alcançar melhores valores do que o ATPS à base de K^+. As previsões provaram que, apesar da alta complexidade de tais sistemas, as estratégias de modelação adoptadas neste trabalho, para a equação de estado ePC-SAFT podem ser aplicadas com sucesso para prever a partição em sistemas de múltiplos componentes, como ATPS. O trabalho experimental e os resultados de previsão do modelo ePC-SAFT também contribuíram de forma clara para uma melhor compreensão dos fenómenos que regem tanto a solubilidade em água quanto a partição em ATPS.

Keywords: vitaminas, DNP-AA, pouca solubilidade, ATPS, ePC-SAFT, equilíbrio de fases

Zusammenfassung

Aminosäuren und Vitamine erfahren ein zunehmendes Interesse im Bereich der Wissenschaft und der Industrie. Dennoch ist die Aufreinigung dieser Moleküle immer noch eine herausfordernde Aufgabe. Häufig werden bei der Aufreinigung von Aminosäuren und Vitaminen umweltschädliche Lösemittel eingesetzt. Eine Alternative dazu stellen bioabbaubare flüssig-flüssig Extraktionssysteme (ATPS) dar. Diese verhindern den Verlust der biomolekularen Aktivität da das Hauptlösemittel in diesen Extraktionssystemen Wasser ist.

Aus Sicht der Thermodynamik benötigt die Auswahl und die Anwendung von ATPS zur Aufreinigung von Biomolekülen ein tiefergehendes Verständnis des ATPS Phasengleichgewichtes und dem Verhalten der Biomoleküle in Wasser. Aus diesem Grund wurde im Rahmen dieser Arbeit die Erhöhung der Löslichkeit in Abhängigkeit des pH-Wertes und der Zugabe von Additiven untersucht. Weiterhin wurde die Auswahl der ATPS Phasenformer auf der Grundlage von zwei Kriterien durchgeführt: Zum einen muss eine breite Mischungslücke und zum anderen ein hoher Verteilungskoeffizient gegeben sein. In dieser Arbeit wurden deshalb eine große Anzahl an Experimenten mit einem prädiktiven thermodynamischen Modell (electrolyte PC-SAFT) gekoppelt. Die in dieser Arbeit untersuchten Biomoleküle waren DNP -AA und wasserlösliche Vitamine.

Die Wasserlöslichkeit dieser Moleküle wurde in Abhängigkeit des pH-Wertes und unter Zugabe von Co-Vitaminen untersucht. Dabei zeigten die Vorhersagen eine sehr gute Übereinstimmung mit den experimentellen Daten. Der Schlüssel zu diesem Erfolg war die korrekte Beschreibung der Speziesverteilung in Abhängigkeit des pH/Co-Vitamins. ATPS wurden bezüglich der Bionodalen und der entsprechenden Konoden charakterisiert. Der Verteilungskoeffizient von vier DNP-AA und fünf wasserlöslichen Vitaminen wurde in ATPS, bestehend aus Polyethylenglykol (M_{PEG} = 4000 – 8000 g·mol^{-1}) und organischen Salzen (Na_3Citrate, Na_2Tartrate, K_3Citrate, KNaTartrate) bei T=298.15 K und p=1 bar, bestimmt. Der größte Verteilungskoeffizient wurde in den Citrat-basierten ATPS bestimmt. Weiterhin wurde nachgewiesen, dass Na^+-basierte ATPS einen höheren Verteilungskoeffizienten als K^+-basierte ATPS aufweisen. Die Vorhersagestrategie welche in dieser Arbeit entwickelt wurde hat gezeigt, dass auch für sehr komplexe Systeme eine Vorhersage des Verteilungskoeffizienten möglich ist. Weiterhin haben die experimentellen Ergebnisse und die ePC-SAFT Vorhersagen zu einem besseren Verständnis hinter den Effekten, welche die Löslichkeit und den Verteilungskoeffizienten beeinflussen, beigetragen.

Keywords: Vitamine, DNP-AA, schwerlöslich, ATPS, ePC-SAFT, Phasengleichgewichte

Acknowledgments

This dissertation is presented to the Faculty of Engineering of the University of Porto for obtaining the degree of Ph.D. in Chemical and Biological Engineering.

The experimental research was carried out at the Associate Laboratory LSRE (Laboratory of Separation and Reactions Engineering) – LCM (Laboratory of Catalysis and Materials). Thus, I would like to thank the head of LSRE-LCM, Prof. Doutora Madalena Dias, for this opportunity. I would like to also thank the director of the PDEQB, Prof. Doutora Alexandra Pinto, for the doctoral program orientation. I would like to acknowledge the financial support of the Portuguese Foundation of Science and Technology of Ph.D. scholarship PD/BD/114315/2016.

I would like to express special gratitude to my supervisor Prof. Doutora Maria Eugénia Rebello de Almeida Macedo for all the support, suggestions, and encouragement during the whole Ph.D. period. I would like to thank her for the constant trust in my work and for allowing me to grow as a research scientist. Her advice and opportunity to present the work on multiple occasions, including national and international conferences, have significantly raised my motivation and passion for science.

I would like to thank committee members, Prof. Doutora Maria Arminda Costa Alves, Prof. Doutora Ana Isabel Nobre Martins Aguiar de Oliveira Ricardo, Prof. Doutora Ángeles Domínguez Santiago, Prof. Doutora Maria Eugénia Rebello de Almeida Macedo, Prof. Doutor Domingos Azavedo Gonçalves Barbosa, and Doutora Elena Gómez Costas, for their positions as assessors and examiners.

Special thanks to my supervisor, Prof. Doutora Maria Eugénia Rebello de Almeida Macedo, also for establishing the collaboration with the Technical University of Dortmund, where I had an opportunity to perform the modeling work. Being a member of the CRUP – DAAD joint project among the Technical University of Dortmund and Faculty of Engineering of the University of Porto has broadened the framework of my Ph.D. studies. The latter would not be possible without the agreement of the head of the Laboratory of Thermodynamics of the Technical University of Dortmund, Prof. Gabriele Sadowski, to carry out the work at her Chair. I would like to thank Prof. Gabriele Sadowski for fruitful discussions, dedication, and support during my stay in Dortmund. I would like to express special thanks to Dr. -Ing. hab. Christoph Held for being my supervisor in Dortmund, and particularly for the introduction to the world of ePC-SAFT modeling. It was my biggest

pleasure to work with him and listen to the critical comments and suggestions that have been a great contribution to my work. Without the positive spirit of Dr. -Ing. hab. Christoph Held toward scientific research and constant availability to answer the questions, maintaining the enthusiasm for solving complex modeling issues would be very difficult, if even possible. I would like to thank Prof. Gabriele Sadowski and Dr. -Ing. hab. Christoph Held for giving me an opportunity to present my work at the German Thermodynamik Kolloquium conference. I am very grateful for a warm welcome in Dortmund and for all support provided, also in non-scientific related issues.

I deeply thank Prof. Doutor José Miguel Loureiro from the University of Porto, Prof. Doutor Oscar Rodríguez, and Prof. Andrzej Górak from the Technical University of Dortmund for all the encouraging conversations and great support provided during the time of my Ph.D. I am also very thankful to Prof. Andrzej Górak for recognition of my scientific outcomes and for inviting me to the conferences at which I could share the results of my work with Polish scientists.

I would like to express my appreciation for the work of M.Sc. Hoang Tam Do and B.Sc. Birte Nierhauve from the Technical University of Dortmund that I had a pleasure to supervise and for their contribution to my research. I would also like to thank my dear colleagues from the University of Porto and the Technical University of Dortmund. Working time would not be that enjoyable and encouraging without them.

I also would like to thank my friends I met during the Ph.D. period in Portugal, Eduarda, Filipa, Ioana, Catalina, Patrícia, and Nuno, for making me feel happy and comfortable while staying abroad. Also, special thanks to Canan, Jurek, Konrad, Patrick, Slawa, Katrin, Richard, and Alex for a great time in Germany. I deeply would like to thank Anton for motivating me, as well as for the never-ending patience and support.

Last, but not least, I would like to express special thanks to my family and friends from Poland for their unconditional emotional assistance.

Publications and Reproduction Clearance

This thesis includes the results that were published in scientific articles. Thus, the content of some publications was reused in the present work with the permission of a given publisher. This concerns just selected articles of Wysoczanska *et al.* published as full papers and applies to the following chapters:

Chapter 1	[1-8]	Chapter 7	[1, 3, 4, 7, 8]
Chapter 2	[5-8]	Chapter 8	[5, 6, 8]
Chapter 3	[1-8]	Chapter 9	[2-4, 7, 8]
Chapter 4	[5-8]	Chapter 10	[1, 3, 4, 7, 8]
Chapter 5	[5, 6, 8]	Chapter 11	[1-8]
Chapter 6	[2-4, 7]		

[1] Reprinted (adapted) with permission from ref. [1] (Wysoczanska, K., Silvério, S. C., Teixeira, J. A., & Macedo, E. A. (2015). Cation effect on the (PEG 8000+ sodium sulfate) and (PEG 8000+ magnesium sulfate) aqueous two-phase system: Relative hydrophobicity of the equilibrium phases. J. Chem. Thermodyn., 91, 321-326). **Copyright (2020) Elsevier**.

[2] Reprinted (adapted) with permission from ref. [2] (Wysoczanska, K., & Macedo, E. A. (2016). Influence of the molecular weight of peg on the polymer/salt phase diagrams of aqueous two-phase systems. J. Chem. Eng. Data, 61(12), 4229-4235). **Copyright (2020) American Chemical Society**.

[3] Reprinted (adapted) with permission from ref. [3] (Wysoczanska, K., & Macedo, E. A. (2016). Effect of molecular weight of polyethylene glycol on the partitioning of DNP-amino acids: PEG (4000, 6000) with sodium citrate at 298.15 K. Fluid Phase Equilib., 428, 84-91). **Copyright (2020) Elsevier**.

[4] Reprinted (adapted) with permission from ref. [4] (Wysoczanska, K., Do, H. T., Held, C., Sadowski, G., & Macedo, E. A. (2018). Effect of different organic salts on amino acids partition behaviour in PEG-salt ATPS. Fluid Phase Equilib., 456, 84-91). **Copyright (2020) Elsevier**.

[5] Reprinted (adapted) with permission from ref. [5] (Wysoczanska, K., Sadowski, G., Macedo, E. A., & Held, C. (2019). Toward Thermodynamic Predictions of Aqueous Vitamin Solubility: An Activity Coefficient-Based Approach. Ind. Eng. Chem. Res., 58(17), 7362-7369). **Copyright (2020) American Chemical Society**.

[6] Reprinted (adapted) with permission from ref. [6] (Wysoczanska, K., Macedo, E. A., Sadowski, G., & Held, C. (2019). Solubility enhancement of vitamins in water in the presence of covitamins: measurements and ePC-SAFT predictions. Ind. Eng. Chem. Res., 58(47), 21761-21771). **Copyright (2020) American Chemical Society**.

[7] Reprinted (adapted) with permission from ref. [7] (Wysoczanska, K.; Do, H. T.; Sadowski, G.; Macedo, E. A.; Held, C., Partitioning of water-soluble vitamins in biodegradable ATPS: ePC-SAFT predictions and experimental validation. AIChE, doi:10.1002/aic.16984). **Copyright (2020) Wiley.**

[8] Reprinted (adapted) with permission from ref. [8] (Wysoczanska, K.; Nierhauve, B..; Sadowski, G.; Macedo, E. A.; Held, C. (2021) Solubility of DNP-amino acids and their partitioning in biodegradable ATPS: experimental and ePC-SAFT modeling. Fluid Phase Equilib, 527, 112830). **Copyright (2020) Elsevier.**

Contents

Contents

List of Figures

List of Figures

List of Figures

List of Tables

Roman symbols

a_i	thermodynamic activity of component *i* [-]
A	Helmholtz energy [J]
a^{assoc}	associative contribution to a^{res} [J·mol^{-1}]
a^{disp}	dispersive contribution to a^{res} [J·mol^{-1}]
a^{hc}	hard chain contribution to a^{res} [J·mol^{-1}]
a^{ion}	electrostatic contribution to a^{res} [J·mol^{-1}]
a^{res}	molar residual Helmholtz energy [J·mol^{-1}]
A_i, B_i	association sites A and B of component *i* [-]
A_j, B_j	association sites A and B of component *j* [-]
$\Delta_{cr}^{L} Cp_{m,i}^{0}$	difference of the heat capacity of the solid and the liquid component *i* at its melting point [kJ·K^{-1}·kg^{-1}]
d	temperature dependent segment diameter [Å]
f	fugacity [bar]
G^E	the excess Gibbs energy [J]
$\Delta_{cr}^{L} H_{m,i}^{0}$	heat of fusion of component *i* [kJ·kg^{-1}]
H_zA	acid able to dissociate *z* times
H_zX	amphoteric compound able to dissociate *z* times
H_2O	water
H_3O^+	hydronium ion
K_i	partition coefficient of component *i* [-]
K_a	acid dissociation constant [-]
$K_{a,th}$	thermodynamic dissociation constant [-]
k_B	Boltzmann constant 1.38065·10^{-23} [J·K^{-1}]
k_{ij}	binary interaction parameter [-]
K_{sp}	solubility product [mol·kg$_{water}^{-1}$]
M	molar mass [g·mol^{-1}]
m	molality [mol·kg$_{water}^{-1}$]
$m_{0,i}^{L}$	intrinsic solubility of component *i* [mol·kg$_{water}^{-1}$]
m_i^L	solubility of component *i* [mol·kg$_{water}^{-1}$]
m_i^{seg}	segment number of component *i* [-]
n_i	mole number of component *i* [-]
N^{assoc}	association scheme [-]
NP	number of experimental data points [-]
osm	osmolality [mmol·kg$_{water}^{-1}$]
p	pressure [bar]
q	charge [-]
R	universal gas constant [J·mol^{-1}·K^{-1}]
RFU	relative fluorescence unit [-]
T	temperature [K]
t	time [s]
$T_{m,i}$	melting temperature of component i [K]
u_i/k_B	dispersion-energy parameter [K]
v	stoichometric coefficient [-]
V	volume [m^3]
w	mass fraction [-]
x_i	mole fraction of component *i* [-]

X_i	abbreviation for expression in equation (2.82)
y	thermodynamic property used for parameter estimation [-]
z	number of protons that acid can donate [-]
Z	compressibility factor [-]

Greek symbols

α	molal fraction [-]
γ_i	activity coefficient of component *i* [-]
Δ	delta [-]
ε^{AiBi} / k_B	association-energy parameter [K]
κ	Debye screening length [$1 \cdot Å^{-1}$]
κ^{AiBi}	association-volume parameter [-]
λ	wavelength [nm]
μ	chemical potential [$J \cdot mol^{-1}$]
ρ	mass density [$kg \cdot m^{-3}$]
σ	segment diameter [Å]
φ	fugacity coefficient [-]
ϕ	osmotic coefficient [-]

Superscript

A	absorbance based
A_iB_i, A_jB_j	association sites A and B on molecule *i* and j
exp	experimental
I	top phase of ATPS
II	bottom phase of ATPS
id	ideal
L	liquid phase
pred	predicted
res	residual
S	solid phase
seg	segment
x	molality based
∞	at infinite dilution
+,-	positive or negative charge

Subscripts

0i	pure component *i* reference state
A^-	anion
A, B,…,π	different phases
assoc	association
B	Boltzmann
cr	critical
disp	dispersion

hc	hard chain
i	component i
j	component j
k	component k
l	component l
m	melting
P	polyethylene glycol (PEG)
ref	reference
S	salt
th	therdmodynamic
W	water

Abbreviations

AA	amino acid
API	Active Pharmaceutical Ingredient
AAD	average absolute deviation
ARD%	average relative deviation [%]
ATPS	aqueous two-phase system
CAS	registry identifier of chemical
COSMO-RS	COnductor-like Screening MOdel for Real Solvents
DF	Dilution Factor
DNP-AA	2,4-dinitrophenyl amino acid
DNP-alanine	N-(2,4-Dinitrophenyl)-L-alanine
DNP-glycine	N-(2,4-Dinitrophenyl)glycine
DNP-leucine	N-(2,4-Dinitrophenyl)-L-leucine
DNP-valine	N-(2,4-Dinitrophenyl)-L-valine
eCPA	electrolyte Cubic Plus Association equation of state
eNRTL	electrolyte NonRandom Two-Liquid model
EOS	Equation Of State
ePC-SAFT	Perturbed-Chain Statistical Associating Fluid Theory
HCl	hydrochloric acid
H-H	Henderson-Hasselbalch
H-NMR	proton nuclear magnetic resonance spectroscopy
J-PM	joint-parameter modeling method
K_2Oxalate	disodium oxalate
K_2Tartrate	disodium tartrate
K_3Citrate	tripotassium citrate
KFormate	potassium formate
KNaTartrate	potassium sodium tartrate
KOH	potassium hydroxide
Li_3Citrate	trilithium citrate
LLE	Liquid-Liquid Equilibrium
ME	Merck
MgSulfate	magnesium sulfate
MM	Molecular Modeling method
Na_2HCitrate	disodium hydrogen citrate

Na_2Succinate	disodium succinate
Na_2Sulfate	disodium sulfate
Na_2Tartrate	disodium tartrate
Na_3Citrate	trisodium citrate
NaFormate	sodium formate
NaOH	sodium hydroxide
$(NH_4)_2$HCitrate	diammonium hydrogen citrate
$(NH_4)_3$Citrate	triammonium citrate
OF	objective function
PEG	polyethylene glycol
PR	PanReac (supplier)
PXRD	powder X-ray diffraction
ref	reference
SA	Sigma-Aldrich (supplier)
SA^-	anion of a salt
SC^+	cation of a salt
SAFT	Statistical Associating Fluid Theory
SLE	solid-liquid equilibrium
SRK	Soave Redlich Kwong
TCI	Tokyo Chemicals Industry (supplier)
TL	tie-line
TLL	tie-line length
UNIFAC	UNIversal Quasichemical Functional Group Activity Coefficient model
UNIQUAC	UNIversal QUAsichemical Activity Coefficient model
UV	ultraviolet
UV-VIS	ultraviolet-visible spectrophotometry
VB12	cyanocobalamin
VB2	riboflavin
$VB3^{acid}$	nicotinic acid
$VB3^{amide}$	nicotinamide
VB9	folic acid
VC	ascorbic acid
VIS	visible
wt-%	weight percentage [%]
X^-	anion of amphoteric component

1. Introduction

This chapter addresses the high merit of studying the physicochemical properties of aqueous solutions containing biomolecules, i.e. amino acid derivatives and water-soluble vitamins, and selecting biodegradable aqueous two-phase systems (ATPS) centered on the partitioning of these molecules. ATPS can assist in the mitigation of the two major problems that often occur when conventional extraction techniques and solvents are used: loss of biomolecular activity of the biomolecules and production of harmful waste. Thus, the present chapter summarizes the last attempts contributing to the above goals that have been reported in literature. It presents the aim of this work and the approach used to characterize the biomolecules in their aqueous solutions, as well as partitioning in biodegradable ATPS. It also covers the topics related to selection of ATPS appropriate for the separation of considered biomolecules.

1.1. Motivation and State-of-the-Art

In this chapter, the high importance of studying the physicochemical properties of biomolecules, including aqueous solubility, as well as their partitioning in biodegradable aqueous two-phase systems (ATPS) is addressed. Section 1.1.1 provides and explains the major issues that have been driving the research carried out within this work, while section 1.1.2 presents the up-to-date knowledge on these issues. Since studies performed in this work involve many different aspects that must be considered while studying aqueous systems of high complexity, for clarity enhancement section 1.1.2 is divided into subsections. At first, the actual knowledge of the physicochemical properties of some amino acid derivatives and water-soluble vitamins is covered. This includes the knowledge of physicochemical properties such as density and osmotic coefficients published in the literature for aqueous solutions of the considered biomolecules, as well as their solubility in water. The second part of section 1.1.2 is dedicated to Aqueous Two-Phase Systems (ATPS). It evaluates the past research on the polyethylene glycol (PEG) – organic salt ATPS that has been so far discussed in the literature. The last part presents the possible applications of biodegradable ATPS for the partitioning of different components. Each subsection is followed by presenting the corresponding state-of-the-art of thermodynamic modeling for correlating or predicting data (if available) from the scope of these three main topics.

1.1.1. Motivation

Water is the main compound that occurs in humans' bodies, thus, studying the behavior of biomolecules in an aqueous environment is of very high merit [9, 10]. However, the physicochemical properties of many biomolecules are often underexplored. Among different physicochemical properties, the solubility in water is one of the most important and should be known before planning any experiment or designing the process in which biomolecules are involved [11-13]. Furthermore, understanding the mechanisms that rule the solubilization processes is crucial not just for unit operations, but also for drug-delivery studies, which nowadays are willingly discussed in the literature [14-16]. Water-soluble vitamins and amino acids are biomolecules that play important roles in human's metabolism [17]. On one hand, they are known as essential

molecules for human health, on the other hand, their application is not limited only to health-promoting actions such as dietary supplementing.

Besides vital functions, some vitamins are considered as model components for drugs, and this further points to the high importance of studying different interactions in their aqueous solutions [18-20]. Recent publications have significantly broadened the scope of the research on water-soluble vitamins by showing a high interest of using them, e.g., as precursors for sensing materials, which are readily applied in the field of environmental protection [21]. Furthermore, the literature proposed vitamins as agents in the recycling processes of rechargeable power suppliers - Li-ion batteries [22-25]. According to former studies, amino acids were applied to various scientific fields as well, since they can assist in the synthesis of nanocrystals for sensors and solar cells production [26, 27] or may be used as biosurfactants in oil recovery or lubricants and cosmetics production, among others [28-30]. Although using vitamins and amino acids can be attractive to many scientific areas, there is relatively scarce characterization of their physicochemical properties and lack of understanding of the phenomena that rule the separation and purification of these molecules in aqueous environmentally friendly systems. This strongly limits their “green” production on an industrial scale [31, 32]. “Green” means that the media used to obtain biomolecules of certain purity grades are not polluting the environment and do not lead to harmful waste production [33-36]. Another aspect is related to the usage of the separation systems that prevent also from biomolecular activity loss of biomolecules [37, 38].

The lack of solubility data can be observed for both amino acid derivatives and essential components such as water-soluble vitamins. In some cases, the low availability of physicochemical data in literature is related to low solubility that drastically decreases the interest of studying their properties. This is especially notable for cyanocobalamin (VB12), which is difficult to characterize not just due to its limited solubility but also through its complex molecular structure [39]. A high structural complexity can lead to a huge number of possible molecular interactions in the solution and some structural changes, which can occur in aqueous solutions under variable conditions, and in the presence of additional components [40-42]. To study the interactions of very complex and large biomolecules such as proteins, often smaller compounds that share the same functional groups as macromolecules are introduced to the research[43-46]. Thus,

2,4-dinitrophenyl derivatives of amino acids (DNP-AA) have been commonly selected to evaluate the interactions of the amino acid side-chain groups in aqueous environment[43, 46-49]. Being yellow in visible light they are readily detected and analyzed using spectrophotometry[50].

The experimental procedures used to characterize the aqueous systems composed of low-soluble components such as some of DNP-AA or water-soluble vitamins, e.g. riboflavin (VB2), folic acid (VB9), cyanocobalamin (VB12), are usually time-intensive and challenging[51]. To measure the properties of the solutions (e.g. liquid density or osmotic coefficients) containing poorly soluble components in a significant concentration range, enhancing the solubility of biomolecules is of importance. The solubility is usually improved by variation of the temperature and the pH or by the addition of so-called hydrotropes [52-56]. It is well known that changing the temperature can significantly increase the solubility of solutes in solvents[57]. Although the pH also dramatically influences solubility, the information on pH is often neglected in literature when reporting aqueous solubility data. If experimental results reported for aqueous solutions are given without corresponding pH, they are practically worthless. The lack of information on the pH becomes even more troublesome when trying to unravel the phenomena which rule the solubilization upon addition of different solubilizers, e.g., hydrotropes [58]. The hydrotropic solubilization is a technique used to increase the solubility of poorly water-soluble components by the addition of excess amounts of a second solute—the so-called hydrotrope [53, 59]. According to the literature, such a procedure can lead even to 1000- to 10 000-fold enhancement of solute solubility [52]. The term “hydrotropic solubilization” can be misused and applied where the same solubility increase can be achieved by pH shift upon addition of small amounts of an acid or a base (e.g. HCl or NaOH)[60].

Scarce knowledge on the behavior of DNP-AA and vitamins in aqueous solutions in the presence of additives is a limiting factor for industrial applications such as process design and optimization. Knowing the pH-solubility profiles is fundamental for understanding and controlling the behavior of these compounds in aqueous solutions [60, 61]. Overall, a high experimental input to fully characterize aqueous systems that involve considered biomolecules is required to fill a great lack of knowledge in the literature. Some attempts of modeling solubility data with different thermodynamic approaches that

could reduce the number of experiments needed, have been already taken for relatively well soluble water-soluble vitamins, namely ascorbic acid (VC), nicotinic acid ($VB3^{acid}$), and nicotinamide ($VB3^{amide}$) [62-66]. However, modeling and predicting the aqueous solubility of DNP-AA and poorly soluble vitamins using any predictive model has not been yet reported in literature. Thus, this is still very challenging task. The difficulty in studying the aqueous solubility of DNP-AA and water-soluble vitamins is the fact that these molecules can dissociate in water leading to the formation of different ionic species. To predict the interactions in complex aqueous systems containing biomolecules and their different ionic species, an appropriate thermodynamic model is required that can cover important molecular interactions in these multicomponent mixtures. It concerns among others Coulomb or hydrogen-bonding forces [67, 68].

A thermodynamic model could assist in this study by separating the effects of pH and cross-interactions on solubility. Activity coefficients are an appropriate indicator for the interactions, and different models exist in the literature to calculate them [69-73]. Statistical Association Fluid Theory (SAFT)-based models are very often proposed because of their predictive character and physical background, e.g. Electrolyte Perturbed-Chain SAFT (ePC-SAFT) [74-76]. Since ePC-SAFT was already very successful for modeling and predicting various physicochemical properties of different organic components [77-82], it was also very promising for the purpose of this work. Novel modeling strategies applied to a thermodynamic model ePC-SAFT and the measurements performed for experimental validation, could further help in understanding complex problems that occur in the systems where these biomolecules are involved [83, 84]. This may involve studies on different separation systems that can be used for the partitioning.

The partitioning in aqueous two-phase systems (ATPS) is a separation technique, with very low environmental impact, considered as an accurate and very adequate methodology for purification of biomolecules [85-88]. It could be also used for partitioning of the components in the present study. This promising and still developing method for the separation of biomolecules in a gentle and environmentally friendly condition has great potential for the biotechnological industry [86, 89, 90]. Due to the high content of water, it provides a mild environment with a rare loss of biomolecular activity to these kinds of components. Furthermore, the technique offers substantial advantages, such as biocompatibility, low interfacial tension, high capacity and yield,

ease of up-scale [91-94]. Although it presents many advantages over other conventional separation processes, it is still not widely implemented at an industrial level, as the understanding of the phenomena that rule the partition is highly complex and still under study.

To date studies have been conducted on the two major types of ATPS: formed by mixing two solutions of different polymers and of a polymer and a salt. Polyethylene glycol (PEG), being a biodegradable, low-toxicity, and relatively inexpensive component, is a widely chosen polymer to form ATPS. It also presents interesting properties such as low melting point and very low volatility, when compared to other, commonly used, toxic organic solvents [86, 95]. PEG together with another polymer or salt, can form two immiscible phases and, as reported in the literature, can enhance protein refolding, and decrease aggregation [85, 96]. Systems formed by a polymer and a salt are usually more adopted due to the larger difference in densities, higher selectivity, lower viscosity, and the lower cost of salts compared to polymers [37].

It has been reported that PEG combined with salts can form very adequate ATPS, for the partitioning of various compounds – amino acids and their derivatives [97], proteins [98-101], enzymes [102, 103], proenzymes [104], antibiotics [105-108], among others. Widely studied salts for ATPS with PEG are phosphates [101, 108-110], and sulfates [101, 111-114]. However, at an industrial level, they can cause environmental pollution. The environmental risk of classical ATPS formed by polymer and inorganic salt [115-117] can only overcome by the development, evaluation, and application of new systems based on biodegradable compounds, so by replacing the inorganic salts with some organic alternatives, e.g. citrates or tartrates. These salts are commonly used as food additives and present health advantages [118, 119].

Missing comprehension of the dependencies of the partitioning of biomolecules such as DNP-AA and water-soluble vitamins on system properties still limits the application of ATPS at an industrial level. Thermodynamic models able to accurately predict influences of system properties controlling the partitioning in ATPS would significantly help as time-consuming and cost-intensive experiments can be reduced to a minimum extent. However, due to many dependencies of the partitioning behavior in ATPS, understanding the phenomena which rule the partitioning in these complex systems and modeling requires much more effort (e.g. availability of data) than in

conventional separation systems. Both ATPS phases contain high water concentrations, thus, solubility data of a solute in each phase is not enough to predict the partitioning in ATPS and cannot be done on the modeling basis already published in the literature for conventional separation systems in which organic solvents were involved [65]. Biomolecule partitioning in PEG – biodegradable salt ATPS is highly influenced by pH, a solute can dissociate in ATPS, and both the pH and interactions strongly depend on the kind and composition (the tie-line length - *TLL*) of ATPS, as well as on the properties of ATPS phase formers, e.g. PEG´s molecular weight, type of anion and cation of salt [86, 87]. The modeling and predicting the partitioning of biomolecules in PEG – organic salt ATPS using any thermodynamic predictive model have not been yet reported in the literature. Thus, the challenge of predicting the above with a thermodynamic model ePC-SAFT was a great opportunity to be taken in this work.

1.1.2. State-of-the-Art

This section is divided into three main parts that cover the topics in the scope of the present work. In the present section, at first, up-to-date knowledge of physicochemical properties of 2,4-dinitrophenyl derivatives of amino acids (DNP-AA) and water-soluble vitamins, selected in this work, is presented (*I*). The second part focus on the current state of the literature on different biodegradable PEG – salt aqueous two-phase systems (ATPS) and the availability of the properties of these systems in former publications (*II*). In the end, the actual stage of knowledge on the partitioning of different organic molecules in various biodegradable PEG - salt ATPS is discussed (*III*).

The elaboration provided in this section involved the current state of the literature on experimental studies, as well as thermodynamic modeling. The latter was given in more detail only if it was available in previously published works.

I. Physicochemical properties of DNP-AA and water-soluble vitamins

The state of knowledge of solute properties considered in this work is presented in the following. The experimental data published in literature is discussed separately for aqueous solutions of DNP-AA and water-soluble vitamins. In the end, the availability of thermodynamic models that allow accounting for non-ideality of both DNP-AA and water-soluble vitamin systems is addressed.

DNP-AA: experimental

A major interest of studying DNP-AA in literature resulted from sharing the same functional groups by DNP-AA as the macromolecules, i.e. peptides and proteins. Former publications on DNP-AA focused mainly on the determination of the sequence of amino acids in peptides and proteins, among others[120-122]. Later works have shown different applications of DNP-AA e.g. to evaluate the possible cell interactions[123, 124]. More recent publications used DNP-AA for stereochemical analysis [125, 126]. Besides these research scopes, DNP-AA were rather poorly characterized in the literature, especially in terms of their physicochemical properties.

Although physicochemical data for solid DNP-AA are very scarce in literature, the melting points of DNP-AA $T_{m,DNP-AA}$ were studied by Rao *et al.*, Abderhalden *et al.*, and Rice *et al.* in the last century, leading to several publications [127-129]. Unfortunately, other caloric properties such as melting enthalpies $\Delta_{cr}^{L}H_{m,DNP-AA}^{0}$ and heat capacities $\Delta_{cr}^{L}Cp_{m,DNP-AA}^{0}$ have not been determined yet, to the best of my knowledge. Furthermore, to date, literature has not provided the basic knowledge of the physicochemical properties of DNP-AA in their aqueous solutions such as liquid density, osmolality, or solubility in water. Although these data can be very important for understanding DNP-AA behavior in water, there were some steps taken to unravel the phenomena in DNP-AA aqueous solutions. Thus, Madeira and Zaslavsky *et al.* [45] selected DNP-AA to study the interactions of amino acid side-chain groups in aqueous systems. Ramachandran *et al.* presented the work in which dissociation constants pK_a required for understanding the dissociation equilibrium of DNP-AA were provided [130]. Data provided by Ramachandran *et al.* [130] have proven that the acid-base character of DNP-AA is different than of aliphatic amino acids. Ramachandran *et al.* [130] have listed only a single pK_a value for each DNP-AA, since DNP-AA are acidic, in contrast to amphoteric aliphatic amino acids. These were very important findings in terms of pH-solubility profiling of DNP-AA.

Water-soluble vitamins: experimental

Although water-soluble vitamins VC (ascorbic acid), VB2 (riboflavin), $VB3^{acid}$ (nicotinic acid), $VB3^{amide}$ (nicotinamide), VB9 (folic acid), and VB12 (cyanocobalamin) are common substances in human`s life, readily applied and discussed in literature due to the

important role they play in metabolism [131-134], the knowledge of their different physicochemical properties is relatively scarce. Unfortunately, most vitamins are not synthesized in the body at all, while only a few (vitamins B3 and D) are synthesized in inadequate quantities [135, 136]. In contrast to fat-soluble vitamins (A, D, E, K), water-soluble vitamins (VC, complex B) dissolve in aqueous body fluids [38, 137]. Further, excess amounts of water-soluble vitamins cannot be stored in the body for later use due to the constant physiological excretion of body liquids [135]. For these reasons, past research works from literature focused mainly on a deeper understanding of the biological functions of water-soluble vitamins and on the design of different methods of their supply [138-143]. These studies have been mostly carried out for the prevention of various diseases, as several body dysfunctions are caused by water-soluble vitamin deficiencies [144, 145]. Some publications have significantly broadened the scope of the research on water-soluble vitamins by showing a high interest of using them, e.g., like reported by Zhang *et al.* as precursors for sensing materials, which are readily applied in the field of environmental protection [21] or proposed by Poschlad *et al.* as model compounds and ligands in new controlled-release and targeting drug delivery systems [16]. The latter are often evaluated from the anticancer treatment standpoint [14, 15, 146].

Despite the organic components classified as water-soluble vitamins (VC, B-complex) differ significantly in molecular structure and consequently also in physicochemical mixture properties, not much attention has been given in literature to study aqueous solubility of water-soluble vitamins [135, 147]. Additionally, solubility data provided for each vitamin at a given temperature are very divergent among different sources. However, Yalkowsky *et al.* present some data on vitamin aqueous solubility in different temperature ranges withdrawn from literature [148]. Shalmashi *et al.* [149] published solubility in water of VC in the range of T = 293 K and T = 323 K and Gonçalves *et al.* [150] have shown data obtained for $VB3^{acid}$ in the range of T = 283 K to T = 333 K. According to Ottaway and Ball (1993), some vitamins are not stable at high temperatures, T>298.15 K [151, 152]. There are some studies that report water-soluble vitamin aqueous solubility at T=298.15 K and p=1 bar, but these are only a few works among all published on the topics related to vitamins [148-150, 153-155]. Amongst publications on aqueous solubility data at T=298.15 K found for vitamins considered in this work, the highest

number of works is for VC. Aqueous solubility values of VC at T=298.15 K were published by Shalmashi *et al.* [149], Deritter [156], Nixon et al. [157], and Apelblat [158]. However, the deviations between these solubility data reached even ~100%. The values of solubility in water obtained for $VB3^{acid}$ and $VB3^{amide}$ at T=298.15 K were reported by Gonçalves *et al.* [150] and Lange *et al.* [66], respectively. Aqueous solubility data for VB2 were included in the book of Dawson *et al.* [159] and in the publication of Derriter [156]. The solubility of VB9 in water was published by Wu *et al.* [155] and Taub *et al.* [42]. Among the two vitamins VB2 and VB9, the latter presents the highest deviations if compared with different literature sources and solubility may vary of order 10^3 from reported absolute solubility values in different works. Solubility data at T=298.15 K for VB12 could not be found in the literature, only aqueous VB12 solubility reported by Freier *et al.* at T=293.15 K was available. Based on solubility data from the reports and European Pharmacopoeia terms [57], some of the vitamins are classified as only sparingly water-soluble (e.g., cyanocobalamin—VB12) or poorly soluble in water (e.g., riboflavin—VB2, folic acid—VB9) at T = 298.15 K and at their intrinsic pH. Low-solubility also limits the interest of studying their physicochemical properties and can be a reason for the high inconsistency of the solubility values provided in literature as the experimental methodologies for poorly-soluble compounds are typically coupled with high uncertainty of the measurements. Although the pH has a significant influence on solubility, the information on pH is often not provided in the literature when reporting aqueous solubility data. So far, there are only a few works in which aqueous solubility data of vitamins have been reported together with the pH of equilibrated solutions. These are mainly studies reporting the solubility of VB3 ($VB3^{acid}$, $VB3^{amide}$) published by Gonçalves *et al.* [150] and Lange *et al.* [66], as well as the solubility of VB9 from the articles of Taub *et al*. [42] and Wu *et al.* [155].

Dissociation equilibrium data which help to estimate the pH-solubility profiles, towards dissociation constant pK_a, were published for almost all considered vitamins using different methods, UV-VIS, a combination of potentiometric and spectrophotometric techniques, H-NMR, titration, or electrophoresis [160-163]. Although having dissociation data only does not fully ascertain the solubility at different pH, it gives an idea of the solubility lines course in pH-solubility profile. Dissociation equations based on Henderson-Hasselbalch equations, that use pK_a and intrinsic solubility [164]

measurements, were presented in the work of Avdeef [60]. The exception was VB12 which has not been characterized in literature in terms of acid-base behavior in aqueous solutions yet. Therefore, the pK_a values for VC were provided in the work of Brittain *et al.* [165], while for VB3^{acid} this data was given by Klingsberg *et al.* [166]. Dissociation behavior of VB2 has been discussed in literature, thus pK_a data could be withdrawn from works of Rivlin *et al.* [167], Michaelis *et al.*[168], Kuhn *et al.*[169], and Suelter[170]. The pK_a values for VB9 could be found in studies published by Szakács *et al.* using pressure-assisted capillary electrophoresis [161]. A review of Hofsäss *et al.* [171] on pK_a data for VB9 available in literature [155, 161, 172] confirms that data provided by Szakács *et al.* [161] was a breakthrough to define the previously inaccessible complete set of pK_a values for VB9. Difficulty in obtaining reliable pK_a data for VB2, VB9, and VB12, relates to the low solubility of these vitamins classified according to European Pharmacopoeia terms [57]. Since there has not been any report yet discussing the dissociation behavior of VB12, the pK_a values of VB12 could be only approximated using calculation tools, such as Chemicalize [173]. In overall, based on data and discussions published in literature (VB2, VB3^{acid}, VB9, VB12) or approximated with calculation tools (VB12), vitamins considered in this work are acidic (VC) or amphoteric (VB2, VB3^{acid}, VB9, VB12).

The solubility can be improved by the addition of so-called, in literature, hydrotropes [53, 54, 59]. To date, at least two vitamins were classified as hydrotropes, VC, and VB3^{amide}, and they have been used to dissolve some active pharmaceutical ingredients (APIs) [174], as well as vitamins according to table 1.1.

Table 1.1. Aqueous vitamin – hydrotrope systems.

Low water-soluble vitamin	*hydrotrope*	*reference*
VB2	VB3^{amide}	[153, 154, 175, 176]
	VC	[177]
	urea	[153, 154]
	caffeine	[176, 178, 179]
VB9	VB3^{amide}	[42]

Thus far, there are just a few publications in the literature that contain other physicochemical data of aqueous vitamin solutions such as density or osmotic

coefficients. These are the works published by Banipal *et al.* and Seng *et al.* for aqueous solutions of VC and VB3^{acid} [180, 181]. Also, data on caloric properties such as melting points $T_{m,vitamin}$, melting enthalpies $\Delta_{cr}^{L}H_{m,vitamin}^{0}$, and heat capacities $\Delta_{cr}^{L}Cp_{m,vitamin}^{0}$ for water-soluble vitamins are very scarce in literature. Among water-soluble vitamins considered in this work, a complete set of melting data are available only for VB3^{acid} and VB3^{amide}. These data could be found in the works of Gonçalves *et al*. [150], Joseph *et al.* [182] for VB3^{acid}, and in the publication of Laube *et al.* for VB3^{amide} [65]. For VC, both $T_{m,vitamin}$ and $\Delta_{cr}^{L}H_{m,vitamin}^{0}$ were available from Schröder *et al.* [64]. For VB2 and VB9 only $T_{m,vitamin}$ were provided in the literature in the works of Lide *et al.* [183] and Bradley *et al*.[184]. The caloric properties of VB12 have not been reported in literature yet.

Thermodynamic non-ideality of DNP-AA and water-soluble vitamins in aqueous solutions

Thermodynamic models allow describing phase equilibria (in the scope of this work solid-liquid and liquid-liquid equilibria) by means of activity coefficients of organic molecules in aqueous mixtures, using melting properties as well (for solid-liquid equilibrium calculations). So far, different thermodynamic approaches have been proposed in literature for modeling, and prediction of the properties of multicomponent systems. These were the Gibbs excess energy (G^E) models and equations of state (EOS) [185, 186].

In G^E models the excess Gibbs energy of liquid mixtures could be correlated with molecular local-composition models like Non-Random Two Liquid (NRTL) of Renon and Prausnitz [187] or UNIversal QUAsiChemical (UNIQUAC) developed by Abrams and Prausnitz [188, 189]. The excess Gibbs energy can be also predicted with a semi-empirical group-contribution model like UNIversal Quasichemical Functional Group Activity Coefficients (UNIFAC) of Fredenslund and Prausnitz [70, 190, 191]. The relative simplicity of these models allowed a wide range of applications in literature and was used to model a significant number of systems and their properties, in a variety of conditions [192-196].

The alternatives to G^E models are EOS. The elaboration considering the capabilities and limitations, current state, and the future of EOS has been recently published in extraordinary work resulting from the expertise and significant contribution of Kontogeorgis *et al.* [197]. One of the EOS appropriate for modeling of solutions containing

organic molecules is the Cubic-Plus-Association (CPA) postulated by Kontogeorgis *et al.* [72]. CPA EOS is the combination of a cubic EOS of Soave-Redlich-Kwong (SRK) with the association term of the Wertheim theory [198-200]. The SRK contribution allows accounting for the physical interactions between molecules, while the association term considers the intermolecular hydrogen bonding as well as solvation effects. Polarity and quadrupolar interactions are not explicitly involved in CPA [201]. Another highly recommended in literature EOS for modeling the systems containing complex components are Statistical Associating Fluid Theory (SAFT) models [202]. SAFT concept originates from an extension of Wertheim`s theory [203-206] to mixtures and it was derived by Chapman *et al.* [207, 208]. It accounts for deviations of a real system from the reference hard-sphere system. The perturbations considered by SAFT can be caused among others by different interactions, i.e. attractive van der Waals, association, polar and quadrupolar, and the non-spherical shape of the molecules. This theory was used and extended by Huang and Radosz [209, 210] who introduced to SAFT a dispersion term of Chen and Kreglewski [211]. A modification of SAFT, the perturbed-chain SAFT developed by Groß and Sadowski [75, 76] resulted from adopting the perturbation theory to the reference system of hard chains composed by spherical segments. PC-SAFT was already successfully applied to a variety of multicomponent systems including the ones containing different organic components of high complexity [212-216].

An alternative to the above-mentioned models might be the approaches based on conductor-like screening model (COSMO) [71] and their extensions, e.g. conductor-like screening model for real solvents (COSMO-RS) [217, 218]. However, the reliability of COSMO-RS models is strongly dependent on the geometry of the molecule [219]. If this is not represented accordingly, then the large deviations from reality are observed. As stated by Chemat *et al.* this can be the limitation for modeling the large molecules [220].

To model electrolyte solutions, the extensions of different models were proposed in the literature, e.g. the electrolyte NRTL (eNRTL) of Chen [69, 221, 222], the modified UNIQUAC of Thomsen [223, 224], the modified UNIFAC-Dortmund model of Gmehling [225, 226], the electrolyte CPA (eCPA) of Inchekel *et al.* [227], or the electrolyte PC-SAFT of Cameretti *et al.* (ePC-SAFT) [74]. Most of thermodynamic models adopted for modeling electrolyte solutions involve a term for long-range electrostatic interactions besides the term for short-range interactions. The contribution for electrostatic interactions is

commonly derived from Debye-Hückel theory [228]. It describes the interactions in an ideal solution in which charged species are present. To apply this theory to the non-ideal electrolyte solutions, the Debye-Hückel term and the short-range interactions are considered [229]. In general, the determination of physicochemical properties of the components under study is possible with any of these models. However, the difference in the precision of the predictions may differ in a significant manner.

Thermodynamic modeling of DNP-AA properties has not been reported yet. However, literature presented the modeling that involved amino acids (AA) or peptides that share the molecular similarity to DNP-AA. To date, the correlating, modeling, and predicting the behavior of amino acids and peptides in aqueous solutions was done with different thermodynamic models. Soto *et al.* measured and modeled the solubility of a mixture of two amino acids in their aqueous solutions using NRTL [230], while Chen *et al.* carried out the modeling of different amino acids and peptides in aqueous solutions using the electrolyte extension of this model, namely eNRTL [231]. Khoshbarchi and Vera applied UNIFAC for predicting the activity coefficients of amino acids and peptides in aqueous solutions [232]. Also, UNIQUAC has shown to be adequate for modeling of amino acid solubility as reported by Peres et al. [233]. Held *et al.* [79, 81] have proven that very reliable predictions of amino acid solubility can be obtained with PC-SAFT and its electrolyte extension (ePC-SAFT). However, based on the knowledge presented by Ramachandran *et al.* [130], it is expected that DNP-AA behave differently in aqueous solutions than AA, thus thermodynamic properties of DNP-AA are likely to be very different than of aliphatic parenteral AA (AA involved in DNP-AA structure). Also, thermodynamic modeling of water-soluble vitamins is relatively scarce in literature. Among all models above mentioned, CPA EOS has already been evaluated for the prediction of the solubilities of ascorbic acid and nicotinic acid only in organic solvents [62], whereas COSMO-RS has been used for calculations of solubilities of these vitamins in water [64]. SAFT-based models are recommended for such complex systems due to their predictive nature and physical background on which they are based. Thus, according to studies reported in literature, Perturbed-Chain (PC-SAFT) was suitable for the prediction of the aqueous solubilities of nicotinamide [65, 66] and many different organic components, sugars, amino acids, and APIs [79, 215, 234, 235] in very good agreement to experimental data.

II. Phase separation in biodegradable PEG – organic salt ATPS (T=298.15±2 K and p=1 bar)

Although ATPS have been already reported by Albertson in 1958[236], the research is still ongoing and the design of new ATPS is attractive for academia and promising for industry. Prior to the evaluation and application of ATPS, much experimental data is required. The state of knowledge of biodegradable PEG – organic salt ATPS considered in this work is presented in the following. Firstly, the experimental data published in literature is discussed. This involves the physicochemical characterization of ATPS, namely the availability of biphasic diagrams. Then, the availability of different empirical equations and thermodynamic models that allow describing phase equilibrium of PEG – salt ATPS was addressed.

The present work has given more emphasis on PEG – organic salt ATPS that are more biodegradable, and do not lead to the production of waste that could be inconvenient for the environment. Additionally, it evaluates ATPS at constant T=298.15 K and p=1 bar since such conditions are appropriate for sensitive compounds considered. For this reason, the following elaboration focus on presenting the current state of knowledge on such environmentally friendly systems at T=298.15±2 K and p=1 bar and lists different types of biodegradable PEG – organic salt ATPS that found an interest in literature.

Experimental data on PEG – organic salt ATPS

A number of revisions has been presented in the literature, in articles or book chapters that involved different types of ATPS [86, 87, 237-240]. Pereira *et al.* published recently a document centered on the novel applications, advantages, and bottlenecks of ATPS [241]. Most of the available elaborations provided a general knowledge on ATPS or focused on selecting appropriate media for ATPS, but some of the components chosen for these systems are questionable regarding environmental protection [242], e.g. ionic liquids [243-247] or reproducibility, e.g. deep eutectic solvents [242, 248, 249].

Works on ATPS formed by PEG and organic salt have recently found to be very promising in terms of phase separation and environmental protection [250]. The PEG - citrate salt ATPS were often studied by different scientific groups if comparing the research input thorough literature between different PEG – organic salt ATPS. This can be seen from table 1.2 where different ATPS studied in literature are listed. Vernau and Kula

[251] characterized liquid-liquid equilibrium (LLE) of ATPS formed by PEG 1550 and sodium citrate ($Na_3Citrate$). Application of higher molar mass PEG can often lead to larger biphasic region formation, therefore many authors, e.g. Zafarani *et al.* [252] have further extended the research of Vernau and Kula [251] by presenting the biphasic diagrams of systems composed by $Na_3Citrate$ and PEG of different molar mass [253-256]. High heterogeneous regions observed in these systems allow decreasing the concentration of the salt needed to form two immiscible phases. Efficient phase separation in PEG - $Na_3Citrate$ systems inspired many authors to evaluate different organic salts, e.g. formates or tartrates, for the potential phase formers of ATPS.

Table 1.2. Experimental liquid-liquid equilibria (LLE) of PEG – organic salt ATPS at T=298.15±2 K and p=1 bar.

Organic salt	M_{PEG} [g·mol^{-1}]	*reference*
$Na_3Citrate$	400	[257]
	1500	[254, 256, 258]
	1550	[251]
	2000	[255]
	6000	[253, 254]
	8000	[258]
$Na_2HCitrate$	600	[259]
	1000	[259]
	2000	[259]
	4000	[259]
	6000	[259]
	20 000	[259]
$K_3Citrate$	600	[260]
	1500	[258]
	6000	[253, 261]
	8000	[258]
$Li_3Citrate$	4000	[262]
	6000	[262]
	8000	[262]

$(NH_4)_2$HCitrate	2000	[263]
$(NH_4)_3$Citrate	2000	[264]
Na_2Succinate	6000	[265, 266]
NaFormate	600	[260, 267]
	1500	[258, 267]
	3000	[267]
	6000	[265, 267]
	8000	[258]
KFormate	600	[260, 267]
	1500	[258, 267]
	3000	[267]
	6000	[267]
	8000	[258]
Na_2Tartrate	600	[268]
	1000	[268]
	2000	[268]
	4000	[268, 269]
	6000	[268]
	8000	[268]
K_2Tartrate	4000	[270]
	8000	[258]
KNaTartrate	4000	[270]
K_2Oxalate	4000	[270]

Modeling of PEG - organic salt ATPS

For a better understanding of ATPS and to correlate phase composition data, empirical equations have been proposed in literature. The most common expressions are equations of Othmer-Tobias [271] and of Bancroft [272] that allow characterizing ATPS using two adjustable parameters. Besides that, empirical equations are also considered appropriate for a description of the binodal curve like in the work published by Hu *et al.* [273], Tubío *et al*. [274], or expression proposed by Merchuk *et al.* [275].

Other common methods to model phase composition data of ATPS are virial equations or activity coefficient models. Zafarani-Moattar *et al.* [252] used an osmotic virial equation as well as the UNIQUAC activity coefficient model to correlate the phase behavior of PEG 6000 – Na_3Citrate ATPS. The authors of the work [252] found that for this system, a better fit could be obtained with virial model. The tie-lines of the same ATPS (PEG 6000 – Na_3Citrate) have been modeled also by Perumalsamy *et al.* [276] using other activity coefficient model namely UNIFAC. Also, an extended NRTL model has been used for modeling of the tie-line compositions of ATPS composed by citrate salt, namely Na_2HCitrate [277]. Furthermore, Ketabi *et al.* used extended UNIQUAC and UNIFAC to model the tie-lines in a system composed by PEG 3000 and K_3Citrate [278]. Zafarani-Moattar *et al.* [265] applied NRTL for modeling tie-line data of ATPS composed of PEG 6000 and Na_2Succinate or NaFormate.

Although local composition models have presented potential in the modeling of LLE, they were not lacking the limitations, e.g. applicability to more complex systems. Therefore, the addition of a new component to ATPS required adopting a separate modeling procedure if these models were considered. The equations of the local composition model demand a novel derivation to represent data of more complex systems. Thus, equations of state are very promising in predicting the phase separation in ATPS composed of four (or even more) components, namely ePC-SAFT. Reschke *et al.* [279, 280] developed the heterosegmented approach for PEG-based ATPS, as well as a multispecies approach for organic electrolytes. The approach was very successful for modeling different PEG – organic salt ATPS, but it required a remarkably greater number of parameters. Since accounting for many more salt species as well as for different PEG segments leads to a huge computational effort, there is still a challenge to model ATPS composed by PEG and organic salts with a more accessible and less demanding approach.

III. Partitioning in biodegradable PEG – organic salt ATPS (T=298.15±2 K and p=1 bar)

Understanding the behavior of different organic molecules in aqueous solutions is of importance for process design with special attention on separation processes. Separating a compound of interest among the two aqueous phases has been also considered in the literature as an appropriate approach to evaluate interactions in water systems [43, 47].

To study the applicability of ATPS, as well as to unravel the phenomena that rule the partitioning and different interactions, a high experimental input is required.

The state of knowledge of partitioning in biodegradable PEG – organic salt ATPS is presented in the following. Firstly, the experimental data published in literature for the partitioning of different solutes in PEG – organic salt ATPS is discussed. Then, the availability of models that were used in former studies for correlating the partition coefficients of different solutes in ATPS is addressed.

Experimental data on partitioning in PEG – organic salt ATPS

Table 1.3 presents an overview of the partitioning data that are available in literature for different solutes in PEG – organic salt ATPS. It proves the high applicability of these systems in separating different organic compounds. In general, data measured for solutes included in table 1.3 have shown that these media can be very appropriate also in terms of separation efficiency. The partitioning in PEG – biodegradable salt ATPS can be still optimized by the change of several factors. The works published in literature evaluated the influence of PEG´s molar mass, pH, ATPS composition (tie-line length, TLL), temperature, and the presence of displacement agents (e.g. NaCl) [281, 282]. Given the data presented in table 1.3 there are already few studies in literature on the practical application of PEG – organic salt ATPS, however, there is still not enough data to unravel all phenomena which rule the partitioning in ATPS.

Table 1.3. Experimental partitioning of different solutes in PEG – organic salt ATPS at T=298.15±2 K and p=1 bar.

ATPS	*Solute*	*reference*
PEG – Citrate	immunoglobulin G	[283]
	bovine trypsin	[282]
	α-chymotrypsin	[282]
	α-amylase	[284]
	phytase	[285]
	bovine lactoferrin	[286]
	cephalexin	[254]

	phenolic compounds (eucaliptus)	[287]
	concanavalin A	[288]
	lactate dehydrogenase	[289]
	bovine serum albumin	[290]
	α-lactalbumin	[100]
	cefazolin	[106]
	glycomacropeptide	[281]
PEG – Tartrate	cephalexin	[291]
	cefazolin	[106]
PEG - Succinate	bovine serum albumin	[98]
	catalase	[98]
	β-lactoglobulin	[98]
	α-amylase	[98]
	lysozyme	[98]
	pepsin	[98]
	urease	[98]
	trypsin	[98]
PEG-Oxalate	lipase	[292]

Modeling of partitioning in PEG – organic salt ATPS

Measuring the partitioning of different solutes in PEG – organic salt at different moderating conditions is usually time- and cost-intensive. Thermodynamic models that can describe the interactions in aqueous systems could reduce the number of experiments needed to determine the partitioning. Thus, in literature, at least several models have been proposed to correlate and describe the partitioning in PEG – organic salt ATPS.

Perez *et al.* [98] have proposed an extended Pitzer model to describe the LLE and model partition coefficients of different proteins: bovine serum albumin, catalase, β-lactoglobulin, α-amylase, lysozyme, pepsin, urease, and trypsin. The partitioning was

modeled for ATPS composed by PEG and biodegradable salt, namely Na_3Citrate, Na_2Succinate, and Na_2Tartrate at T=295.15 K. This is slightly different temperature value than chosen in the present work, T=298.15 K. Edrisi et al. carried out thermodynamic modeling with extended NRTL and modified UNIQUAC models to correlate cephalexin partitioning data obtained in ATPS formed by PEG and Na_2Tartrate [291] at T=298.15 K.

This scarcity of works available in literature focusing on modeling the partitioning in PEG – organic salt ATPS is related to the very high complexity of these systems. One of the challenges is the fact that organic salts can dissociate forming different species at a given pH. Thus, to the best of my knowledge, any of the predictive thermodynamic models has not been totally successful yet in predicting the partitioning of ionizable components that can also partially dissociate leading to the species formation, e.g. DNP-AA or vitamins, in these systems.

1.2. Aim of this Work and Approach

1.2.1. Aim of this Work

The aim of this work is to contribute to a better understanding of the behavior of different biomolecules, DNP-AA (DNP-glycine, DNP-alanine, DNP-valine, DNP-leucine) and water-soluble vitamins (VC – ascorbic acid, VB2 – riboflavin, $VB3^{acid}$ – nicotinic acid, $VB3^{amide}$ – nicotinamide, VB9 - folic acid, VB12 – cyanocobalamin) in their aqueous solutions. This goal could be achieved through experimental measurements and thermodynamic modeling contributions. The intention of this work was to lower the lack of understanding of partitioning in ATPS, so to break the biggest limitation that disable the implementation of ATPS at industrial scale. The consequence of better understanding DNP-AA or vitamin behavior in water and ATPS would be a design of new separation systems and better screening for ATPS applicability. This knowledge would match the needs of food and pharmaceutical industry. The availability of experimental data was scarce in literature, thus the measurements carried out in this study were considered as an essential background to improve the understanding of aqueous solutions. For all the measurements the value of the standard atmospheric pressure was considered. The pressure has not been measured, but as the work concerns liquid phases, it does not have any relevance or cause any changes to the properties from this work. Prior to the predictions, ePC-SAFT parameters had to be estimated using liquid densities (T = 298.15

K – 318.15 K, p = 1 bar) and freezing-point depressions measured in this work. Also, the modeling and predictions approaches applied to ePC-SAFT were established in this work.

In principal, to improve the understanding of DNP-AA or water-soluble vitamins behavior in aqueous solutions both the experiments and the ePC-SAFT predictions were carried out at T = 298.15 K and p = 1 bar, to obtain the following:

a) Solubility of DNP-AA and water-soluble vitamins in water, at different pH, and in the presence of additives (covitamins).

This study has been carried out to find an appropriate method to enhance the solubility of poorly soluble components such as DNP-AA or some of water-soluble vitamins (VB2, VB9, VB12). It was a very important task of this work since low-solubility often limits the applicability (DNP-AA, vitamins) and bioavailability (vitamins). A special attention was given to pH effect. It also involved studying the hydrotropic solubilization. All data have been determined experimentally and predicted with ePC-SAFT. In general, the solubility of DNP-AA and water-soluble vitamins in pure water, at different pH and in the presence of additives were evaluated at T=298.15 K, p=1 bar. However, to present the influence of temperature on solubility, the two additional aqueous solubility data points for each DNP-AA were measured in this work: at T=308.15±0.1 K, p=1 bar and T=318.15±0.1 K, p=1 bar (only in pure water, without additives). The temperature influence was shown also for $VB3^{acid}$ at T = 283.59 K – 332.01 K and for and for VC at T = 293 K – 323 K since these data were found in literature [149, 150].

b) Biphasic diagrams of PEG (M_{PEG} = 4000 – 8000 g·mol^{-1}) – organic salt ($Na_3Citrate$, $K_3Citrate$, $Na_2Tartrate$, KNaTartrate) ATPS (T = 298.15 K, p = 1 bar).

This objective relied on defining if ATPS composed of PEG and organic salt are efficient media for the separation and evaluating how to optimize phase separation efficiency. The latter allowed to find whether the range of PEG molar mass considered in this work influences the phase separation in a significant way. At this point, the work was centered on identifying a way to compensate for the disadvantage in handling more viscous PEG of M_{PEG} = 8000 g·mol^{-1} with advantages for the separation. Also, the salt influence was studied to understand the dependence on the phase behavior resulting from selecting salts of different cations (Na^+, K^+) and anions ($Citrate^{3-}$, $Tartrate^{2-}$). To better understand

the non-ideality that can be caused by different interactions, ePC-SAFT predictions were performed.

c) Partition coefficients of DNP-AA and water-soluble vitamins in ATPS (T = 298.15 K, p = 1 bar).

Improving the understanding of the partitioning in ATPS could be done only if numerous experiments on ATPS were provided. Such measurements had to be carried out in this work. Partition coefficients allowed estimating the affinity of a solute to the top or bottom phase of ATPS. This objective relied on evaluating the influence of a solute and phase forming ATPS components on partitioning. Non-ideality determined with ePC-SAFT was helpful in finding explanations for a step forward in understanding the phenomena which rule the partitioning.

1.2.2. Approach

The approach was based on performing experiments and carrying out thermodynamic predictions with ePC-SAFT to achieve the objectives listed in section 1.2.1 and to better understand the behavior of different organic molecules: DNP-AA (figure 1.1) and water-soluble vitamins (figure 1.2) in aqueous solutions and in ATPS containing different phase forming compounds (figure 1.3).

Different physicochemical properties of water solutions were measured in this work: aqueous solubility, density, osmotic coefficients, phase separation, and solute partitioning in ATPS. The experimental procedures used for the measurements were built-on the methods available from the literature [97, 153, 258, 293-295]. To understand the influence of different factors on the measured properties, some of the experiments were performed under different conditions, i.e., the pH, temperature, or the presence of additives. For example, the aqueous solubility of DNP-AA and water-soluble vitamins was evaluated in pure water, upon addition of pH-adjusting agents, or covitamins. Covitamins chosen in this work (VB3 and VC) were considered as hydrotropes in previous works in literature [153, 176, 177].

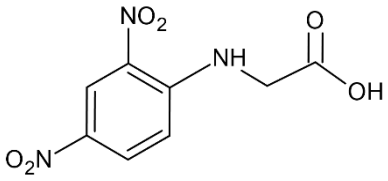

DNP-glycine

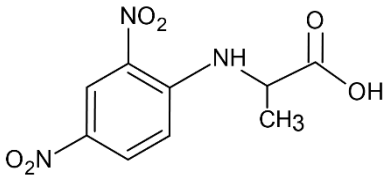

DNP-alanine

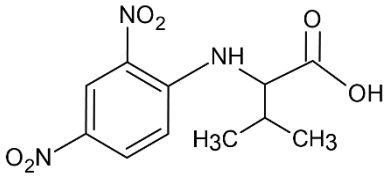

DNP-valine

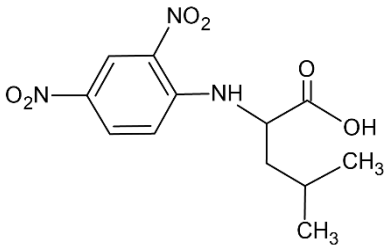

DNP-leucine

Figure 1.1. N-(2,4-Dinitrophenyl) amino acids (DNP-AA) considered in this work; DNP-glycine: N-(2,4-Dinitrophenyl)glycine, DNP-alanine: N-(2,4-Dinitrophenyl)-L-alanine, DNP-valine: N-(2,4-Dinitrophenyl)-L-valine, DNP-leucine: N-(2,4-Dinitrophenyl)-L-leucine.

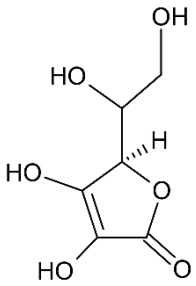

VC

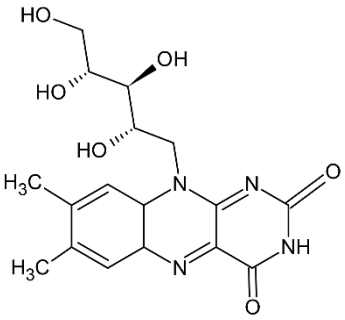

VB2

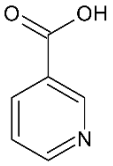

VB3^{acid}

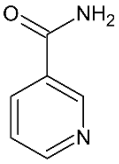

VB3^{amide}

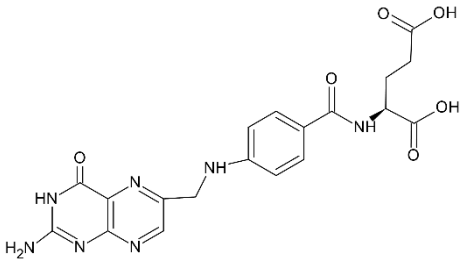

VB9

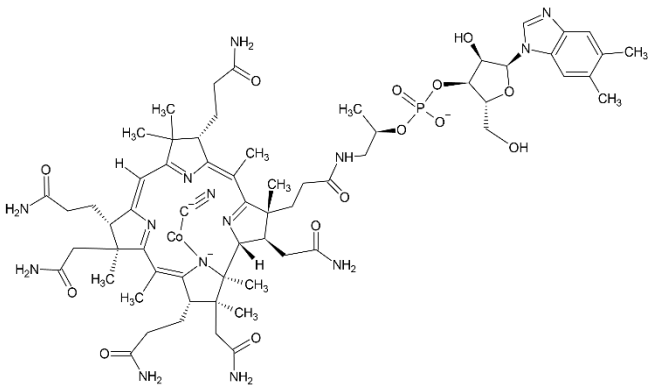

VB12

Figure 1.2. Water-soluble vitamins considered in this work; VC: L(+)-ascorbic acid, VB2: riboflavin, VB3^{acid}: nicotinic acid, VB3^{amide}: nicotinamide, VB9: folic acid, VB12: cyanocobalamin.

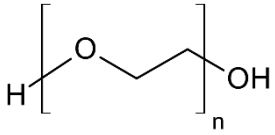

PEG

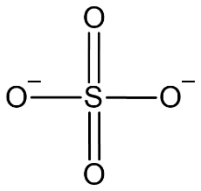

$Sulfate^{2-}$

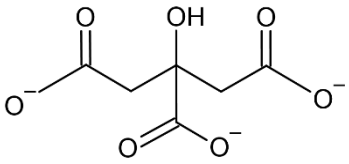

$Citrate^{3-}$

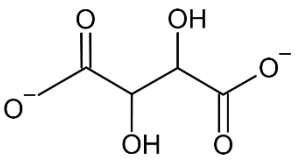

$Tartrate^{2-}$

Figure 1.3. ATPS phase formers considered in this work: polyethylene glycol (PEG) and salt anions. The salts under study containing presented in this figure anions and cations Na^+, Mg^{2+} or K^+ were Na_2Sulfate, MgSulfate, Na_3Citrate, K_3Citrate, Na_2Tartrate, KNaTartrate.

Once the aqueous solubility of DNP-AA and water-soluble vitamins, as well as basic physicochemical properties of these molecules in their aqueous solutions were known, the focus of the work was dedicated to the partitioning of these molecules in ATPS, at T=298.15 K and p=1 bar. However, prior to this, efficient biodegradable PEG – salt ATPS were selected. This involved studying the applicability of different organic salts to form the two phases with polyethylene glycol (PEG) of different molar mass and was done to evaluate the efficiency in phase separation using biphasic diagrams. Tie-lines, i.e. equilibrium compositions and binodals were found experimentally. Biphasic diagrams were used as a pre-selective tool to determine which salts can form ATPS with large two-phase regions. Therefore, ATPS selected in this work were formed by PEG (M_{PEG} = 4000 – 8000 g·mol^{-1}) and organic salts (Na_3Citrate, K_3Citrate, Na_2Tartrate, KNaTartrate). The systems were characterized using ePC-SAFT pure-component and binary interaction k_{ij} parameters. Only after these procedures, the partitioning in designed ATPS of solutes: DNP-AA (DNP-glycine, DNP-alanine, DNP-valine, DNP-leucine) and water-soluble vitamins (VB2 – riboflavin, $VB3^{acid}$ – nicotinic acid, $VB3^{amide}$ – nicotinamide, VB9 - folic acid, VB12 – cyanocobalamine) was carried out. The partition coefficients were determined for different ATPS compositions (tie-line length – TLL). The results were evaluated based on the solute, as well as ATPS phase formers: salt and PEG influence.

Since obtaining reliable data relied on carrying anumber of time-intensive and laborious experiments, the experimental framework presented in this document was further used to validate the predictions obtained with thermodynamic electrolyte PC-SAFT model (ePC-SAFT based on perturbed-chain statistical associating fluid theory). The intention of using ePC-SAFT was to predict aqueous solubility, phase equilibria of ATPS, and partitioning of biomolecules in ATPS. ePC-SAFT pure-component and binary interaction k_{ij} parameters were established through the two novel methods designed in this work specifically for modeling DNP-AA and vitamins, molecular method (MM, for DNP-AA, vitamins) and joint-parameter method (J-PM, for DNP-AA). Both MM and J-PM were designed based on the former approaches found in literature [81, 296]. Caloric properties needed for aqueous solubility predictions were either taken from literature or estimated in this work.

1.3. Outline of The Thesis

This document was elaborated to present the new knowledge on solubility and partitioning of biomolecules acquired based on experimental results and thermodynamic modeling. Both methods were applied to better understand the phenomena that rule the behavior of biomolecules in aqueous solutions, thus their solubility in water, and partitioning in ATPS. Besides that, one of the major intentions of writing this document was to highlight the importance of designing and optimizing environmentally-friendly and cost-efficient separation systems that could be appropriate for the partitioning of biomolecules (DNP-AA and water-soluble vitamins).

The thesis begins by presenting the motivation and actual state-of-the knowledge under the framework of this study. The introduction highlights the objectives of this work, as well as the approach that had to be fulfilled to achieve the aim of this work. These contents are involved in Chapter 1. Chapter 2 was introduced to provide a background on the major topics, namely: thermodynamic fundamentals, phase equilibria, dissociation constants, and thermodynamic modeling (ePC-SAFT). Although it required presenting some basic knowledge, the descriptions were targeted to solve the problems encountered specifically for the compounds under study.

This work required choosing experimental and modeling methods. Chapter 3 focus on presenting the materials used in the experiments, as well as the procedures that were

followed to obtain experimental data. The modeling methods designed in this work to especially model the solutions containing DNP-AA and water-soluble vitamins are given in Chapter 4, together with all ePC-SAFT parameters and caloric properties, estimated in this work or obtained from literature.

The next chapters 5-10 present the results and discussion on the aqueous solubility of biomolecules, experimental phase equilibria of ATPS, and partitioning of biomolecules in ATPS. They are divided into two blocks: experimental (chapters 5, 6, 7) and predictions (chapters 8, 9, 10). Therefore, experimental chapter 5 corresponds to prediction chapter 8, and both cover the discussion on the results of aqueous solubility. Experimental chapter 6 corresponds to prediction chapter 9 and involves a discussion on the results obtained on phase equilibria of ATPS. Analogous to that, experimental chapter 7 relates to chapter 10, and covers the topic of the DNP-AA and vitamin partitioning in ATPS. Each of the chapters 5-10 ends up with a conclusion that consist of the most important findings based on the results obtained experimentally (chapters 5, 6, 7) or with ePC-SAFT (chapters 8, 9, 10).

Chapter 11 summarizes the contribution to the research that has been added through carrying out the studies in this work, as well as it shows further insights that should be considered.

2. Theoretical Background

Understanding the behavior of DNP-AA and water-soluble vitamins in aqueous systems requires insight into fundamental knowledge of equilibria. To account for non-ideality while calculating the thermodynamic properties, the models based on Equation-of-State (EOS) are relevant. Thus, this chapter involves an insight into the thermodynamic theory which is behind these approaches. This is essential knowledge for phase equilibria calculations with EOS. Further, in the present chapter there is a basic description that covers the dissociation equilibria theory. In the end, the concept of SAFT-based EOS (ePC-SAFT) to account for non-ideality is addressed.

2.1. Thermodynamic Fundamentals

This subchapter presents thermodynamic fundamentals for the modeling using EOS -based models. EOS are based on the calculation of Helmholtz energy A. In practice, once the residual Helmholtz energy A^{res} is known, then all thermodynamic properties (like pressure, density, activity coefficients) are reachable. A^{res} is defined with equation (2.1). According to equation (2.1) fundamental variables for A^{res} are temperature T and volume V. A^{id} stands for the ideal contribution to the Helmholtz energy.

$$A^{res}(T,V) = A(T,V) - A^{id}(T,V) \tag{2.1}$$

2.1.1. Chemical Potential and Fugacity Coefficient

The chemical potential μ_i of component *i* in a non-ideal fluid mixture is described according to equation (2.2). In this expression μ_{0i} is the chemical potential of the pure component, R is the universal gas constant, T and p stand for the temperature and pressure, respectively, and a_i corresponds to the activity of component *i*. The a_i in equation (2.2) can be replaced by relating it with the mole fraction (x_i) and the activity coefficient (γ_i) of component *i*. The definition of the activity coefficient that describes the non-ideality of a system is given in detail in the next section (2.1.2).

$$\mu_i(T,p,x_i) = \mu_{0i}(T,p) + RTlna_i = \mu_{0i}(T,p) + RTlnx_i + RTln\gamma_i \tag{2.2}$$

Given the definition of the activity coefficient, equation (2.2) can be transformed into expression (2.3) by substituting γ_i with the ratio of the fugacity coefficient φ_i at particular (T,p,x_i) conditions and the fugacity coefficient φ_{0i} of the pure component φ_{0i} at the same temperature and pressure (T,p).

$$\mu_i(T,p,x_i) = \mu_{0i}(T,p) + RTlnx_i + RT\ln\left(\frac{\varphi_i}{\varphi_{oi}}\right) \tag{2.3}$$

According to equation (2.1) A^{res} is dependent on variables (T,V) instead of (T,p) so further equations are formulated using this condition and follow the expression (2.4).

$$\mu_i(T,p,x_i) = \mu_i(T,V,x_i) \tag{2.4}$$

Bilateral subtraction of an ideal contribution to the chemical potential $\mu_i^{id}(T,V,x_i)$ from equation (2.3) leads to expression(2.5).

$$\mu_i(T,V,x_i) - \mu_i^{id}(T,V,x_i) = \mu_{0i}(T,p) - \mu_i^{id}(T,V,x_i) + RT\ln\left(\frac{x_i\varphi_i}{\varphi_{0i}}\right) \tag{2.5}$$

Introducing equations (2.6) and (2.7):

$$\mu_{0i}(T,p) = \mu_i^{id}(T,p) + RT\ln\varphi_{0i} \tag{2.6}$$

$$\mu_i^{id}(T,V,x_i) = \mu_i^{id}(T,V) + RT\ln x_i \tag{2.7}$$

into equation (2.5) allows the calculation of the residual part of the chemical potential $\mu_i^{res}(T,V,x_i)$ as shown in expression (2.8).

$$\mu_i^{res}(T,V,x_i) = \left(\mu_i^{id}(T,p) - \mu_i^{id}(T,V)\right) + RT\ln\varphi_i \tag{2.8}$$

Subsequently, the relation with compressibility factor Z presented in equation (2.9) can be introduced[75].

$$\mu_i^{id}(T,p) - \mu_i^{id}(T,V) = RT\ln Z \tag{2.9}$$

Implementing expression (2.9) and further conversions lead to equation (2.10) which allows obtaining fugacity coefficient φ_i.

$$\ln\varphi_i = \frac{\mu_i^{res}(T,V,x_i)}{RT} - \ln Z \tag{2.10}$$

Further transformations lead to the expression (2.11) for the residual part of the chemical potential $\mu_i^{res}(T,V,x_i)$ [297].

$$\mu_i^{res}(T,V,x_i) = \frac{A^{res}}{nRT} + \left(\frac{\partial\left(\frac{A^{res}}{nRT}\right)}{\partial x_i}\right)_{T,V,x_{k\neq i}} - \sum_{=1}^{N}\left(x_l \cdot \left(\frac{\partial\left(\frac{A^{res}}{nRT}\right)}{\partial x_l}\right)_{T,V,x_{k\neq l}}\right) + Z - 1 \tag{2.11}$$

In the present study, the residual Helmholtz energy with respect to the mole number n (molar residual Helmholtz energy, $a^{res}=\frac{A^{res}}{n}$) and the compressibility factor (Z) are calculated with ePC-SAFT[74].

2.1.2. Activity Coefficient and Osmotic Coefficient

The activity coefficient γ_i of a component *i* involved in equation (2.2) describes the non-ideality in solutions. According to equation (2.12) γ_i is expressed as a ratio of the fugacity coefficient of component *i* at the actual conditions (T, p, x_i) to the fugacity coefficient of the pure component at the reference state (T, p)[298].

$$\gamma_i = \frac{\varphi_i(T, p, x_i)}{\varphi_{0i}(T, p)} \tag{2.12}$$

If infinitesimal amount of component *i* is dissolved in aqueous solution, then equation (2.13) that allows calculating so-called "rational activity coefficient" is more relevant [80, 299].

$$\gamma_i^* = \frac{\varphi_i(T, p, x_i)}{\varphi_i^\infty(T, p, x_i)} = \frac{\gamma_i}{\gamma_i^\infty} \tag{2.13}$$

The fugacity coefficient at infinite dilution φ_i^∞ and activity coefficient at infinite dilution γ_i^∞ can be defined according to equations (2.14) and (2.15), respectively [80]. However, the condition is that the ratio of the mole fraction $\frac{x_l}{x_k}$ of each pair of components l and k in a mixture (l, k ≠ i) remains constant when $x_i \to 0$.

$$\varphi_i^\infty = \lim_{x_i \to 0} \varphi_i \tag{2.14}$$

$$\gamma_i^\infty = \lim_{x_i \to 0} \gamma_i \tag{2.15}$$

To describe the non-ideality of aqueous solution the osmotic coefficient ϕ is also appropriate. The ϕ can be calculated using equation (2.16) in which a_W and x_W denote the solvent (water) activity and solvent (water) mole fraction, accordingly[300].

$$\phi = \frac{ln(a_W)}{ln(x_W)} \tag{2.16}$$

The ϕ can be calculated with the alternative simplified equation (2.17), in which $M_{0,W}$ stands for the molecular weight of water ($g \cdot mol^{-1}$), m_i is the concentration of component *i* expressed in molality ($mol \cdot kg^{-1}$), and ν_i denotes the stoichiometric coefficient. This

expression is widely applied in studies published in literature [80]. This equation has been used in this work to calculate ϕ.

$$\phi = -\frac{1000 \cdot ln(a_W)}{M_{0,W} \sum_{i \neq W} \nu_i m_i} \tag{2.17}$$

2.2. Phase Equilibria

In this subchapter, the theoretical background for modeling of phase equilibria is provided. These are solid-liquid equilibrium (SLE) (section 2.2.1) and liquid-liquid equilibrium (LLE) in ATPS together with the relations required to characterize the solute partitioning equilibria (section 2.2.2). The conditions and thermodynamic equations included in the following were used in the present work for parameter estimation of thermodynamic model. Since the methods of calculating LLE can be accessed from the literature and have been broadly applied already [301-303], in section 2.2.2 more attention is paid to the expressions derived in this work specifically for modeling of solute partitioning. In this work, the modeling was done using equation of state (EOS) predictive model, namely the Electrolyte Perturbed-Chain Statistical Associating Fluid Theory (ePC-SAFT). However, as mentioned in section 1.1.2, other models might also be used for calculating thermodynamic properties of electrolyte solutions, such as EOS [304-307] or G^E-models (excess Gibbs energy models) [69, 218, 308-315].

At thermodynamic equilibrium, the pressure (p), temperature (T) and chemical potential of component i (μ_i) in each coexisting phase (A, B, ..., π) of a system must follow the conditions presented with equations (2.18) – (2.20).

$$T^A = T^B = \cdots = T^\pi \tag{2.18}$$

$$p^A = p^B = \cdots = p^\pi \tag{2.19}$$

$$\mu_i^A = \mu_i^B = \cdots = \mu_i^\pi \tag{2.20}$$

From the presented above conditions (2.18) - (2.20), isofugactity criterion can be derived (2.21). Expression (2.21) where f_i corresponds to fugacity of component i is the starting point for all phase equilibrium calculations performed in this work.

$$f_i^A = f_i^B = \cdots = f_i^\pi \tag{2.21}$$

2.2.1. Solid-Liquid Equilibrium

In this work, the calculations of equilibrium concerning heterogenous system containing solute *i* (DNP-AA or vitamin) in both solid phase (S) and in the liquid phase (L) were performed based on the isofugacity criterion ($f_i^S = f_i^L$) as shown previously in equation (2.21). The fugacity f_i^S can be calculated with equation (2.22) and analogically to that f_i^L is then obtained with equation (2.23).

$$f_i^S = x_i^S \gamma_i^S f_{0i}^S \tag{2.22}$$

$$f_i^L = x_i^L \gamma_i^L f_{0i}^L \tag{2.23}$$

Since in this work it was assumed that in all SLE the solid crystallizes in pure form and there are no other crystals formed, the fugacity f_{0i}^S of the pure component is the same as the fugacity f_i^S of component *i.* Thus, $x_i^S \gamma_i^S$ from equation (2.22) equals 1. By means of isofugacity criterion and the above assumption, x_i^L can be calculated according to equation (2.24).

$$x_i^L = \frac{1}{\gamma_i^L} \frac{f_{0i}^S}{f_{0i}^L} \tag{2.24}$$

The γ_i^L is accessible with ePC-SAFT and its calculation is based on theory provided in section 2.1.2. ePC-SAFT parameters required for these calculations are estimated in this work. However, equation (2.24) besides γ_i^L still requires knowledge of the quotient of fugacities of pure component *i* (DNP-AA or vitamin) in both phases. If knowing the melting properties of such component, namely melting temperature ($T_{m,i}$), melting enthalpy ($\Delta_{cr}^L H_{m,i}^0$), and the difference between liquid and solid heat capacity ($\Delta_{cr}^L Cp_{m,i}^0$), then $x_i^{L,pred}$ could be predicted with equation (2.25) postulated by Prausnitz [316]. The caloric properties required for these calculations were, in this work, taken from the literature or estimated.

$$x_i^{L,pred} = \frac{1}{\gamma_i^L} exp\left[-\frac{\Delta_{cr}^L H_{m,i}^0}{RT} \left(1 - \frac{T}{T_{m,i}}\right) - \frac{\Delta_{cr}^L Cp_{m,i}^0}{R} \left(\frac{T_{m,i}}{T} - 1 - \ln\left(\frac{T_{m,i}}{T}\right)\right)\right] \tag{2.25}$$

The solubility expressed by $x_i^{L,pred}$ can be converted to molality $m_i^{L,pred}$ using equation (2.26).

$$m_i^{L,pred} = \frac{x_i^{L,pred} \cdot 1000}{\left(1 - x_i^{L,pred}\right) \cdot M_{0,W}} \tag{2.26}$$

The maximum solubility of a component in the pH-equilibrium solubility profile is limited by the solubility product K_{sp} [317]. When a solid being low-soluble ionic compound is in equilibrium with its ions in saturated aqueous solution, the thermodynamic solubility product K_{sp} is described by activity of present species *i* (ion A and counter ion B) according to equation (2.27) [318]. In this expression the activity coefficients γ_A and γ_B are varying with ionic strength just in a way that $K_{sp,th}$ is numerically constant and stays independent of ionic strength.

$$K_{sp,th} = \prod_i a_i^{v_i} = (m_A\gamma_A)^{v_A}(m_B\gamma_B)^{v_B} \tag{2.27}$$

2.2.2. Liquid-Liquid Equilibrium and Partition Coefficient

To fit the binary PEG/salt interaction parameters (k_{ij}) of ePC-SAFT EOS, LLE calculations are performed. Any LLE with *n* components is calculated through the isoactivity expression originated from isofugacity criterion. In equation (2.28) γ_i^I and γ_i^{II} represent the activity coefficients that can be obtained with ePC-SAFT and x_i^I and x_i^{II} are the equilibrium mole fractions of a component *i* in the two liquid phases named I and II, respectively. To calculate the activity coefficients of components in ATPS, ePC-SAFT requires the parameters of all compounds present in solution.

$$x_i^I\gamma_i^I = x_i^{II}\gamma_i^{II} \tag{2.28}$$

As DNP-AA and water-soluble vitamins are usually present at very small concentrations, the infinite dilution activity coefficient γ_i^∞ can be very relevant [319]. The γ_i^∞ is defined with equation (2.15) in section 2.1.2. Depending on the pH of ATPS, solutes DNP-AA or vitamins, can be present as different species in solution. The partition coefficient at infinite dilution $K_j^{pred,\infty}$ of species *j* is defined as a concentration ratio (in mole fraction and x_j^I and x_j^{II}) of species *j* in the two phases I (PEG phase) and II (salt

phase), respectively. This is presented in equation (2.29) in which $\gamma_i^{\infty,I}$ and $\gamma_i^{\infty,II}$ are the activity coefficients at infinite dilution in the two phases. In this thesis, superscript ∞ applied for $K_j^{pred,\infty}$ implicitly refers to the mole fraction-based partition coefficient obtained with ePC-SAFT (instead of using $K_j^{pred,x}$).

$$K_j^{pred,\infty} = \frac{\gamma_j^{\infty,II}}{\gamma_j^{\infty,I}} = \frac{x_j^I}{x_j^{II}} \tag{2.29}$$

The charge q of vitamin species is explicitly considered in ePC-SAFT modeling. The ePC-SAFT pure-component parameters and k_{ij} parameters for different species are estimated. The experimentally measured partition coefficient of component *i* (DNP-AA or vitamin) is the total partition coefficient $K_i^{pred,\infty}$ that is summed over all the DNP-AA or vitamin species present in ATPS. This value may differ from the ePC-SAFT predicted $K_j^{pred,\infty}$ if $pH^I \neq pH^{II}$. Conversion between the two values requires the species distributions according to equation (2.30). Due to a difference in pH between the ATPS phases, the species distributions of each solute species were calculated separately for phase *I* and *II*. The theoretical basis for the species calculation is given in the following subchapter of this thesis (2.3).

$$K_i^{pred,\infty} = K_j^{pred,\infty} \cdot \frac{\alpha_j^{II}}{\alpha_j^I} \tag{2.30}$$

2.3. Dissociation Equilibrium

The behavior of ionizable organic components such as DNP-AA and vitamins in aqueous solutions varies with the pH. To estimate the influence of pH on the solute property such as solubility, some mathematical approaches have been already proposed, e.g. the Henderson-Hasselbalch (*H-H*) equation. The principal assumptions behind the *H-H* equation are based on the idealized dissociation equilibria. The idealized expressions describe the dissociation and allow calculating the solubility of poorly soluble DNP-AA and water-soluble vitamins in aqueous solutions. However, for many compounds, deviations between the so-calculated solubilities and experimental data are frequently observed [320]. In this work, the solubility calculations with an idealized *H-H*-based approach were used just for the reliability of experimental data evaluation, as well as to

present a general overview of pH-solubility profiles of different DNP-AA and vitamins. The EOS-based approach that accounts for non-ideality was introduced to accurately predict the behavior of these solutes in aqueous solutions. The latter approach was based on expressions presented in this chapter that involve an activity coefficient.

In section 2.3.1 of the present chapter, possible dissociation mechanisms are included and further followed by the expressions which allow idealized dissociation-based solubility calculations [6-8]. At the end (section 2.3.2), the pH dependence on species fraction of acidic and amphoteric ionizable compound is presented. Similar mass balance equations for calculating the non-idealized species distribution of weak acid (i.e. silicic acid) are provided elsewhere [321, 322].

2.3.1. Equilibrium Expressions

DNP-AA and water-soluble vitamins considered in the present work are acidic (DNP-AA, VC) or amphoteric (VB2, $VB3^{acid}$, VB9, VB12). To estimate different properties, e.g. solubility, reliable dissociation mechanisms must be provided. Only then, the solubility expressions can be derived. Respective transformation of the *H-H* expression allows solubility estimation if pH and dissociation constants (K_a or pK_a) are known. The *H-H*-based solubility equations presented in the following involve acid dissociation constant K_a (or pK_a) which is a quantitative measure of acid strength in a solution and can be accessed experimentally. The pK_a values considered in this work are included in table 2.1[6, 8].

Table 2.1. Dissociation constants (pK_a=-$\log_{10}K_a$), T=298.15 K [6, 8]. Data obtained from the literature [130, 161, 165-171] or estimated [8]. Most data concerning DNP-AA and vitamins are provided in the literature [130, 161, 165-171] without precise description of the conditions for pK_a determination, thus it is assumed that the values presented in the table concern the ideal conditions and apply to the infinite dilution (ionic strength, $I \to 0$).

Compound	pK_{a_1}	pK_{a_2}	pK_{a_3}	pK_{a_4}	*reference*
VC	4.17	11.57			[165]
VB2	1.7	6.1	10.2		[167-170, 173]
VB3^{acid}	2.07	4.81			[166]
VB9	2.38	3.34	4.7	8.1	[161, 171]
VB12	1.82	13.99			[173]
DNP-glycine	2.8				[130]
DNP-alanine	3.5				[130]
DNP-valine	2.9				[8]
DNP-leucine	2.8				[8]

A general description of pK_a determination and the H-H-based mathematical approach to define pH-solubility profiles is widely available in the literature [60, 323-325]. Thus, this section contains equations derived in the present work that solely concern DNP-AA and vitamins considered in the current thesis. The values from table 2.1 that for most of compounds were found in the literature are used just for solubility calculations with an idealized approach. However, this section shows solubility equations that include thermodynamic dissociation constant $pK_{a,th}$ ($K_{a,th}$) and allow accounting on system non-ideality. $K_{a,th}$ values are not accessible experimentally, thus they can be estimated in thermodynamic modeling.

Equilibrium in Solutions Containing DNP-AA

A solution of low soluble weak monoprotic acid, such as DNP-AA, can be described with equation (2.31) where H^+ stands for the hydrated hydronium ion (H_3O^+) and A^- is the ionized form of this acid.

$$HA \rightleftharpoons H^+ + A^- \tag{2.31}$$

The dissociation constant $K_{a,th}$ is the quotient of activities a_j of the species j present in aqueous solution as shown in equation (2.32). It considers the non-ideality of a solution and can be expressed using concentrations and activity coefficients γ_j of the species j. The concentrations of species are presented in the brackets, since both molal fraction x_j and molality m_j could apply and x_j can be easily converted to molality m_j using an expression analogous to equation (2.26).

$$K_{a,th} = \frac{[a_{H^+}][a_{A^-}]}{[a_{HA}]} = \frac{[H^+][A^-]}{[HA]} \cdot \frac{\gamma_{H^+}\gamma_{A^-}}{\gamma_{HA}} \tag{2.32}$$

Given the assumption behind the *H-H* equation that the quotient of activity coefficients γ_j of the species j is constant, the K_a for low soluble compound can be expressed solely with species concentrations according to equation (2.33). This is the foundation of idealized *H-H*-based approach [320, 326, 327]. K_a is given in the literature at infinite dilution [303]. According to Lange [328] this approach is appropriate for poorly-soluble components since their concentrations are close to infinite dilution.

$$K_a = \frac{[H^+][A^-]}{[HA]} \tag{2.33}$$

Dissociation constants $K_{a,th}$ and K_a are used in this work as a basis for solubility calculations. At first, the idealized *H-H*-based approach that uses K_a was applied. Then, the thermodynamic modeling with EOS with $K_{a,th}$ was carried out.

Equation (2.34) represents an equilibrium between a solute molecule HA (dissolved in aqueous solution) and its solid (precipitated) form $HA(s)$. Intrinsic solubility expressed in mol·kg^{-1} ($m^L_{0,i}$) of neutral (unionized) weak acid e.g. DNP-AA, is accessed according to equations (2.34) and (2.35)[8]. This unit of concentration was considered in the present work as more convenient for solubility data presentation and was also used in the literature to describe equilibrium expressions of acidic components [329].

$$HA(s) \rightleftharpoons HA \tag{2.34}$$

$$m^L_{0,i} = m_{HA} \tag{2.35}$$

The sum of all the species concentrations present in the saturated solution defines the total solubility of component *i*, m_i^L [mol·kg^{-1}], at given pH, according to equation (2.36).

$$m_i^L = m_{A^-} + m_{HA} \tag{2.36}$$

These expressions can be transformed into idealized equation (2.37) by substituting equations (2.33) and (2.35) to equation (2.36).

$$m_i^L = m_{0,i}^L \left(\frac{K_a}{m_{H^+} + 1}\right) \tag{2.37}$$

Further conversions that use $K_a = 10^{-pK_a}$ and assumption m_{H^+}=10^{-pH} (activity coefficient γ_{H^+} is neglected in ideal *H-H* approach)[330] lead to idealized *H-H*-based solubility equations (2.38) or (2.39) which contain already pH and pK_a.

$$m_i^L = m_{0,i}^L(10^{-pK_a+\mathrm{pH}} + 1) \tag{2.38}$$

$$\log m_i^L = \log m_{0,i}^L + \log\ (10^{-pK_a+\mathrm{pH}} + 1) \tag{2.39}$$

To account for non-ideality of a system, the solubility equations (2.40) and (2.41) can be used. These expressions contain activity coefficients γ_j that are accessible with a thermodynamic model.

$$m_i^L = m_{0,i}^L \left(\frac{\gamma_{HA}}{\gamma_{A^-}} \cdot 10^{-pK_{a,th}+\mathrm{pH}} + 1\right) \tag{2.40}$$

$$\log m_i^L = \log m_{0,i}^L + \log\ (\frac{\gamma_{HA}}{\gamma_{A^-}} \cdot 10^{-pK_{a,th}+\mathrm{pH}} + 1) \tag{2.41}$$

Equilibrium in Solutions Containing Diprotic Acidic Vitamins

A solution of a diprotic weak acid such as VC can be described with equilibrium equations (2.42) and (2.45) and corresponding to them expressions (2.43) - (2.44) and (2.46) - (2.47) for dissociation constants ($K_{a,th}$ and K_a), respectively[6]. Like in the previous example, the concentrations are presented in brackets, since both mole fraction x_j and molality m_j of the species *j* could be applied. According to equation (2.42) deprotonation of VC leads to formation of ascorbate ion HA^-. In alkaline aqueous solutions

further deprotonation to the ascorbate di-anion A^{2-} is observed [331]. Expressions (2.44) and (2.47) are only valid if the idealized approach is considered.

$$H_2A \rightleftharpoons H^+ + HA^- \tag{2.42}$$

$$K_{a_1,th} = \frac{[H^+][HA^-]}{[H_2A]} \cdot \frac{\gamma_{H^+}\gamma_{HA^-}}{\gamma_{H_2A}} \tag{2.43}$$

$$K_{a_1} = \frac{[H^+][HA^-]}{[H_2A]} \tag{2.44}$$

$$HA^- \rightleftharpoons H^+ + A^{2-} \tag{2.45}$$

$$K_{a_2,th} = \frac{[H^+][A^{2-}]}{[HA^-]} \cdot \frac{\gamma_{H^+}\gamma_{A^{2-}}}{\gamma_{HA^-}} \tag{2.46}$$

$$K_{a_2} = \frac{[H^+][A^{2-}]}{[HA^-]} \tag{2.47}$$

Equation (2.48) represents an equilibrium between a solute molecule H_2A (dissolved in aqueous solution) and its solid (precipitated) form $H_2A(s)$. Solubility of the neutral vitamin $m_{0,i}^L$ from equation (2.49) can be expressed in mol·kg^{-1}.

$$H_2A(s) \rightleftharpoons H_2A \tag{2.48}$$

$$m_{0,i}^L = m_{H_2A} \tag{2.49}$$

Similar to the previous example, the sum of all the species concentrations present in the saturated solution defines the total pH-dependent solubility, m_i^L [mol·kg^{-1}], according to equation (2.50).

$$m_i^L = m_{A^{2-}} + m_{HA^-} + m_{H_2A} \tag{2.50}$$

Finally, the substitution of equilibrium expressions (2.42), (2.45) and (2.47) into equation (2.48) and appropriate conversions similar to the former example lead to equations (2.51) and (2.52) which allow idealized solubility calculation.

$$m_i^L = m_{0,i}^L\left(10^{-\mathrm{p}K_{a_2}-\mathrm{p}K_{a_1}+2\mathrm{pH}} + 10^{-\mathrm{p}K_{a_1}+\mathrm{pH}} + 1\right) \tag{2.51}$$

$$\log m_i^L = \log m_{0,i}^L + \log\ (10^{-\mathrm{p}K_{a_2}-\mathrm{p}K_{a_1}+2\mathrm{pH}} + 10^{-\mathrm{p}K_{a_1}+\mathrm{pH}} + 1) \quad (2.52)$$

If considering non-ideality, the solubility can be calculated according to equation (2.53) or (2.54).

$$m_i^L = m_{0,i}^L \left[\gamma_{H_2A}\left(\frac{10^{-\mathrm{p}K_{a_2,th}-\mathrm{p}K_{a_1,th}+2\mathrm{pH}}}{\gamma_{A^{2-}}} + \frac{10^{-\mathrm{p}K_{a_1,th}+\mathrm{pH}}}{\gamma_{HA^-}}\right) + 1\right] \quad (2.53)$$

$$\log m_i^L = \log m_{0,i}^L + \log\left[\gamma_{H_2A}\left(\frac{10^{-\mathrm{p}K_{a_2,th}-\mathrm{p}K_{a_1,th}+2\mathrm{pH}}}{\gamma_{A^{2-}}} + \frac{10^{-\mathrm{p}K_{a_1,th}+\mathrm{pH}}}{\gamma_{HA^-}}\right) + 1\right] \quad (2.54)$$

The two examples presented for an acidic compound show steps that must be taken to derive solubility equations. The proposed approaches consider ideality or non-ideality of DNP-AA or water-soluble vitamins in aqueous solutions. Since these expressions at first require reliable dissociation schemes, further content of this chapter focuses more on the determination of such reactions for more complex vitamins. Equations that account for ideality or non-ideality can be derived analogously. The *H-H*-based solubility equations must consider all dissociation constants K_a. The latter approach uses activity coefficient in expressions for dissociation constant $K_{a,th}$. To provide a general overview, the solubility expressions for other water-soluble vitamins are given in the following.

Equilibrium in Solutions Containing Polyprotic Amphoteric Vitamins

As it has been shown in the previous examples, respective conversions allow obtaining the expressions for idealized *H-H*-based and non-idealized approaches for any equilibrium system. The only condition to achieve this is to define reliable equilibrium equations. According to that, the solubility in water of amphoteric VB3$^{\mathrm{acid}}$ can be expressed with equation (2.57) or (2.58), if the equilibrium of vitamin solution follows expressions (2.55) and (2.56) [6].

$$H_2X^+ \rightleftharpoons H^+ + HX \quad (2.55)$$

$$HX \rightleftharpoons H^+ + X^- \quad (2.56)$$

$$\log m_i^L = \log m_{0,i}^L + \log\ (10^{\mathrm{p}K_{a_1}-\mathrm{pH}} + 10^{-\mathrm{p}K_{a_2}+\mathrm{pH}} + 1) \quad (2.57)$$

$$\log m_i^L = \log m_{0,i}^L + \log \left[\gamma_{HX}\left(\frac{10^{\mathrm{p}K_{a_1,th}-\mathrm{pH}}}{\gamma_{H_2X^+}} + \frac{10^{-\mathrm{p}K_{a_{2,th}}+\mathrm{pH}}}{\gamma_{X^-}}\right) + 1\right] \quad (2.58)$$

As stated with equations (2.55) and (2.56), the amphiprotic system of VB3^{acid} contains the three types of species that might be present at equilibrium. Thus, VB3^{acid} can be negatively charged at the carboxylic functional group (at high pH), positively charged at the pyridinyl hydrogen (at low pH), or neutral (pH≈3.4) [135, 147, 332, 333].

The equilibrium equations (2.55) - (2.57) can be valid also for VB12 if considering the existence of just two pK_a values for this vitamin[6]. The molecular structure of VB12 is very complex and it is expected that VB12 undergoes multi-step dissociation. However, the simplified mechanism presented in equations (2.55) and (2.56) is accurate enough for the purpose of this work. Such a statement can be given based on the experimental data presented further in this thesis.

Equations (2.55) - (2.58) are applicable also to VB2 if considering just its two pK_a values [6]. Therefore, equation (2.55) would correspond to deprotonation within the isoalloxazine ring of VB2, while equation (2.56) could relate to deprotonation of its ribityl chain. By means of Chemicalize-Chem Axon online tool [173] and in agreement with the literature [168], one additional pK_a value can be found. The mechanism of VB2 dissociation if three pK_a values are involved is presented in equations (2.59) - (2.61). Consequently, the solubility is then calculated using equation (2.62) or (2.63), if considering idealized or non-ideality-oriented approach, respectively.

$$H_3X^+ \rightleftharpoons H^+ + H_2X \quad (2.59)$$

$$H_2X \rightleftharpoons H^+ + HX^- \quad (2.60)$$

$$HX^- \rightleftharpoons H^+ + X^{2-} \quad (2.61)$$

$$\log m_i^L = \log m_{0,i}^L + \log\left(10^{-\mathrm{p}K_{a_3}-\mathrm{p}K_{a_2}+2\mathrm{pH}} + 10^{-\mathrm{p}K_{a_2}+\mathrm{pH}} + 10^{\mathrm{p}K_{a_1}-\mathrm{pH}} + 1\right) \quad (2.62)$$

$$\log m_i^L = \log m_{0,i}^L + \log \left[\gamma_{H_2X}\left(\frac{10^{-\mathrm{p}K_{a_{3,th}}-\mathrm{p}K_{a_{2,th}}+2\mathrm{pH}}}{\gamma_{X^{2-}}} + \frac{10^{-\mathrm{p}K_{a_{2,th}}+\mathrm{pH}}}{\gamma_{HX^-}} + \right.\right.$$
$$\left.\left. + \frac{10^{\mathrm{p}K_{a_{1,th}}-\mathrm{pH}}}{\gamma_{H_3X^+}}\right) + 1\right] \quad (2.63)$$

The H-H-based solubility equations can be adjusted to any vitamin system, even if this requires accounting for many pK_a values of the vitamin. Equilibrium equations (2.64) - (2.67) present several dissociation steps of triacidic monobasic VB9, corresponding to deprotonation (equations (2.64) and (2.67) within its pteridine ring, and to deprotonation of the two carboxyl groups (equations (2.65) and (2.66) [161, 171]. Depending on the approach applied for calculations, the pH-dependent solubility of VB9 can be then calculated through equation (2.68) or (2.69) [6].

$$H_4X^+ \rightleftharpoons H^+ + H_3X \tag{2.64}$$

$$H_3X \rightleftharpoons H^+ + H_2X^- \tag{2.65}$$

$$H_2X^- \rightleftharpoons H^+ + HX^{2-} \tag{2.66}$$

$$HX^{2-} \rightleftharpoons H^+ + X^{3-} \tag{2.67}$$

$$\log m_i^L = \log m_{0,i}^L + \log\,(10^{-\mathrm{p}K_{a_4}-\mathrm{p}K_{a_3}-\mathrm{p}K_{a_2}+3\mathrm{pH}} + 10^{-\mathrm{p}K_{a_3}-\mathrm{p}K_{a_2}+2\mathrm{pH}} + 10^{-\mathrm{p}K_{a_2}+\mathrm{pH}} + 10^{\mathrm{p}K_{a_1}-\mathrm{pH}} + 1) \tag{2.68}$$

$$\log m_i^L = \log m_{0,i}^L + \log\left[\gamma_{H_3X}\left(\frac{10^{-\mathrm{p}K_{a_4,th}-\mathrm{p}K_{a_3,th}-\mathrm{p}K_{a_2,th}+3\mathrm{pH}}}{\gamma_{X^{3-}}} + \frac{10^{-\mathrm{p}K_{a_3,th}-\mathrm{p}K_{a_2,th}+2\mathrm{pH}}}{\gamma_{HX^{2-}}} + \frac{10^{-\mathrm{p}K_{a_2,th}+\mathrm{pH}}}{\gamma_{H_2X^-}} + \frac{10^{\mathrm{p}K_{a_1,th}-\mathrm{pH}}}{\gamma_{H_4X^+}}\right) + 1\right] \tag{2.69}$$

2.3.2. The pH Influence on the Speciation

Weak electrolytes do not completely dissociate in water; thus, it is expected that different species of DNP-AA, water-soluble vitamins and organic salts are present in aqueous solutions. The species distribution of those compounds in aqueous solution depends on pH. Calculation of the species fraction α_j of each type of species j of a component can be done using pK_a (or K_a) values and pH (or $[H^+]$). At pH = pK_a the species fraction of the neighboring species is equal.

As an example, the species distribution for low soluble monoprotic acid HA (e.g. DNP-AA) is calculated using equations (2.70) - (2.71) in which α_{HA} and α_{A^-} are the species fractions of HA and A^-, respectively[8]. This is an idealized approach that can be used for poorly soluble components. In both equations, K_a and $[H^+]$ can be replaced by 10^{-pK_a} and 10^{-pH}, accordingly. Expression $[H^+] = 10^{-pH}$ is only an assumption that neglects the non-ideality. The calculations with equations (2.70) - (2.71) are appropriate for very low concentrations. This statement is made according to Lange [328].

$$\alpha_{HA} = \frac{[HA]}{[A^-] + [HA]} = \frac{[H^+]}{[H^+] + K_a} \tag{2.70}$$

$$\alpha_{A^-} = \frac{[A^-]}{[A^-] + [HA]} = \frac{K_{a_1}}{[H^+] + K_a} \tag{2.71}$$

If considering non-ideality, the species distribution of DNP-AA is expressed as shown in equations (2.72) and (2.73)[8]. In these expressions $[a_{H^+}] = 10^{-pH}$.

$$\alpha_{HA} = \frac{[a_{H^+}]}{[a_{H^+}] + \frac{K_{a,th} \cdot \gamma_{HA}}{\gamma_{A^-}}} \tag{2.72}$$

$$\alpha_{A^-} = \frac{\frac{K_{a,th} \cdot \gamma_{HA}}{\gamma_{A^-}}}{[a_{H^+}] + \frac{K_{a,th} \cdot \gamma_{HA}}{\gamma_{A^-}}} \tag{2.73}$$

Equations (2.74)-(2.76) might be derived to calculate α_j in solutions containing any polyprotic compound, e.g. amphoteric VB3^{acid} or VB12[7].

$$\alpha_{H_2X^+} = \frac{[H_2X^+]}{[H_2X^+] + [HX] + [X^-]} = \frac{[H^+]^2}{[H^+]^2 + [H^+]K_{a_1} + K_{a_1}K_{a_2}} \tag{2.74}$$

$$\alpha_{HX} = \frac{[\mathrm{HX}]}{[H_2X^+] + [HX] + [X^-]} = \frac{[H^+]K_{a_1}}{[H^+]^2 + [H^+]K_{a_1} + K_{a_1}K_{a_2}} \tag{2.75}$$

$$\alpha_{X^-} = \frac{[X^-]}{[H_2X^+] + [HX] + [X^-]} = \frac{K_{a_1}K_{a_2}}{[H^+]^2 + [H^+]K_{a_1} + K_{a_1}K_{a_2}} \tag{2.76}$$

If considering the non-ideality, the species distribution of an amphoteric VB3^{acid} or VB12 is expressed as shown in equations (2.77) - (2.79).

$$\alpha_{H_2X^+} = \frac{[a_{H^+}]^2 \cdot \frac{\gamma_{HX}}{\gamma_{H_2X^+}}}{[a_{H^+}]^2 \cdot \frac{\gamma_{HX}}{\gamma_{H_2X^+}} + [a_{H^+}]K_{a_{1,th}} + K_{a_{1,th}}K_{a_{2,th}} \cdot \frac{\gamma_{HX}}{\gamma_{X^-}}} \tag{2.77}$$

$$\alpha_{HX} = \frac{[a_{H^+}]K_{a_{1,th}}}{[a_{H^+}]^2 \cdot \frac{\gamma_{HX}}{\gamma_{H_2X^+}} + [a_{H^+}]K_{a_{1,th}} + K_{a_{1,th}}K_{a_{2,th}} \cdot \frac{\gamma_{HX}}{\gamma_{X^-}}} \tag{2.78}$$

$$\alpha_{X^-} = \frac{K_{a_{1,th}}K_{a_{2,th}} \cdot \frac{\gamma_{HX}}{\gamma_{X^-}}}{[a_{H^+}]^2 \cdot \frac{\gamma_{HX}}{\gamma_{H_2X^+}} + [a_{H^+}]K_{a_{1,th}} + K_{a_{1,th}}K_{a_{2,th}} \cdot \frac{\gamma_{HX}}{\gamma_{X^-}}} \tag{2.79}$$

The species distribution of DNP-glycine and VB3^{acid} as a function of pH can be presented graphically as shown in figure 2.1. The species shown in figure 2.1 are calculated using an idealized approach according to equations (2.70) and (2.71) for DNP-glycine and equations (2.74) - (2.76) for VB3^{acid}. Other equations allowing determination of α_j for more complex systems can be derived analogously to presented in this section examples. This includes also expressions that may be used to calculate the species distribution of organic salts, however, in this work at the pH of salt-rich solutions (pH~8), all salts are considered as fully dissociated [334, 335].

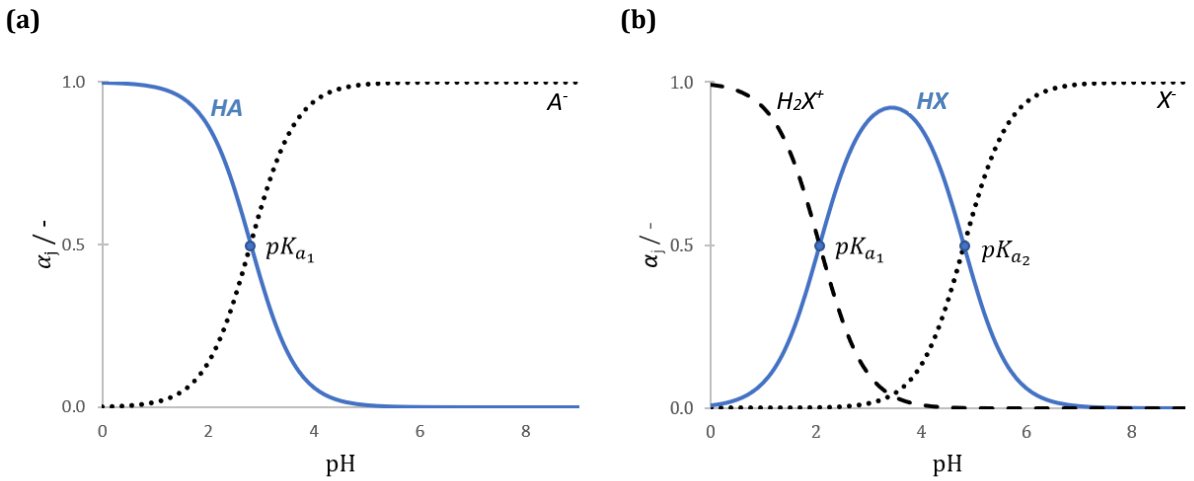

Figure 2.1. Dissociation equilibrium of aqueous solutions containing DNP-glycine (a) and VB3^{acid} (b) as a function of pH at T=298.15K. The lines represent the molar fractions α_j of species j calculated using equations (2.70) and (2.71) (a) and equations (2.74) - (2.76) (b), as well as dissociation constants (pK_a) from table 2.1 (ideal conditions assumed). Species j: neutral (solid lines), positively charged (dashed lines), negatively charged (dotted lines). The lines crossover at half-equivalence points, where pH=pK_a.

2.4. The ePC-SAFT Equation of State

Molecular-based models founded on equation of state (EOS) that account for the non-ideality are often very successful in overcoming the biggest bottlenecks of the idealized approaches. The Perturbed-Chain SAFT (PC-SAFT) model developed by Gross and Sadowski [75, 76] is an equation of state based on the Statistical Associating Fluid Theory (SAFT) of Chapman *et al.* [207, 208]. Electrolyte PC-SAFT (ePC-SAFT) was introduced by Cameretti *et al.* [74] to describe the mixtures containing ionic components and it is an extension of the original PC-SAFT. The thermodynamic perturbation theory behind original PC-SAFT is applied to the reference hard-chain system. According to equation (2.75), the residual Helmholtz energy (a^{res}) is calculated from the sum of different energy contributions resulting from hard-chain forces (a^{hc}), dispersive van der Waals attractions (a^{disp}), and hydrogen bonding (a^{assoc}). Besides these contributions ePC-SAFT also involves an expression that describes Coulomb interactions (a^{ion}). Since an extensive description of ePC-SAFT and all mentioned contributions is included in literature [75, 76, 336-339], in this thesis just the principals of ePC-SAFT concept are presented.

$$a^{res} = a^{hc} + a^{disp} + a^{assoc} + a^{ion} \tag{2.80}$$

Any component *i* is characterized by three pure-component parameters: the segment number (m_i^{seg}), the segment diameter (σ_i), and the dispersion-energy parameter (u_i/k_B) [75]. Moreover, for associating components the two additional fitting parameters are implemented: the association-energy parameter ($\varepsilon^{A_iB_i}/k_B$), where k_B stands for Boltzmann constant, and the association-volume parameter ($k^{A_iB_i}$) [76]. In total, at maximum five parameters are used to describe a pure component with ePC-SAFT. For an associating compound such as water, DNP-AA, or vitamin, the number of acceptor/donor association sites (N_i^{assoc}) is defined before the modeling [209]. The electrostatic contribution of a^{ion} is based on Debye-Hückel [340] term according to equation (2.81) and was introduced to ePC-SAFT by Cameretti et al. [74]. In this equation, κ stands for the Debye screening length, q_i is the charge of component *i*, and χ_i can be defined according to expression (2.82).

$$\frac{a^{ion}}{k_BT} = -\frac{\kappa}{12\pi k_B T_\varepsilon}\sum_i x_i q_i^2 \chi_i \tag{2.81}$$

$$\chi_i = \frac{3}{(\kappa q_i)^3}\left[\frac{3}{2} + \ln(1+\kappa q_i) - 2(1+\kappa q_i) + \frac{1}{2}(1+\kappa q_i)^2\right] \quad (2.82)$$

No additional pure-component parameter to account on electrostatic interactions is considered in ePC-SAFT modeling. Thus, the a^{ion} expression requires only that the charge q_i is set prior to the modeling [74].

To apply ePC-SAFT to mixtures, combining rules from Berthelot-Lorentz [341, 342] and Wolbach-Sandler [343] are introduced according to equations (2.83) - (2.86). Using these expressions for a mixture in which components *i* and *j* are present, the mean segment diameter (σ_{ij}), the mean dispersion-energy parameter (u_{ij}), the mean association-energy parameter ($\varepsilon^{A_iB_j}$), and the mean association-volume parameter ($\kappa^{A_iB_j}$) can be determined. Also, involving the binary interaction parameter (k_{ij}) between components *i* and *j* can be worthwhile for the modeling of mixtures.

$$\sigma_{ij} = \frac{1}{2}\cdot(\sigma_i + \sigma_j) \quad (2.83)$$

$$u_{ij} = \sqrt{u_i \cdot u_j}\cdot(1 - k_{ij}) \quad (2.84)$$

$$\varepsilon^{A_iB_j} = \frac{1}{2}\cdot(\varepsilon^{A_iB_i} + \varepsilon^{A_jB_j}) \quad (2.85)$$

$$\kappa^{A_iB_j} = \sqrt{\kappa^{A_iB_i}\cdot\kappa^{A_jB_j}}\cdot\left(\frac{2\cdot\sqrt{\sigma_i\cdot\sigma_j}}{(\sigma_i+\sigma_j)}\right)^3 \quad (2.86)$$

The k_{ij} is implemented in case the correction of the cross-dispersion energy in a mixture is needed. More precisely, it is introduced if the deviations of this energy from the geometric mean of the pure-component are significant. The k_{ij} can be linearly related to the temperature T (expressed in K), however, in this work, all k_{ij} are considered as temperature-independent.

3. Materials and Experimental Methods

Missing comprehension of the dependencies of the partitioning of organic compounds on system properties still limits the application of ATPS at the industrial level. This chapter provides the materials and methodologies required to design new ATPS suitable for the partitioning of DNP-AA and water-soluble vitamins. The results obtained through these procedures allow a better understanding of solute behavior in an aqueous environment. Thus, the chapter involves a description of the methodologies used for both solute and ATPS characterization, as well as of the procedures applied for the evaluation of solute partitioning. Experimental data acquired through procedures presented in this chapter are essential for industrial applications. Also, thermodynamic modeling, namely parameter estimation and validation of model predictions requires some experimental input.

3.1. Materials

All chemicals applied for the experiments were used without any further purification. No additional analyses to confirm the purity were carried in this work. An overview of all chemicals used in the experiments, together with the names of Suppliers and purities, is given in table 3.1. The purity of each product was given as declared in certificate of analysis provided by the respective Supplier.

Table 3.1. Chemical provenance with specification of the Chemical Abstract Service (CAS) and the purity given in mass fraction of each component. Supplier: SA = Sigma-Aldrich, TCI = Tokyo Chemicals Industry, PR = PanReac, ME = Merck. Average molar mass M_{PEG} (Supplier) = 1500 g·mol^{-1} (ME), 4000 g·mol^{-1} (SA), 6000 g·mol^{-1} (SA), and 8000 g·mol^{-1} (SA).

Compound	*Abbreviation*	*CAS*	*Supplier*	*Mass Purity*
		N-(2,4-dinitrophenyl)-Amino Acids (DNP-AA)		
N-(2,4-Dinitrophenyl)-L-alanine	DNP-alanine	1655-52-3	TCI	≥0.97
N-(2,4-Dinitrophenyl)glycine	DNP-glycine	1084-76-0	TCI	≥0.99
N-(2,4-Dinitrophenyl)-L-valine	DNP-valine	1694-97-9	TCI	≥0.97
N-(2,4-Dinitrophenyl)-L-leucine	DNP-leucine	1655-57-8	TCI	≥0.97
		Water-Soluble Vitamins		
L(+)-Ascorbic acid	VC	50-81-7	PR	≥0.99
Riboflavin	VB2	83-88-5	SA	≥0.98
Nicotinic acid	$VB3^{acid}$	59-67-6	SA	≥0.98
Nicotinamide	$VB3^{amide}$	98-92-0	SA	≥0.98
Folic acid	VB9	59-30-3	SA	≥0.97
Cyanocobalamin	VB12	68-19-9	SA	≥0.98
		ATPS Phase Formers		
Polyethylene glycol	PEG	25322-68-3	SA/ME	#
Sodium citrate tribasic dihydrate	Na_3Citrate	6132-04-3	SA	≥0.99
Potassium citrate tribasic monohydrate	K_3Citrate	6100-05-6	SA	≥0.99
Sodium tartrate dibasic dihydrate	Na_2Tartrate	6106-24-7	SA	≥0.99
Potassium sodium tartrate tetrahydrate	KNaTartrate	6381-59-5	SA	≥0.99

Sodium sulfate anhydrous	Na_2Sulfate	7757-82-6	ME	≥0.99
Magnesium sulfate anhydrous	MgSulfate	7487-88-9	SA	≥0.99
	pH-Adjusting Agents			
Hydrogen chloride	HCl	7647-01-0	ME	≥0.99
Sodium hydroxide	NaOH	1310-73-2	ME	≥0.99
Potassium hydroxide	KOH	1310-58-3	ME	≥0.85

[#] The purity of PEG was not declared by SA/M.

The abbreviations provided in table 3.1 were required to improve the readability of this document. Some of these, especially for N-(2,4-dinitrophenyl)-amino acids, became widespread terms in previous publications [344, 345]. Shortened names VC and VBx (x=2, 3^{acid}, 3^{amide}, 9, 12) which in this work refer to water-soluble vitamins are based on vitamin generic descriptor names (C, B-complex). This nomenclature is in common usage in literature and connects vitamins of similar biological activity and solubility, rather than of alike chemical structure [137]. The abbreviation for salts (e.g. $Na_3C_6H_5O_7$ = Na_3Citrate; $Na_2C_4H_4O_6$ = Na_2Tartrate), constituted by a symbol of the cation (e.g. Na^+) and long name of the anion (e.g. Citrate, Tartrate), was introduced for better legibility and distinguishability. Detailed information about the chemical structure of each compound can be approached using specification CAS included in table 3.1.

In regard to polymer, table 3.1 contains average molar masses of polyethylene glycol (PEG) declared by Supplier. A narrow molar mass distribution of PEG allows an assumption that just one polymer species is present (low polydispersity of PEG). This statement was made based on an explanation of molar mass distribution of polymers (including PEG) elaborated by Reschke [346] that was based on distribution theory published by Hosemann and Schramek [347]. All dilutions and stock solutions were prepared with deionized Millipore water. The salts used in this work were purchased as hydrates. The concentrations (wt-%) of PEG and salts were at first pre-determined using an analytical balance, while the real concentrations were calculated from dried mass of samples withdrawn from these solutions. This procedure was applied according to the literature [260, 348, 349]. Drying method (heating or freeze-drying) was chosen based on physicochemical properties of each compound. More detailed description on that is

provided in the following section 3.2.2 of this chapter. The pH was adjusted by addition of HCl, NaOH, or KOH whenever it was required by the experimental procedure.

3.2. Experimental Methods

This subchapter describes methodologies that allowed measuring the solubility of biomolecules considered in the present work, as well as characterizing ATPS equilibria, and evaluating the behavior of biomolecules in different ATPS. Section 3.2.1 involves the experimental setup and analytical procedures to determine the solubility of DNP-AA and vitamins in water at T = 298.15 K and p = 1 bar, at different pH, and in the presence of additives (covitamins)[5, 6, 8].

The measurements which assisted in the design of ATPS suitable for the partitioning of DNP-AA and vitamins were performed according to the methodologies described in sections 3.2.2 (ATPS Equilibria Characterization) [2, 3] and 3.2.3 (Partition Coefficient Determination) [1, 3, 4, 7]. Experimental methods for DNP-AA and vitamin solutions characterization are given in Section 3.2.4 (Density and Osmotic Coefficient Measurements) [5].

3.2.1. Solubility

The experimental shake-flask method was used to determine the equilibrium concentrations m_i^L (i.e. aqueous solubilities) of DNP-AA (DNP-glycine, DNP-alanine, DNP-valine, DNP-leucine) and water-soluble vitamins (VC, VB2, VB3^{acid}, VB9, VB12) in water, at T=298.15±0.1 K and p=1 bar. The technique was applied to measure the solubility in pure water (aim A), to obtain the pH-solubility profiles (aim B), and to test the influence of cosolute on solubility (aim C). The solubility measurements were performed according to scheme presented in figure 3.1.

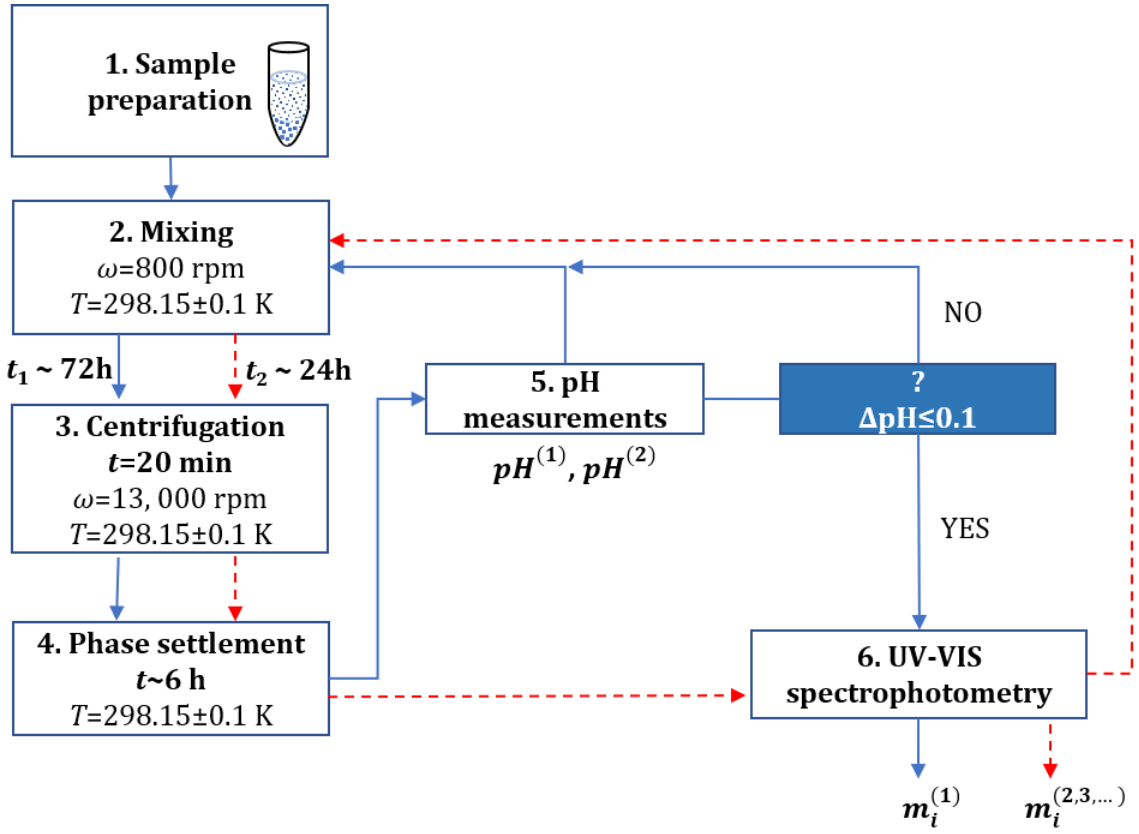

Figure 3.1. Procedure applied for solubility determination; Solid lines: measuring the concentration $m_i^{(1)}$[mol·kg^{-1}] (steps 1→6) - the equilibrium is verified with pH of saturated solutions (ΔpH≤0.1) taken out in time intervals (~72h). Dashed lines: further concentration measurements $m_i^{(2,3,\dots)}$ (steps 2→3→4→6) - the equilibrium ($m_i = m_i^L$) is considered as reached if Δm_i≤6% measured in time intervals (~24h).

Step 1: Sample preparation

The samples were prepared accordingly to reach the aims (figure 3.2). The tubes containing solid DNP-AA or vitamin were filled with water or aqueous solutions containing additives (NaOH, HCl, covitamins). The weighting of stock solutions of additives (m_{HCl}=0.05-0.5 mol·kg^{-1}, m_{NaOH}=0.05-0.5 mol·kg^{-1}, m_{VC}=0.5-1 mol·kg^{-1}, m_{VB3}^{acid}=0.05-0.1 mol·kg^{-1}, m_{VB3}^{amide}=0.1-0.2 mol·kg^{-1}) was done using Mettler Toledo analytical balance (XS205 Dual Range) with an uncertainty of ±0.01 mg. The amount of DNP-AA or vitamin was not weighted, as the condition in this step was solely to add an amount that allows having a solid (undissolved DNP-AA or vitamin) and liquid phase in a tube. The tubes with samples were shaken on a Vortex mixer for 15 min. After the preliminary tests, this time was considered enough for this step. If after that, the systems became homogeneous, then more solid DNP-AA or vitamin was added to the solution.

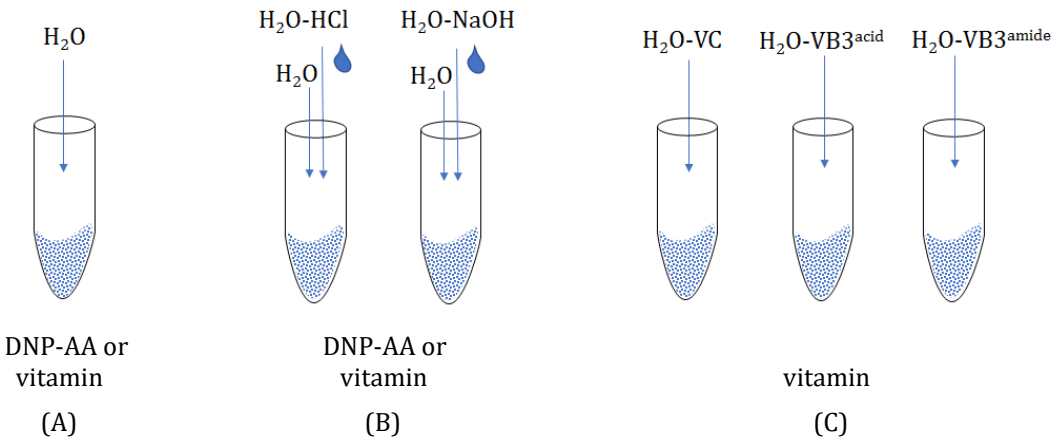

Figure 3.2. Sample preparation for different aims considered in solubility experiments; Aims A-C: (A) filling the tube containing solid DNP-AA (DNP-glycine, DNP-alanine, DNP-valine, DNP-leucine) or vitamin (VC, VB2, $VB3^{acid}$, VB9, VB12) with water, (B) filling the tube containing solid DNP-AA (DNP-glycine, DNP-alanine, DNP-valine, DNP-leucine) or vitamin (VC, VB2, $VB3^{acid}$, VB9, VB12) with water and adding dropwise different amounts of aqueous solutions HCl, or NaOH, (C) filling the tube containing vitamin (VB2, VB9, VB12) with aqueous solution of covitamin VC, $VB3^{acid}$, or $VB3^{amide}$.

Step 2: Mixing

Only in the case that the solutions were heterogeneous (solid + liquid), the tubes were moved to a thermomixer (Thermomixer comfort, Eppendorf) and constantly shaken (ω=800 rpm) at T=298.15±0.1 K for at least 72h. Over incubating time, the samples were very well protected from light and thoroughly sealed. However, in time intervals (every 12h) the presence of solid-state in the tubes was visually inspected. If within the incubation time it was found that DNP-AA or vitamin became dissolved in liquid, then more solid was added to the solution and the incubation continued. If after 72h counting from the initial incubation time the addition of a solute was still required to keep the system heterogenous, then after adding more solid the samples were left for at least 24h in thermomixer and after that inspected again. The solid was added and samples were incubated until the two phases (solid + liquid) were observed for at least 24h counting from the moment of each addition.

Steps 3-4: Centrifugation and phase settlement

Subsequently, after incubation, the tubes were centrifuged for 20 min at ω=13.0·10^3 rpm, T=298.15 K (refrigerated centrifuge 5418 R, Eppendorf). For phase settlement at isothermal conditions, the samples were placed back into the thermomixer

and incubated at T=298.15±0.1 K for at least 6h without shaking. This centrifugation and incubation times were considered being enough for complete phase separation based on preliminary tests [6].

Step 5: pH measurements

The pH values of the saturated liquid phase were determined with pH meter (glass electrode QpH 70, VWR, accuracy of ±0.01 pH units). After that, the whole procedure (incubation with shaking, centrifugation, and phase settlement) was repeated until the pH did not change of more than pH≤0.1.

Step 6: UV- VIS spectrophotometry

When the pH requirement (ΔpH≤0.1) had been met, small aliquots of the saturated liquid phase were withdrawn with a micropipette (in duplicate) and properly diluted with water. All the dilutions were prepared by weight using analytical balance (XS205 Dual Range, uncertainty of ±0.01 mg). The concentrations of DNP-AA or water-soluble vitamins were measured by UV-VIS spectrophotometry (Tecan Microplate Reader Infinite M200 Pro) using the following wavelengths based on the reports from the literature: $\lambda_{DNP-AA}^{max} = 362\ nm$ [350, 351], $\lambda_{VC}^{max} = 270\ nm$ [352], $\lambda_{VB2}^{max} = 270\ nm$ / $445\ nm$ [153, 353, 354], $\lambda_{VB3acid}^{max} = 270\ nm$ [355], $\lambda_{VB9}^{max} = 280\ nm$ / $360\ nm$ [354, 356], $\lambda_{VB12}^{max} = 360\ nm$ [357]. Calibration curves for all DNP-AA and vitamins were prepared before concentration analyses. The concentrations of vitamins in pure water and aqueous solutions containing covitamins or the pH adjusting agents (HCl, NaOH) were determined precisely according to the procedures previously reported in similar studies [42, 153, 177]. The absorbance of samples containing VB2 and VB9 in pure water (aim A) was measured at a different wavelength than in covitamin influence studies (aim C). The reason for using different wavelengths for VB2 and VB9 solutions in studies with covitamin was related to the coexistence of maximum peaks for vitamin and covitamin (at the wavelengths chosen for testing vitamin solubility in pure water). This methodology was already reported in the literature [42, 153, 177]. To assure that the equilibrium state was reached, the same samples with supersaturated solutions were shaken in the thermomixer for at least one additional day. After complete phase separation (as in the previous step), again new aliquots were withdrawn, diluted with water and the concentrations were determined. Appropriate dilutions were very important to avoid possible interferences, especially in

vitamin + covitamin mixtures, or vitamin/DNP-AA + the pH adjusting agent (HCl, NaOH). The absorbance of a conveniently diluted sample containing water and an additive (covitamin, HCl, NaOH) was equal to the absorbance measured for pure water. This requirement has ensured that there were no interferences from an additive (covitamin, HCl, NaOH) in concentration measurements.

If for several samples measured in different time intervals, the concentration deviations were lower than 6%, the equilibrium was considered as being achieved (thus, $m_i = m_i^L$). This value was chosen based on the literature, as well equipment accuracy (obtained with samples of known concentration) [153]. The deviations between experimental solubility measurements ($m^{L,exp}$) and the arithmetic mean of solubility data ($m^{L,mean}$) measured from a given number of solubility points (NP_m) were calculated according to equation (3.1) that expresses an average relative deviation ARD%.

$$\mathrm{ARD\%} = 100 \cdot \frac{1}{\mathrm{NP}_m} \cdot \sum_{\mathrm{k}=1}^{\mathrm{NP}_m} \left| 1 - \left(\frac{m^{L,exp}}{m^{L,mean}} \right)_{\mathrm{k}} \right| \tag{3.1}$$

Samples taken from the solutions of different pH were dried in a vacuum drying oven at T=298.15±0.1 K, p=2±0.1 mbar (Binder VD 53). Solid was characterized by powder X- ray diffractometer PXRD (Rigaku MiniFlex600, Japan) (Appendix: A6, A7). Approximately 5 mg of solid sample was required. The angle 2Θ range considered for the analyses was 2°<2Θ<30°.

3.2.2. ATPS Equilibria

ATPS considered in this work were characterized using biphasic diagrams. In this section, at first, the methodology used to define the liquid immiscibility regions of ATPS (binodal curves) is presented. Afterwards, the procedure which allows the measurement of the equilibrium composition of the two phases (defined by tie-lines) is described.

Determination of Binodal Curves

The binodal curve of each ATPS was determined using the cloud point method. The procedure used for these measurements was based on the methodology reported in the literature [258, 349]. All weighting was carried out on an Adam Equipment balance model AAA250L, with an uncertainty of ±0.2 mg.

At first, aqueous stock solutions of PEG with average molar mass M_{PEG}: 1500, 4000, 6000, 8000 g·mol^{-1} (~50 wt-%), and salt: Na_3Citrate, K_3Citrate, Na_2Tartrate, KNaTartrate (~30 wt-%) were prepared. The concentration of PEG and salt in stock solutions was measured gravimetrically and calculated from PEG/salt dry mass, obtained using a freeze-dryer (Scan Vac, CoolSafe 55–4) for PEG, KNaTartrate, and Na_2Tartrate, or after evaporating on a heating plate (Stuart hot plate SB300), for Na_3Citrate and K_3Citrate. After drying the samples were moved to vacuum desiccator and taken out just for short times required for weighting.

Different heterogeneous mixtures of known composition of polymer and salt were prepared in assay tubes by weighting different amounts of PEG and salt stock solutions. Then the tubes were vigorously shaken in a vortex mixer (VWR, model VV3) for 3 min and afterwards placed into a thermostatic bath (Techne, Tempette TE-8D) at $T = 298.15 \pm 0.2$ K for 20 minutes. Known amounts of water were added dropwise to the tubes until one homogenous phase was reached. After each water addition, the tubes with samples were again shaken in a vortex mixer for 3 min and located in a thermostatic bath at T=298.15 ± 0.2 K for at least 15 min. Time of shaking and settlement at each step of this procedure was chosen according to the literature [358]. Each measurement procedure was repeated until the whole binodal curve was obtained (in average 23 data points were used to determine one binodal curve) . For the presentation and comparison of different experimental data, the binodal curves were adjusted to the empirical equation (3.2) according to Merchuk et al. [275]. In this expression, w_S and w_P are the salt and PEG compositions given in mass fraction, respectively, and a, b and c are adjustable parameters, obtained by nonlinear least squares regression.

$$w_P = a \cdot exp(b \cdot {w_S}^{0.5} - c \cdot {w_S}^3) \qquad (3.2)$$

Determination of Tie-lines

Tie-lines were measured for different feed compositions of PEG – salt ATPS according to the procedure reported in the literature [258, 349]. For each ATPS at least three (up to six) tie-lines were determined. All weighting was carried out on an Adam Equipment balance model AAA250L, with an uncertainty of ±0.2 mg. Biphasic systems were prepared by weight in 15 mL tubes using PEG and salt stock solutions from the previous test (binodal curve determination). The tubes with samples were shaken thoroughly in a

vortex mixer for 3 min and afterwards they were left for phase separation for at least 48 h, in a thermostatic bath at T = 298.15 ± 0.2 K. The duration of mixing and phase clearance was chosen according to the literature and preliminary experiments carried out in this work [258, 349, 358].

Subsequently, for each tie-line, samples of top and bottom phases were withdrawn using a syringe and conveniently diluted with water. Salt concentration was determined in both phases, at T = 298.15 K, by electrical conductivity using a Crison GLP31 Meter with a platinum conductivity cell Crison 52 93, precise to within ±0.5%. Calibration curve was established by measuring the electrical conductivity of standard solutions with known salt concentrations (aqueous solutions of Na_3Citrate, K_3Citrate, Na_2Tartrate, KNaTartrate), within the range 1–4 wt-%. In this range, no PEG interference in the electrical conductivity measurements was observed. For all measurements, the error associated with the calculation of the average salt concentration, using the calibration line, was below 1%. Total salt concentration of each phase was obtained from three measurements and corrected with the dilution factor (standard deviations were calculated to be less than 0.2%). Water concentration in the top and bottom phase was measured gravimetrically after freeze-drying (Scan Vac, CoolSafe 55–4). Samples of the top phase were withdrawn in triplicate, conveniently diluted with water (1/5), frozen at T = 255 K for 24 h, and placed into freeze dryer for at least 72h. These conditions were chosen according to t literature [349]. In all cases, the standard deviation of the average dry weight was assessed to be less than 0.15%. The PEG concentration was obtained from a mass balance. Such methodology for obtaining polymer and salt concentration was reported in at least several publications [258, 295, 349].

The tie-line lengths (TLL) were determined as shown in equation (3.3), where w_P^I , w_P^{II} and w_S^I , w_S^{II} are the mass fractions of PEG (P) or salt (S) in the top (I) and bottom (II) phases at equilibrium.

$$TLL = \sqrt{(w_P^I - w_P^{II})^2 + (w_S^I - w_S^{II})^2} \tag{3.3}$$

It is very common in literature to provide phase equilibrium compositions of ATPS in mass fractions and to calculate TLL based on this unit of concentration. Thus, for better data comparison between data from different sources, phase compositions are given in

this thesis in mass fractions. However, the mass fractions w_i can be converted to mole fractions x_i with equations (3.4) and (3.5). In these equations, v_{SC^+} and v_{SA^-} denote the number of moles of salt ions v_j : salt cation (SC^+) and salt anion (SA^-) into which a salt dissociates in aqueous solution. While expression (3.4) allows calculation of the mass fraction of component *i*: PEG (P) and water (W), equation (3.5) can be used to determine the mass fraction of ionic species *j* originated from salt dissociation: SC^+ and SA^-.

$$x_i = \frac{\frac{w_i}{M_i}}{\frac{w_P}{M_P} + (v_{SC^+} + v_{SA^-}) \cdot \frac{w_S}{M_S} + \frac{w_W}{M_W}} \tag{3.4}$$

$$x_j = \frac{v_j \cdot \frac{w_S}{M_S}}{\frac{w_P}{M_P} + (v_{SC^+} + v_{SA^-}) \cdot \frac{w_S}{M_S} + \frac{w_W}{M_W}} \tag{3.5}$$

In the ATPS studied in this thesis (pH~8), the salts considered as phase formers fully dissociate leading to the presence of ions Na^+, K^+, $Citrate^{3-}$, and $Tartrate^{2-}$ in a solution (the species fractions $\alpha_{Citrate^{3-}} \approx \alpha_{Tartrate^{2-}} = 0.99$). The pH of each ATPS phase was measured with pH meter (glass electrode QpH 70, VWR, accuracy of ±0.01 pH units). For this analysis, the samples from the top and bottom phases were withdrawn with a syringe.

To verify the reliability of the tie-lines, the correlations widely applied in the literature [260, 349, 359, 360] suggested by Othmer-Tobias (3.6) [271] and Bancroft (3.7) [272] were used in this work.

$$\log\left(\frac{1 - w_P^I}{w_P^I}\right) = k_1 + n_1 \cdot \log\left(\frac{1 - w_S^{II}}{w_S^{II}}\right) \tag{3.6}$$

$$\log\left(\frac{w_W^{II}}{w_S^{II}}\right) = k_2 + n_2 \cdot \log\left(\frac{w_W^I}{w_P^I}\right) \tag{3.7}$$

3.2.3. Partition Coefficient

Measuring partitioning of DNP-AA (DNP-alanine, DNP-glycine, DNP-valine, DNP-leucine) and water-soluble vitamins (VB2, $VB3^{acid}$, $VB3^{amide}$, VB9, VB12) in ATPS was carried out based on the methodology from the literature [361]. The weighting was done on an Adam Equipment balance model AAA250L, with an uncertainty of ±0.2 mg. All procedure was performed at T=298.15±0.2 K, and p=1 bar (controlled with air

conditioning and a thermostatic bath Techne, Tempette TE-8D). The partition coefficients were determined as presented in figure 3.3.

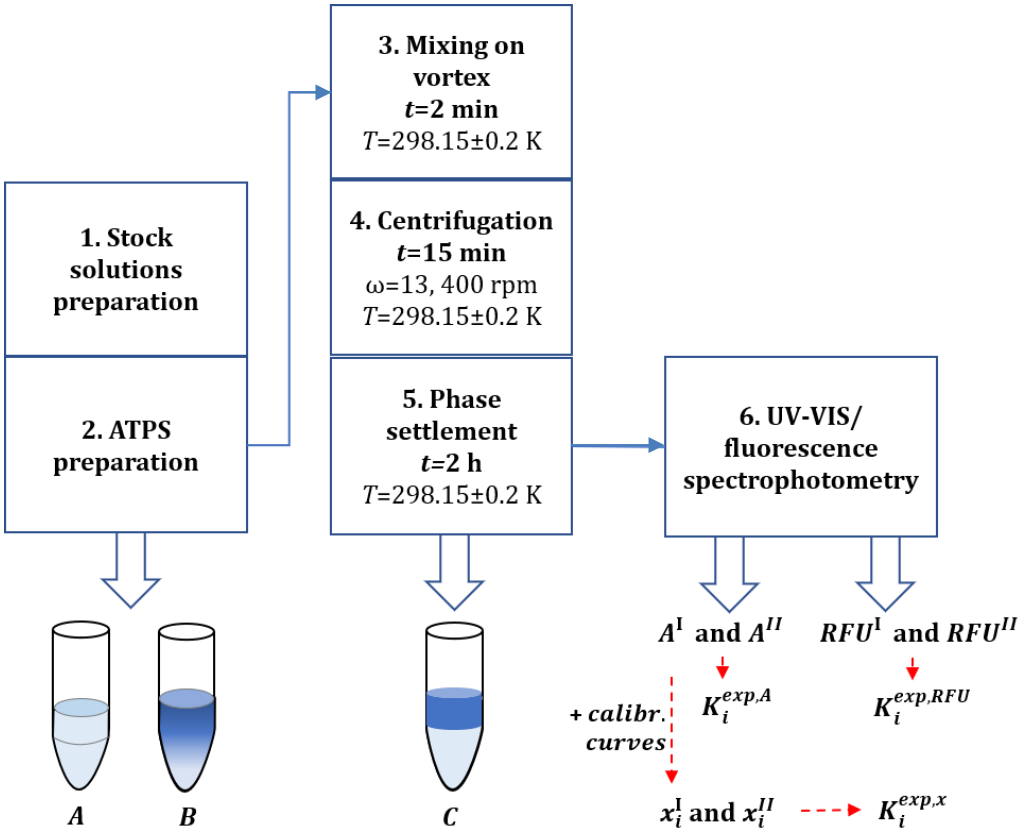

Figure 3.3. Procedure applied for determination of solute (DNP-AA, vitamin) partitioning in ATPS; Step 1: preparation of PEG, salt and solute (DNP-AA, vitamin) stock solutions; Step 2: the addition of PEG and salt stock solutions (A), the addition of solute (DNP-AA, vitamin) stock solution and water to PEG-salt ATPS (B). Steps 3→5: mixing and establishment of phase equilibrium in ATPS (C). Step 6: measuring the absorbance and fluorescence of samples withdrawn from the top (*I*) and the bottom (*II*) phase to obtain *K* ($K_i^{exp,A}$, $K_i^{exp,RFU}$); the calibration curves (absorbance of DNP-AA/vitamin solution of known concentration vs. mole fraction of DNP-AA/vitamin) allow calculation of mole fractions of a solute in each phase and determination of concentration-based *K* ($K_i^{exp,x}$).

Step 1: Stock solutions preparation

ATPS were prepared from aqueous stock solutions containing PEG of different average molar mass M_{PEG}: 1500, 4000, 6000, 8000 g·mol^{-1} (~50 wt-%), and salt: Na_3Citrate, K_3Citrate, Na_2Tartrate, KNaTartrate (~30 wt-%). The concentration of PEG and salt in stock solutions was obtained gravimetrically and calculated as described in section 3.2.2. The aqueous stock solutions of solutes (DNP-AA or vitamin, 0.2 wt-%) were done in 5 mL

glass tubes by weighting the mass of solid DNP-AA/vitamin and adding an appropriate mass of water. If necessary NaOH (1-2 drops of m_{NaOH}=0.5 mol·kg^{-1}) was added to completely dissolve DNP-AA/vitamin in water. All stock solutions were well protected from light and thoroughly sealed.

Step 2: ATPS preparation

At first, PEG/salt stock solutions and water were added to 2 mL Eppendorf tubes according to the feed composition (wt-%) of the respective tie-lines. All the additions were done by volume (µL) using an automatic pipette (Multipipette® XStream, Eppendorf). The amounts of PEG and salt stock solutions added were based on the prior established volume (µL) – mass (g) relation for each PEG/salt stock solution. The calibration procedure involved weighing on a balance different amounts of stock solutions pipetted in the volume unit and then choosing the volume of PEG/salt solution corresponding to the mass of a solution required to form ATPS. The mass of each component was calculated from composition expressed in wt-% assuming 1g as the total mass of ATPS. For each tie-line, six replicates with the same feed composition (PEG, salt, water) were prepared. Then, different amounts of the solute (DNP-AA, vitamin) stock solutions (20–100 mg) and water (100-20 mg) were added according to figure 3.4.

ATPS were prepared with an adequate amount of water needed to achieve a total ATPS mass of 1 g. For this reason, 100 mg corresponding to an addition of a solute solution and the respective amount of water was subtracted from the total mass of water calculated for ATPS. Then, 100 mg was total mass of water + solute solution added according to the scheme shown in figure 3.4.

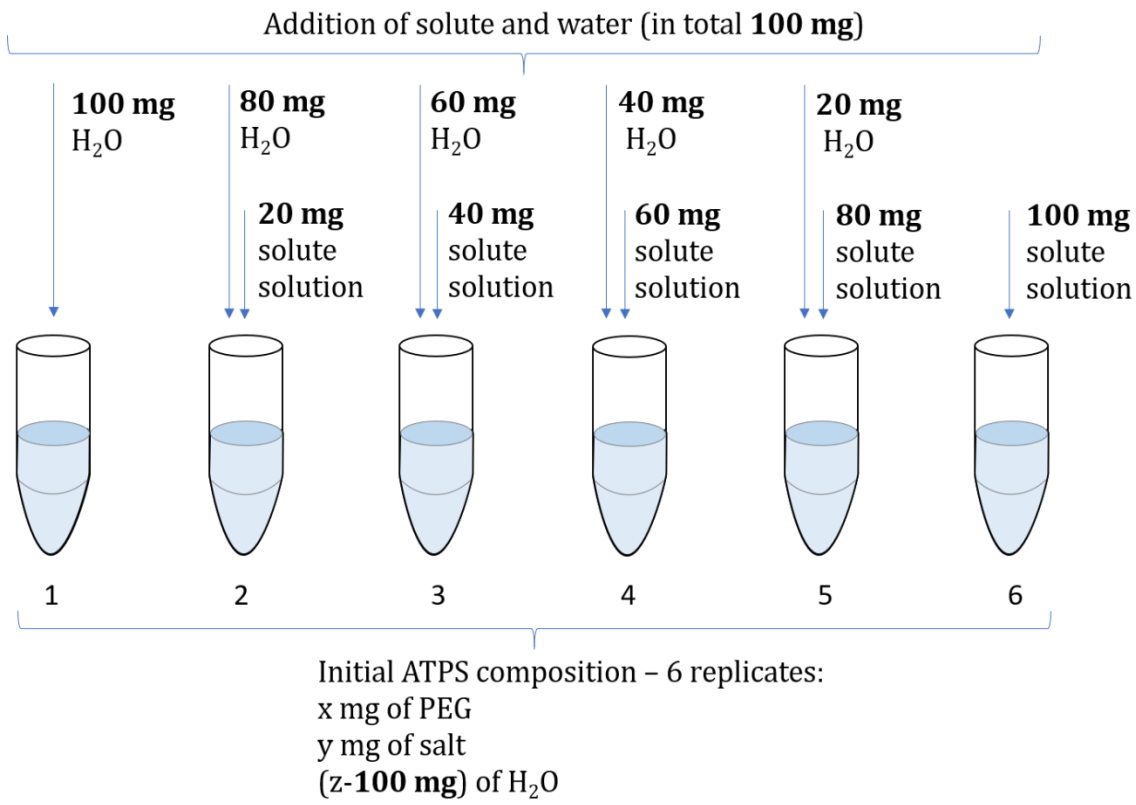

Figure 3.4. ATPS preparation: ATPS prepared in 6 replicates containing x mg of PEG, y mg of salt and (z-100 mg) of water (according to the tie-line composition) are filled with water and solute (DNP-AA, vitamin) stock solutions. The mass of water and solute added is 100 mg. The total mass of each ATPS after all additions is 1g.

Steps 3-5: Mixing, centrifugation, and phase settlement

The tubes containing water, PEG and salt, with or without DNP-AA/vitamin, were vigorously shaken for 2 min on a vortex mixer and right after that centrifuged for 15 min at ω=13.4·10^3 rpm (Minispin, Eppendorf) to obtain phase separation. This time duration of both procedures was reported in the literature and confirmed as enough in the present work with preliminary tests for different solutes [361, 362]. For the next 2h, ATPS were left at T=298.15 K for total interface clearance. This time was also tested before in the preliminary tests. During this equilibration time, the temperature T=298.15 K was controlled with air conditioning or if necessary, the tubes with ATPS were placed in a thermostatic bath (Techne, Tempette TE-8D).

Step 6: UV- VIS and fluorescence spectrophotometry

Samples withdrawn in duplicate from the top and bottom phases of ATPS were appropriately diluted with water to avoid interferences from PEG and salt. The absorbance (*A*) and fluorescence (*RFU* = Relative Fluorescence Unit) were determined spectrophotometrically (Thermo Scientific Varioskan Flash) using UV-VIS spectroscopy at $\lambda_{DNP-AA}^{max} = 362\ nm$ [350], $\lambda_{VB2}^{max} = 270\ nm$ [354], $\lambda_{VB3acid}^{max} = 260\ nm$ [363], $\lambda_{VB3amide}^{max} = 260\ nm$ [364], $\lambda_{VB9}^{max} = 280\ nm$ [354], $\lambda_{VB12}^{max} = 360\ nm$ [357], and fluorescence spectroscopy at $\lambda_{VB2}^{emission} = 520\ nm$, $\lambda_{VB2}^{excitation} = 270\ nm$ [365]. The measurements were also performed for aliquots of ATPS not containing DNP-AA/vitamin. The values of *A* or *RFU* were equal as obtained for pure water, ensuring that there are no interferences of PEG and salt in these measurements. The partition coefficients were obtained using the two ways commonly found in literature: through the slope of the straight lines from *A* or *RFU* measurements corrected with the dilution factor and by the mean of the calibration curve [1, 3, 4, 7, 97, 366-368].

The slope of the straight lines from representation of A^I (or RFU^I) in the top phase (*I*) versus A^{II} (or RFU^{II}) in the bottom phase (*II*), corrected with the respective dilution factors (DF, fraction of final volume to initial volume) allowed the determination of experimental absorbance- (or florescence) based partition coefficient of component *i* ($K_i^{exp,A}$ and $K_i^{exp,RFU}$, respectively). In this work, *i* corresponds to DNP-AA or vitamin. $K_i^{exp,A}$ and $K_i^{exp,RFU}$ were obtained according to equations (3.8) and (3.9), respectively:

$$K_i^{exp,A} = \frac{A^I \cdot DF}{A^{II} \cdot DF} \tag{3.8}$$

$$K_i^{exp,RFU} = \frac{RFU^I \cdot DF}{RFU^{II} \cdot DF} \tag{3.9}$$

From calibration curves representing the absorbance of a DNP-AA/vitamin versus the respective concentrations of DNP-AA/vitamin, it was possible to calculate the mole fraction of a solute (x_i^I, x_i^{II}) in each phase (*I*, *II*) for different tie-line compositions. The experimental concentration-based partition coefficient $K_i^{exp,x}$ at high DNP-AA/vitamin dilution was determined using equation (3.10).

$$K_i^{exp,x} = \frac{x_i^I}{x_i^{II}} \tag{3.10}$$

Each DNP-AA and vitamin considered in this work, except VB9, is fully present as just one species in both ATPS phases, and the experimental partition coefficient of component *i* ($K_i^{exp,x}$) is the same as for the respective species *j* ($K_j^{exp,x}$). In the case of VB9, two species ($VB9^{2-}$, $VB9^{3-}$) will be present at the conditions under investigation (pH ~ 8). Thus, both species will contribute to the experimental partition coefficient of component *i* ($K_i^{exp,x}$). The two species of VB9 ($VB9^{2-}$, $VB9^{3-}$) will be differently partitioned in ATPS due to a pH difference between the phases. Equation (3.11) allows calculating partition coefficient of *j* species $K_j^{exp,x}$ that is based on experimental partitioning data measured in this work. Equation (3.11) includes the fractions α_j^I and α_j^{II} of species *j* in each phase (*I* - top, *II* - bottom). These fractions can be calculated as previously shown in section 2.3.2 (Appendix A1-A2).

$$K_j^{exp,x} = K_i^{exp,x} \cdot \frac{\alpha_j^I}{\alpha_j^{II}} \tag{3.11}$$

3.2.4. Density and Osmotic Coefficient

To characterize DNP-AA and vitamin aqueous solutions, both properties liquid density and osmolality were used. The technique used for density measurements is based on the principle of the oscillating U-tube technique, in which densities are determined through the differences in frequencies of oscillation. The osmolality that is a measure of the total number of all particles present in a solution is determined through the difference in the freezing point between a solution and pure solvent (water) [369]. These experimental measurements are thvery relevant for thermodynamic modeling. The methodologies used for each property are presented in the following.

Density measurements

In this work, the densities of aqueous solutions containing DNP-AA or vitamin were carried out using Anton Paar density meter (DMA 4200 M) with maximum uncertainty of ±1.5 $kg \cdot m^{-3}$. Samples for the analysis were prepared gravimetrically using Mettler Toledo analytical balance (XS205 Dual Range) with an uncertainty of ±0.01 mg. Before the

measurements, the equipment was calibrated with air and deionized water. Liquid density was determined from the mean value of at least three replicates.

Densities of ternary solutions water - DNP-AA - NaOH were determined at p=1 bar and T=298.15 K – 318.15 K. The samples were prepared by dissolving different amounts of solid DNP-AA (DNP-glycine, DNP-alanine, DNP-valine, DNP-leucine) in aqueous solutions ($m_{DNP\text{-}AA} \leq 0.015$ mol·kg^{-1}) which contained NaOH in concentrations required for complete DNP-AA dissolution ($m_{NaOH} \leq 0.038$ mol·kg^{-1}).

Densities of binary solutions water – vitamin were determined at p=1 bar and T=298.15 K. The samples were prepared by dissolving different amounts of solid vitamin (VC, VB2, VB3^{acid}, VB9, and VB12) in water. The final vitamin concentrations varied strongly for freely soluble ($m_{VC} \leq 1.49$ mol·kg^{-1}), sparingly soluble ($m_{VB3^{acid}} \leq 0.14$ mol·kg^{-1}, $m_{VB12} \leq 0.006$ mol·kg^{-1}) and very low soluble ($m_{VB2} \leq 0.001$ mol·kg^{-1}, $m_{VB9} \leq 0.01$ mol·kg^{-1}) vitamins. Due to the limited solubility of VB2 and VB9, the homogenous samples with fully dissolved vitamin were obtained with KOH solution (m_{KOH}=0.5 mol·kg^{-1}) added dropwise. A negligible amount of KOH in solution allowed to increase the solubility of VB2 and VB9 without changing the species kinds present in the aqueous system (ΔpH<1). The pH of VB2 and VB9 solutions was controlled with pH meter (glass electrode QpH 70, VWR, accuracy of ±0.01 pH units).

Determination of Osmotic Coefficients

In this work, the osmolality of water – vitamin binary systems was measured using a freezing-point depression Gonotec osmometer (FP Osmomat 010, Knauer, Germany). During the measurements, the apparatus cools the sample and measures the temperature with a thermistor. An ideal 1 mol·kg^{-1} aqueous solution has the osmolality of 1 Osmol·kg^{-1} and freezes at T = -1.858° C. The apparatus uses this dependency and displays the result in mOsmol·kg^{-1}.

The samples for the measurements were prepared gravimetrically on Mettler Toledo analytical balance (XS205 Dual Range, uncertainty of ±0.01 mg) by dissolving water-soluble vitamin (VC, VB3^{acid}, VB12) in water ($m_{VC} \leq 0.85$ mol·kg^{-1}, $m_{VB3^{acid}} \leq 0.12$ mol·kg^{-1}, $m_{VB12} \leq 0.0086$ mol·kg^{-1}). The equipment was calibrated using certified (Knauer) 400 mOsmol and 850 mOsmol standard NaCl solutions (v=2). The baseline was set by measuring the osmolality of pure water. These calibrating procedures were repeated also

in between the measurements to ensure the highest accuracy, as well as to exclude any baseline drifts of the equipment. Tubes with 50µl of the sample were in sequence placed inside the osmometer, measured, and the displayed results in mOsmol·kg^{-1} were recorded. Each sample in this experiment was measured at least three times and the mean value was considered. This method allowed measuring osmotic coefficients with ARD%<2. Similar accuracy has been already reported in the literature for different solutes [370].

The osmotic coefficient (ϕ) was calculated from experimental osmolality (osm), according to equation (3.12) [81]. The expression involves the initial molality of the vitamin in each solution (m) and the number of species into which the components present in the solution can dissociate (v). To model neutral vitamins, VC, VB3^{acid} and VB12 were in these calculations considered as molecular non-dissociated species (v=1).

$$\phi = \frac{osm}{\nu_i \cdot m_i} \tag{3.12}$$

Moreover, since the solubility of DNP-AA and other vitamins used in the present work, namely VB2 and VB9, is very low and their solutions could not reach the detection limit for osmolality tests (the osmolality of solutions containing different vitamin concentrations ~ osmolality of pure water), the measurements for DNP-AA, VB2, and VB9 systems were not considered.

4. Modeling Methods and their Accuracy

This chapter presents the electrolyte PC-SAFT (ePC-SAFT) EOS modeling strategies found in this work and used to accurately characterize the pure components and their interactions in aqueous solutions. Thus, the modeling methods: Molecular Method (MM) and Joint-Parameter Method (J-PM), both introduced in this work for the modeling of different organic components, are presented. The description of the modeling methods is accompanied by an overview of the parameters established in this work and the accuracy calculations based on experimental data. The chapter also shows literature data on melting properties that are necessary for solubility calculations.

4.1. ePC-SAFT Parameter Estimation

This subchapter provides ePC-SAFT parameters and evaluates modeling accuracy. As explained in subchapter 2.4, ePC-SAFT requires five pure-component parameters to characterize an associating component. An additional parameter, namely binary interaction parameter k_{ij}, can be optionally used to describe the interactions in a mixture containing this component. In the present work, two main methods were applied to estimate ePC-SAFT pure-component parameters and binary interaction parameters k_{ij}: Molecular Method (MM) and Joint-Parameter Method (J-PM). These two modeling approaches were built on the conceptions from the literature and have been designed in this work specifically for the modeling of DNP-AA and vitamins. The principals of the modeling approaches for MM and J-PM from this work have an origin in strategies published by Held *et al*., as well as by Hübner and Lodziak *et al.* [79, 80, 296, 303]. The conception adopted to J-PM was also used by Knierbein & Wangler *et al.* and Greinert *et al.* for modeling of α-chymotrypsin and 1,3-bisphospho-D-glycerate, respectively [371, 372].

In the present study, the MM relied on fitting the parameters to experimental data like in the works published by Held *et al*. [79, 80, 303], but it included also novel modeling procedures adopted for the purpose of this work. These new procedures considered interactions of negatively charged components (DNP-AA, vitamins) in aqueous solutions and the dissociation equilibrium. The J-PM proposed in this work shared the similarity to the approach designed by Hübner and Lodziak *et al.* for connecting the parameters, but it did not follow the same idea used for obtaining each parameter. The reason for applying different procedures to J-PM than in the method published by Hübner and Lodziak *et al.* was related to a different character of connected molecules. The J-PM has joint the parameters of two components of different type: aromatic DNB considered as non-associating compound (three ePC-SAFT pure-component parameters) with associating aliphatic amino acid (five ePC-SAFT pure-component parameters), while the original work published by Hübner and Lodziak *et al.* relied on connecting the sets of parameters of the same kind molecules (associating amino acids). In the J-PM solely the two of ePC-SAFT pure-component parameters m_i^{seg} and σ_i were joint and no deviation to the dispersion energy was assumed.

By means of these two modeling methods, MM and J-PM, it was possible to estimate pure-component parameters of neutral and charged DNP-AA, vitamins, as well as DNB and salt ions. The methods allowed estimating also the binary interaction parameters k_{ij}, e.g. between a solute (DNP-AA or vitamins) and ions of ATPS phase forming components. Besides that, the present study used some sets of ePC-SAFT parameters published previously in the literature (water, PEG, salt ions, amino acids, $VB3^{amide}$) [79, 303, 338, 373-375]. The major reason for using the two different modeling methods was related to a distinct data available before the modeling (experimental or ePC-SAFT parameters). For example, ePC-SAFT parameters for most of water-soluble vitamins were not available in the literature, so they were fitted using the MM. The J-PM was designed for homological series of DNP-AA. From the molecular standpoint, DNP-AA molecule (DNP-glycine, DNP-alanine, DNP-valine, DNP-leucine) is composed by DNB (dinitrobenzene) group connected with a given amino acid chain (aliphatic amino acid, AA: glycine, alanine, valine, leucine). Thus, already established ePC-SAFT parameters for AA [79] could be joint with parameters for DNB estimated within this work, leading to new set of parameters for DNP-AA.

Since the procedures behind modeling methods used in this work are rather complex, more detailed explanation of the two modeling methods: MM and J-PM and their evaluation is described in detail in sections 4.1.1 and 4.1.2, accordingly. These two methods were used to obtain ePC-SAFT parameters from the current study. Table 4.1 and table 4.2 present a general overview of all ePC-SAFT pure-component and binary interaction $k_{\text{ij water}}$ (between water and a given molecule) parameters for neutral (non-charged) and charged components that were estimated in this work or taken from the literature.

Table 4.1. ePC-SAFT pure-component parameters and binary interaction parameters with water of neutral molecules considered in this work: dinitrophenyl amino acids (DNP-AA), aliphatic amino acids (AA), dinitrobenzene (DNB), water-soluble vitamins, PEG, and water. The parameters listed were obtained using Molecular Method (MM), Joint-Parameter Method (J-PM) or they were taken from the literature.

Component	M [g·mol^{-1}]	m_i^{seg} [-]	σ_i [Å]	u_i/k_B [K]	ε^{AiBi}/k_B [K]	κ^{AiBi} [-]	N_i^{assoc} #1	$k_{ij\ water}$ (T=298.15 K)	*Ref.* #2
DNP-glycine	241.16	9.2035	2.8636	216.96	2598.06	0.039	2/2		TW[8] J-PM
DNP-alanine	255.18	9.8187	2.9612	287.59	3176.6	0.082	2/2		TW[8] J-PM
DNP-valine	283.24	11.8391	2.9945	306.41	3183.8	0.039	2/2		TW[8] J-PM
DNP-leucine	297.26	12.6577	3.0501	330	3600	0.02	2/2		TW[8] J-PM
glycine	75.07	4.8495	2.327	216.96	2598.06	0.039	1/1	$-6.12\cdot10^{-2}$	[79]
L-alanine	89.09	5.4647	2.5222	287.59	3176.6	0.082	1/1	$-6.12\cdot10^{-2}$	[79]
L-valine	117.15	7.4851	2.5888	306.41	3183.8	0.039	1/1	$-7.57\cdot10^{-2}$	[79]
L-leucine	131.17	8.3037	2.7	330	3600	0.02	1/1	$-6.30\cdot10^{-2}$	[79]
DNB#3	168.11	4.354	3.4001	340.002				$3.00\cdot10^{-2}$	TW[8] MM
VC	176.13	11.7082	2.367	353.442	2600.675	0.039	1/4	$-1.80\cdot10^{-2}$	TW[5] MM
VB2	376.36	15.9238	2.63	150.315	2548.107	0.034	5/5	$-4.70\cdot10^{-2}$	TW[5] MM
VB3^{amide}	122.12	4.6485	1.7143	166.25	1056.2	0.002	1/1	$1.64\cdot10^{-2}$	[65]
VB3^{acid}	123.11	8.0883	2.3522	209.045	1088.56	0.002	3/1	$-3.90\cdot10^{-2}$	TW[5] MM
VB9	441.40	16.7167	2.6907	152.016	2379.471	0.034	8/4		TW[6] MM
VB12	1355.37	21.8544	4.05	346.45	2136.56	0.01	23/6	$-2.11\cdot10^{-2}$	TW[5] MM
PEG		$M_{PEG}\cdot0.050$	2.9	204.6	1799.8	0.02	2/2	$-1.35\cdot10^{-1}$	[374]
water	18.02	1.2047	#4	353.95	2425.67	0.045	1/1		[373]

#1 Association Scheme: acceptor/donor

#2 fitting method in this work: MM (Molecular Method), J-PM (Joint-Parameter Method)

#3 DNB=1,3-dinitrobenzene

#4 $\sigma_i = 2.7927 + 10.11\cdot\exp(-0.01775\cdot T[K]) - 1.417\cdot\exp(-0.01146\cdot T[K])$

Table 4.2. ePC-SAFT pure-component parameters and binary interaction parameters with water of charged molecules considered in this work. The parameters listed were obtained using Molecular Method (MM), Joint-Parameter Method (J-PM) in this work (TW) or they were taken from the literature.

Component	M [g·mol^{-1}]	m_i^{seg} [-]	σ_i [Å]	u_i/k_B [K]	ε^{AiBi}/k_B [K]	κ^{AiBi} [-]	N_i^{assoc} #1	$k_{ij\ water}$ (T=298.15 K)	q_i	*Ref.* #2
DNP-glycine$^-$	240.16	9.204	2.8635	216.96	2598.06	0.039	2/2	-2.29·10^{-2}	-1	TW[8] J-PM
DNP-alanine$^-$	254.18	9.819	2.9611	287.59	3176.6	0.082	2/2	-2.22·10^{-2}	-1	TW[8] J-PM
DNP-valine$^-$	282.24	11.839	2.9944	306.41	3183.8	0.039	2/2	-2.09·10^{-2}	-1	TW[8] J-PM
DNP-leucine$^-$	296.26	12.658	3.05	330	3600	0.02	2/2	-4.75·10^{-3}	-1	TW[8] J-PM
VB2$^+$	377.36	15.924	2.63	150.315	2548.107	0.034	5/5	-5.80·10^{-2}	1	TW[6] MM
VB2$^-$	375.36	15.924	2.63	150.315	2548.107	0.034	5/5	-6.10·10^{-2}	-1	TW[6] MM
VB3^{acid-}	122.11	8.0883	2.3522	209.045	1088.56	0.002	3/1	-6.30·10^{-2}	-1	TW[7] MM
VB9$^+$	442.40	16.717	2.6907	152.016	2379.471	0.034	8/4	-1.60·10^{-2}	1	TW[6] MM
VB9$^-$	440.40	16.717	2.6907	152.016	2379.471	0.034	8/4	-1.60·10^{-2}	-1	TW[6] MM
VB9^{2-}	439.40	16.717	2.6907	152.016	2379.471	0.034	8/4	-4.00·10^{-2}	-2	TW[6] MM
VB9^{3-}	438.40	16.717	2.6907	152.016	2379.471	0.034	10/2	-3.20·10^{-2}	-3	TW[6] MM
Citrate^{3-}	189.09	1.000	4.46	250				-2.2687·10^{-1}	-3	[375]
Tartrate^{2-}	148.07	1.000	4.49	200				-2.002·10^{-1}	-2	TW[7] MM
OH$^-$	17.01	0.416	1.6401	2444.756				-2.5·10^{-1}	-1	[303, 338]
Na$^+$	22.99	1.000	2.4122	646.05				4.60·10^{-4}	1	[303, 338]
K$^+$	39.10	1.000	2.9698	271.052				1.9972·10^{-1}	1	[303, 338]

#1 Association Scheme: acceptor/donor

#2 fitting method in this work: MM (Molecular Method), J-PM (Joint-Parameter Method)

Table 4.3 contains the binary interaction parameters between different species (neutral and charged) present in multicomponent aqueous systems considered in this work. Since, the two methods described in the following sections of this thesis (MM, J-PM) were used to model both neutral and charged components, for a better ordination, tables 4.1 - 4.3 are already given in this subchapter. Besides that, the tables contain association schemes that were established before the modeling since they are independent of the modeling

approach used. The method of their estimation is described in the following. The association schemes are required for most of the components considered in ePC-SAFT modeling in this work.

Table 4.3. ePC-SAFT binary interaction parameters k_{ij} between components in ATPS. The parameters listed were obtained using Molecular Method (MM) or they were taken from the literature.

Component	Na^+	K^+	OH^-	$Citrate^{3-}$	$Tartrate^{2-}$	PEG	*Ref.* [#1]
Na^+	-	-	0.649	-1	-1	0	[303, 375], TW[7] MM
K^+	-	-	1	0.237	-0.3	0.34	[303],TW[8] MM
$Citrate^{3-}$				-	-	0.1	TW[7] MM
$Tartrate^{2-}$				-	-	0.07	TW[7] MM
DNP-$glycine^-$	0.15	0.4		-	-	0.015	TW[8] MM
DNP-$alanine^-$	0.15	0.4		-	-	-0.035	TW[8] MM
DNP-$valine^-$	0.15	0.4		-	-	-0.033	TW[8] MM
DNP-$leucine^-$	0.15	0.4		-	-	-0.026	TW[8] MM
$VB2^-$	0	-		0.39	0.29	0.142	TW[7] MM
$VB3^{acid\ -}$	0	-		0.48	0.1	0	TW[7] MM
$VB3^{amide}$	0	-		0	-0.25	0	TW[7] MM
$VB9^{2-}$	0	-		0.92	0.6	0.159	TW[7] MM
$VB9^{3-}$	0	-		0.95	0.45	0.11	TW[7] MM
VB12	-0.2	-		-0.168	-0.08	0	TW[7] MM

[#1] fitting method in this work: MM (Molecular Method)

Before the modeling the association schemes N_i^{assoc} of each associating component *i* (DNP-AA, vitamin) were assigned (table 4.1 and table 4.2). Also, prior to the parameter estimation the charge q_i of each charged component was set as shown in table 4.2. For water, the 2B association model has been used according to the literature [373]. Even though the 2B model is less realistic than the 4C model, the 2B model has been recommended in the literature for modeling thermodynamic properties of biological solutions [79, 293].

The association schemes of DNP-AA and vitamins were set as a compromise between the best modeling result and the counted numbers of possible acceptor and

donor sites. The decision on choosing the same number of donor sites as acceptor sites and equal scheme for all DNP-AA was taken based on association scheme (1/1) published for parent aliphatic AA by Held *et al.* [79]. Because of the high structural diversity of the considered vitamins, a high number of different kinds of interactions exist for every vitamin, and the association schemes were set for each molecule individually. For this purpose, available online tools which characterize the molecules through chemical structure analyses, e.g., *Chemicalize* [173] or *PubChem database* [376] were used. Analyzing the vitamins with these tools yielded the number of association sites that are compared in table 4.4. For VB12, the molecule was too complex for the molecular structure analysis and the result could not be obtained with *Chemicalize*.

Table 4.4. Comparison of association sites (A=acceptor/D=donor) assigned to vitamins in this work (TW) with schemes obtained using online tools Chemicalize [173] and PubChem database [376].

Component	*Chemicalize*	*PubChem*	*TW*
VC	5/4	6/4	4/1
VB2	9/5	7/5	5/5
$VB3^{acid}$	3/1	3/1	3/1
VB9	12/6	9/6	8/4
VB12	n.a.	21/9	23/6

Overall, it can be observed that the association sites that were set to the vitamins are generally in good agreement to the association sites obtained by counting the theoretically maximal acceptor and donor sites using *Chemicalize* or *PubChem database*.

Further, the association schemes of both VB2 and VB9, for charged species: VB^{+}, VB^{-}, and VB^{2-}, were set equal to the scheme of the neutral pendants VB (neutral). For VB9 (possible four dissociation steps, section 2.3.1), a different association scheme was required for the species $VB9^{3-}$. On the one hand, the donor sites of $VB9^{3-}$ were reduced by two ($4 \rightarrow 2$) compared to neutral VB9. On the other hand, two new acceptor sites were considered ($8 \rightarrow 10$) compared to neutral VB9. Illustration of this mechanism in simplified form is shown in figure 4.1. This was found to be required to quantitatively model the pH-dependent solubility of negatively charged VB9 at pH > 6.5 ($VB9^{3-}$ not negligible).

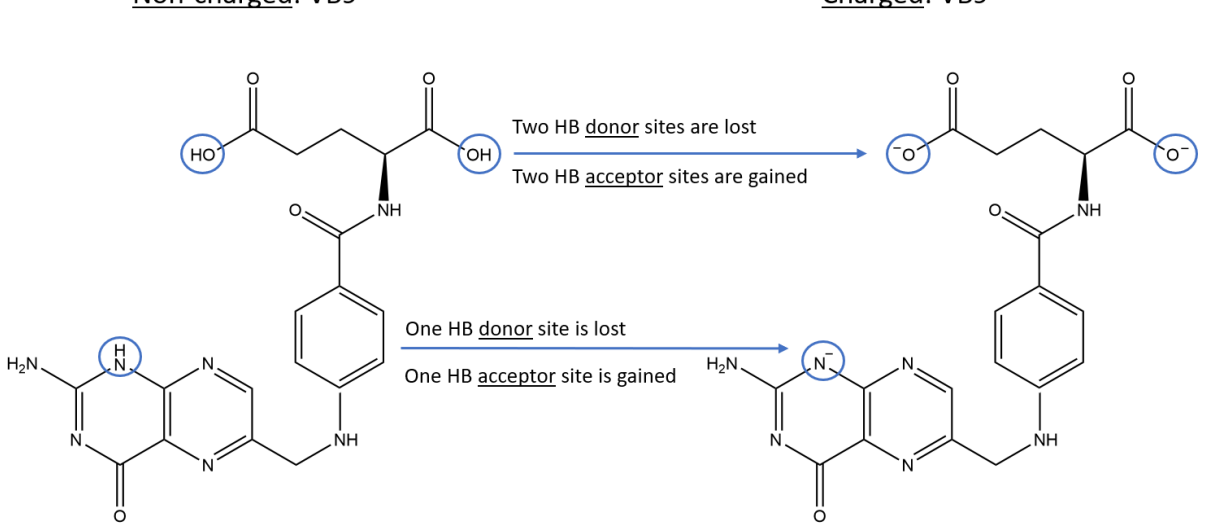

Figure 4.1. Influence of the different species on the association scheme of VB9 (neutral VB9 vs ionized species VB9^{3-}) according to the dissociation steps postulated by Szakács *et al.* [161].

4.1.1. Molecular Method (DNP-AA, Vitamins)

The methodology of MM for estimating the pure-component and binary interaction parameters k_{ij} was applied for neutral and charged water-soluble vitamins, as well as for salt ions and negatively charged DNP-AA. Different physicochemical properties were used to estimate ePC-SAFT parameters, e.g. liquid density, osmotic coefficients, solubility. For fitting the parameters of the compound to experimental data, the objective function is minimized with a Levenberg-Marquardt algorithm (the damped least-squares method) as shown in equation (4.13). In this expression y_n is the property and NP_y stands for the number of data points. The superscripts in y_n express the origin of data: ePC-SAFT modeling (*mod*) and experimental (*exp*).

$$\mathrm{OF} = \sum_{\mathrm{n=1}}^{y_n} \sum_{\mathrm{k=1}}^{\mathrm{NP}_y} \left(1 - \left(\frac{y^{mod}}{y^{exp}}\right)_{\mathrm{k}}\right)^2 \tag{4.13}$$

The accuracy of modeling results is evaluated in this work using an average relative deviation expressed in % (ARD%) or an average absolute deviation (AAD). Both can be calculated according to equations (4.14) and (4.15), respectively. While equation (4.14) was applied for evaluation of the modeling results in which experimental ρ and ϕ were used, expression (4.15) was applied to calculate the deviations in modeling of ternary LLE data. In equation (4.15) the number of tie-lines, phases and components is represented by l, m and n, accordingly.

$$\mathrm{ARD\%} = 100 \cdot \frac{1}{\mathrm{NP}_y} \cdot \sum_{\mathrm{k}=1}^{\mathrm{NP}_y} \left| 1 - \left(\frac{y^{mod}}{y^{exp}} \right)_{\mathrm{k}} \right| \tag{4.14}$$

$$\mathrm{AAD} = \frac{1}{\mathrm{l}} \cdot \frac{1}{\mathrm{m}} \cdot \frac{1}{\mathrm{n}} \cdot \sum_{\mathrm{i}=1}^{\mathrm{l}} \sum_{\mathrm{z}=1}^{\mathrm{m}} \sum_{\mathrm{k}=1}^{\mathrm{n}} \left| (y^{exp} - y^{mod})_{\mathrm{i,z,k}} \right| \tag{4.15}$$

Fitting pure-component parameters and k_{ij} to ρ and ϕ: vitamins (neutral) and organic salt ions

The pure-component and k_{ij} parameters for neutral vitamins considered as associating components (table 4.1), as well as for non-associating Tartrate^{2-} (table 4.2), were fitted to solubility-independent experimental densities ρ and osmotic coefficients ϕ. Regarding vitamins, experimental data required for the fitting were found in the literature only for VC and VB3 [180, 181]. Data for tartrate salts are widely available, thus, the parameters for Tartrate^{2-} were established by fitting them to experimental ρ and ϕ of binary water – Na_2Tartrate solutions reported in the literature [269, 377]. Since the experimental description of vitamin properties is relatively scarce in the literature, both ρ and ϕ measurements were carried out in the present study according to procedures described in section 3.2.4. Experimental ρ and ϕ of aqueous vitamin solutions and ARD% for this modeling are included in the Appendix (A3). As an example, the outcome after the application of this modeling method can be also evaluated based on data shown in figure 4.2(a-c).

For a better visibility, the densities of aqueous solutions containing VC are plotted in a separate figure 4.2b. The highest average relative deviation among experimental and ePC-SAFT modeled densities was ARD%=0.16 (VC). This result is still of high accuracy. Among all vitamins studied in this work, VC is the most soluble and liquid densities of water + VC have been already reported in the literature for a wide range of concentrations [180]. It can be observed from figure 4.2(b) that literature data and data from this work are in good agreement. The lowest ARD% between PC-SAFT and experimental liquid densities was calculated for water + VB2 solution (ARD%=0.0007). This is because ePC-SAFT parameters for VB2 were fitted solely to densities of binary systems water – VB2.

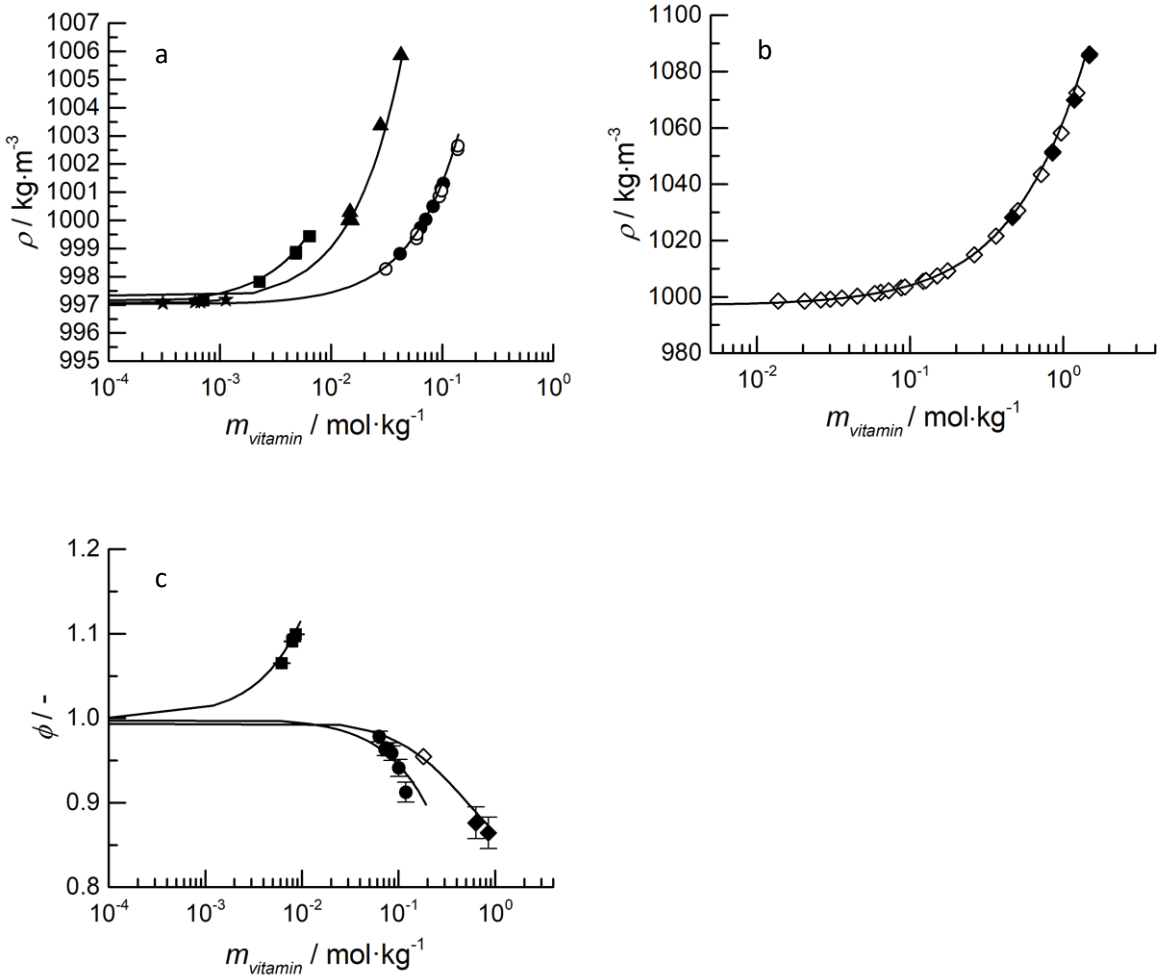

Figure 4.2. Application of MM to obtain ePC-SAFT pure-component and $k_{ij\ water}$ parameters for neutral vitamins; The parameters were fitted to densities ρ (a,b) and osmotic coefficients ϕ (c) of binary systems water–vitamin. They are plotted versus vitamin molality $m_{vitamin}$, at T = 298.15 K, p = 1 bar. Full symbols: data from this work for VC (◆), VB2 (★), VB3 (●), VB9 (▲), and VB12 (■). Open symbols: data from the literature for VC (◇), VB3 (○), refs [180, 181]. Lines: ePC-SAFT modeling using parameters from table 4.1.

Osmotic coefficients of water – VB2 were not accessible experimentally due to the very low solubility of VB2. The same procedure was applied to another practically insoluble vitamin VB9. Nevertheless, at very low concentrations, osmotic coefficients of aqueous solutions containing uncharged components are very close to one. For this reason, ϕ_{VB2} and ϕ_{VB9} were assumed to be one at maximum VB2 and VB9 molality (i.e., at the solubility limit at T=298.15 K). This assumption was an additional condition in the parameter fit for VB2 and VB9. Even addition of KOH to VB2 and VB9 solutions did not allow for reliable experimental osmotic coefficients. The lowest ARD% of modeled osmotic coefficients

(ARD%=0.9) was observed for the most soluble vitamin studied in this work (VC). To accurately describe the interactions in aqueous solutions containing organic salts, e.g. Na_2Tartrate, introducing an additional k_{ij} (beside $k_{ij\ water}$) between salt cation (e.g. Na^+) and salt anion (e.g. $Tartrate^{2-}$) was very relevant (table 4.3) [375].

The results of the modeling obtained with parameters from table 4.2 and table 4.3 for aqueous solutions containing $Tartrate^{2-}$ are presented in figure 4.3(a-b). They are in good agreement to experimental data [269, 377]. The parameters for Na^+ were already available in the literature [303, 338]. The average relative deviation (ARD%) between experimental and ePC-SAFT modeled densities yields ARD%=0.38. The deviations between experimental and modeled osmotic coefficients (ARD%=3.46) are also acceptable as experimental uncertainty is in the same order of magnitude.

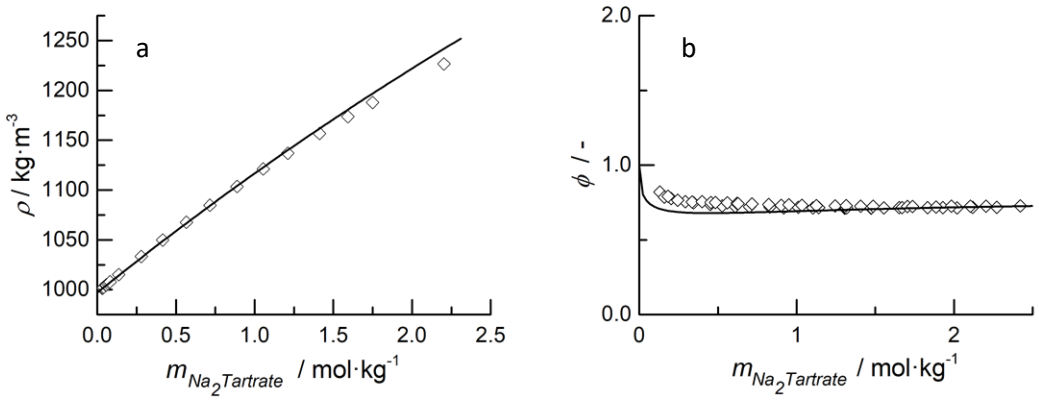

Figure 4.3. Application of MM to obtain ePC-SAFT pure-component and k_{ij} parameters for $Tartrate^{2-}$. Parameter fitting to (a) densities ρ and (b) osmotic coefficients ϕ of binary water – Na_2Tartrate system vs molality of Na_2Tartrate $m_{Na_2Tartrate}$, at T = 298.15 K, p = 1 bar. Points: experimental data from the literature [269, 377]. Lines: ePC-SAFT modeling (parameters from table 4.2 and table 4.3).

The relevance of introducing k_{ij} between the salt ions (table 4.3) can be also confirmed with the results of modeling carried out for other salts, e.g. containing K^+ and organic anion ($Citrate^{3-}$, $Tartrate^{2-}$) as presented in figure 4.4(a-b). Since the parameters for K^+ and $Citrate^{3-}$ have been already published in the literature [303, 338, 375] and the parameters for $Tartrate^{2-}$ were estimated in this work as shown in the previous example (figure 4.3), the only parameter fitted in this step was k_{ij} between K^+ and organic anion. Experimental data used for this modeling were ρ and ϕ of binary systems: water - K_3Citrate and water - K_2Tartrate [378-380]. The deviations of experimental and obtained

with ePC-SAFT for densities (water - K_2Tartrate: ARD%=1.73; water - K_3Citrate: ARD%=0.26) and osmotic coefficients (water - K_2Tartrate: ARD%=4.35; water - K_3Citrate: ARD%=4.45) were of reasonable magnitude.

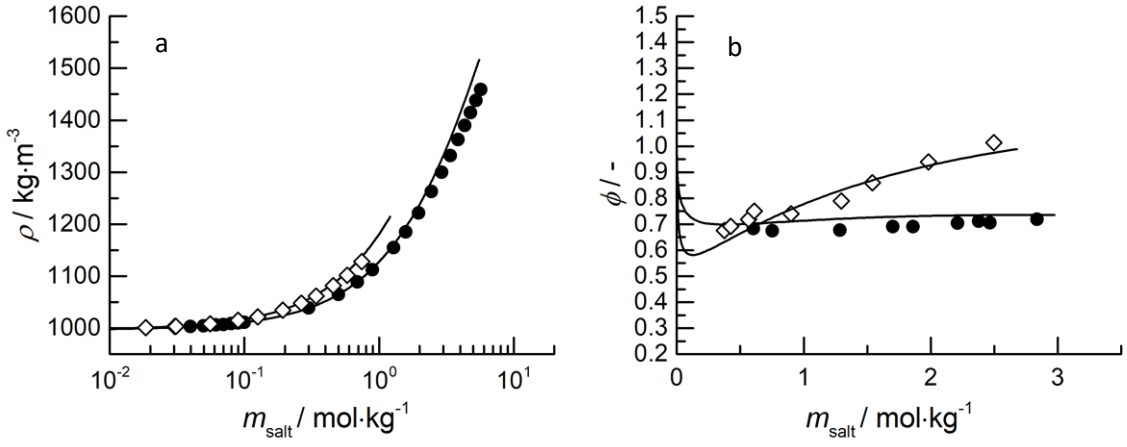

Figure 4.4. Application of MM to obtain ePC-SAFT pure-component and k_{ij} parameters for K_2Tartrate and K_3Citrate. Parameter fitting to (a) densities ρ and (b) osmotic coefficients ϕ of binary water – K_2Tartrate (◇) and water - K_3Citrate (●) system. Results plotted against molality of K_2Tartrate $m_{K_2Tartarte}$ and K_3Citrate $m_{K_3Citrate}$, at T = 298.15 K, p = 1 bar. Points: experimental data from the literature [378-380]. Lines: ePC-SAFT modeling (parameters from table 4.2 and table 4.3). The range of m_{salt} for modeling of ϕ was adjusted to the m_{salt} that could be possibly found in the salt-rich phase of ATPS. According to binodal data it can be assumed that m_{salt} in bottom phase is >10 wt-% [2].

Fitting k_{ij} between water and charged species of vitamins and DNP-AA

Each binary interaction $k_{ij\ water}$ parameter for charged DNP-AA or vitamin species (table 4.2) was adjusted to a single experimental solubility data point measured at T = 298.15 K and p = 1 bar. The $k_{ij\ water}$ was not treated as an independent variable. Rather, it was found to depend on the kind of species. The $k_{ij\ water}$ accounted simultanously for the thermodynamic non-ideality with activity coefficients of the species and thermodynamic constants $K_{a,th}$, according to Lange *et al.*[381]. For this modeling, a pH was chosen at which only the respective species was present exclusively or (in the case of VB9) where the species j was at high content ($\alpha_j \rightarrow 1$). The thermodynamic basis for the calculation of solubility equilibria with ePC-SAFT has been given in section 2.2.1. It is important to mention that equations (2.25) and (2.26) (for the conversion x_0^L to m_0^L) were

used to predict the solubility m_i^L of component *i* at the pH at which $m_i^L = m_0^L$ (m_0^L is the intrinsic solubility). At this pH, just neutral species are present in the solution and solubility m_0^L can be predicted using parameters fitted to solubility-independent properties (figure 4.2). At pH at which also charged species are expected, the solubility m_i^L of component *i* (DNP-AA or vitamin) can be predicted according to solubility equations (2.41), (2.54), (2.58), (2.63), and (2.69). To account for solubility change over pH, the values of thermodynamic dissociation constants $K_{a,th}$ need to be estimated(table 4.5). This can be done using solubility equations (2.41), (2.54), (2.58), (2.63), (2.69). Thus, aqueous solubility m_i^L and corresponding pH are substituted in these expressions with experimental solubility data. Then, the activity coefficients of the species γ_j^L and intrinsic solubility m_0^L (calculated according to equation (2.25) and (2.26)) are introduced. A comparison of $K_{a,th}$ and K_a allows the conclusion that the behavior of DNP-AA in aqueous solutions might have greater deviations from ideality than of vitamins in aqueous solutions.

Table 4.5. Dissociation constants (K_a and $K_{a,th}$), T=298.15 K. K_a values were calculated from pK_a reported in the literature [6, 8, 130, 161, 166-171, 173] or estimated [6, 8]. pK_a for this calculation are included in table 2.1. $K_{a,th}$ were calculated from solubility equations (2.41), (2.54), (2.58), (2.63), (2.69).

Compound	K_{a_1}	$K_{a_1,th}$	K_{a_2}	$K_{a_2,th}$	K_{a_3}	$K_{a_3,th}$	K_{a_4}	$K_{a_4,th}$
VB2	$2.00 \cdot 10^{-2}$	$7.94 \cdot 10^{-2}$	$7.94 \cdot 10^{-7}$	$2.00 \cdot 10^{-7}$	$6.31 \cdot 10^{-11}$	$6.31 \cdot 10^{-11}$		
VB3^{acid}	$8.51 \cdot 10^{-3}$	$2.24 \cdot 10^{-2}$	$1.55 \cdot 10^{-5}$	$6.31 \cdot 10^{-6}$				
VB9	$4.17 \cdot 10^{-3}$	$2.24 \cdot 10^{-3}$	$4.57 \cdot 10^{-4}$	$9.02 \cdot 10^{-5}$	$2.00 \cdot 10^{-5}$	$3.16 \cdot 10^{-7}$	$7.94 \cdot 10^{-9}$	$6.31 \cdot 10^{-9}$
DNP-glycine	$1.58 \cdot 10^{-3}$	$1.00 \cdot 10^{-4}$						
DNP-alanine	$3.16 \cdot 10^{-4}$	$5.60 \cdot 10^{-5}$						
DNP-valine	$1.26 \cdot 10^{-3}$	$1.40 \cdot 10^{-5}$						
DNP-leucine	$1.58 \cdot 10^{-3}$	$3.50 \cdot 10^{-4}$						

In this modeling, the $k_{ij\ water}$ was the only parameter fitted for charged species. The pure-component parameters for charged species were assumed to be equal to their neutral pendants. The molar masses *M* of each species were corrected by the number of protons (added or removed compared to the neutral species). The charge *q* of each charged species was considered explicitly in the Debye–Hückel energy contribution a^{ion}

to a^{res} (equation (2.80)). The association schemes for charged molecules were chosen according to the procedure provided already in this chapter. This modeling was performed using single experimental data points and the major purpose of the procedure used for the parameter fit was to later predict the whole pH-solubility profile at a given pH range (approximately 2<pH<7). This could be done only while having the parameters established for each species (table 4.2). Thus, the accuracy (expressed in ARD%) of the method considered in the perspective to its application is evaluated just in the following chapter 8.

Fitting k_{ij} to ATPS: components in ATPS

The k_{ij} helps describing the non-ideality caused among others by interactions in ATPS between the components forming the system (PEG – salt ions), as well as of interplay of a solute (in this work species of DNP-AA and vitamin) with PEG and with salt ions. The liquid-liquid equilibrium (LLE) and partition coefficients data required for this modeling were obtained according to the methods described in sections 3.2.2 and 3.2.3. The modeling procedure of LLE using isoactivity criterion and methodology applied for partition coefficient determination have been provided in section 2.2.2.

The k_{ij} values between PEG and salt ions (Na^+, K^+, $Citrate^{3-}$, $Tartrate^{2-}$) were estimated by fitting them just to one tie-line (TL) of each selected ATPS. In total, three ATPS (and accordingly to this just three TL in total) were used for the fitting. ATPS considered for the modeling contained PEG (M_{PEG} = 4000 g·mol^{-1}) and salt ($Na_3Citrate$, $K_3Citrate$, $Na_2Tartrate$). Since at the pH of ATPS (pH∼8), all salts considered in the present work are solely present as fully dissociated spherical species, methodology for LLE modeling accounts in this thesis just for fully dissociated salt species and homosegmented PEG. This conventional strategy used in this work (instead of more complex approach from the literature [280]) allows later predicting the LLE and can be applied for partitioning predictions with more reasonable computing time. A very high computational effort related to ePC-SAFT copolymer approach from the literature [280] was the factor that has limited further application of this approach in this work for predicting the partitioning of complex molecules, such as DNP-AA and vitamins that dissociate into different ionic species in ATPS.

To eliminate additional effects (e.g. precipitation) during the partitioning that might be induced by higher solute concentration, aqueous solute solution added to ATPS contained low concentration of DNP-AA or vitamin. For this reason, modeling of partitioning involved the activity coefficient at infinite dilution (section 2.2.2). At pH of ATPS (pH~8), the partitioned solutes considered in this work are present as differently charged species. According to Lange [328] the dissociation equilibria of components at infinite dilution can be calculated with pK_a (K_a) values (widely available in the literature). This means, that in this particular case equations (2.74) - (2.76) may be used to calculate species distribution of DNP-AA. Based on pK_a data included in table 2.1 and theoretical basis given in sections 2.3.1 - 2.3.2, at this pH range, DNP-AA are negatively charged and present as DNP-AA$^-$ (q = -1, α_{DNP-AA^-}≈1). The two pK_a values for DNP-AA (namely, DNP-valine, DNP-leucine) provided in table 2.1 were adjusted to experimental pH-dependent solubility data. The fitting was done in a way that the pH-solubility profiles calculated with H-H equations (section 2.3.1) match experimental data measured at different pH values. A more complex situation regarding the species presence is observed for vitamins due to the higher variety of their pK_a values (table 2.1). The mean charges of all vitamin species occurring in ATPS at given pH can be depicted in figure 4.5.

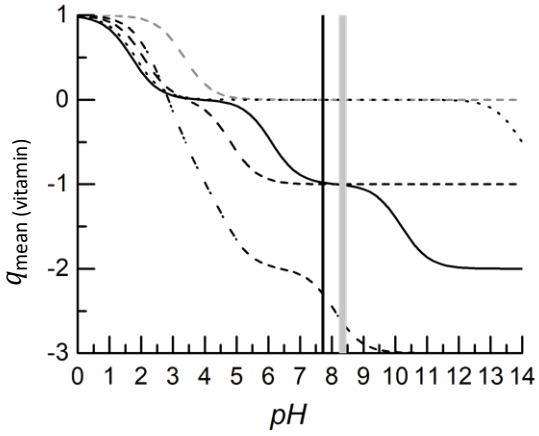

Figure 4.5. The mean charge q_{mean} of all vitamin species in aqueous solution (calculated from the ionic distribution using pK_a values from table 2.1) as a function of pH. Lines: dashed - VB3 (gray – VB3^{amide}, black – VB3^{acid}), solid - VB2, dashed-dot - VB9, dotted - VB12. The pH range in ATPS is shown as vertical lines: PEG - Na_3Citrate (gray), PEG - Na_2Tartrate (black). The thickness of the vertical lines represents the range of pH in considered ATPS (Appendix, A4).

The data in figure 4.5 were calculated using equations derived as presented in section 2.3.2 Thus, based on pK_a values vitamin species kinds present in ATPS are VB2, $VB3^{acid-}$, $VB3^{amide}$, $VB9^{2-}$, $VB9^{3-}$, VB12.

The non-ideality caused by interactions between a solute and ATPS phase formers was described with ePC-SAFT pure-component parameters and k_{ij} parameters fitted just to one $K_i^{exp,x}$ of vitamins and DNP-AA partitioned in two (for vitamins) or three (for DNP-AA) PEG 6000 - salt (vitamins: $Na_3Citrate$, $Na_2Tartrate$, DNP-AA: $Na_3Citrate$, $K_3Citrate$, $Na_2Tartrate$) ATPS. The k_{ij} was fitted just to $K_i^{exp,x}$ obtained in one TL of ATPS (the one closest to the binodal curve). In all, only two (for vitamins) or three (for DNP-AA) $K_i^{exp,x}$ values for each component were used in this modeling. It is important to mention that all k_{ij} between components present in ATPS were introduced solely to improve the description of the interactions that can occur in ATPS. Also, like the previously described fitting method, the accuracy (expressed in AAD for LLE and ARD% for experimental and predicted K) of the methods considered in the perspective to their application is evaluated just in the following chapters of this thesis (chapters 9 and 10).

4.1.2. Joint-Parameter Method (DNP-AA)

The pure-component and $k_{ij\ water}$ parameters for neutral DNP-AA included in table 4.1 were estimated using the Joint-Parameter Method (J-PM). The J-PM has been designed in this work specifically for the modeling of these compounds. The sets of ePC-SAFT parameters for neutral DNP-AA were acquired by combining ePC-SAFT parameters of amino acids (AA; table 4.1) published previously by Held *et al.* [79] and ePC-SAFT parameters for dinitrobenzene (DNB; estimated in this study and listed in table 4.1). The parameters for DNB were modeled in the present work using experimental data taken from the literature (liquid densities ρ, vapor pressures p) [382, 383]. The results of DNB modeling that followed the fitting procedure described already in the previous section (4.1.1) are presented in the Appendix (A5).

In the J-PM the number of segments of DNP-AA (m_i) is the number of segments of AA and DNB summed together. The segment diameter (σ_i) is an arithmetic average of segment diameters of AA and DNB. As mentioned at the beginning of section 4.1, also association schemes were changed (AA: 1/1, DNP-AA: 2/2) in order to account for additional donor and acceptor sites and this is related to the presence of aromatic ring in

DNP-AA structure. The dispersion energy (u_i), the association-energy parameter (ε^{AiBi}), the association-volume parameter (κ^{AiBi}), are assumed to be the same as for AA. The binary interaction parameters with water ($k_{ij\ water}$) for DNP-AA were set to zero.

The J-PM overcomes the problem related to the unavailability of reliable experimental data for low-soluble DNP-AA. Due to poor solubility, the osmotic coefficients could not be measured in this work as the detection limits for this technique have not been met. However, another solubility-independent physicochemical property – liquid density, was used to characterize the solutions containing DNP-AA. The densities of water – NaOH – DNP-AA solutions were measured in this work at T=298.15 – 318.15 K according to the procedure provided in section 3.2.4. Nevertheless, density data was not enough to obtain reliable parameter sets with MM and was used just for validation of ePC-SAFT parameters obtained with J-PM. The results of the validation are presented in figure 4.6.

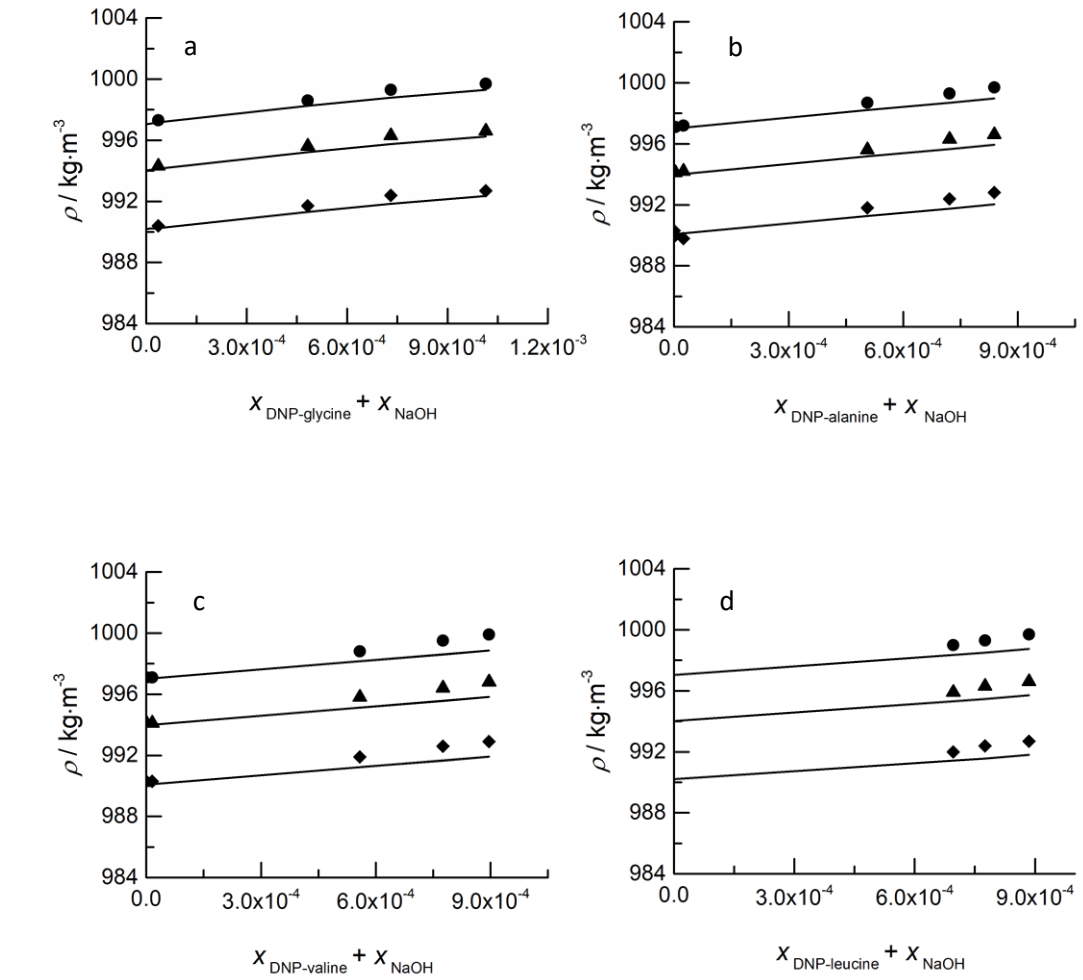

Figure 4.6. Validation of pure-component parameters fitted with J-PM: densities ρ of ternary solutions: water – NaOH - DNP-AA vs. mole fractions of DNP-AA ($x_{DNP\text{-}AA}$) + NaOH (x_{NaOH}), at T=298.15 K [●], T = 308.15 K [▲], and T = 318.15 K [◆], p=1 bar. Symbols: experimental, solid lines: ePC-SAFT modeling using parameters from table 4.1 and table 4.2.

ePC-SAFT parameters used to calculate the density of these ternary solutions are included in table 4.1 (DNP-AA, water) and table 4.2 (Na^+, OH^-). The experimental density data and ARD% values for the modeling are included in the Appendix (A3). The highest deviation calculated with equation (4.14) for densities measured at the temperature range of T=298.15 – 318.15 K was ARD%=0.08 (water – DNP-leucine – NaOH). The average value of relative deviation (ARD%=0.05) calculated for all amino acids together was equal for each temperature considered in this test (T=298.15 K, T=308.15 K, and T=318.15 K).

4.2. Caloric properties

Melting properties necessary for SLE modeling that were taken from the literature or estimated in this work are listed in table 4.6. For DNP-AA and the least soluble vitamins among all considered in this study, namely VB2, VB9, and VB12, it was not possible to find all required melting properties in the literature.

Table 4.6. Melting properties of DNP-AA, DNB, and vitamins, obtained from the literature, or estimated in this work (TW).

Component	$T_{m,i}$ [K]	$\Delta_{cr}^{L}H_{m,i}^{0}$ [kJ/mol]	$\Delta_{cr}^{L}Cp_{m,i}^{0}$ [J/(mol·K)]	*Ref.*
DNP-glycine[#1]	478.15	27.02	n.a.	TW, [127, 128, 130]
DNP-alanine[#1]	451.15	25.49	n.a.	TW, [127-130]
DNP-valine[#1]	458.15	25.89	n.a.	TW, [127-129]
DNP-leucine[#1]	476.15	26.9	n.a.	TW, [127, 128]
DNB	363	17.36	60.84	[384-386]
VC[#2]	465.15	29.12	43	TW, [64]
VB2[#1]	553.15	31.25	n.a.	TW, [183]
VB3^{acid}	509.91	28.2	38	[150, 182]
VB3^{amide}	401.15	28	78.12	[65]
VB9[#1]	523.15	29.56	n.a.	TW, [184]
VB12[#1]	665.15	37.58	n.a.	TW, [387]

[#1] $\Delta_{cr}^{L}H_{m,i}^{0}$ calculated in this work (TW) with Walden Rule ($\Delta_{cr}^{L}H_{m,i}^{0} = \Delta_{cr}^{L}S_{m,i}^{0}\cdot\Delta T_{m,i}$) using an established value $\Delta_{cr}^{L}S_{m}^{0}$ = 56.5 J/(mol·K)

[#2] $\Delta_{cr}{}^{L}Cp_{m}{}^{0}$ estimated in this work (TW) using solubility data in T = 293.15–323.15 K.

While melting points $T_{m,i}$ were in general available in the literature for all components considered in this work, the melting enthalpies $\Delta_{cr}^{L}H_{m,i}^{0}$ needed to be estimated in this work using Walden Rule [388]. This method relies on the estimation of $\Delta_{cr}^{L}H_{m}^{0}$ using the average value of melting entropies of some organic compounds (among others 1,3-chloronitrobenzene which has a similar structure as DNB). Walden Rule has been used in previous solubility studies and it seems to be appropriate also for the purpose of this work [82]. The reason for obtaining data with this technique is the difficulty in getting reliable experimental melting enthalpy data. Also, according to observation reported in the previous publication for DNP-AA, some molecules can course

decomposition while melting [129]. This inconvenience is also expected to occur for vitamins [151, 389-392]. The change of heat capacity $\Delta_{cr}^{L}Cp_{m,i}^{0}$ could be provided only for VC, VB3^{acid} and VB3^{amide}. That is, for all four DNP-AA, VB2, VB9, and VB12 the value had to be neglected in the modeling. $\Delta_{cr}^{L}Cp_{m,i}^{0}$ was fitted with ePC-SAFT to experimental solubility data in temperature range T = 293.15–323.15 K from the literature [149].

5. Experimental Aqueous Solubility of Biomolecules

This chapter presents experimental aqueous solubility results measured for DNP-AA and vitamins. For the correlation and evaluation of experimental data approaches based on the theoretical basis from chapter 2 were used. These were the H-H equation-based solubility equations derived for the studied components and expressions for the species distribution calculations. In the following, the effects on solubility in water caused by different factors (pH, temperature, covitamin presence) were discussed.

5.1. Experimental Results: Amino Acid Derivatives

This section presents experimental solubility results which were obtained for DNP-AA (DNP-glycine, DNP-alanine, DNP-valine, DNP-leucine) at constant temperature T=298.15 K±0.1 K and pressure p=1 bar, according to the methodology given in section 3.2.1. The discussion given in the following sections 5.1.1-5.1.2 covers the evaluation of the solubility of a homologous series of DNP-AA (section 5.1.1) and shows the pH influence on the course of experimental solubility curves of DNP-AA (section 5.1.2). The results of the measurements of DNP-AA solubility in water (T=298.15±0.1 K and p=1 bar) accompanied by ARD% values, with and without the usage of pH-adjusting agents, are presented in Appendix (A6). Additionally, section 5.1.3 provides a reasoning of studying in this work the solubility of DNP-AA at constant temperature (T=298.15 K±0.1 K) by providing a brief comparison of temperature vs pH effect on solubility. Data required for this analysis are also included in Appendix (A6, table A6.3).

Experimental measurements were an essential part of the present work that allowed achieving the objectives of the study. This subchapter refers to experimental data measured in this work that for clarity reasons were placed into Appendix (A6). The discussion presented in the following uses the figures based on the results of multiple measurements that were grouped into tables A6.1, A6.2, and A6.3, in the Appendix (A6). It was done according to the scheme shown in figure 5.1 that has been provided with the intention to facilitate finding the experimental background of data plotted and discussed in the next sections (5.1.1, 5.1.2, 5.1.3).

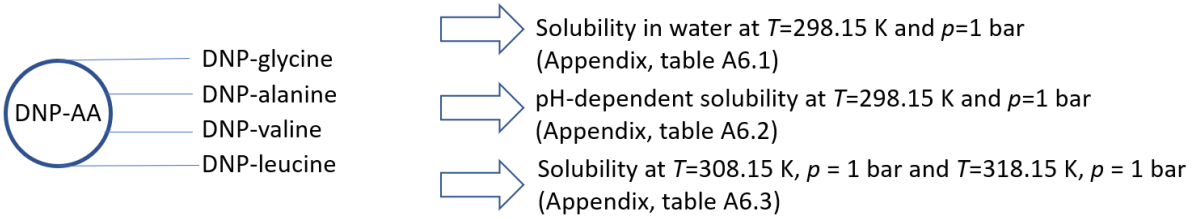

Figure 5.1. Experimental solubility data measured for DNP-AA in this work plotted in figures and discussed in subchapter 5.1 (Appendix).

5.1.1. Intrinsic Aqueous Solubility at Constant Temperature

At first, DNP-AA solubility measurements were performed without the addition of any acidity or basicity modifier (i.e. HCl, NaOH). The pH values of DNP-AA saturated

solutions were ≈ 3. At this pH, an aqueous solution of DNP-AA contains neutral and negatively charged species *j* (in this case *j* are neutral DNP-AA or charged DNP-AA$^-$). Each species of DNP-AA can differently behave in aqueous solution and thus lead to a difference in the experimental solubility value of DNP-AA, m^L_{DNP-AA}, that has been defined by expression (2.36). For a better understanding of DNP-AA solubility, very relevant at this point is to obtain equilibrium concentrations of DNP-AA in solutions where only neutral species occur. The solubility of neutral species of DNP-AA, called intrinsic solubility ($m^L_{0,DNP-AA}$), is defined with the previously shown equation (2.35). Intrinsic solubility data allows better solubility comparison within the DNP-AA homologous series since a saturated solution of each DNP-AA reaches different pH when being at equilibrium. Otherwise, the differences in DNP-AA experimental solubility m^L_{DNP-AA} caused by the pH effect could lead to wrong assumptions.

In this work, experimental solubility data m^L_{DNP-AA} (Appendix, A6) and pK_a values from table 2.1 substituted to solubility equation (2.38) based on idealized H-H equation allowed calculating the molality of neutral DNP-AA i.e. $m^L_{0,DNP-AA}$ if solely neutral species (DNP-AA) are present in the solution at equilibrium. The results of $m^L_{0.DNP-AA}$ calculations are included in the Appendix (table A6.4) and are graphically presented in figure 5.2.

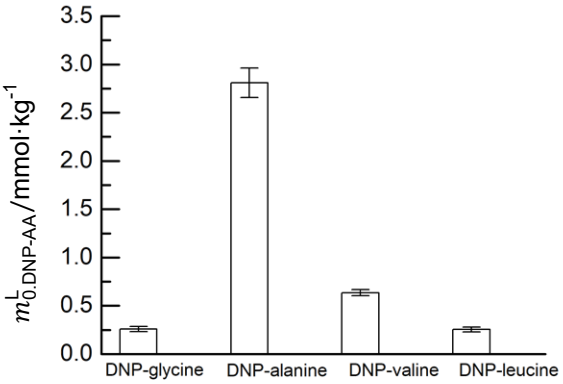

Figure 5.2. Intrinsic aqueous solubility of DNP-AA $m^L_{0,DNP-AA}$. Intrinsic solubility was calculated from experimental solubility data obtained in this work at T=298.15 K and p=1 bar and pH=3.42 (DNP-glycine), pH=3.09 (DNP-alanine), pH=3.17 (DNP-valine, DNP-leucine) (Appendix, A6.4). The calculations were performed using experimental solubilities, pK_a values from table 2.1, and solubility equation (2.38). ARD% of experimental solubility data ≤5.1.

Based on figure 5.2 the trend of DNP-AA solubility (assuming the same trend of $m^L_{0,DNP-AA}$ and m^L_{DNP-AA} at constant pH) is the following: $m^L_{DNP-alanine}$> $m^L_{DNP-valine}$ > $m^L_{DNP-glycine}$ and $m^L_{DNP-leucine}$. Undoubtedly, DNP-alanine is the most soluble among the four studied DNP-AA. However, which DNP-AA from the two least soluble (DNP-glycine or DNP-leucine) has higher solubility, is not clear enough from inspection of figure 5.2. The difficulty results from the fact that the differences in the solubility of these two DNP-AA are within experimental uncertainty (ARD%≤5.1). If comparing the results obtained in this work for DNP-AA with solubility data reported in the literature for aliphatic AA [81, 393, 394], it can be deducted that DNP-AA do not follow the same solubility trend as AA, i.e. $m^L_{glycine}$< $m^L_{L-alanine}$ < $m^L_{L-valine}$ < $m^L_{L-leucine}$. Besides that, the solubility of each DNP-AA is also of lower magnitude than for its parent aliphatic AA.

Possibly, the differences in solubility of DNP-AA are related to the molecular structure of the compound and the melting properties values (provided in table 4.6), which if different, will lead to different solubilities. More precisely, both melting points and solubility can be influenced by the intermolecular forces. Higher melting points result from stronger intermolecular bonds and this can mean that breaking them during dissolving can be also more troublesome. If the aqueous solubility trend of DNP-AA (decreasing m^L_{DNP-AA}) follows the reverse trend of melting properties (increasing $T_{m,DNP-AA}$), then DNP-alanine should be the one which dissolves easiest in water (the lowest $T_{m,DNP-AA}$). DNP-AA considered in this work with a second lower $T_{m,DNP-AA}$ is DNP-valine. In fact, this trend fits the result presented in figure 5.2. Melting properties and the solubilities of DNP-glycine and DNP-leucine are too alike to conclude if they follow this relation.

Even if there is some correlation in the trends of both properties $T_{m,DNP-AA}$ and m^L_{DNP-AA}, the reason of lower m^L_{DNP-AA} (if comparing to m^L_{AA} of aliphatic AA) lies mostly in lower similarity of DNP-AA to solvent (water) than it is for aliphatic AA - water. Nonpolar solutes dissolve better in nonpolar solvents, and in contrast to that polar solutes dissolve better in polar solvents [57]. The presence of the aromatic dinitrophenyl group in DNP-AA structure may likely influence the intermolecular forces in a way that dissolving DNP-AA in water is more difficult than dissolving aliphatic AA in water. For this reason, in that case, the similarity to the solvent (water) seems to play a major role. This can be explained by the hydrogen bonding of the molecule. A proof that the similarity of a

compound to solvent more probably relates to DNP-AA solubility can be provided if comparing the melting temperature of each DNP-AA ($T_{m,DNP-AA}$) and its parent aliphatic AA ($T_{m,AA}$). Each of these aliphatic AA has much higher melting temperature if comparing it to DNP-AA. However, parent aliphatic AA have higher solubility than DNP-AA. This comparison is based on melting data published for L-alanine and glycine by Chua *et al.* [395] and solubility data reported in the literature [168-170]. However, based on observations from this section, the conclusion is the following; if $T_{m,i}$ data is given for a separate group of homological compounds e.g. DNP-AA or AA series, then there can be found some indirect correlation for each series. Possibly this behavior originates from the presence of similar molecular interactions influencing both properties.

5.1.2. Influence of pH on Aqueous Solubility

The solubility of DNP-AA changes with pH in a way that the presence of ionized molecules (charged DNP-AA) with the pH increase of a solution, leads to an increase of DNP-AA solubility m^L_{DNP-AA}. This observation is based on figure 5.3 that shows experimental pH-dependent solubility data measured according the procedure from section 3.2.1 (Appendix, table A6.2). The pH-dependent theoretical solubility curves of DNP-AA were calculated using an idealized H-H-based approach by means of intrinsic solubility $m^L_{0,DNP-AA}$ (obtained using experimental data like described in the previous section 5.1.1), pK_a values from table 2.1, and solubility expression (2.38) that is based on H-H equation.

Figure 5.3 shows that there is a different acid-base character of DNP-AA if comparing it to aliphatic parent AA. These parent AA (glycine, alanine, valine, leucine) are known to be amphoteric[373, 393, 394, 396], while DNP-AA behave just like acids. Thus, the solubility of DNP-AA decreases at very low pH values. Also, Ramachandran *et al.* report that there are just single pK_a values for each DNP-AA [130]. According to the species distribution calculations performed using equations (2.70) and (2.71), around pH~6 all DNP-AA are solely present in an aqueous solution as negatively charged (DNP-AA$^-$) species (figure 2.1).

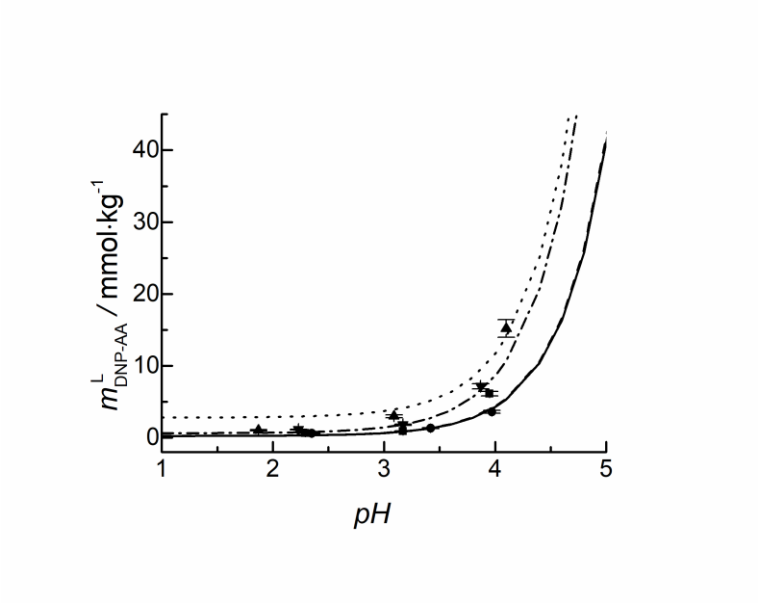

Figure 5.3. Experimental solubilities m^L_{DNP-AA} as a function of pH, determined at T=298.15 K and p=1 bar. The symbols: experimental data measured in this work (Appendix, table A6.2), the lines: pH-solubility curves calculated with H-H-equation-based expression (2.38); DNP-glycine (dashed), DNP-alanine (dotted), DNP-valine (dashed-dotted), DNP-leucine (solid).

5.1.3. Combined pH and Temperature Effect on Aqueous Solubility

The pH effect is often neglected in studies that report solubility data. In contrast to this, the temperature at which data have been determined is usually provided. The main purpose of this work was to study the solubility of DNP-AA at constant temperature T=298.15±0.1 K and p=1 bar. However, just to provide an idea of the importance of pH effect, figure 5.4 presents a comparison of solubility increase after pH and temperature change. Since solubility data of DNP-AA could not be found in the literature, only for the purpose of this comparison, the two additional aqueous solubility data points for each DNP-AA were measured in this work: at T=308.15±0.1 K, p=1 bar and T=318.15±0.1 K, p=1 bar (without additives). The procedure was analogous to the description provided in section 3.2.1. These data are also included in Appendix (table A6.3).

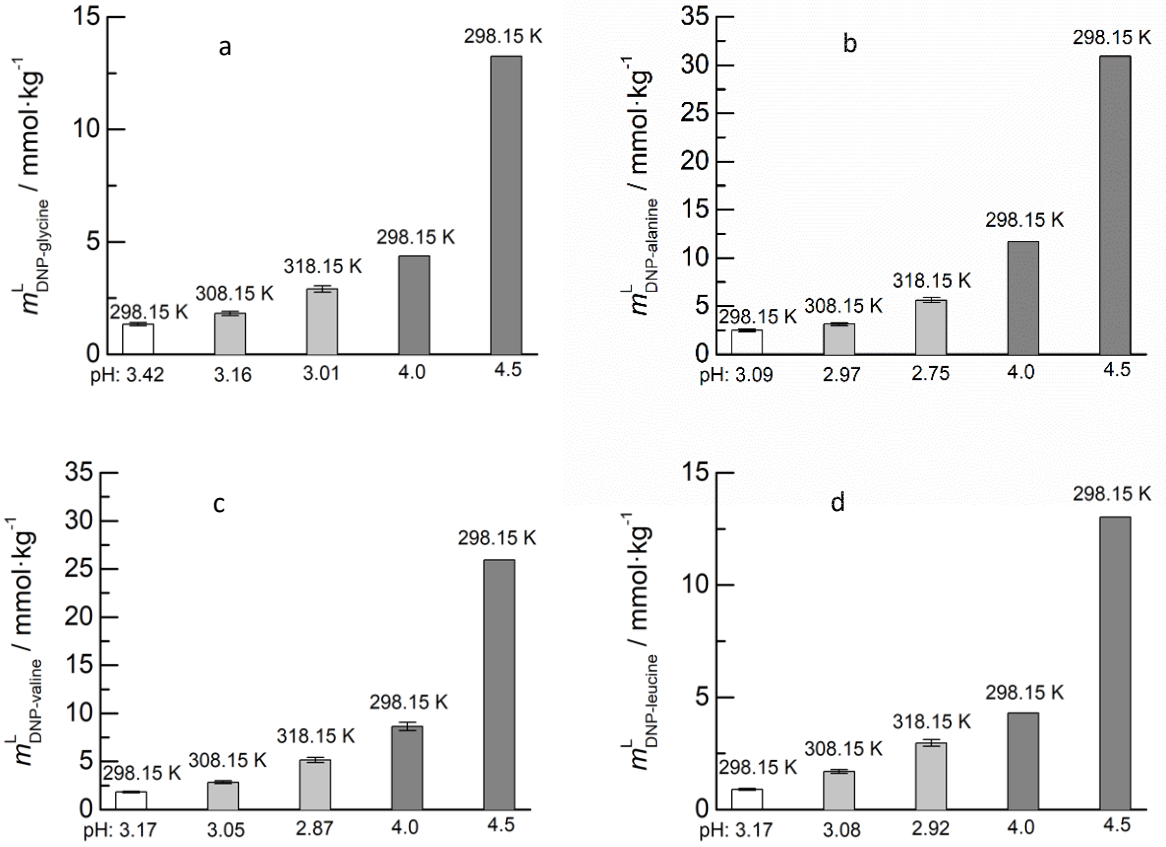

Figure 5.4. Influence of pH and temperature on experimental solubility m^L_{DNP-AA} of DNP-AA (a – DNP-glycine, b – DNP-alanine, c – DNP-valine, d – DNP-leucine). White bars: data obtained at T=298.15 K and p=1 bar, without any additive at pH of the saturated solution (pH ranged from 3.09 – 3.42). Light gray bars: data obtained at T=308.15 K, p=1 bar and T=318.15 K, p=1 bar, without any additive at pH of the saturated solution (pH ranged from 2.75 – 3.16). Dark gray bars: data obtained at T=298.15 K and p=1 bar, pH=4 and pH=4.5 (for better comparison between each DNP-AA), using solubility curves from figure 5.2 (calculated with equation (2.38) based on experimental solubility and pK_a values from table 2.1).

The main conclusion from figure 5.4 is that just a slight DNP-AA solubility increase is observed when changing the temperature of 10 K or 20 K. However, if the pH of DNP-AA solution increases only of 0.5 units (from pH = 4 to pH = 4.5), then more than a double increase of the DNP-AA solubility is obtained. Besides that, if the solutions are not buffered, then dissolving more acid leads also to a decrease in pH. Thus, increasing the temperature allows to dissolve more DNP-AA, but also leads to the pH change (as shown in figure 5.3 such pH change also causes DNP-AA solubility decrease). For this reason, if the measurements are performed at different temperatures and in non-buffered DNP-AA

solutions, the two effects of pH and temperature are coupled and hard to separate. These are the reasons why the temperature effect on DNP-AA solubility has not been further studied in this work and all the measurements were performed at constant temperature T=298.15±0.1 K.

5.2. Experimental Results: Water-Soluble Vitamins

This section provides the results of experimental aqueous solubility obtained for water-soluble vitamins VC, VB2, $VB3^{acid}$, VB9, VB12, at constant temperature T=298.15±0.1 K and pressure p=1 bar, according to the methodology given in section 3.2.1. The results are presented in the Appendix (A7) and accompanied by ARD% values. The discussion included in the following at first involves the evaluation of the vitamin solubility in saturated aqueous solutions without pH adjustment (5.2.1). In further sections, it also presented the influence of different factors on vitamin solubility such as pH (5.2.2), temperature and pH combined (5.2.3), and the presence of covitamin (5.2.4). The combined temperature and pH effects are based on a comparison of VC, VB2, and VB3 solubility data obtained in this work at T=298.15 K with solubilities reported in the literature [148-150] at different temperatures than in the present study.

This subchapter refers to experimental data measured in this work that for clarity reasons were placed into Appendix (A7). The discussion presented in the following uses the figures based on the results of multiple measurements that were grouped into tables A7.1, A7.2, and A7.3, in the Appendix (A7). It was done according to the scheme shown in figure 5.5 that has been provided with the intention to facilitate finding the experimental background of data plotted and discussed in the next sections (5.2.1, 5.2.2, 5.2.3, 5.2.4).

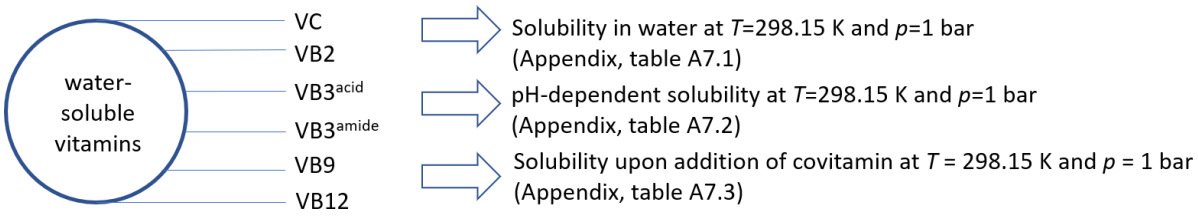

Figure 5.5. Experimental solubility data measured for water-soluble vitamins in this work plotted in figures and discussed in subchapter 5.2 (Appendix, A7).

5.2.1. Intrinsic Aqueous Solubility at Constant Temperature

At first, the vitamin solubility measurements were performed without the addition of acidity or basicity modifier (i.e. HCl, NaOH). The pH values of vitamin saturated solutions ranged from pH=1.93 to pH=5.75 (Appendix, table A7.1). Analogically to the reasoning given already in section 5.1.1 (concerning DNP-AA), for a better understanding of vitamin solubility, very relevant at this point is to consider equilibrium concentrations for vitamin neutral species in solutions where only these occur. Intrinsic solubility data allow better solubility comparison within different vitamins.

In this work, experimental solubility data $m^L_{vitamin}$ (Appendix, table A7.1) and pK_a values from table 2.1 substituted to accordingly transformed H-H-based solubility equations from section 2.3.1 allowed calculating the intrinsic solubility of vitamin $m^L_{0,vitamin}$, so the solubility if solely neutral vitamin species are present in the solution at equilibrium. Upon the pK_a values from table 2.1 and calculations of species distribution performed based on section 2.3.2, only the three vitamins VC, VB3^{acid}, and VB12, were present in their saturated solutions (VC: pH=1.94, VB3^{acid}: pH=3.42, VB12: pH=5.55) as solely neutral species. Thus, in this case, experimental solubility measured for VC, VB3^{acid}, and VB12 is intrinsic solubility.

The species distribution calculated for VB2 at non-adjusted pH of saturated solution showed that although this vitamin can exist in aqueous solution at pH=5.68 as both neutral and charged species (q=0, q=-1), experimental solubility value measured for VB2 is quite alike to intrinsic solubility value. Experimental value for VB2 is assumed to be close enough since ARD% between them (ARD%$_{max}$ between m^L_{VB2} and calculated $m^L_{0,VB2}$ ≤4.08) is in the range of experimental uncertainty (ARD%≤5). Thus, experimental solubility value measured for VB2 can be also be treated as intrinsic solubility.

More troublesome situation than in above cases concerns VB9, which in its saturated solution (pH=4.28) was present almost solely as charged species (q=-1, q=-2). Since VB9 is only marginally soluble in water ($m^L_{VB9} = 1.07 \cdot 10^{-4}$ mol · kg^{-1}), a higher experimental deviation is expected. This can be confirmed with a high divergence in experimental solubility values reported in the literature [148]. The experimental solubility deviation from calculated intrinsic solubility ($m^L_{0,VB9} = 4.16 \cdot 10^{-5}$ mol · kg^{-1}) is higher than ARD%=4.08, however, the calculations performed with equation (2.68) strongly depend

also on reliability of pK_a values. Besides that, still a need of trustworthy experimental solubility value is of importance. For this reason, the assumption that intrinsic solubility of VB9 $m^L_{0,VB9}\sim 0$ was in this case feasible.

Experimental aqueous solubility data for all considered vitamins, which were measured in this work at T=298.15±0.1 K and p = 1 bar, together with the corresponding pH values, are given in the Appendix (table A7.1). $m^L_{0,vitamin}$ plotted in in figure 5.6 were calculated with equations based on idealized H-H-based expressions (section 2.3.1) using pK_a data (table 2.1). Experimental solubility values $m^L_{vitamin}$ measured for VC, VB2, VB3^{acid}, VB12 in pure water were comparable with calculated intrinsic solubility values $m^L_{0,vitamin}$ (ARD% ≤4.08 between experimental $m^L_{vitamin}$ and calculated $m^L_{0,vitamin}$). Although ARD% between experimental m^L_{VB9} and calculated $m^L_{0,VB9}$ for VB9 ≥ 4.08, the assumption that $m^L_{0,VB9} \rightarrow 0$ was made since VB9 is just marginally soluble. According to figure 5.6 and common terms used in literature to describe the solubility in water, just one vitamin studied in this work (VC) is freely soluble. While VB3 and VB12 can be still classified as sparingly soluble, VB2 and VB9 are already considered as practically insoluble. More precisely, the order of vitamin solubility is the following $m^L_{VC} > m^L_{VB3acid} > m^L_{VB12} > m^L_{VB2} > m^L_{VB9}$ (assuming the same trend of $m^L_{0,vitamin}$ and $m^L_{vitamin}$ at constant pH).

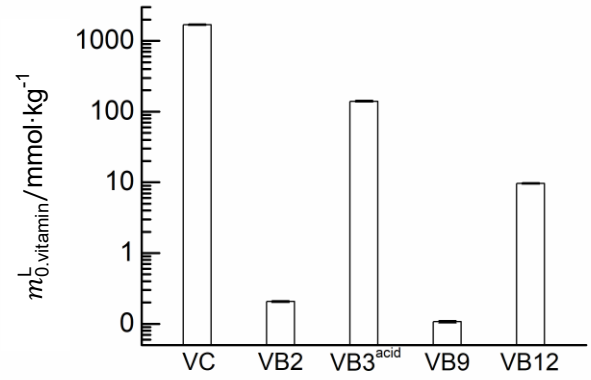

Figure 5.6. Intrinsic solubility of vitamins $m^L_{0,vitamin}$ determined in pure water at T=298.15 K and p=1 bar (Appendix, A7.1). ARD%^{exp}≤4.56. pH of saturated solutions: pH=1.94 (VC), pH=5.68 (VB2), pH=3.42 (VB3^{acid}), pH=4.28 (VB9), pH=5.55 (VB12).

The solubility trend (figure 5.6) could be correlated to melting points if compounds belonged to homologous series. Since molecular structures of vitamins diverge a lot, it is rather not expected that the melting properties will show a correlation with solubility data of each vitamin. Namely, it seems not possible to find out the solubility trend of vitamins (considered in this work) based on melting data. According to table 4.5 the melting temperatures of vitamins follow the order $T_{m,VB12} > T_{m,VB2} > T_{m,VB9} > T_{m,VB3acid} > T_{m,VC}$. This trend fits the previously given observation for DNP-AA (section 5.1.1) that smaller molecules with polar bonds and with lower melting temperatures, have also higher solubility (VC, VB3^{acid}) than the big ones (VB12). Thus, more possible is that one of the factors that rule water-soluble vitamin solubility is the complexity of molecular structure, as well as the presence of hydroxyl- and carbonyl groups and different interactions (e.g. hydrogen bonding). The latter, namely hydrogen bonding, is in general convenient for aqueous solubilization.

5.2.2. Influence of pH on Aqueous Solubility

In this work, experimental data on pH-dependent vitamin solubility in water was obtained at T=298.15±0.1 K and p=1 bar according to the procedure described in section 3.2.1. The results of measurements are included in Appendix (table A7.2). The three amphoteric (VB2, VB3^{acid}, VB9, and VB12) and one acidic (VC) water-soluble vitamins were considered. The solubility of vitamins changes with pH in a way that the presence of charged species after the pH increase (amphoteric, acidic vitamin) or the pH decrease (amphoteric vitamin) leads to the improved vitamin solubility $m^L_{vitamin}$. This observation can be seen in figure 5.7 that presents experimental pH-dependent solubility data measured in this work.

The pH-dependent theoretical solubility curves shown in figure 5.7 were calculated by means of intrinsic solubility $m^L_{0,vitamin}$ (section 5.2.1), pK_a values from table 2.1, and solubility expressions from section 2.3.1 that are based on idealized H-H equation. These results are only valid if no additional vitamins are added to the saturated water + vitamin solutions, i.e. just for binary water + vitamin systems. In general, reasonably accurate description of the pH-solubility profiles of vitamins under investigation can be obtained using idealized H-H-based solubility equations and the pK_a values presented in this work (table 2.1). However, despite a good agreement between experimental and theoretical

solubility profiles for most vitamins (VC, VB3^{acid}, VB9, and VB12), the VB2 solubility profiles calculated with equation (2.57) do not match the experimental data at pH > 5.5. Equation (2.57) was derived in case amphoteric VB2 has just the two pK_a values reported in the literature (table 2.1; pK_a =1.7 and pK_a =10.2) [167]. There might be many reasons for the unexpected experimental solubility profile of VB2 [170]. However, one simple argument might be the existence of one additional pK_a value as explained in section 2.3.1. By means of Chemicalize - ChemAxon online tool and confirmed with the literature [168, 173] one additional pK_a value (pK_a=6.1) applied to equation (2.62) enables the accurate description of experimental VB2 solubility data.

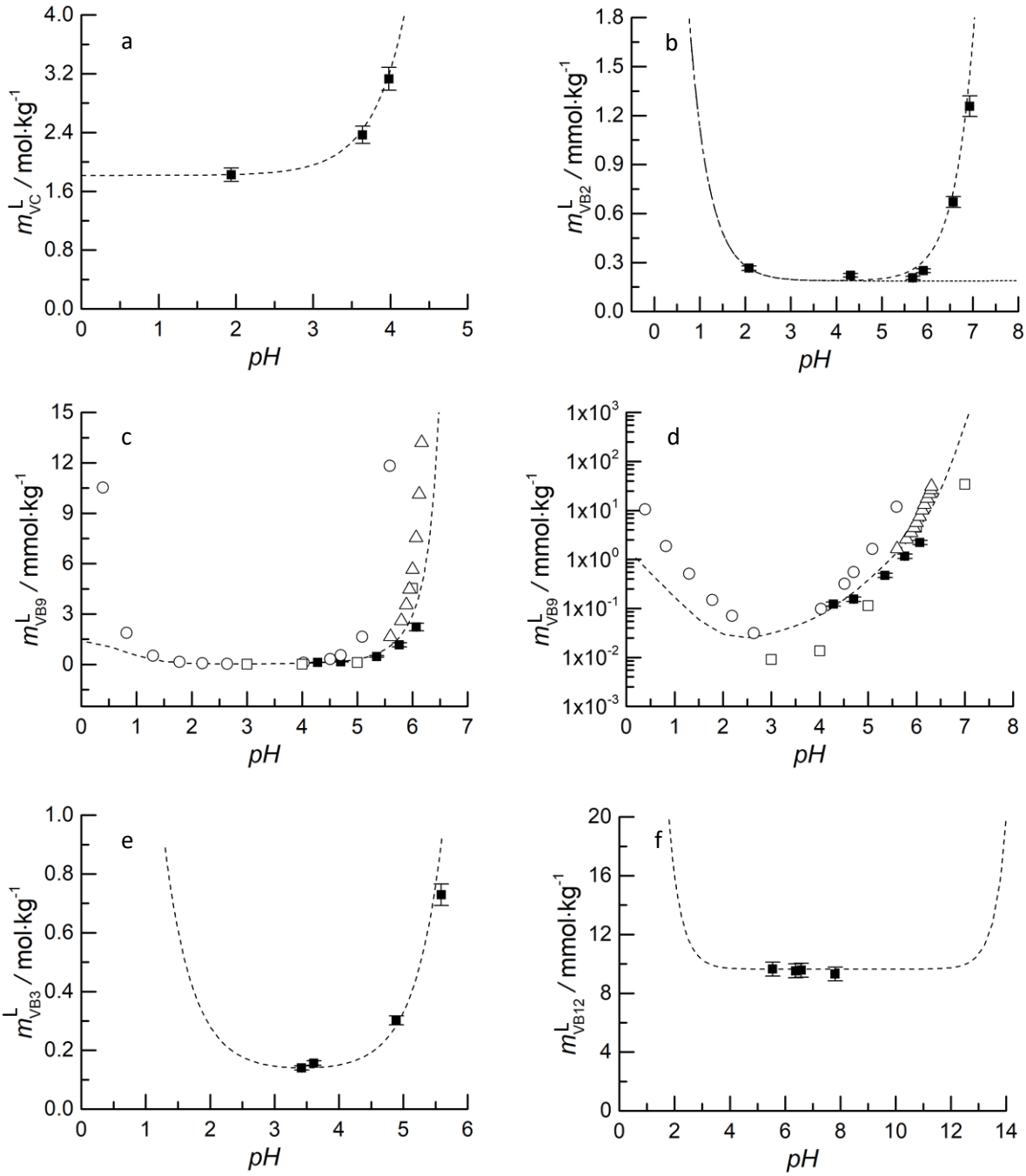

Figure 5.7. Experimental vitamin solubilities $m^L_{vitamin}$ as a function of pH, measured at T=298.15 K, p=1 bar. a - VC, b – VB2, c, d – VB9, e - VB3^{acid}, f - VB12. Data from this work (black squares) or from the literature (open symbols) [40, 42, 155, 156]. Dashed lines represent theoretical pH-solubility curves estimated with idealized H-H-based solubility equations (section 2.3.1). Special case: VB2 with pK_a 1.7 and 10.2 (dotted line), pK_a 1.7, 6.1, and 10.2 (dashed line). Solubility profile of VB9 is presented at two scales, normal (for better visibility in which region a significant increase of solubility is expected) and logarithmic (for better data comparison between different sources).

Incomplete and possibly inconsistent data on aqueous solubility of vitamins is the biggest problem emerging in literature. For VB9 some solubility data are already published in the literature, however, deviations between data found in different sources are large and reach ARD%=300 [42, 148, 155, 156]. This might be related to the fact that VB9 is practically insoluble in water and measuring very low solubilities is accompanied with high relative uncertainties. Anyhow, using the pK_a values from the literature [161, 171] and idealized H-H-based solubility equation (2.68) allows calculating a reasonably accurate pH-solubility profile for VB9. This profile matches the experimental data reported elsewhere at T = 298.15 K and p = 1 bar [156], as well as data measured in this work.

5.2.3. Combined pH and Temperature Effect on Aqueous Solubility

The pH effect is often neglected when studying the effect of temperature on solubility. The present work is focused on the aqueous solubility of vitamins at constant temperature T=298.15±0.1 K and p=1 bar. However, both pH and temperature can influence vitamin solubility. There are some data available in literature measured at different temperatures than T=298.15 K. Nevertheless, studies on temperature influence on vitamin solubility are relatively scarce in literature and involve just the solubility of VC, VB3^{acid}, and VB2 among all considered in this work. Additionally, in these publications, only solubility data for VB3^{acid} has been reported together with the pH of saturated solutions.

In this section, solubility data at different temperatures obtained from the literature [148-150] for VC, VB3^{acid}, and VB2, have been compared to experimental solubility measured in this work at T=298.15±0.1 K. The temperature influence on the solubility of the two most soluble vitamins (VC, VB3^{acid}) is presented in figure 5.8. According to figure 5.8, and as expected, the increase in solubility of VC and VB3^{acid} upon increasing the temperature is observed. By increasing the temperature of 25 K, namely from T=298.15 K to T=323 K, it is possible to double the solubility of VC and VB3^{acid}. The temperature can influence the pH of aqueous solution during the solubilization. This was confirmed in the literature for VB3^{acid} solubility [150]. The same observation was made in section 5.1.3 based on experimental aqueous solubility of DNP-AA (Appendix, table A6.3). In the work published by Gonçalves et al. [150] the increase in temperature of 34 K (from T=298.15 K to T=332.01 K) led to a lower pH of 0.3 unit (from pH 3.42 to pH 3.12). This can be related

to the fact that more acid dissolved in the aqueous solution after increasing the temperature, leads to the higher hydrogen ion activity (leading to a lower pH value). Thus, the major drawback of solubility data for VC that was taken from the literature and presented in figure 5.8 (gray bars) is lack of the pH measured for saturated solutions. The pH effects observed for each vitamin considered in this work have been already discussed in section 5.2.2.

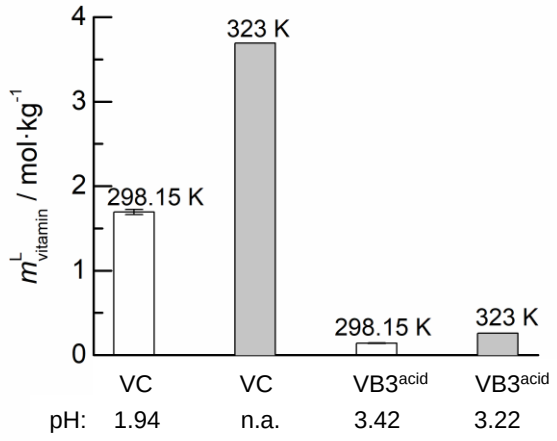

Figure 5.8. Temperature influence on VC and VB3^{acid} aqueous solubility m^L_{VC} and $m^L_{VB3acid}$ based on data determined in this work at T=298.15 K and p=1 bar (white bars) and data from the literature [149, 150] at T=323 K and p=1 bar (gray bars), pH of vitamin saturated solutions provided under the figure. Data from the literature measured for VC has not been accompanied by pH values of saturated solution.

One of the reasons for studying the influence of pH on the aqueous solubility of vitamins raised from the observation presented in figure 5.9. It shows the pH and the temperature effects on VB2 solubility using data measured in this work and from the literature [148]. Data reported in the literature at T=310.15 K have not been accompanied by the pH of saturated solution and this is the major drawback for this evaluation. However, approximately double solubility increase can be observed when changing the pH of a solution of 1 pH unit (from pH=5.68 to pH=6.68) than if increasing the temperature of 12 K (from T=298.15 K to T=310.15 K). The same solubility enhancement of VB2 caused by pH or temperature can be observed by changing the pH of only ~0.5 pH units (from pH=5.68 to pH=6.15) or after increasing the temperature from T=298.15 K (data from this work) to T=310.15 K (data from the literature [148]). The solubility calculations for each pH increase were obtained with idealized H-H-based solubility

equation (2.62). Increasing the pH over changing the temperature could be especially beneficial for other vitamins, e.g. VB9 that can undergo some structural changes if exposed to the heat [389, 397, 398]. Probably due to a temperature sensitivity found in the literature for VB9, there is no VB9 solubility data that could allow evaluating the combined pH and temperature influence on VB9 solubility.

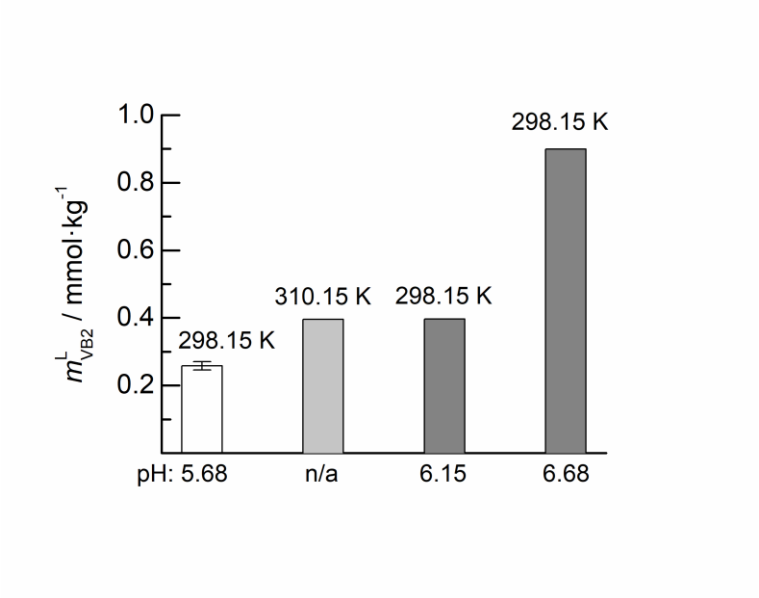

Figure 5.9. Combined pH and temperature effect on VB2 aqueous solubility m^L_{VB2} based on data determined in this work at T=298.15 K and p=1 bar (white bars), data from the literature at T=310.15 K and p=1 bar (light gray bar)[148], and data calculated from experimental solubility and pK_a values from table 2.1 using idealized H-H-based solubility equation (2.62) (dark gray bars). While temperature values are provided above the bars, the values of pH of saturated solutions are given under the bars. The pH value corresponding to solubility data point obtained from the literature [148] has not provided.

5.2.4. Influence of Covitamin on Aqueous Solubility

Some solubility data of vitamins with coexisting vitamins, so-called covitamins [399, 400], are already available in the literature at high covitamin concentrations [42, 153, 154, 175-177]. Covitamins might show a hydrotropic behavior [175]. To cover all the possible effects (resulting from the pH and cross-interactions), solubility data at a wide range of covitamin concentration were required in addition to the few existing literature data.

The aqueous solubility of poorly water-soluble vitamins (VB2, VB9, and VB12) at T=298.15 K and p=1 bar upon addition of better-soluble covitamins (VC, VB3^{acid}, VB3^{amide}) was measured according to the procedure described in section 3.2.1 and these data are included in Appendix (table A7.3). These data are accompanied by the corresponding pH

of the solutions and ARD% values. The concentrations of covitamins used in this study were: $m_{VB3acid} = 0.05 - 0.1\ \text{mol} \cdot \text{kg}^{-1}$, $m_{VB3amide} = 0.1 - 0.2\ \text{mol} \cdot \text{kg}^{-1}$, $m_{VC} = 0.5 - 1\ \text{mol} \cdot \text{kg}^{-1}$. The pH values of vitamin saturated solutions mixed with covitamins ranged from pH~2 to pH~6 ($pH_{VB2+covitamin}$ = 1.91-6.43, $pH_{VB9+covitamin}$ =5.32-6.00, and $pH_{VB12+covitamin}$=3.43 -6.4). Figure 5.10 shows experimental solubilities of VB2 (figure 5.10a), VB9 (figure 5.10b), and VB12 (figure 5.10c), upon addition of $VB3^{acid}$, $VB3^{amide}$, or VC, to the respective aqueous vitamin solutions.

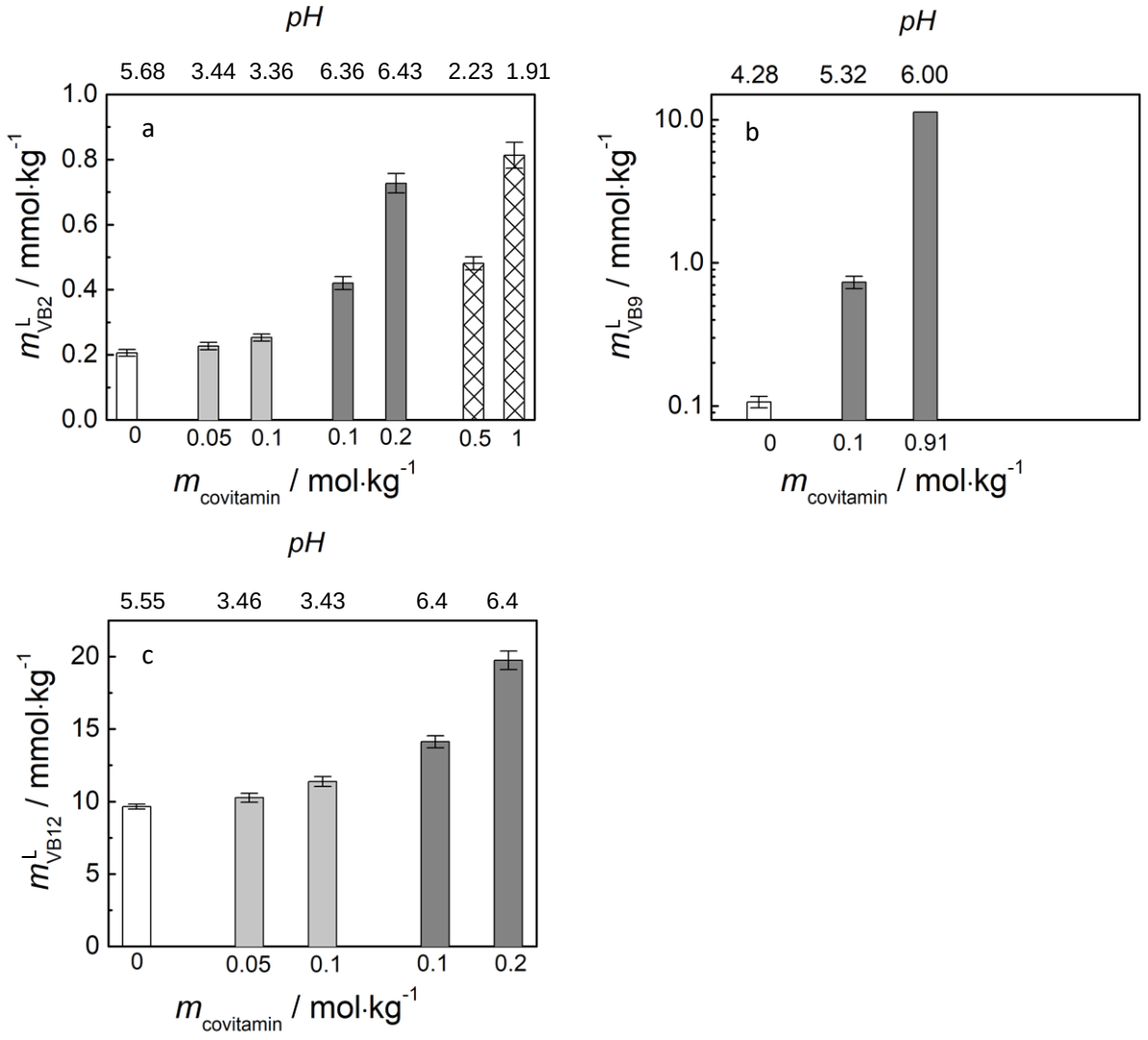

Figure 5.10. Experimental aqueous solubility of vitamins VB2 (a), VB9 (b), and VB12 (c), measured in this work at T=298.15 K and p=1 bar in pure water (white bars) and upon addition of covitamins $VB3^{acid}$ (light gray bars), $VB3^{amide}$ (dark gray bars), and VC (patterned bars). Additional solubility data point for VB9 ($m_{VB3amide}$ = 0.91 mol·kg^{-1}) was taken from the literature [42]. The numbers above the figures are the pH values of the saturated solutions.

In general, the solubility of vitamins is related to the concentration of covitamin introduced to vitamin solution and to the covitamin and vitamin types itself. Based on the data presented in figure 5.10, it can be observed that covitamin VB3^{amide} strongest enhances the solubility of VB2, VB9, and VB12. About a 5-fold higher concentration of covitamin VC than VB3^{amide} is required to increase the solubility of VB2 to the comparable level. The advantage of using VB3^{amide} over VC is better highlighted in figure 5.11 where the experimental solubility obtained in this work is joint with data available from the literature. The solubility enhancement levels upon addition of covitamins vary, and they can be very different for each vitamin. The same concentration of covitamin VB3^{amide} ($m_{VB3amide}$= 0.91 mol·kg^{-1}) added to aqueous solutions of VB2 and VB9, leads to about 100-fold solubility enhancement of VB9, while for VB2, a 15-fold increase is observed. Moreover, covitamins VC and VB3^{acid} added at comparable concentrations have less influence than VB3^{amide} on VB2, VB9, and VB12 solubility.

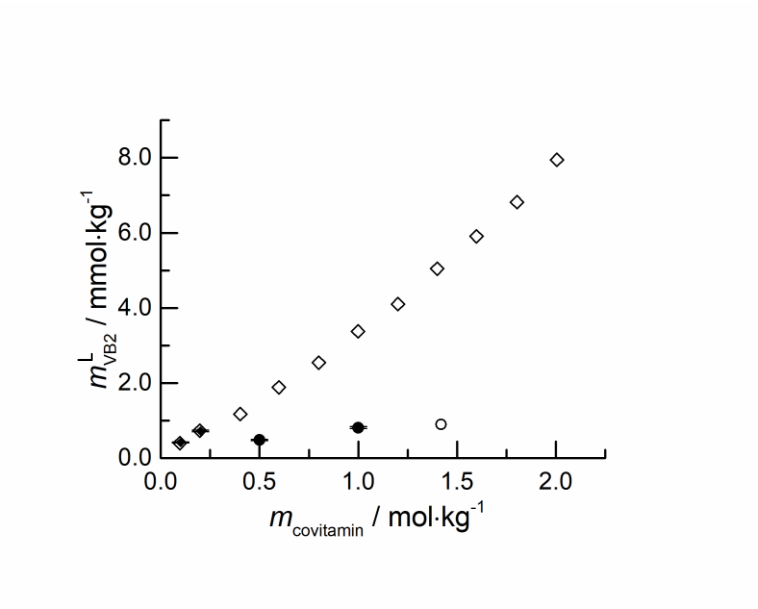

Figure 5.11. Experimental aqueous solubility of VB2 upon addition of covitamins VB3^{amide} (diamonds) and VC (circles), at T=298.15 K and p=1 bar. Black symbols – this work, white symbols – literature [153, 177]. The pH of solutions from this work (black symbols) are provided in figure 5.10. The pH of solutions from the literature: pH~6.4 for VB2 + VB3^{amide} - white diamonds (involves all these data since the pH has not been precisely specified for each solution); pH=1.8 for VB2 + VC – white circle. Note that data from reference [153] was reported at T = 303.15 K, however this causes only slight deviation to the solubility at T=298.15 K.

The dissimilarities in the effects of covitamins on vitamin solubility enhancement are possibly related to the differences in the interplay of different factors, e.g. pH and

interactions. The so-called (in the literature) "hydrotropes" might cause pH changes that strongly influence molecular interactions, species distribution, or even both. The strength of these factors is evaluated in detail in section 8.3 of this work.

5.3. Conclusion

In this chapter, the aqueous solubility of four DNP-AA, namely DNP-glycine, DNP-alanine, DNP-valine, and DNP-leucine, as well as five vitamins VC, VB2, VB3^{acid}, VB9, VB12, has been experimentally evaluated, at T = 298.15 K and p = 1 bar. The results of pH-dependent solubility obtained after addition of HCl or NaOH have been presented. Intrinsic aqueous solubilities and pH-solubility curves were determined using experimental data, pK_a values from the literature, and idealized H-H-based approach. Additionally, the influence of pH and temperature, as well as the combined effect of these two factors on DNP-AA and vitamin solubility in water, were considered in the present study. In the end, the enhancement of aqueous solubility of low-soluble vitamins (VB2, VB9, and VB12), at T = 298.15 K and p = 1 bar, after the addition of covitamins (VC, VB3^{acid}, VB3^{amide}) was discussed.

In regards to DNP-AA, the solubility trend observed was as following $m^L_{DNP-alanine}$> $m^L_{DNP-valine}$ > $m^L_{DNP-glycine}$ and $m^L_{DNP-leucine}$. This was rather unclear which DNP-AA from the two least soluble (DNP-glycine or DNP-leucine) has higher solubility since the difference in solubility of DNP-glycine and DNP-leucine was within the experimental error. The aqueous solubility trend of DNP-AA (decreasing m^L_{DNP-AA}) follows the reverse trend of melting properties (increasing $T_{m,DNP-AA}$). Based on data from the literature for aliphatic AA, the solubility trends observed for DNP-AA and AA do not match ($m^L_{glycine}$< $m^L_{L-alanine}$ < $m^L_{L-valine}$ < $m^L_{L-leucine}$). Also, the solubility of each DNP-AA is of lower magnitude than for its parent aliphatic AA. The difference between DNP-AA and aliphatic amino acids is also in the dissociation equilibrium. In contrast to aliphatic amino acids that are amphoteric, DNP-AA are acidic components. Thus, a decrease of the pH leads to a lower DNP-AA solubility, while an increase of the pH enhances the solubility of DNP-AA.

A slight DNP-AA solubility increase is observed when changing the temperature of 10 K or 20 K (from T=298.15 K to T=318.15 K). In contrast to that, if the pH of DNP-AA solution increases of 0.5 units (from pH=4 to pH=4.5), there is more than a double increase of the DNP-AA solubility. In non-buffered DNP-AA solutions, the increase of

temperature causes the improvement of aqueous solubility of DNP-AA, however, due to dissolving more of acidic DNP-AA leads also to a decrease in the pH. For this reason, it is very important to consider the pH effect while studying the temperature influence on DNP-AA solubility in non-buffered aqueous solutions.

The observed trend of vitamin solubility in water is the following m^L_{VC}> $m^L_{VB3acid}$ > m^L_{VB12} > m^L_{VB2} > m^L_{VB9}. The melting properties could not be correlated with solubility data of each vitamin since the molecular structures of vitamins are very diverged. Thus, it was not possible to find the solubility trend of vitamins based on melting data. The vitamins considered in this chapter were either acidic (VC) or amphoteric (VB2, VB3^{acid}, VB9, and VB12). This means that in all cases, an increase in pH could enhance the solubility of a vitamin. Except for VC, the solubility was improved by decreasing the pH. Curves obtained with pK_a values from the literature and idealized H-H-based solubility equations have shown a very good fit for the pH-dependent experimental data obtained for vitamins.

Based on data from the literature, by increasing the temperature of 25 K, namely from T=298.15 K to T=323 K, it is possible to double the solubility of VC and VB3^{acid}. Also, a double VB2 solubility increase can be observed when changing the pH of a solution of 1 pH unit. The same solubility enhancement of VB2 caused by pH or temperature can be observed by changing the pH of only ~0.5 pH units or after increasing the temperature from T=298.15 K to T=310.15 K. However, the temperature can also influence the pH of vitamin aqueous solution during the solubilization. This was confirmed with solubility data published in the literature since an increase in temperature of 34 K could lower the pH of VB3^{acid} solution of 0.3 unit. Thus, in this evaluation, the importance of studying the combined pH and temperature effect was highlighted.

Studies on the influence of different covitamins VC, VB3^{acid}, and VB3^{amide}, on poorly soluble vitamins VB2, VB9, and VB12, have shown that the solubility of vitamins is related to the concentration of covitamin introduced to vitamin solution and to the covitamin and vitamin type itself. It has been observed that covitamin VB3^{amide} the strongest enhances the solubility of VB2, VB9, and VB12. To increase the solubility of VB2 to the comparable level, about a 5-fold higher concentration of covitamin VC than VB3^{amide} was required. It was found that the same concentration of covitamin VB3^{amide} added to aqueous solutions of VB2 and VB9, can lead to about 100-fold solubility enhancement of VB9, while for VB2, a 15-fold increase was observed. Besides that, covitamins VC and VB3^{acid} added at

comparable concentrations have less influence than $VB3^{amide}$ on VB2, VB9, and VB12 solubility. Based on these results, it could be concluded that different covitamin effects on the enhancement of vitamin solubility are possibly related to the differences in the interplay of different factors, e.g. pH and interactions. Overall, it was proven that the so-called in literature "hydrotropes" can cause pH changes that strongly influence molecular interactions, species distribution, or even both.

6. Experimental Phase Equilibrium of ATPS

This chapter presents the experimental phase equilibria measured for different ATPS formed by non-toxic compounds, namely PEG and organic salts. For the correlation and evaluation of experimental data, widely applied in the literature equations such as Merchuk, Othmer-Tobias, Bancroft were used. Based on experimental results, in the following, the influence of using PEG of different average molar mass and salt type on ATPS phase forming is discussed.

6.1. Experimental Results: ATPS Diagrams

Experimental binodal and tie-line data for PEG - organic salt ATPS were measured in this work at T=298.15 K and p=1 bar. Experimental equilibrium concentrations, as well as the tie-line lengths (TLL) determined according to equation (3.3), were included in Appendix (A8). The results of the measurements are in this subchapter evaluated in terms of the effects resulting from the presence of different components in ATPS. As such, these have an influence on ATPS phase formation. Thus, sections 6.1.1 and 6.1.2 involve the discussion centered on the application of different average molar mass of PEG (section 6.1.1) and salt type (section 6.1.2) in ATPS.

The results of the experiments performed in this study were placed into Appendix (A8) for clarity reasons. The discussion presented in the following uses the figures based on the results of multiple measurements that were grouped into tables A8.1, A8.2, A8.3 and A8.4, in the Appendix (A8). It was done according to the scheme shown in figure 6.1 that has been provided with the intention to facilitate finding the experimental background of data plotted and discussed in subchapter 6.1.

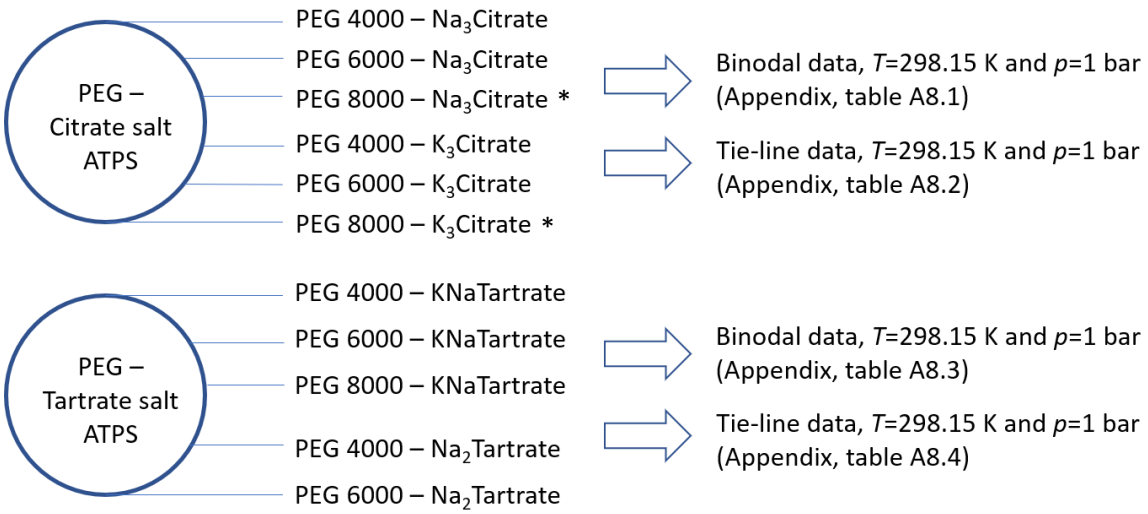

Figure 6.1. Experimental binodal and tie-line composition data measured in this work plotted in figures and discussed in subchapter 6.1 (Appendix, A8). Symbol (*) indicates data that was taken from literature and used in this work [258].

Experimental data presented in sections 6.1.1 and 6.1.2 were correlated using empirical expressions such as Merchuk equation (3.2) [275], Othmer-Tobias equation

(3.6) [271], and Bancroft equation (3.7) [272]. Binodal curves were obtained by fitting the parameters of Merchuk equation to experimental data. These adjustable parameters are given in table 6.1. Based on coefficient of determination values ($r^2 \geq 0.999$) included in table 6.1, Merchuk equation was very successful in correlating experimental binodal data. The results of this fitting are graphically presented in sections 6.1.1 and 6.1.2. Despite the availability of binodals for PEG 8000 – Na_3Citrate and PEG 8000 – K_3Citrate ATPS in the literature, some points of the binodal data were measured also in this work [258]. Since they agree with the previous study, the tie-line data for these two ATPS were cohered from the literature [258]. Othmer-Tobias and Bancroft correlations were used to verify the reliability of the tie-lines in (liquid-liquid) equilibrium (LLE) as suggested in the literature [114, 349, 401, 402]. Adjustable parameters obtained from the Othmer-Tobias and Bancroft equations are given in table 6.2. The application of both equations gives good linearity of the LLE data (figure 6.2, figure 6.3). This can be confirmed with coefficient of determination values (average $r^2 \geq 0.997$) included in table 6.2. Thus, the results of experimental data correlation with these equations prove high measurement reliability obtained in the present work.

Table 6.1. Number of data points used to determine each binodal curve (*NP*), together with the adjustable parameters (*a*, *b*, and *c*) obtained from the Merchuk equation (3.2), and respective coefficients of determination (r^2). TW – parameters fitted in this work.

ATPS	*NP*	*a*	*b*	*c*	r^2	*ref*
PEG 4000 – Na_3Citrate	27	0.84 ± 0.01	−5.15 ± 0.07	595 ± 23	0.9994	TW [3]
PEG 6000 – Na_3Citrate	32	0.87 ± 0.01	−5.51 ± 0.07	700 ± 19	0.9995	TW [3]
PEG 8000 – Na_3Citrate	25	0.955 ± 0.028	−5.73 ± 0.17	581 ± 29	0.9993	TW [4], [258]
PEG 4000 – K_3Citrate	14	1.41 ± 0.07	−5.86 ± 0.11	224 ± 21	0.999	TW [2]
PEG 6000 – K_3Citrate	16	1.51 ± 0.07	−6.24 ± 0.12	281 ± 18	0.999	TW [2]
PEG 8000 – K_3Citrate	14	1.38 ± 0.08	−6.17 ± 0.13	348 ± 34	0.999	TW [2]
PEG 4000 – KNaTartrate	14	1.33 ± 0.04	−5.67 ± 0.07	177 ± 15	0.9995	TW [2]
PEG 6000 – KNaTartrate	18	1.10 ± 0.06	−4.92 ± 0.09	264 ± 18	0.999	TW [2]
PEG 8000 – KNaTartrate	17	1.24 ± 0.05	−5.54 ± 0.10	312 ± 17	0.9993	TW [2]
PEG 4000 – Na_2Tartrate	45	1.048 ± 0.009	−5.36 ± 0.067	314 ± 13	0.9994	TW [7]
PEG 6000 – Na_2Tartrate	28	1.037 ± 0.01	-5.66± 0.063	418 ± 20	0.9995	TW [7]

Table 6.2. Adjustable parameters n_1, k_1 and n_2, k_2 obtained using equations of Othmer-Tobias equation (3.6) and Bancroft equation (3.7), respectively, together with the corresponding coefficients of determination (r^2). Experimental data used for adjusting the parameters was measured in this work [2-4, 7] or taken from the literature (PEG 8000 – Citrate Salt) [258]. NP – number of experimental data points used to determine the parameters. TW – parameters fitted in this work.

ATPS	*Othmer-Tobias*				*Bancroft*			*ref*
	NP	n_1	k_1	r^2	n_2	k_2	r^2	
PEG 4000 – Na_3Citrate	12	1.4663	-0.6043	0.9966	0.6812	0.4259	0.9941	TW [3]
PEG 6000 – Na_3Citrate	12	1.3939	-0.5841	0.9999	0.7305	0.4285	0.9995	TW [3]
PEG 8000 – Na_3Citrate	10	1.6677	-0.6473	0.9894	0.5983	0.4024	0.9857	TW [4], [258]
PEG 4000 – K_3Citrate	6	1.7721	-0.5426	0.9992	0.5706	0.3242	0.9991	TW [2]
PEG 6000 – K_3Citrate	6	1.2578	-0.3143	0.9999	0.8084	0.2735	0.9999	TW [2]
PEG 8000 – K_3Citrate	6	1.6861	-0.5092	0.9183	0.5506	0.3354	0.9138	TW [4], [258]
PEG 4000 – KNaTartrate	6	1.7183	-0.4483	0.9986	0.5701	0.2874	0.9980	TW [2]
PEG 6000 – KNaTartrate	6	1.8025	-0.5231	0.9997	0.5462	0.3147	0.9994	TW [2]
PEG 8000 – KNaTartrate	6	1.8450	-0.5790	0.9993	0.5520	0.3312	0.9996	TW [2]
PEG 4000 – Na_2Tartrate	12	1.7373	-0.6964	0.9946	0.5488	0.4233	0.9942	TW [7]
PEG 6000 – Na_2Tartrate	12	1.6757	-0.6533	0.9902	0.5941	0.4059	0.9886	TW [7]

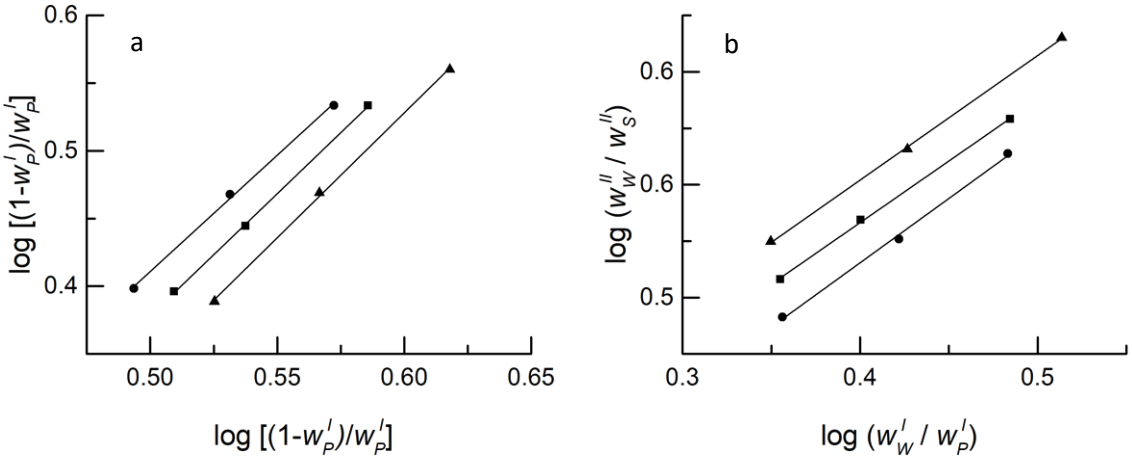

Figure 6.2. Linearization of the liquid-liquid equilibrium data obtained with Othmer-Tobias (a) and Bancroft (b) equations using experimental data measured in this work at T=298.15 K and p=1 bar for ATPS formed by KNaTartrate and PEG: PEG 4000(●), PEG 6000(▪), and PEG 8000 (▲).

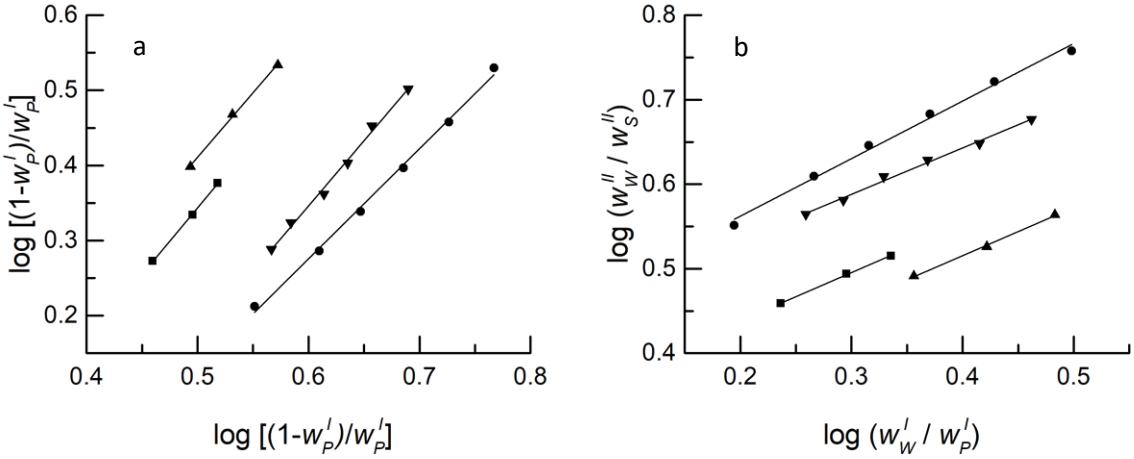

Figure 6.3. Linearization of the liquid-liquid equilibrium data obtained with Othmer-Tobias (a) and Bancroft (b) equations using experimental data measured in this work at T=298.15 K and p=1 bar for ATPS formed by PEG 4000 (P) and organic salt (S): $Na_3Citrate$(●), $K_3Citrate$(■), $Na_2Tartrate$(▼), KNaTartrate (▲).

6.1.1. PEG Influence on ATPS

The binodal data for ATPS composed by PEG of different average molar mass (M_{PEG}: 4000, 6000, 8000 g·mol^{-1}) and organic salt ($Na_3Citrate$, $K_3Citrate$, $Na_2Tartrate$, and KNaTartrate), at T=298.15 K and p=1 bar, are graphically presented in figure 6.4. The binodal curves were calculated with the Merchuk equation using the adjustable parameters from table 6.1.

Figure 6.4 compares binodals obtained for different ATPS in terms of PEG´s molecular weight used. Among all systems considered in this thesis, a slightly higher "working area" was obtained when PEG of higher molecular weight was used. This means that PEG 8000 has better two-phase forming ability (with organic salts considered and water) than PEG 6000 and PEG 4000. Thus, among all ATPS studied in this work, systems composed by PEG 8000 and biodegradable salt can be considered as the most efficient ATPS regarding the phase separation.

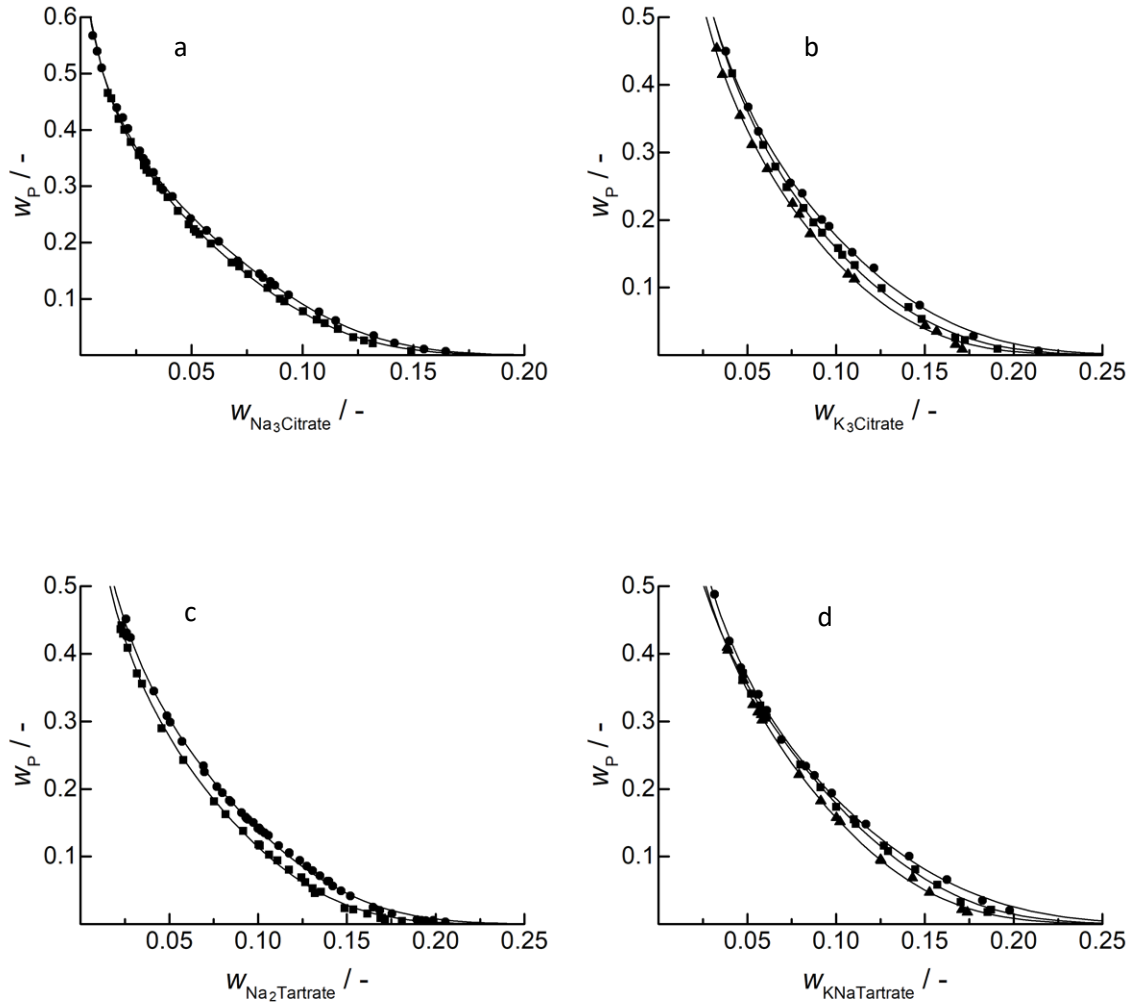

Figure 6.4. Binodal experimental data (in mass fraction, *w*) measured at *T*=298.15 K and *p*=1 bar for ATPS: PEG (P) – $Na_3Citrate$ (a), PEG (P) - $K_3Citrate$ (b), PEG (P) – $Na_2Tartrate$ (c), and PEG (P) - KNaTartrate (d). ATPS formed by PEG of different molar mass: PEG 4000(●), PEG 6000(▪), and PEG 8000 (▲). Lines were calculated using Merchuk equation (3.2) and parameters from table 6.1.

The behavior of PEG in aqueous solution observed in figure 6.4 can be explained with physical properties of its chain and interactions, e.g. hydrogen bonding [403]. However, it

can be seen in figure 6.4 that the difference in the position of the two-phase regions for ATPS formed by PEG of average molar mass ranged from M_{PEG} = 4000 – 8000 g·mol^{-1} is not significant. Thus, less viscous aqueous solutions of lower molar mass of PEG (e.g. PEG 6000 or PEG 4000) can be more convenient for the application of ATPS than more viscous solutions of PEG 8000[404]. This is especially important if considering an industrial scale application of ATPS.

6.1.2. Salt Influence on ATPS

The binodal data for ATPS composed by PEG (PEG 4000, PEG 6000) and organic salts (N_3Citrate, K_3Citrate, Na_2Tartrate, and KNaTartrate), at T=298.15 K and p=1 bar, are plotted in figure 6.5. The binodal curves were calculated with the Merchuk equation using adjustable parameters from table 6.1.

Figure 6.5 compares binodals obtained for different ATPS in terms of the kind of organic salt used. Among all systems considered in this thesis, the highest "working area" was obtained if Na_3Citrate was used. This means that Na_3Citrate has better two-phase forming ability (with PEG and water) than any other salt used in this work (K_3Citrate, Na_2Tartrate, and KNaTartrate). The salts have followed the order regarding the two-phase region formation (the largest - the lowest): Na_3Citrate, Na_2Tartrate, K_3Citrate, KNaTartrate. However, the biphasic area for the ATPS formed by PEG and K_3Citrate was just marginally higher than for PEG – KNaTartrate. The differences in PEG mass fractions (within a range shown in figure 6.5) between these two ATPS were ≈2% in the regions of low PEG or low salt concentrations. Undoubtedly, based on data plotted in figure 6.4 (section 6.1.1) and figure 6.5 presented in this section, the salt effect has higher influence for binodal curves position than that of the PEG´s average molar mass, in the range of M_n considered in this work. It is of importance, however, to unravel which of the two salt constituents: anion or cation contributes more to the observed salt effect.

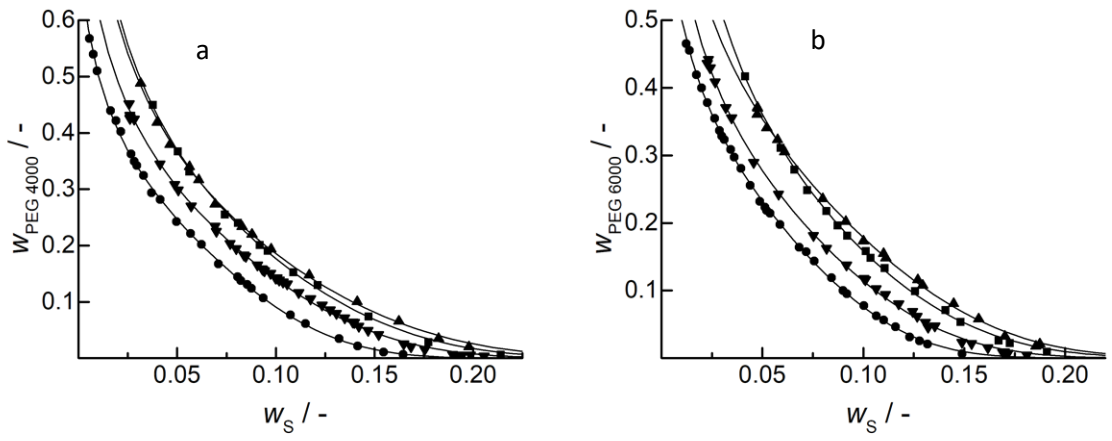

Figure 6.5. Binodal experimental data (in mass fraction, *w*) measured in this work at *T*=298.15 K and *p*=1 bar for ATPS: PEG 4000 – organic salt (a) and PEG 6000 – organic salt (b). ATPS formed by different salt: $Na_3Citrate$(●), $K_3Citrate$(■), $Na_2Tartrate$(▼), KNaTartrate (▲). Lines calculated using Merchuk equation (3.2) and parameters from table 6.1.

The anion effect on PEG (M_{PEG} = 4000 and 6000 g·mol^{-1}) – sodium salt ($Na_3Citrate$, $Na_2Tartrate$) ATPS are presented in figure 6.6 where additionally the tie-lines measured in this work are plotted (Appendix, A8).

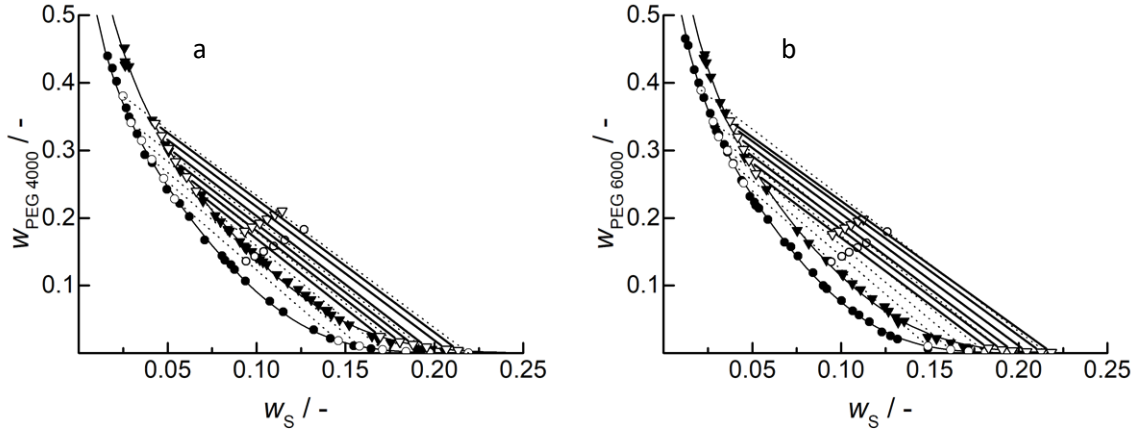

Figure 6.6. Binodal and tie-line experimental data (in mass fraction, *w*) measured in this work at *T*=298.15 K and *p*=1 bar for ATPS: PEG 4000 – organic salt (a) and PEG 6000 – organic salt (b). ATPS formed by different salt: $Na_3Citrate$ (●) and $Na_2Tartrate$ (▼). Binodal curves are calculated using Merchuk equation (3.2) and parameters from table 6.1. The open points (○,▽) refer to the feed and equilibrium composition.

Through the comparison of the biphasic regions (figure 6.6) influenced by the presence of different salt anion, citrate salt ($Na_3Citrate$) is more efficient than tartrate ($Na_2Tartrate$). This means that more salt is needed to form ATPS composed by tartrate salt. However, in this case, the effect caused by a different number of sodium salt cations cannot be separated from the anion effect. This means that since the anion also determines the number of cations present in salt, the case presented in figure 6.6 is not enough to draw general and irrefutable conclusions on anion effect.

The cation effect on PEG (M_{PEG} = 4000 and 6000 g·mol^{-1}) – organic salt ($Na_3Citrate$, $K_3Citrate$, and $Na_2Tartrate$, KNaTartrate) ATPS is presented in figure 6.7 and figure 6.8 where additionally the tie-lines measured in this work were plotted (Appendix, A8). By the comparison of the two-phase regions influenced by the presence of different citrate salt cations (figure 6.7), sodium cation ($Na_3Citrate$) is more efficient in terms of biphasic region formation than potassium ($K_3Citrate$). This means that more salt is needed to form ATPS composed of potassium salt. This observation can be confirmed also with figure 6.8 which evaluates cation influence on LLE of PEG – $Na_2Tartrate$ and PEG – KNaTartrate ATPS.

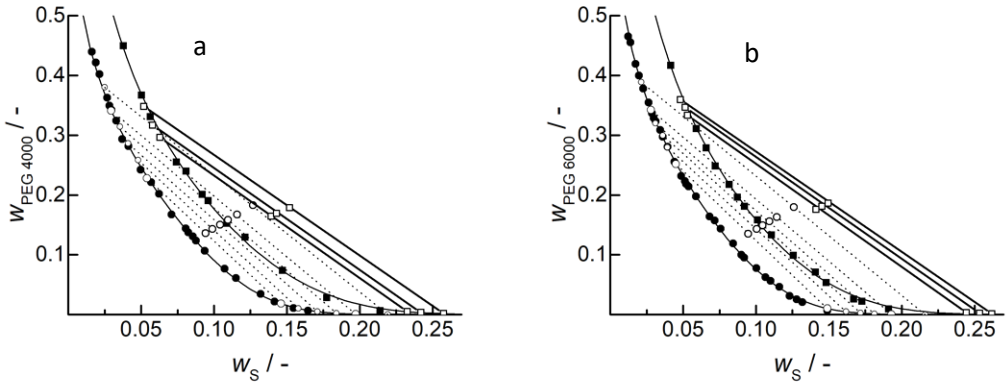

Figure 6.7. Binodal and tie-line experimental data measured in this work at T=298.15 K and p=1 bar for ATPS: PEG 4000 – organic salt (a) and PEG 6000 – organic salt (b). ATPS formed by different salts: $Na_3Citrate$(●) and $K_3Citrate$(■). Lines are calculated using Merchuk equation (3.2) and parameters from table 6.1. The open points (○,□) state for the feed and equilibrium composition.

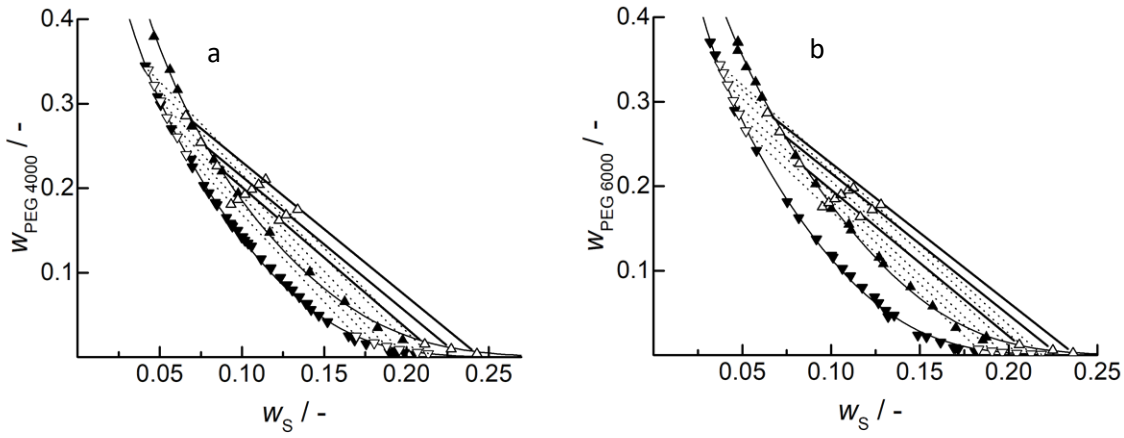

Figure 6.8. Binodal and tie-line experimental data measured in this work at T=298.15 K and p=1 bar for ATPS: PEG 4000 – organic salt (a) and PEG 6000 – organic salt (b). ATPS formed by different salts: Na_2Tartrate(▼) and KNaTartrate (▲). Lines are calculated using Merchuk equation (3.2) and parameters from table 6.1. The open points (▽,△) state for the feed and equilibrium composition.

The presence of two sodium cations in a salt (Na_2Tartrate) used to form ATPS is more advantageous for the two-phase forming than the presence of one sodium and one potassium cation in a salt (KNaTartrate). The system composed of PEG and salt KNaTartrate of the same anion as of Na_2Tartrate, but with just one sodium and one potassium cation leads to a lower biphasic area than for ATPS formed by Na_2Tartrate. Based on figure 6.6, figure 6.7, and figure 6.8, the cation effect of a salt is larger than the anion effect. Undoubtedly, sodium salts are more advantageous in terms of biphasic region formation of ATPS.

6.2. Conclusion

This chapter presents the evaluation of experimental biphasic diagrams measured for different ATPS formed by PEG (average molar mass M_{PEG}: 4000, 6000, 8000 g·mol^{-1}) and biodegradable salt (N_3Citrate, K_3Citrate, Na_2Tartrate, and KNaTartrate), at T=298.15 K and p=1 bar. Widely applied equations of Merchuk, of Othmer-Tobias, and of Bancroft were used for the correlation and evaluation of experimental data. The influence of PEG of different average molar mass, as well as a salt type on ATPS phase forming, has been discussed.

Using the Merchuk equation it was possible to accurately correlate experimental binodal data. Further, Othmer-Tobias and Bancroft correlations applied in this work prove high reliability of measured tie-line composition for each ATPS in this work. The highest biphasic regions were observed for PEG of higher molar mass and for salts that contain sodium cation and citrate anion. This was found by the comparison of the size of two-phase regions related to the presence of different salt cations in citrate salt (Na_3Citrate, K_3Citrate). Among the two ATPS formed by PEG and citrate salt (Na_3Citrate or K_3Citrate), the system formed by PEG and K_3Citrate had a smaller two-phase region. This means that more salt is needed to form ATPS composed of K_3Citrate than for ATPS formed by Na_3Citrate. Thus, it was found that among all ATPS considered, the system formed by PEG 8000 and sodium citrate had the highest biphasic area. Even though PEG of higher molar mass (e.g. PEG 8000) can be more beneficial for ATPS phase formation, the solutions containing PEG 8000 are more viscous and this can be a drawback for industrial application. For this reason, PEG molar mass should be chosen based on the possible application of ATPS rather than just on the size of the biphasic region.

Additionally, it was found that salt influence on phase equilibria of ATPS is much higher than PEG influence. However, the effects caused by anion and cation of salt (Na_3Citrate, Na_2Tartrate) on the ATPS phase forming could not be separated and thus, it was not possible to conclude which of these two effects is stronger. The reason for that is a fact that the salt influence relies not only on the kind of cation but also on the number of cations present in a molecule. Since the number of cations attached to a molecule depends on the valence of anion, it can be assumed that both cation and anion type can influence the phase formation of ATPS in a comparable manner. However, the system composed of PEG and KNaTartrate having one sodium and one potassium cation, led to a noticeable lower biphasic area than it was found for ATPS formed by PEG and Na_2Tartrate with two sodium cations.

7. Experimental Partitioning of Biomolecules in ATPS

This chapter presents experimentally determined partition coefficients for DNP-AA and water-soluble vitamins in PEG – organic salt ATPS. The influence of solute properties, as well as phase formers, have been evaluated in terms of the partitioning in ATPS. Data shown in this chapter proves the merit of replacing inorganic salts by organic biodegradable alternatives that can form ATPS. The effects on partitioning in ATPS originating from the presence of different cation and anion type of salt and different PEG molar mass are discussed.

7.1. Experimental Results: Amino Acid Derivatives

The partition coefficient (K) of amino acid derivatives (DNP-AA) in ATPS formed by PEG of M_{PEG} = 4000 – 8000 g·mol^{-1} and biodegradable salt Na_3Citrate, K_3Citrate, or KNaTartrate depends on DNP-AA properties, especially on their behavior in aqueous solutions and the interactions with phase forming compounds. This involves both the charge state of DNP-AA at given pH and the molecular structure of DNP-AA (e.g. a different number of methylene groups in DNP-AA homological series). The charge state of DNP-AA in ATPS is influenced by the concentration and the properties of all system constituents. The effects ruling DNP-AA partitioning are coupled and hard to separate, however, the choice of different salt anion and cation of salt or molar mass of PEG can be treated as a general requisite for choosing the more efficient ATPS.

In this chapter, the influence of DNP-AA properties on experimental K is covered in section 7.1.1. Further experimental results for studying salt and PEG influence on K of DNP-AA are presented and discussed in sections 7.1.2 and 7.1.3, respectively. Since the deviations between absorbance-based $K_{DNP-AA}^{exp,A}$, and mole fraction-based $K_{DNP-AA}^{exp,x}$ were found in this work to be under the experimental uncertainty levels (ARD%≤5), partitioning data are in the present chapter denoted as K_{DNP-AA}^{exp}. All experimental data involved in subchapter 7.1 are provided in Appendix (A9).

The results of the experiments performed in this study were placed into Appendix (A9) for clarity reasons. The discussion presented in the following uses the figures based on the results of multiple measurements that were grouped into tables A9.1, A9.2, and A9.3, in the Appendix (A9). This was done according to the scheme shown in figure 7.1 that has been provided with the intention to easier find the experimental background of data plotted and discussed in subchapter 7.1.

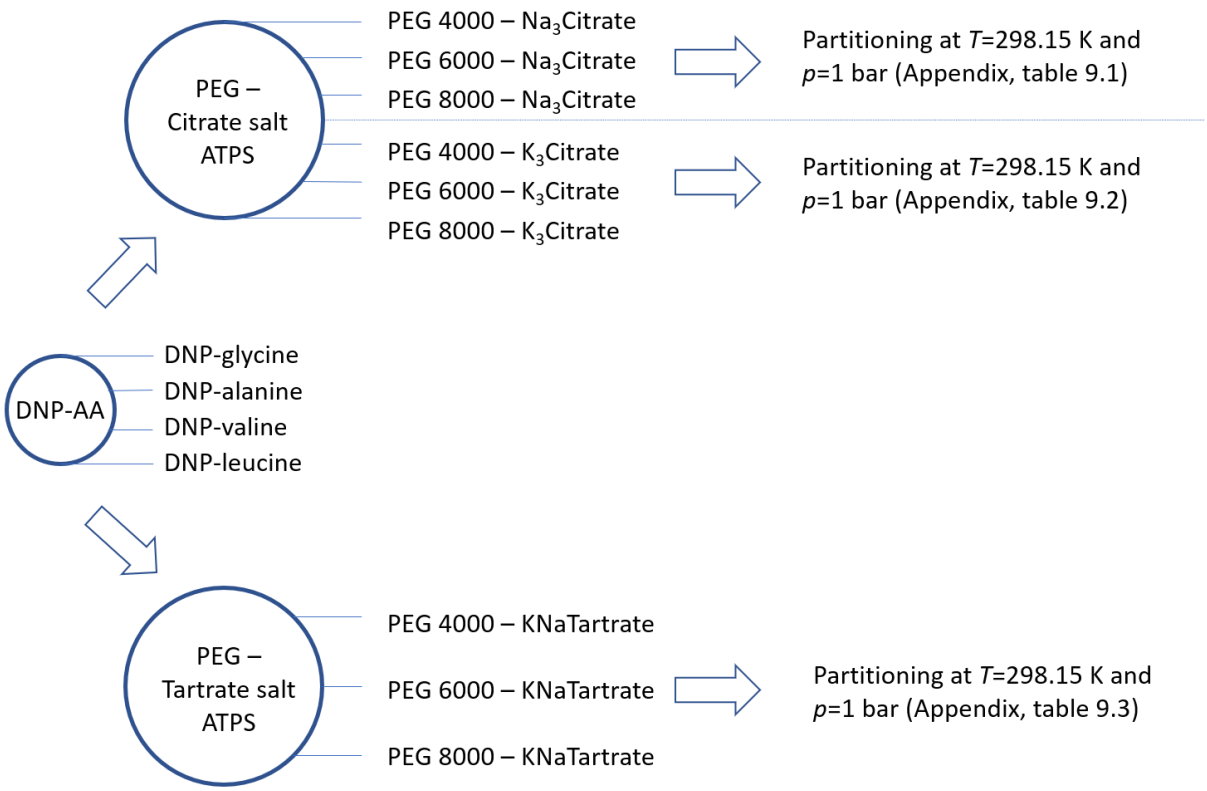

Figure 7.1. Experimental partitioning data measured in this work for DNP-AA, plotted in figures and discussed in subchapter 7.1 (Appendix, A9).

7.1.1. Solute Influence on Partition Coefficient

The partitioning of DNP-AA in ATPS can be influenced by different solute properties, e.g. its charge and molecular structure, as well as by interactions of a solute with phase formers. The latter depends on ATPS composition that in this section is expressed with tie-line length (TLL). All experimental results presented in section 7.1.1 were obtained at T=298.15 K and p=1 bar and are included in Appendix (A9).

The charge of DNP-AA

The pH of ATPS (pH ~ 8, Appendix A4) can change the charge of DNP-AA[8]. The species charge of DNP-glycine at pH of the two ATPS phases (PEG – citrate salts: $\Delta pH_{phases} \leq 0.25$; PEG – tartrate salt: $\Delta pH_{phases} \leq 0.05$) can be deduced from figure 2.1a from section 2.3.2. Figure 2.1a shows the species distribution of DNP-glycine as a function of pH that can be calculated based on its pK_a value (table 2.1). The species distribution data for DNP-AA are also provided in Appendix (A1). The charge of other DNP-AA, namely DNP-alanine, DNP-valine, and DNP-leucine, at pH of ATPS, may be found using similar plot to figure 2.1a

and pK_a values from table 2.1. In sum, each DNP-AA studied in this work is fully present as just negatively charged species (q = -1; $\alpha_{DNP-AA^-} = 1$) in both phases of ATPS: PEG (PEG 4000, 6000, 8000) – biodegradable salt (Na_3Citrate, K_3Citrate, KNaTartrate). Consequently, the experimental partition coefficient K^{exp}_{DNP-AA} measured for DNP-AA is the same as for the respective species ($K^{exp}_{DNP-AA} = K^{exp}_{DNP-AA^-}$). Since there is just one type of the species present in both phases, in this case, a difference in pH of ATPS phases ($\Delta pH_{phases} \leq 0.25$) should not have influence on K^{exp}_{DNP-AA}. It is also important to mention that ΔpH_{phases} of each ATPS studied was not noticeably changed by using PEG of different molar mass, but it was more influenced by changing the anion of a salt.

The molecular structure of DNP-AA

In this work, the homologous series of DNP-AA such as DNP-glycine, DNP-alanine, DNP-valine, and DNP-leucine were considered. DNP-AA have aromatic dinitrophenyl group connected with amino acid group. Since these DNP-AA differ just of the side-chain amino acid group, it is expected that any change within this polar group can influence the behavior of DNP-AA in ATPS. Also, polar group of DNP-AA is responsible for interactions e.g. hydrogen bonding of whole DNP-AA molecule in aqueous solution. The results of DNP-AA partitioning in ATPS formed by PEG 4000 and organic salt (Na_3Citrate, K_3Citrate, KNaTartrate) are presented in figure 7.2. For a better comparison, figure 7.2 contains partitioning data obtained in three ATPS of similar TLL (ARD% ≤ 0.7). TLL were calculated according to equation (3.3). All DNP-AA studied are partitioned mostly to the top PEG-rich phase. The highest K values were observed for DNP-leucine and the lowest for DNP-glycine. According to experimental data (subchapter 5.1) the partitioning trend $K^{exp}_{DNP-leucine} > K^{exp}_{DNP-valine} > K^{exp}_{DNP-alanine} > K^{exp}_{DNP-glycine}$ does not match the order of solubility in water ($m^L_{DNP-alanine} > m^L_{DNP-valine} > m^L_{DNP-glycine}$ and $m^L_{DNP-leucine}$), but it follows the sequence of molar mass M_n of DNP-AA ($M_{DNP-leucine} > M_{DNP-valine} > M_{DNP-alanine} > M_{DNP-glycine}$).

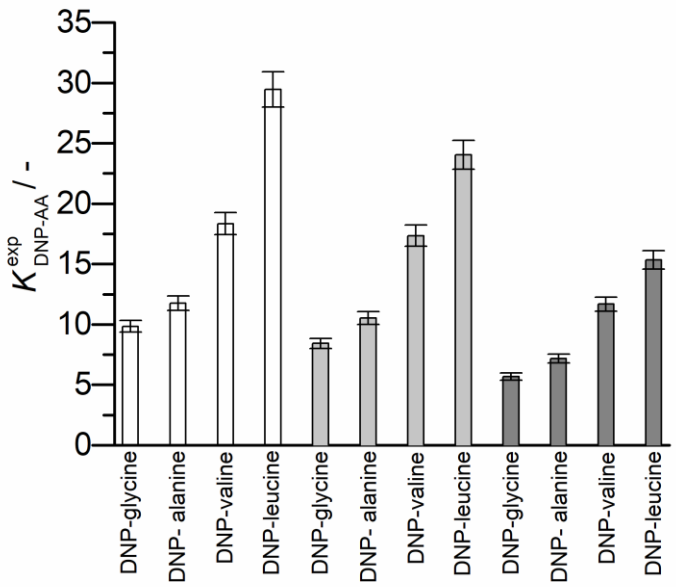

Figure 7.2. Experimental partition coefficients of DNP-AA (K^{exp}_{DNP-AA}) measured at T=298.15 K and p=1 bar in ATPS formed by PEG 4000 and biodegradable salt: Na_3Citrate (white bars, TLL = 0.334), K_3Citrate (gray bars, TLL = 0.337), KNaTartrate (dark gray bars, TLL = 0.333). The feed and equilibrium composition for a given TLL are provided in Appendix (A8).

Combined effects: the molecular structure of DNP-AA and ATPS composition

Since the difference between the homological DNP-AA considered in this work lies in the number of methylene groups in the molecule, the side chains of DNP-AA are the sites that determine the partitioning of these DNP-AA. In the literature, Zaslavsky has reported the estimated average number of methylene groups $n(CH_2)$ of amino acids (table 7.1) [88]. This is experimentally determined value rather than the real number of CH_2 groups in the amino acid molecule and has been established to express the relative hydrophobicity of amino acids.

Table 7.1. Relative hydrophobicity, $n(CH_2)$ for aliphatic AA proposed by Zaslavsky [88].

Amino Acid	$n(CH_2)$
glycine	241.16
alanine	255.18
valine	283.24
leucine	297.26

Figure 7.3 presents the influence of $n(CH_2)$ on partitioning of DNP-AA. A linear correlation between the relative hydrophobicity and partitioning was obtained after linear regression (average r^2=0.999). These lines were provided just to guide the eye and to show the trend of partitioning data. An increase of $n(CH_2)$ improves partition coefficient of studied DNP-AA.

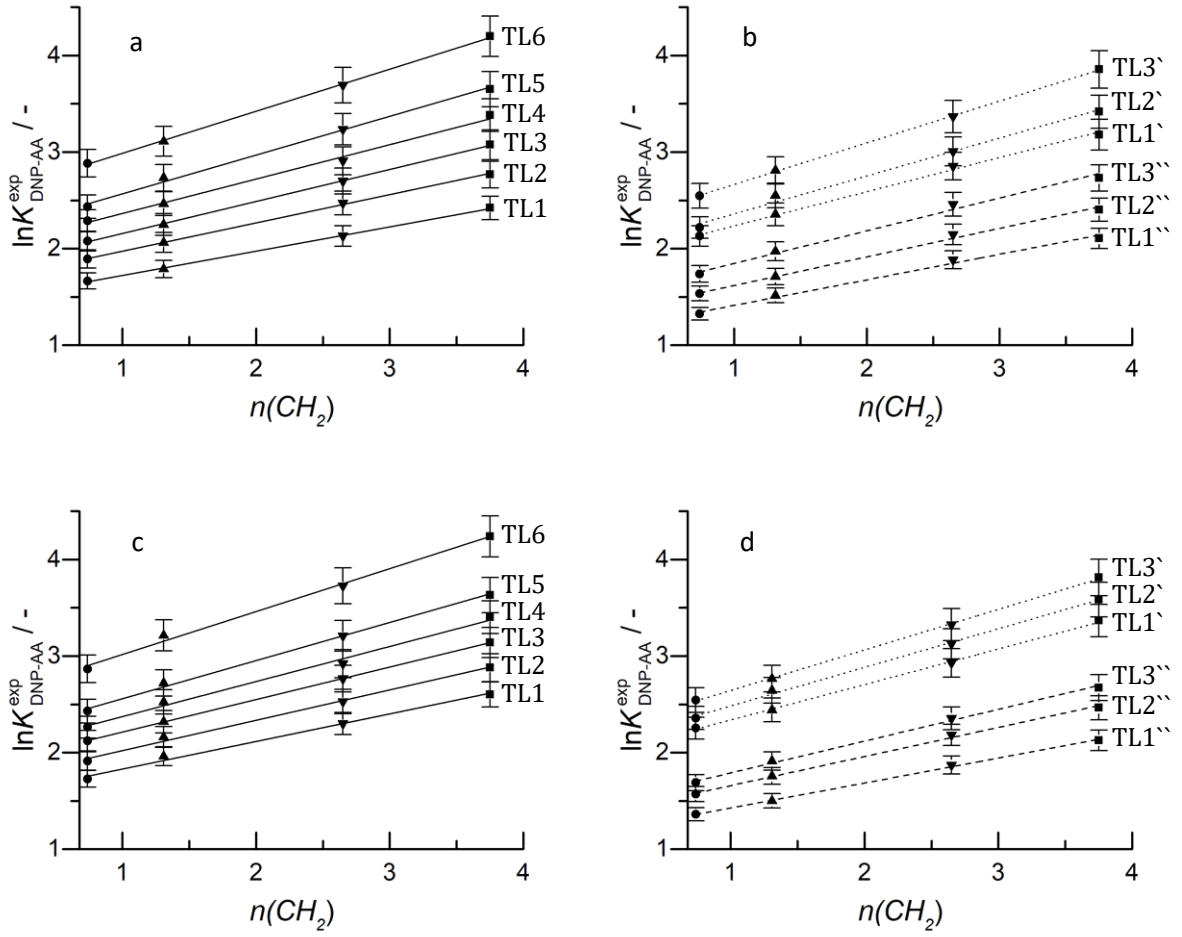

Figure 7.3. Logarithm of experimental partition coefficients of DNP-AA ($\ln K^{exp}_{DNP-AA}$): DNP-glycine(●), DNP-alanine (▲), DNP-valine (▼), DNP-leucine (■) at T=298.15 K and p=1 bar, plotted against average number of $n(CH_2)$ [88]; ATPS formed by PEG (a-b: PEG 4000, c-d: PEG 6000) and biodegradable salt (Na_3Citrate: solid line, K_3Citrate: dotted line, KNaTartrate: dashed line); The lines are obtained after linear regression (average r^2=0.999 for all TL and ATPS considered in this work) and applied just to guide the eye and improve the readability. The feed and equilibrium composition for a given TL are provided in Appendix (A8).

Both figure 7.2 and figure 7.3 present the same trend that points out that PEG - $Na_3Citrate$ can be considered as the most efficient for DNP-AA partitioning (with the highest K_{DNP-AA}^{exp}). The lowest values of partition coefficients can be observed for ATPS composed by PEG and KNaTartrate.

Since the interactions of DNP-AA with ATPS phases depend on the system composition, the most useful representation can be done by plotting partitioning data against TLL. As shown in figure 7.4 the partition coefficient of all DNP-AA increases when the TLL increases.

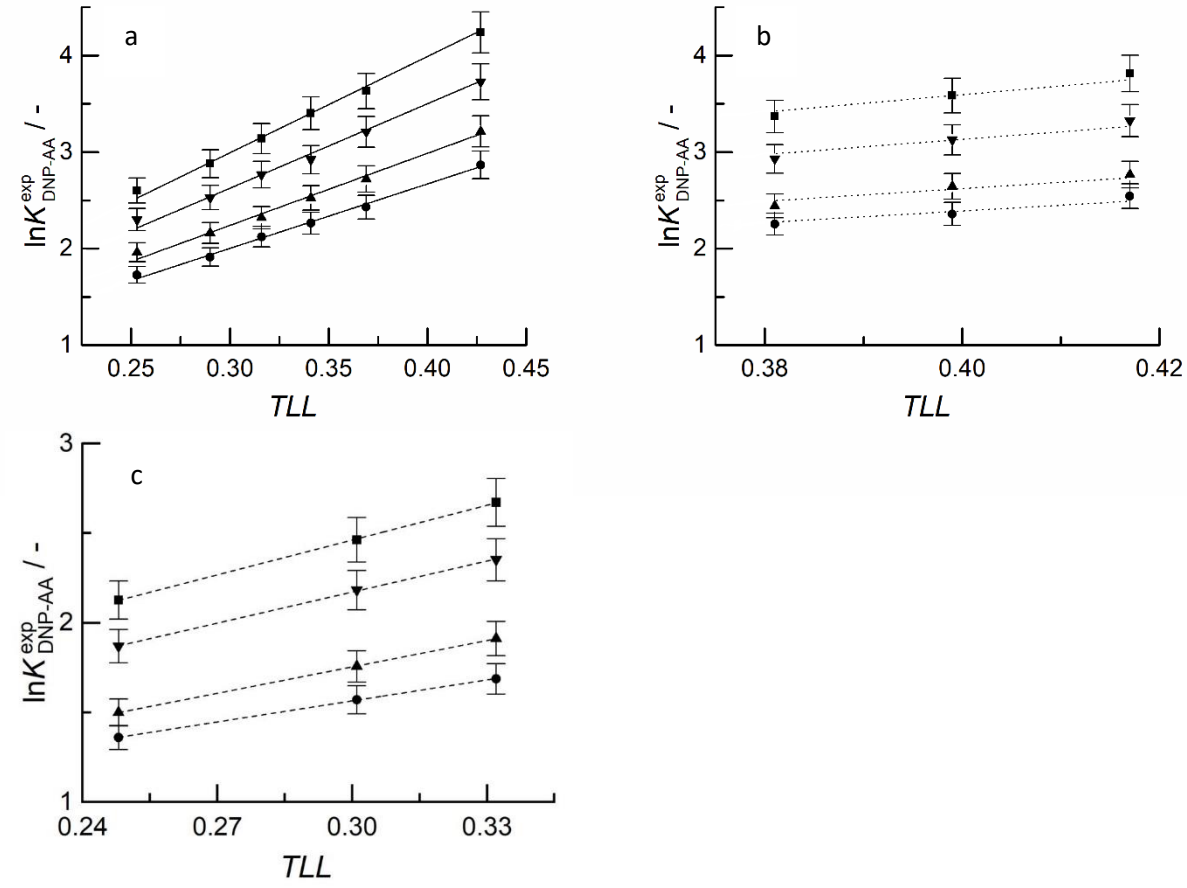

Figure 7.4. Logarithm of experimental partition coefficients of DNP-AA ($\ln K_{DNP-AA}^{exp}$): DNP-glycine(●), DNP-alanine (▲), DNP-valine (▼), DNP-leucine (■) at T=298.15 K and p=1 bar, plotted against TLL of ATPS formed by PEG 6000 and biodegradable salt - $Na_3Citrate$ (a): solid line, $K_3Citrate$ (b): dotted line, or KNaTartrate (c): dashed line. The lines were obtained after linear regression (average r^2=0.999 for all TL and ATPS considered in this work) and were applied just to guide the eye and improve the readability. The feed and equilibrium composition for a given TL are provided in Appendix (A8).

Figure 7.4 shows only TLL regions at which it could be possible to measure the partitioning with reasonable accuracy. The lines presented in figure 7.4 were included just to show the trend of experimental data and to guide the eye. This way of presenting partitioning data (at just certain range of TLL, as data points, and using the line to guide the eye) was also used in the literature [405-409]. The low regions of TLL might also not be of interest for industrial applications as it is very hard to keep systems of low TLL at their heterogenous state at which the two phases are present (the two-phase system of low TLL can become homogenous i.e. one-phase system after addition of a solute or after a slight change of the temperature or pressure).

In this work, $\ln K_{DNP-AA}^{exp}$ plotted against TLL exhibited the linear trend (if using linear regression $r^2 > 0.99$ for all DNP-AA and ATPS from this study), however, it might be that the linearity of $\ln K_{DNP-AA}^{exp}$ is only valid at a narrow range of TLL considered in this work. Thus, it is possible that at TLL outside of this range, e.g. at very low TLL or very high TLL, a significant deviation from the non-linearity is present [410, 411]. Such a non-linear behavior, when $\ln K_i^{exp}$ was plotted over TLL, has been already observed in the literature, for example for human serum albumin partitioned in different PEG – salt ATPS [407]. However, at certain TLL ranges some linearity was also observed [407]. Since measuring data at very low TLL may be coupled with high experimental uncertainty, in this work the trend lines were not extrapolated to the regions where no experimental data could be provided. Also, the lines obtained with linear regression were added only for better readability of the results [405-409]. The values of $\ln K_{DNP-AA}^{exp}$ obtained in this work at a certain TLL range (and relatively far from TLL = 0) were insufficient for an accurate estimation of $\ln K_{DNP-AA}^{exp}$ observed at TLL $\sim$ 0. Thus, to avoid wrong assumptions, all figures presenting $\ln K_{DNP-AA}^{exp}$ versus TLL only show partitioning data at TLL that could be confirmed with experimental results carried out in this study.

It is suggested in some publications that K_i^{exp} can be described using $\ln K = \alpha \cdot TLL + b$ correlation, and that a linear extrapolation of $\ln K_i^{exp}$ toward TLL reaches the value of zero at TLL = 0 (l nK_i^{exp} = 0 if K_i^{exp}= 1) [97, 350]. However, experimental results obtained in the literature for different solutes (e.g. proteins) partitioned in ATPS (also PEG – salt) and plotted in figures as $\ln K_i^{exp}$ or K_i^{exp}versus TLL, do not fully ascertain an assumption that minimum $\ln K_i^{exp}$ approaches zero with the linear trend [407-409, 412-

414]. Also, in this work the values of intercept calculated only using the range of experimental data ($\ln K = \alpha \cdot TLL + b$) for PEG 6000 – Na_3Citrate ATPS were ≠ 0 (intercepts: b = 0.07 for DNP-glycine, 0.14 for DNP-alanine, 0.20 for DNP-leucine, and 0.21 for DNP-valine). Thus, based on experimental data, the trend lines of $\ln K_i^{exp}$ versus TLL do not necessarily reach the origin of the figure if a straight line is extrapolated to TLL = 0.

The values of $\ln K_i^{exp}$ calculated from experimental K_i^{exp} could be positive (if component has affinity to the top phase) or negative (if component has affinity to the bottom phase). In former publications, $\ln K_i^{exp}$ calculated from experimental data at lower TLL are far from being zero, especially if the component has an affinity to the bottom phase [406, 409]. Negative and positive $\ln K_i^{exp}$ for different components were reported in the literature[406, 409]. In this work, both variants (negative and positive values of $\ln K_i^{exp}$) were also observed, however, the case when the molecule was partitioned to the bottom phase (VC, Appendix A.10) was not further considered due to very low K_{VC}^{exp} obtained in preliminary tests. Thus, ATPS studied in this work were not considered as appropriate media for an efficient separation of VC. Also, the alternating K_{VC}^{exp} datapoints did not allow a correlation and respective conclusion on its behavior in ATPS.

The dependence observed in figure 7.4 can result from higher hydrophobicity of the phases when more PEG and salt is added to a system. An increase of salt concentration influences the ionic strength and can result in the K_{DNP-AA}^{exp} improvement [95, 415]. Also, changing PEG concentration can impact K_{DNP-AA}^{exp} through hydrophobic PEG – DNP-AA interactions or increased cross-association forces[95]. To eliminate additional effects in partitioning that might be induced by higher solute concentration, aqueous solute solution added to ATPS contained low concentration of DNP-AA ($m_{DNP\text{-}AA} \leq 0.008$ g·mol^{-1}). This means that each ATPS of total mass equal to 1 g contained at maximum ≈ 0.2 mg of DNP-AA. The solubility of DNP-AA was low enough to assume that this approach has been appropriate (since just low concentrations of DNP-AA can be found in aqueous solutions). K_{DNP-AA}^{exp} was determined after linear regression from the slope of straight lines ($r^2 \approx 0.999$) obtained by plotting the absorbance/fluorescence/concentration of the top (y axis) versus bottom phase (x axis). All data were collected from the samples containing different concentrations of a given DNP-AA in ATPS.

The following sections (7.1.2 and 7.1.3) evaluate in more detail salt and PEG influence on the partitioning using the relation between K_{DNP-AA}^{exp} and TLL, since the way of data presentation shown in figure 7.4 is the most convenient and frequently found in literature[350, 368, 416-418]. This is especially valuable for comparing the partitioning in different ATPS.

7.1.2. Salt Influence on Partition Coefficient

Selecting biodegradable salts for ATPS that could be also appropriate for DNP-AA partitioning requires experimental partitioning data. The results of DNP-AA partitioning in ATPS composed by PEG and salt, at T=298.15 K and p=1 bar, are included in Appendix (A9). Partition coefficients determined for DNP-AA in a system formed by PEG 8000 and salt (organic and inorganic) are shown in figure 7.5. This figure proves the merit of replacing environmentally inconvenient salts (Na_2SO_4 and $MgSO_4$) with more convenient and non-toxic organic salts (Na_3Citrate, K_3Citrate, KNaTartrate). Na_2SO_4 can be successfully replaced with biodegradable Na_3Citrate leading to very comparable partitioning of DNP-AA, while KNaTartrate allows similar outcomes as $MgSO_4$. In general, the favorable trend observed for DNP-AA partitioning in ATPS composed by PEG and Na_3Citrate (the highest K_{DNP-AA}^{exp}) proves that the presence of sodium cation in a molecule is more beneficial for DNP-AA partitioning than potassium (for citrates) or magnesium (for sulfates). Citrate-based salts may cause higher repulsion to DNP-AA species than the tartrate-based salt KNaTartrate due to presence of higher valency in citrate (-3) over tartrate (-2). Thus, the citrate anion could be more convenient than tartrate. However, it is not possible to fully ascertain the reasons of that behavior being based on figure 7.5 only.

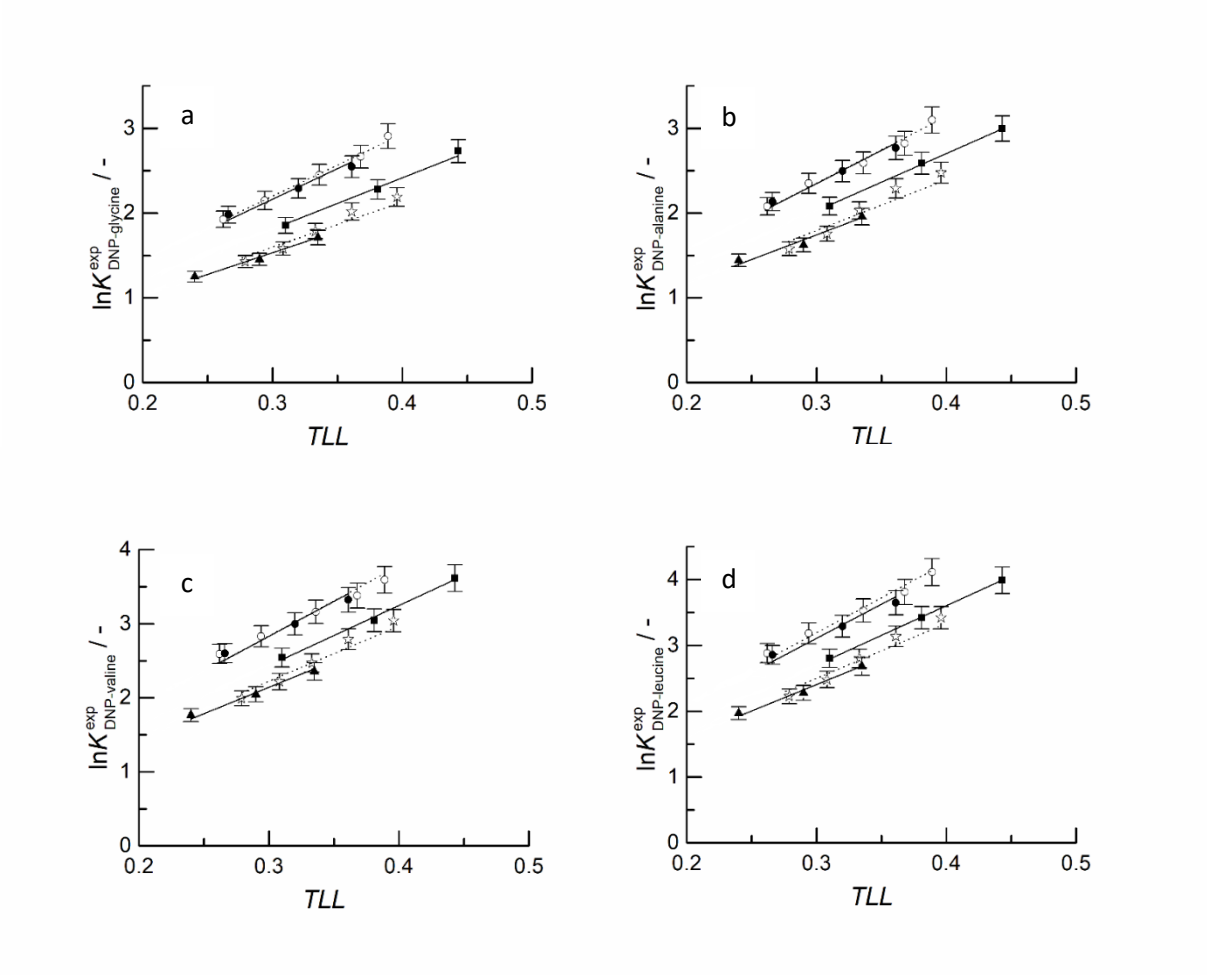

Figure 7.5. Logarithm of experimental partition coefficients of DNP-AA ($\ln K^{exp}_{DNP-AA}$): DNP-glycine (a), DNP-alanine (b), DNP-valine (c), DNP-leucine (d), at T=298.15 K and p=1 bar, plotted against TLL of ATPS: PEG 8000 and inorganic salt (open symbols, dotted lines) or PEG 8000 - organic biodegradable salt (closed symbols, solid lines). Inorganic salts: Na_2SO_4 (○), $MgSO_4$ (☆). Organic salts: Na_3Citrate(●), K_3Citrate(■), KNaTartrate (▲). The lines were obtained after linear regression (average r^2=0.999 for all TL and ATPS considered in this work) and were applied just to guide the eye and improve the readability. The feed and equilibrium composition for a given TL are provided in Appendix (A8). The diagram shows only TLL regions at which it could be possible to measure the partitioning with reasonable accuracy.

7.1.3. PEG Influence on Partition Coefficient

A higher affinity to the upper PEG-phase was observed for all DNP-AA considered. Aqueous solutions containing PEG of different average molar mass can have also different physicochemical properties, such as density or viscosity. However, introducing PEG of different average molar mass may also influence its ability of binding solutes (e.g. through hydrogen bonding interactions). For this reason, it is of importance to study the PEG`s

molar mass effect on DNP-AA partitioning in ATPS. Experimental partitioning data in ATPS composed by PEG 4000, PEG 6000, and PEG 8000 and biodegradable salt (Na_3Citrate, K_3Citrate, KNaTartrate) were measured in this work at T=298.15 K and p=1 bar and the results can be found in Appendix (A9). These data are also plotted in figure 7.6.

The major conclusion based on data plotted in figure 7.6 is that the average molar mass range of PEG (M_{PEG} = 4000 – 8000 g·mol^{-1}) used in the experiment leads to very comparable partitioning results. Based on the examples shown in figure 7.6, PEG 4000 seems to be slightly more advantageous for DNP-AA partitioning than other PEGs. However, in most cases, the differences resulting from the usage of different average molar mass PEG are within an experimental error. The influence of PEG molar mass within the range of M_{PEG} = 4000 – 8000 g·mol^{-1} is much smaller from the salt effect on DNP-AA partitioning presented in the previous section (7.1.2).

a – b: PEG - Na_3Citrate

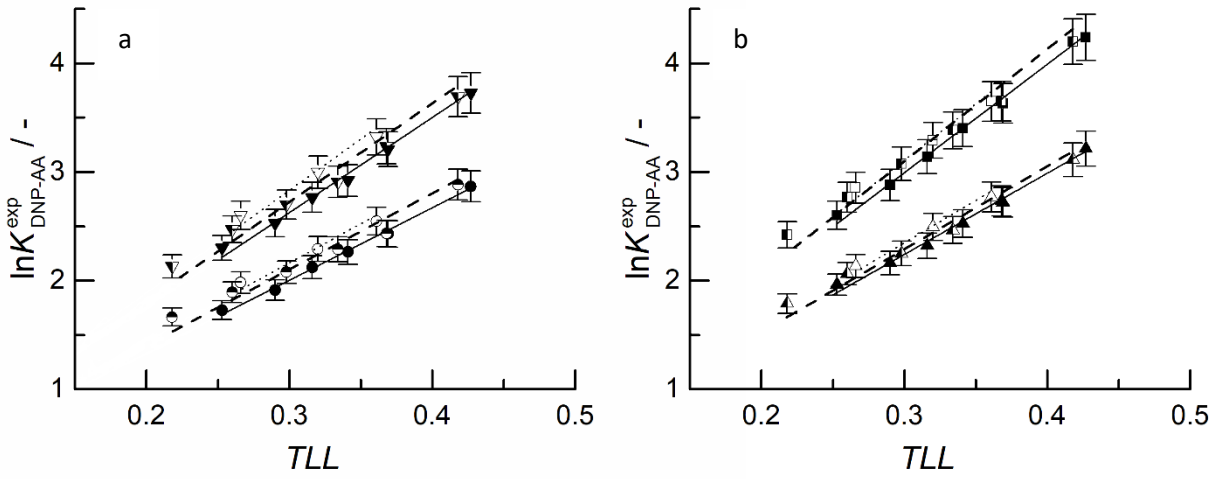

c – d: PEG - K_3Citrate

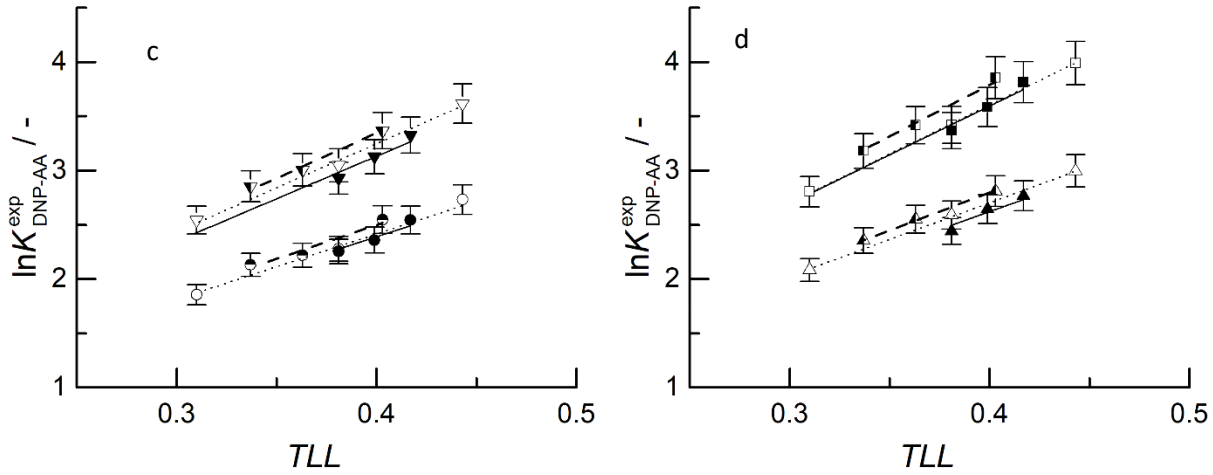

e – f: PEG – KNaTartrate

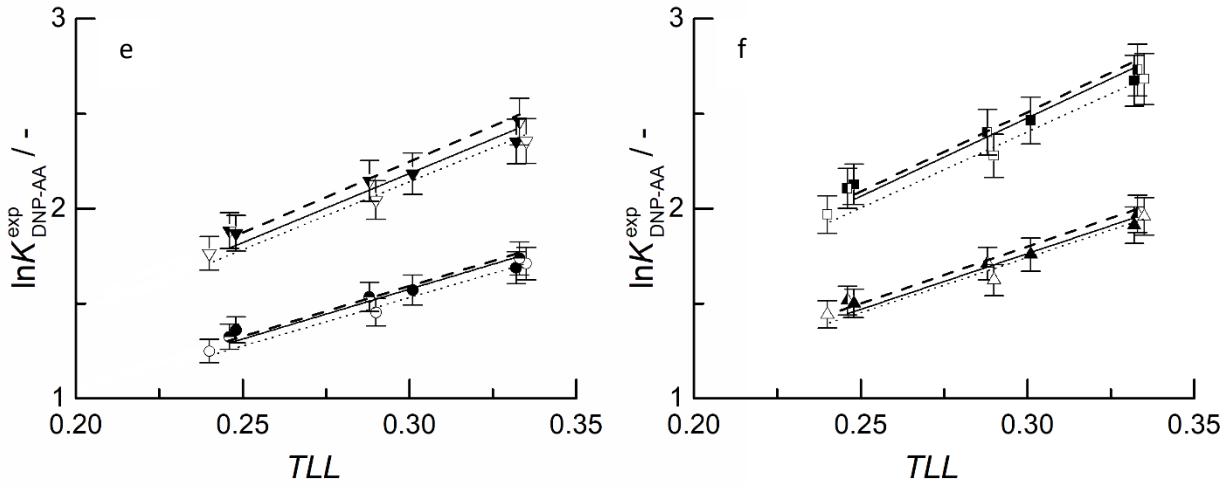

Figure 7.6. Logarithm of experimental partition coefficients of DNP-AA ($\ln K^{exp}_{DNP-AA}$) at T=298.15 K and p=1 bar, plotted against TLL of ATPS formed by PEG: PEG 8000 (open symbols and dotted lines), PEG 6000 (solid symbols and solid lines), or PEG 4000 (half open symbols and dashed lines), and biodegradable salt: Na_3Citrate (a-b), K_3Citrate (c-d), or KNaTartrate (e-f). The lines are obtained after linear regression (average r^2=0.999 for all TL and ATPS considered), applied just to guide the eye and improve the readability. DNP-AA partitioned in ATPS: DNP-glycine (PEG 8000 ○, PEG 6000 ●, PEG 4000 ◓), DNP-alanine (PEG 8000 △, PEG 6000 ▲, PEG 4000 ◭), DNP-valine (PEG 8000 ▽, PEG 6000 ▼, PEG 4000 ▾), DNP-leucine (PEG 8000 □, PEG 6000 ■, PEG 4000 ◧). The feed and equilibrium composition for a given TL: Appendix (A8). The diagram shows only TLL regions at which it could be possible to measure the partitioning with reasonable accuracy.

7.2. Experimental Results: Water-Soluble Vitamins

The partition coefficient (K) of water-soluble vitamins in ATPS formed by PEG of average molar mass M_{PEG} = 4000 – 6000 g·mol^{-1} and biodegradable salt $Na_3Citrate$ or $Na_2Tartrate$ depends on the properties of these vitamins, especially on their behavior in aqueous solutions and the interactions with phase forming compounds. This means that both the charge of vitamin at given pH and the molecular structure of vitamin must be considered. As previously mentioned for DNP-AA in section 7.1, the charge state of a solute in ATPS, is influenced by the concentration and the properties of all system constituents. Water-soluble vitamins are classified based on their biological function, so their molecular structures and properties strongly differ from each other. Selecting the more efficient ATPS in terms of solute partitioning requires extensive studies on the effects that can rule vitamin partitioning and that are caused by introducing to ATPS e.g. different salt anion and cation of salt or PEG of different molar mass.

Sodium salts were chosen based on the previous results, the LLE (chapter 6) and partitioning of organic solutes (DNP-AA, subchapter 7.1). The selection criterium for salt was based on former observation that biphasic regions of ATPS formed by $Na_3Citrate$ were larger than in the systems composed by $K_3Citrate$ or KNaTartrate. Also, higher K_{DNP-AA}^{exp} were obtained in PEG – $Na_3Citrate$ ATPS. However, there was not enough evidence for a good comparison of anion effect in terms of partitioning in ATPS, thus, also in this evaluation the salts of two anions were involved: $Citrate^{3-}$ and $Tartrate^{2-}$. PEG`s molar mass was selected based on the former results, but also on the view of possible future application in industry. Although PEG of M_{PEG} = 8000 g·mol^{-1} has shown to be an efficient media for the two-phase formation (chapter 6), its properties might cause difficulties in handling of the system. Therefore, the application of ATPS formed by PEG of M_{PEG} = 8000 g·mol^{-1} can be limited by its viscosity. In this context, more preferred ATPS could be formed by lower PEG´s molar mass, e.g. M_{PEG} = 4000 g·mol^{-1}. The importance and influence of this factor on vitamin partitioning was evaluated in this subchapter.

Section 7.2.1 of this document presents experimental data and discusses the influence of the properties of water-soluble vitamins on experimental K. Further sections (7.2.2 and 7.2.3, respectively) evaluate an impact of salt and PEG on partitioning of water-soluble vitamin in ATPS. Since the deviations between absorbance-based $K_{vitamin}^{exp,A}$, and mole

fraction-based $K_{vitamin}^{exp,x}$, were in this work under the experimental uncertainty levels (ARD% ≤ 5), partitioning data are in the following sections of this document denoted as $K_{vitamin}^{exp}$. Experimental data involved in subchapter 7.2 are provided in Appendix (A10).

The results of the experiments performed in this study were placed into Appendix (A10) for clarity reasons. The discussion presented in the following uses the figures based on the results of multiple measurements that were grouped into tables A10.1 and A10.2 in the Appendix (A10). It was done according to the scheme shown in figure 7.7 that has been provided with the intention to facilitate finding the experimental background of data plotted and discussed in subchapter 7.2.

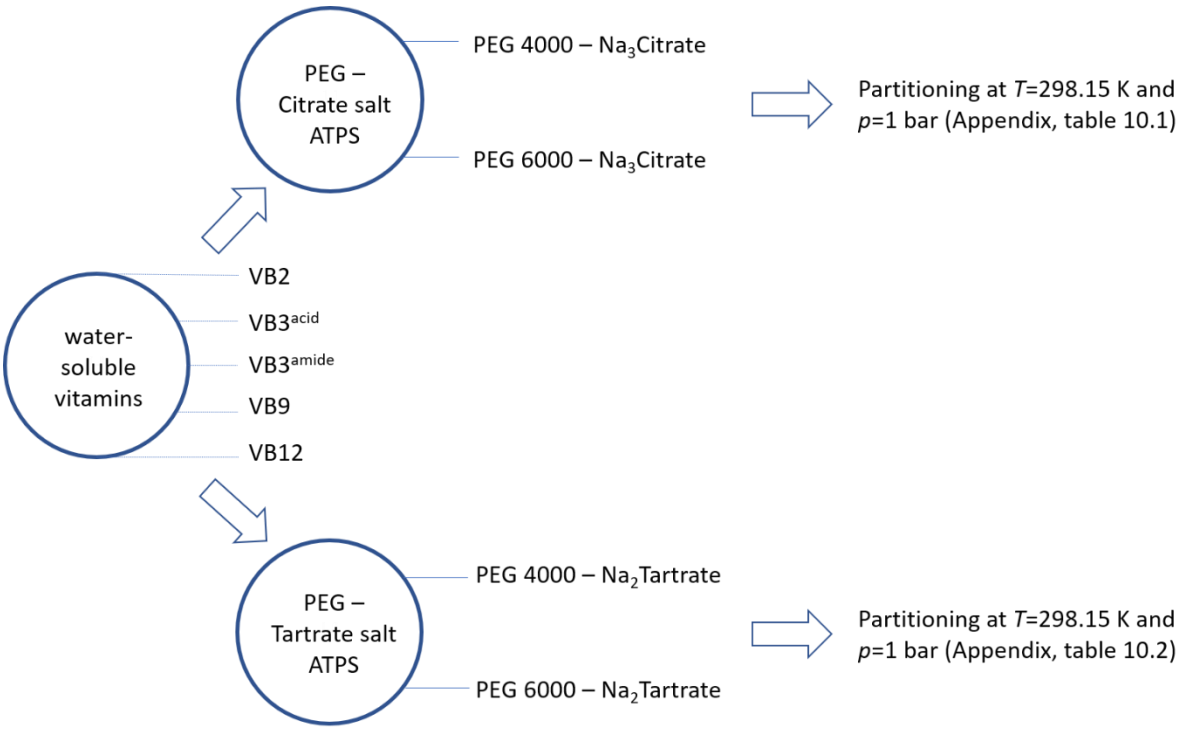

Figure 7.7. Experimental partitioning data measured for water-soluble vitamins in this work, plotted in figures and discussed in subchapter 7.2 (Appendix, A10).

7.2.1. Solute Influence on Partition Coefficient

The partitioning of water-soluble vitamin in ATPS can be influenced by its different properties, e.g. the charge and molecular structure. In general, various interactions which are occurring in ATPS between a solute and phase forming components determine vitamin affinity to each phase. The latter depends on ATPS composition that in this section is expressed with tie-line length (TLL). All experimental results presented in section 7.2.1 were obtained at T=298.15 K and p=1 bar and are included in Appendix (A10).

The charge of water-soluble vitamin

The pH of ATPS (pH~8, Appendix A4) can change the charge of vitamin [6, 7]. The presence of different vitamin species at pH of the phases (PEG – $Na_3Citrate$: $\Delta pH_{phases} \leq 0.25$; PEG – $Na_2Tartrate$: $\Delta pH_{phases} \leq 0.05$) in ATPS formed by PEG of M_{PEG} = 4000 – 6000 g·mol^{-1} and biodegradable salt $Na_3Citrate$ or $Na_2Tartrate$ can be deduced from figure 4.5. It results from calculations of ionic distribution using pK_a values from table 2.1. ΔpH_{phases} for each ATPS considered in this evaluation do not noticeably change by using PEG of different molar mass, but it is much more influenced by changing the anion of a salt.

Based on figure 4.5, at pH~8 the water-soluble vitamins are negatively charged ($VB2^{2-}$, $VB3^{acid\,-}$, $VB9^{2-}$, $VB9^{3-}$) or neutral ($VB3^{amide}$, VB12). At this pH, both VB2 and $VB3^{acid}$ exist solely as single-negatively charged species (q = -1). Others, $VB3^{amide}$ and VB12 are present exclusively as neutral species. Almost all vitamins studied in this work (except VB9) are fully present as just one type of species in both phases of considered ATPS. Thus, the partition coefficient $K_{vitamin}^{exp}$ determined from the experimental measurements for vitamins VB2, $VB3^{acid}$, $VB3^{amide}$, and VB12, is the same as for the respective species ($K_{vitamin}^{exp} = K_{j,vitamin}^{exp}$). Since there is just one type of the species present in both phases (molar fractions in both phases $\alpha_{j,\,vitamin} \approx 1$), in this case, a difference in pH of ATPS phases ($\Delta pH_{phases} \leq 0.25$) should not have an influence on $K_{vitamin}^{exp}$. The species distribution of each vitamin partitioned in ATPS of pH~8 is provided in Appendix (A2).

More complex situation is observed for VB9, which at pH of ATPS can be present as a mixture of species $VB9^{2-}$ and $VB9^{3-}$. Furthermore, a difference in pH of the phases $\Delta pH_{phases} \leq 0.25$ for PEG – $Na_3Citrate$ influences distribution of VB9 species between the phases ($\alpha_{VB9\,2-} = 0.41$ and $\alpha_{VB9\,3-} = 0.59$ at pH = 8.25 of the bottom phase; $\alpha_{VB9\,2-} = 0.31$ and $\alpha_{VB9\,3-} = 0.69$ at pH = 8.45 of the top phase). In contrary, ΔpH_{phases} of ATPS formed by PEG and $Na_2Tartrate$ reached very low level ($\Delta pH_{phases} < 0.05$). Thus, it can be assumed that there is the same VB9 species distribution in both phases (ARD% between the species distribution of $VB9^{2-}$ and $VB9^{3-}$ < 5 %).

The partition coefficient of VB9 species can be calculated with equation (3.11). This requires species distribution of VB9, calculated at pH of ATPS phases ($\alpha_{j,vitamin}^{I}$ and $\alpha_{j,vitamin}^{II}$), as well as experimental partition coefficients, measured in this work at

T=298.15 K and p=1 bar. The $K_{j,vitamin}^{exp}$ of vitamin species (j = $VB9^{2-}$, $VB9^{3-}$), and the experimentally determined $K_{vitamin}^{exp}$ of VB9 in ATPS composed by PEG 6000 and $Na_3Citrate$, are presented in figure 7.8. These data can be also found in Appendix (table A10.1). Through electrostatic interactions, the more negatively charged species $VB9^{3-}$ tend to partition towards the more basic phase (in this case – PEG-rich). This trend has been already reported in the literature [85]. It is then expected that $VB9^{3-}$ will have higher $K_{j,vitamin}^{exp}$ than $VB9^{2-}$ in ATPS considered in the present study.

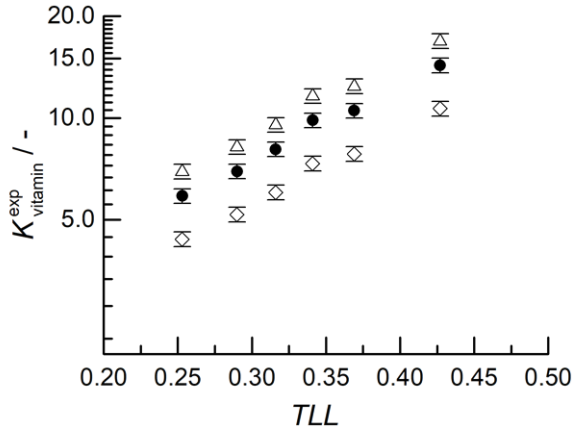

Figure 7.8. Partition coefficients of VB9 species (open symbols: $K_{j,vitamin}^{exp}$) and VB9 (black symbols: $K_{vitamin}^{exp}$) in ATPS: PEG 6000 – $Na_3Citrate$, at different TL compositions, T = 298.15 K and p = 1 bar. Open symbols ◇ ($VB9^{2-}$) and △ ($VB9^{3-}$) represent calculated $K_{vitamin,j}^{exp}$ with equation (3.11). Full symbols ● (VB9) are experimental data points for VB9 (total, contains $VB9^{2-}$ and $VB9^{3-}$) measured in this work. Data plotted in this graph is given in Appendix (table A10.1).

The molecular structure of water-soluble vitamin

In this evaluation, several vitamins that belong to the B-complex water-soluble vitamins group were chosen: VB2, $VB3^{acid}$, $VB3^{amide}$, VB9, VB12. These vitamins were classified to the B-complex group based on their biological function and not the molecular structure. The results of vitamin partitioning in ATPS formed by PEG 4000 and organic salt ($Na_3Citrate$, $Na_2Tartrate$) are presented in figure 7.9. For a better comparison, figure 7.9 contains partitioning data obtained in the two ATPS (PEG 4000 - $Na_3Citrate$, PEG 4000 - $Na_2Tartrate$) of similar TLL (ARD%≤0.7%). TLL were calculated according to equation (3.3). All vitamins studied are partitioned mostly to the top PEG-rich phase.

The partition coefficients of vitamins do not only depend on charge (on their species distribution), and thus not only on electrostatic interactions. The strong pH-dependency of the partition coefficients shown previously in figure 7.8 is caused by the presence of different VB9 species. However, the pH and thus electrostatic interactions are not dominating vitamin partitioning for those vitamins that are exclusively present as one species in the ATPS [7]. This can be seen in figure 7.9 if comparing partitioning of $VB3^{acid}$ and $VB3^{amide}$. $VB3^{acid}$ at pH of considered ATPS exists as negatively charged species (q=- 1, $\alpha_{VB3acid-} = 1$), while $VB3^{amide}$ is in these ATPS neutral (q=0, $\alpha_{VB3amide} = 1$). If these two vitamins are partitioned in ATPS under study, just slightly different $K_{vitamin}^{exp}$ are observed. The highest $K_{vitamin}^{exp}$ values were obtained for VB12 and the lowest for VB2. The partitioning trend $K_{VB12}^{exp} > K_{VB9}^{exp} > K_{VB3}^{exp} > K_{VB2}^{exp}$ also do not really follow the sequence of molar mass M_n of vitamins ($M_{VB12} > M_{VB9} > M_{VB2} > M_{VB3acid} > M_{VB3amide}$). Since the differences in $K_{vitamin}^{exp}$ of $VB3^{acid}$ and $VB3^{amide}$ are close to the experimental error, VB3 in the trend given above refers to both forms of VB3 (acid and amide).

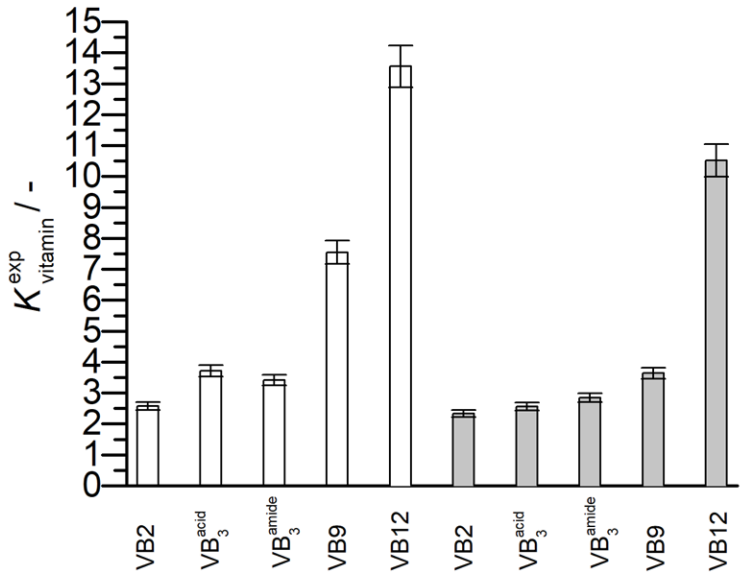

Figure 7.9. Experimental partition coefficients of vitamins ($K_{vitamin}^{exp}$) measured at T=298.15 K and p=1 bar in ATPS formed by PEG 4000 and biodegradable salt: Na_3Citrate (white bars, TLL = 0.298) and Na_2Tartrate (gray bars, TLL = 0.302). The feed and equilibrium composition for a given TLL are provided in Appendix (A8).

The partition coefficient can be influenced by steric entropic effects of the vitamins. VB3 is the smallest vitamin with the lowest molar mass over all studied in this work ($M_{VB3^{acid-}} = M_{VB3^{amide}}$ =122.11 g·mol^{-1}). According to data shown in figure 7.9 the highest *K* determined in this work for PEG 4000 – biodegradable salt was found for VB12. This behavior can be explained by different effects relating to the vitamin properties, e.g. the size. VB12 which is neutral in PEG – Na_3Citrate and PEG – Na_3Tartrate ATPS, is structurally the most complex and the largest vitamin of all water-soluble vitamins (M_{VB12} =1355.37 g·mol^{-1}). The high values of K_{VB12}^{exp} can be related to the fact that large molecules possess larger areas of interactions with the components forming the ATPS [85, 87]. These effects are often discussed in literature when the partitioning of large molecules e.g. proteins is studied [87, 419]. Besides the fact that large molecule of VB12 might have more interactions with PEG due to its size, it can have also stronger interactions due to the presence of functional groups (hydrophobic interactions to PEG, or even hydrogen-bonding effects between PEG and VB12).

Combined effects: the molecular structure of vitamin and ATPS composition

Changing PEG and salt concentration influences the partitioning of vitamins in ATPS in a way that higher $K_{vitamin}^{exp}$ are expected with increasing TLL[7]. This means that since ATPS composition has an influence on the distribution of a solute, it can impact the interactions between the solute and phase forming compounds. This behavior is illustrated in figure 7.10.

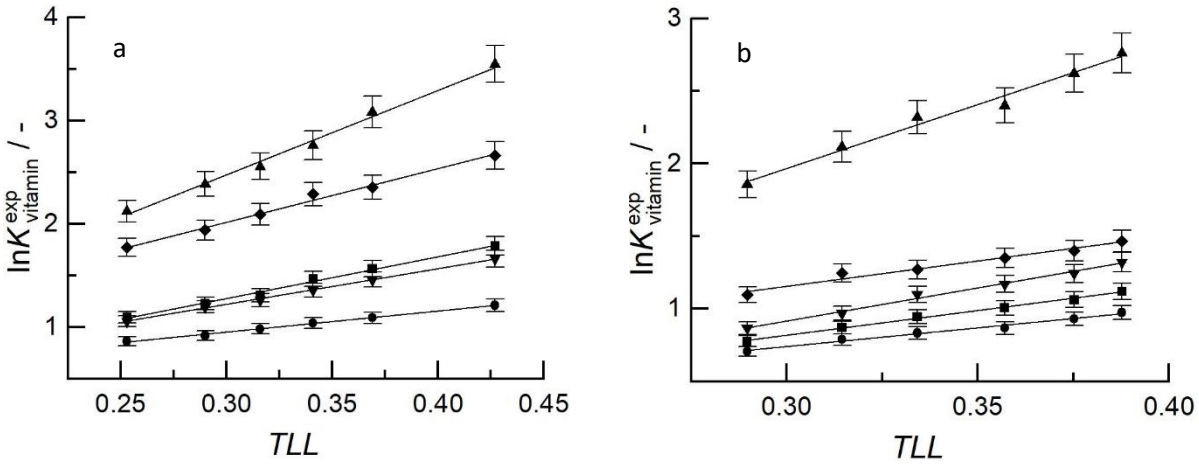

Figure 7.10. Logarithm of experimental partition coefficients of vitamins ($\ln K^{exp}_{vitamin}$): VB2(●), VB3^{acid}(■), VB3^{amide}(▼), VB9(◆), VB12 (▲) at T=298.15 K and p=1 bar, plotted against TLL of ATPS formed by PEG 6000 and biodegradable salt - Na_3Citrate (a) and Na_2Tartrate (b). The lines were obtained after linear regression (average r^2=0.998 for all TL and ATPS considered in this work) and were applied just to guide the eye and improve the readability. The feed and equilibrium composition for a given TL are provided in Appendix (A8).

Figure 7.10 shows only TLL regions at which it was possible to measure the partitioning with reasonable accuracy. The lines presented in figure 7.10 were included just to show the trend of experimental data and to guide the eye. This way of presenting partitioning data (at just certain range of TLL, as data points, and using a linear regression trend to guide the eye) was also used in the literature [405-409]. The reasoning of that was in detail discussed in the previous section 7.1.1. In this work, $\ln K^{exp}_{vitamins}$ plotted against TLL exhibited the linear trend (if using linear regression $r^2 > 0.99$ that did not include critical point at TLL = 0, but only experimental data, for all vitamins and ATPS from this study), however, it might be that the linearity of $\ln K^{exp}_{vitamin}$ is only valid at a narrow range of TLL considered in this work. If this is valid that at TLL = 0 the $\ln K^{exp}_{vitamin}$ reaches also zero, then the intercepts calculated for experimental data in this work would certainly prove the non-linearity of $\ln K^{exp}_{vitamin}$ versus TLL trend. The values of intercept calculated only using the range of experimental data ($\ln K = \alpha \cdot TLL + b$) for PEG 6000 – Na_3Citrate ATPS were ≠ 0 (intercepts: b = 0.02 for VB12, 0.06 for VB3^{acid}, 0.18 for VB3^{amide}, 0.34 for VB2 and 0.45 for VB9).

Increasing the salt concentration impacts the ionic strength and can lead to higher K [95, 415]. Altering PEG concentration might also influence K through hydrophobic PEG – vitamin interactions or increased cross-association forces [95]. Figure 7.10 presents $K_{vitamin}^{exp}$ obtained in ATPS formed by PEG 6000 and salt: Na_3Citrate or Na_2Tartrate. The partitioning trend observed in figure 7.10, namely $K_{VB12}^{exp} > K_{VB9}^{exp} > K_{VB3}^{exp} > K_{VB2}^{exp}$, agrees with the trend that has been found from the previous figure 7.9. To eliminate additional effects in partitioning that might be induced by higher solute concentration, aqueous solute stock solution added to ATPS contained low concentration of vitamin according to their limited solubility (i.e. $0.001 \leq m_{vitamin} \leq 0.016$ mol·kg^{-1}). This means that each ATPS of total mass equal to 1 g contained ≈ 0.2 mg of vitamin at maximum. Also, $K_{vitamin}^{exp}$ values were determined after linear regression from the slope of straight lines ($r^2 \approx 0.998$) obtained by plotting the absorbance/fluorescence/ concentration of the top (y axis) versus bottom phase (x axis). All data were collected from the samples containing different concentrations of a given vitamin in ATPS (0.004 wt-% - 0.02 wt-%).

The following sections (7.2.2 and 7.2.3) evaluate in more detail salt and PEG influence on the partitioning using the relation between $K_{vitamin}^{exp}$ and TLL, since this data presentation is very convenient and frequently found in literature [350, 368, 416-418].

7.2.2. Salt Influence on Partition Coefficient

Selecting biodegradable salt for ATPS that could be also appropriate for vitamin partitioning requires experimental partitioning data. The partitioning results obtained in ATPS composed by PEG and different salts, at T=298.15 K and p=1 bar, are included in Appendix (A10). Partition coefficients $K_{vitamin}^{exp}$ determined for DNP-AA in a system formed by PEG 6000 and PEG 4000 and salt (organic and inorganic) are shown in figure 7.11. The previous results obtained for DNP-AA have shown that the presence of sodium cation in a molecule is more beneficial for DNP-AA partitioning than potassium (for citrates). However, the conclusion regarding the advantage of using citrate anion over tartrate anion for the partitioning of DNP-AA has stayed rather uncertain. Based on figure 7.11 the higher $K_{vitamin}^{exp}$ values are observed for vitamins partitioned in ATPS containing citrate salt.

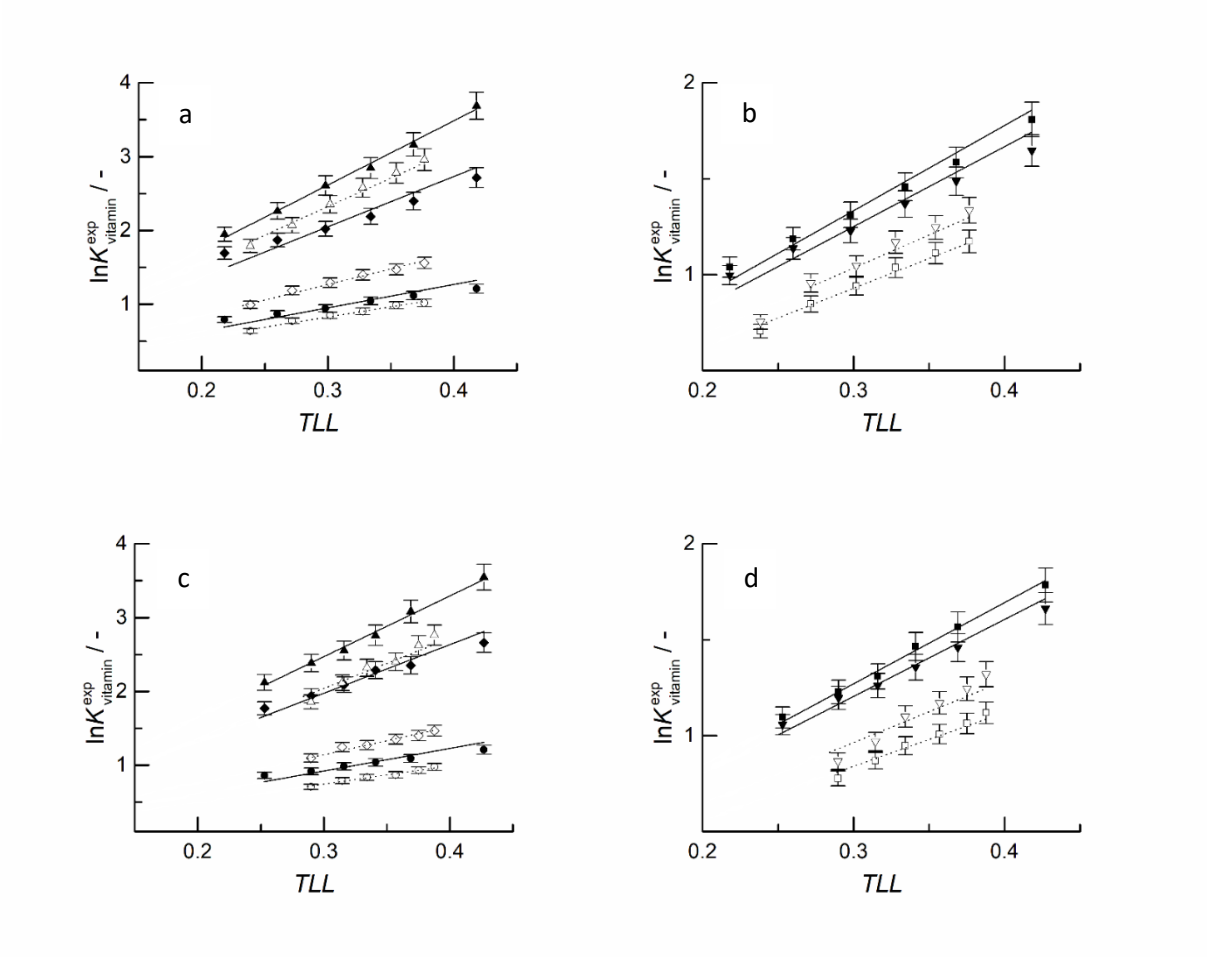

Figure 7.11. Logarithm of experimental partition coefficients of vitamins ($\ln K^{exp}_{vitamin}$): VB2, VB9, VB12 (a,c), VB3^{acid}, VB3^{amide}(b,d), at T=298.15 K and p=1 bar, plotted against TLL of PEG – salt ATPS: PEG 4000 (a-b) or PEG 6000 (c-d) + $Na_3Citrate$ (closed symbols, solid lines) or $Na_2Tartrate$ (open symbols, dotted lines). Vitamins: VB2(●,○), VB3^{acid}(■, □), VB3^{amide}(▼,▽), VB9(◆, ◇), VB12 (▲,△). The lines were obtained after linear regression (average r^2=0.998 for all TL and ATPS considered in this work) and were applied just to guide the eye and improve the readability. The feed and equilibrium composition for a given TL are provided in Appendix (A8).

This is also in agreement with the conclusion regarding DNP-AA from the previous section (7.1.2). Thus, ATPS composed by PEG and $Na_2Tartrate$ do allow only lower $K^{exp}_{vitamin}$ values of vitamins compared to ATPS formed by PEG and $Na_3Citrate$. This partitioning behavior might be related to the fact that the citrate-based salts cause higher repulsion to the vitamin species than the tartrate-based salts The reason for that is the presence of higher valency in citrate (-3) over tartrate (-2). In general, it can be concluded that the highest $K^{exp}_{vitamin}$ values are expected in a system formed by $Na_3Citrate$.

7.2.3. PEG Influence on Partition Coefficient

Experimental partitioning data in ATPS composed by PEG 4000 or PEG 6000 and biodegradable salt (Na_3Citrate, Na_2Tartrate) were measured in this work at T=298.15 K and p=1 bar. Figure 7.12 presents the effect of PEG molar mass on $K_{vitamin}^{exp}$.

The results plotted in figure 7.12 can be found in Appendix (A10). A higher affinity to the upper PEG-phase was observed for all vitamins considered in this evaluation (VB2, $VB3^{acid}$, $VB3^{amide}$, VB9, VB12). Introducing PEG of molar mass in the range selected in this evaluation (M_{PEG} = 4000 g·mol^{-1} or 6000 g·mol^{-1}) influences the partitioning of vitamins. Using PEG of different average molar mass impacts its ability of binding solutes e.g. hydrogen bonding interactions. However, the values of $K_{vitamin}^{exp}$ measured in ATPS formed by PEG 4000 are just slightly higher than their pendants in ATPS formed by PEG 6000. Similar behavior has been already reported in this work for DNP-AA (section 7.1.3). The lower PEG molar mass can lead to the improved $K_{vitamin}^{exp}$. In general, it can be concluded that the highest $K_{vitamin}^{exp}$ values are expected in a system formed by PEG with rather lower molar mass (preferably average M_{PEG} < 4000 g·mol^{-1}).

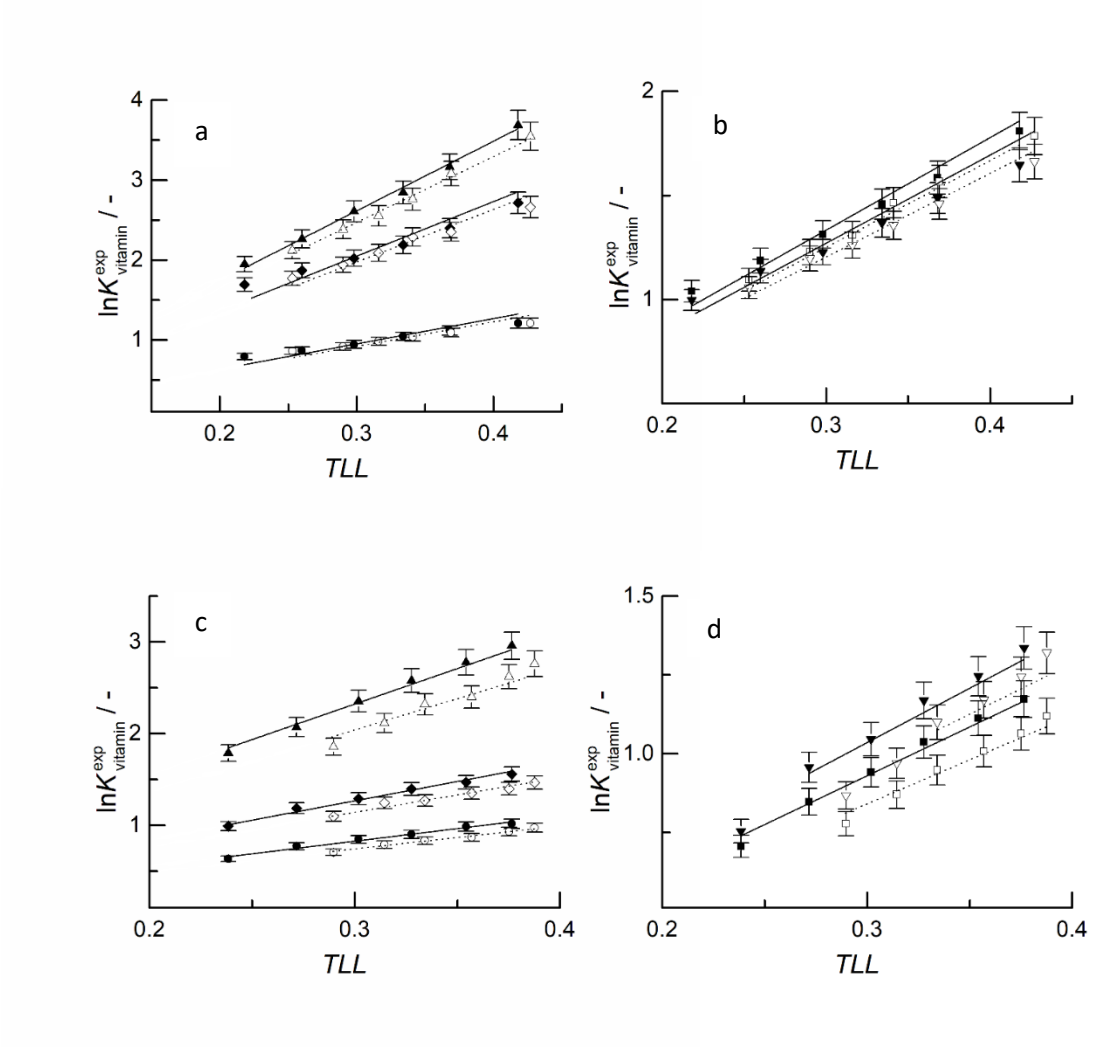

Figure 7.12. Logarithm of experimental partition coefficients of vitamins ($\ln K^{exp}_{vitamin}$): VB2, VB9, VB12 (a,c), VB3^{acid}, VB3^{amide}(b,d), at T=298.15 K and p=1 bar, plotted against TLL of PEG – salt ATPS: PEG 4000 (closed symbols, solid lines) or PEG 6000 (open symbols, dotted lines) + Na_3Citrate (a-b) or Na_2Tartrate (c-d). Vitamins: VB2(●,○), VB3^{acid}(■, □), VB3^{amide}(▼,▽), VB9(◆, ◇), VB12 (▲,△). The lines were obtained after linear regression (average r^2=0.998 for all TL and ATPS considered in this work) and were applied just to guide the eye and improve the readability. The feed and equilibrium composition for a given TL are provided in Appendix (A8). The diagram shows only TLL regions at which it could be possible to measure the partitioning with reasonable accuracy.

7.3. Conclusion

In this chapter, the experimental partitioning results of DNP-AA (DNP-glycine, DNP-alanine, DNP-valine, DNP-leucine) and water-soluble vitamin (VB2, VB3^{acid}, VB3^{amide}, VB9, VB12) in ATPS composed by PEG (M_{PEG} = 4000 – 8000 g·mol^{-1}) and Na_3Citrate, K_3Citrate, or KNaTartrate (for DNP-AA), as well as PEG (M_{PEG} = 4000 – 6000 g·mol^{-1}) and Na_3Citrate

or Na_2Tartrate (for vitamins), at T= 298.15 K and p= 1 bar, were presented and discussed. All solutes partitioned in this work had a higher affinity to the upper PEG phase.

Experimental partition coefficients K_i^{exp} determined in this work follow the trends: $K_{DNP-leucine}^{exp} > K_{DNP-valine}^{exp} > K_{DNP-alanine}^{exp} > K_{DNP-glycine}^{exp}$ for DNP-AA and $K_{VB12}^{exp} > K_{VB9}^{exp} > K_{VB3}^{exp} > K_{VB2}^{exp}$ for vitamins. Partitioning trends for DNP-AA and vitamins do not follow the solubility trends from chapter 5: $m_{DNP-alanine}^{L} > m_{DNP-valine}^{L} > m_{DNP-glycine}^{L}$ and $m_{DNP-leucine}^{L}$ (for DNP-AA) and $m_{VB3amide}^{L} > m_{VB3acid}^{L} > m_{VB12}^{L} > m_{VB2}^{L} > m_{VB9}^{L}$ (for vitamins). This means that different factors that rule the behavior of solutes in aqueous solutions are predominating in the partitioning. The highest K_i^{exp} values were obtained in systems formed by PEG of lower molar mass, namely PEG 4000, and of Na_3Citrate.

The partitioning was evaluated in terms of solute and ATPS properties. The latter involved the choice of different concentrations and type of phase forming components. This evaluation relied on selecting PEG of different molar mass as well as salt anion and cation to form ATPS. Partitioning data was correlated with TLL (obtained previously for each ATPS as explained in chapter 6). A linear correlation between ln$K$ and TLL for all DNP-AA and vitamins partitioned in ATPS was observed. This proves that K_i^{exp} depends on the concentration of all ATPS components.

It has been found that K_i^{exp} of DNP-AA and vitamins in ATPS strongly depends on many factors, and thus, it was hard to separate for an independent evaluation of each influence. These factors involved the properties of solutes, their molecular structures, and the composition of ATPS itself. The latter includes the concentration of phase formers, as well as their properties, e.g. molar mass of PEG, or type of salt. Since the charge of solute changes depending on the pH, the impact of this factor on K_i^{exp} was also studied. In this chapter, it was concluded that the charge of solute never should be neglected, and it is highly recommended to use the charge as an initial evaluation factor for studying the partitioning in ATPS in any future work.

Additionally, the water-soluble vitamins are classified as B-complex according to their biological function, not molecular structure. There is not a unique conclusion saying which factors have predominance in ruling the partitioning of all water-soluble vitamins. Every vitamin in this evaluation needed to be treated individually and required high experimental input. The non-ideality in the behavior of DNP-AA and vitamins in aqueous

solutions that was shown in chapter 4 (e.g. according to liquid density data), can be afterward reflected also in K_i^{exp} divergences. Indeed, the non-ideality of DNP-AA aqueous solutions was reported as less diverged among each DNP-AA solution than among each vitamin aqueous solution. This consequently revealed in the partitioning studies.

ATPS considered in this work have pH~8 and $\Delta pH_{phases} \leq 0.25$. The highest ΔpH_{phases} was observed for ATPS formed by PEG and citrate salt (Na_3Citrate, K_3Citrate) and for both ATPS $\Delta pH_{phases} \approx 0.25$. In contrary, ΔpH_{phases} of ATPS composed by PEG and Na_2Tartrate reached a very low level ($\Delta pH_{phases} < 0.05$),

Based on species distribution data obtained using pK_a values, in pH~8 of ATPS, DNP-AA considered in this study are only present as negatively charged species (-1), whereas vitamins are fully prevalent as neutral (VB12, $VB3^{amide}$) or negatively charged ($VB2^-$, $VB3^{acid-}$) species. All these compounds exist in studied ATPS as one type of species in both ATPS phases. Thus, $\Delta pH_{phases}=0.25$ in PEG - Na_3Citrate ATPS does not influence the K_i^{exp} of these compounds in any significant way. An exception is VB9, which in pH~8 occurs as a mixture of two species $VB9^{2-}$ and $VB2^{3-}$. In PEG – citrate salt systems, ΔpH_{phases} influences the partitioning of VB9 species. The difference in VB9 distribution of the species between PEG - citrate salt ATPS phases is non-negligible and leads to a different K_i^{exp} value of each VB9 species at the same ATPS composition (water, PEG, salt). On the contrary, the difference in the K_i^{exp} values of VB9 species in PEG – tartrate ATPS was smaller than 5%. This resulted from ΔpH_{phases} that was too small to change VB9 species distribution significantly.

The partitioning of the homologous series of DNP-AA follows the trend of their M_n ($M_{DNP-leucine} > M_{DNP-valine} > M_{DNP-alanine} > M_{DNP-glycine}$). This finding was expected as the polar side-chain is the only part in the molecule which differs for selected in this work homologous DNP-AA series. For this reason, the side-chain determines the interactions of these DNP-AA in aqueous solutions. Moreover, it could be proven that there is a linear dependency between $\ln K_i^{exp}$ and the relative hydrophobicity of amino acids expressed as $n(CH_2)$ by Zaslavsky [88]. Since all selected DNP-AA have the same charge (-1) in ATPS considered there must be other effects involved that predominate their partitioning. Possibly deciding factors involve the interactions of side-chain amino acid groups with ATPS phase forming components and take part in hydrogen bonding.

In contrast, K_i^{exp} determined for vitamins do not completely follow the trend of M_n. The highest K_i^{exp} were observed for vitamins of the largest molecule such as VB12 and VB9, but this dependency does not match VB2 and VB3 relation (K_i^{exp} to M_n). This confirms the fact that the partitioning of vitamins in ATPS can be ruled by many effects e.g. the molecular structure, electrostatic interactions with phase formers, complex formation, or hydrogen bonding, among others.

8. Predicting Aqueous Solubility of Biomolecules

Knowing the solubility in an aqueous environment is of crucial importance for life sciences and process design, but still experimental solubility data of DNP-AA and vitamin is rather limited or non-available in literature. Thus, to fully characterize the non-ideality caused by different interactions in aqueous DNP-AA and vitamin solutions, the availability of a predictive thermodynamic models, e.g. ePC-SAFT, is an urgent need. In this chapter, the solubility predictions obtained with novel prediction strategies, designed in this work for DNP-AA and vitamins, are discussed. The effects on aqueous solubility caused by different factors (pH, temperature, covitamin presence) were also considered by the model and evaluated in the following.

8.1. Approach

In this work, novel ePC-SAFT strategies were designed for predicting the solubility of DNP-AA and water-soluble vitamins in water. Thus, this section provides an introduction that is essential for a further discussion of prediction results. It provides a description of strategies that allowed predicting the intrinsic solubility ($m_{0,i}^{L,pred}$), as well as solubility at different pH and upon addition of covitamins ($m_i^{L,pred}$) . The intrinsic solubility of DNP-AA and vitamins was predicted with ePC-SAFT at T=298.15 K and p=1 bar. While the values of $m_{0,i}^{L,pred}$ for some vitamins have been predicted also in a wider temperature range, namely T = 293 – 323 K (VC) and T = 283.59 – 332.09 K (VB3^{acid}), $m_i^{L,pred}$ were predicted only at T = 298.15 K and p=1 bar. ePC-SAFT pure-component and binary interaction parameters required for these predictions have been included in table 4.1 and table 4.2. The methodologies used for the parameter estimation can be found in section 4.1.

Predicting the intrinsic solubility of DNP-AA and vitamin

At first, the intrinsic aqueous solubility $m_{0,i}^{L,pred}$ of DNP-AA (DNP-glycine, DNP-alanine, DNP-valine, and DNP-leucine) and water-soluble vitamins (VC, VB2, VB3^{acid}, VB9, and VB12), at T=298.15 K and p=1 bar, was predicted with ePC-SAFT as presented in figure 8.1. The melting properties required to solubility equation (2.25) have been shown in table 4.6. The activity coefficients of neutral species γ_i^L were predicted using ePC-SAFT pure component and binary interaction k_{ij} (with water) parameters from table 4.1. The solubility values predicted with ePC-SAFT were validated using data included in Appendix (A6 and A7). The same strategy has been used to predict the intrinsic solubilities of vitamins VC and VB3^{acid} at a wider range of temperatures, namely T = 293 – 323 K (VC) and T = 283.59 – 332.09 K (VB3^{acid}). The reliability of these predictions was evaluated using data reported in the literature [149, 150].

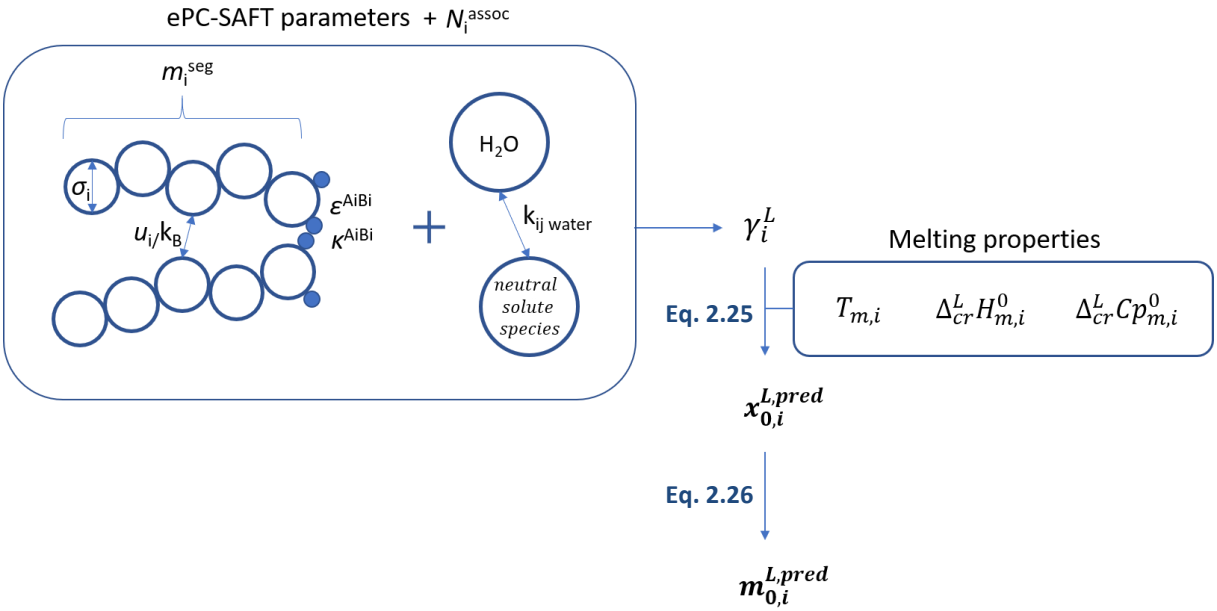

Figure 8.1. Prediction of intrinsic solubility $m_{0,i}^{L,pred}$ of DNP-AA and vitamins with ePC-SAFT. Solubility equation (2.25) postulated by Prausnitz [316] requires melting properties (table 4.6) and γ_i^L that is predicted with ePC-SAFT using pure-component and binary interaction parameters and association schemes from table 4.1. Solubility expressed as $x_{0,i}^{L,pred}$ can be converted into $m_{0,i}^{L,pred}$ using equation (2.26).

Predicting the pH influence on DNP-AA and vitamin solubility

The pH-dependent solubility $m_i^{L,pred}$ of DNP-AA and poorly soluble vitamins VB2, VB9, and VB12, was predicted at T=298.15 K and p=1 bar. The strategy relied on predicting activity coefficients γ_j^L of DNP-AA or vitamin species with ePC-SAFT and introducing them to the respective solubility equations from section 2.3.1. The predictions of activity coefficients of the species γ_j^L were done using ePC-SAFT pure-component and binary interaction parameters from table 4.1 and table 4.2. They were fitted according to the description provided in section 4.1.1. Intrinsic solubility $m_{0,i}^{L,pred}$ required for each of these expressions, i.e. (2.41), (2.54), (2.58), (2.63), and (2.69), was obtained as described in figure 8.1. The dissociation constants $K_{a,th}$ given in table 4.5 were also required ($pK_{a,th}$=-log$K_{a,th}$). The solubility values $m_i^{L,pred}$ predicted with ePC-SAFT were validated using data included in Appendix (A6 and A7) as well as from the literature [40, 42, 155, 156]. This strategy was used to characterize the behavior of DNP-AA and vitamins in aqueous solutions of different pH. Figure 8.2 and figure 8.3 can help to understand the non-ideality caused by different interactions in such solutions and to

relate the presence of species (DNP-AA or vitamins) with solubility since both species distribution and solubility are pH-dependent.

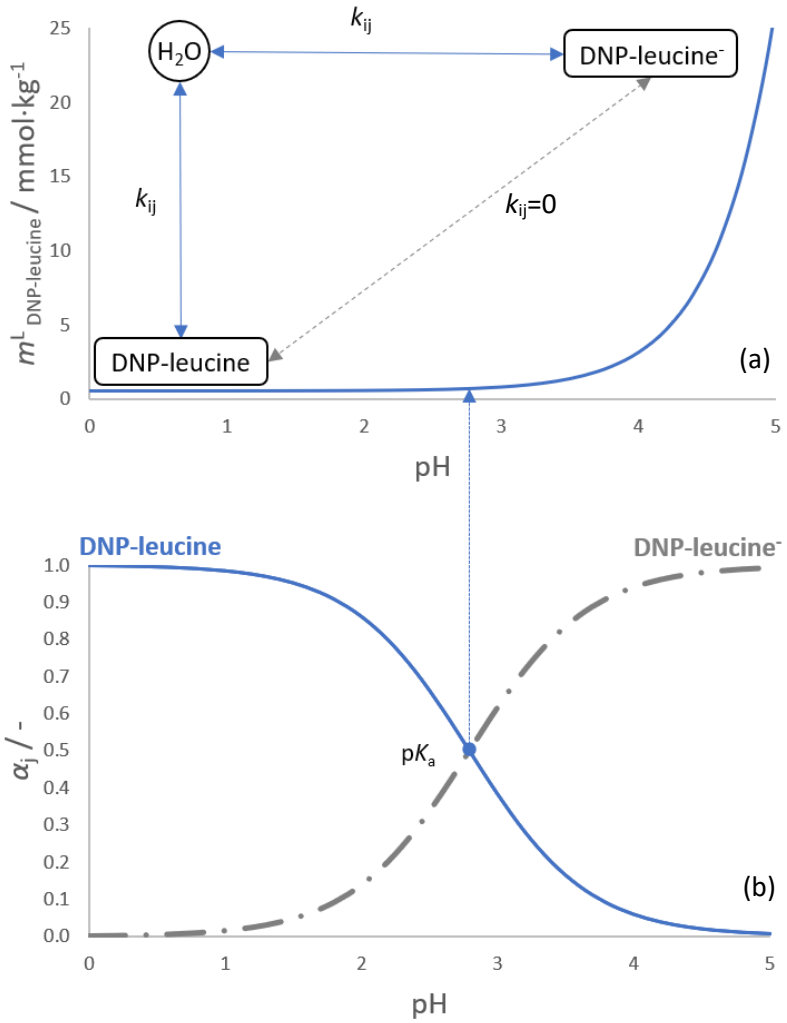

Figure 8.2. Behavior of acidic DNP-leucine in aqueous solution: the pH-solubility profile (a) and the pH-dependent species distribution α_j (b). The species *j* are neutral DNP-leucine and negatively charged DNP-leucine⁻. This scheme presents an ideal system. The pK_a is taken from table 2.1 and corresponds to the pH at which $\alpha_{DNP-leucine} = \alpha_{DNP-leucine^-} = 0.5$. At pH < 2.8 pH neutral molecules of DNP-leucine (dash-dot line in figure b) are in majority in a solution, while at pH > 2.8 mostly negatively charged DNP-leucine⁻ (solid line in figure b) are present. The non-ideality caused by different interactions between water and DNP-leucine species is predicted with ePC-SAFT pure-component parameters and binary interaction parameter k_{ij} (solid arrows in figure a). The k_{ij} between the species was not considered (dotted arrow in figure a).

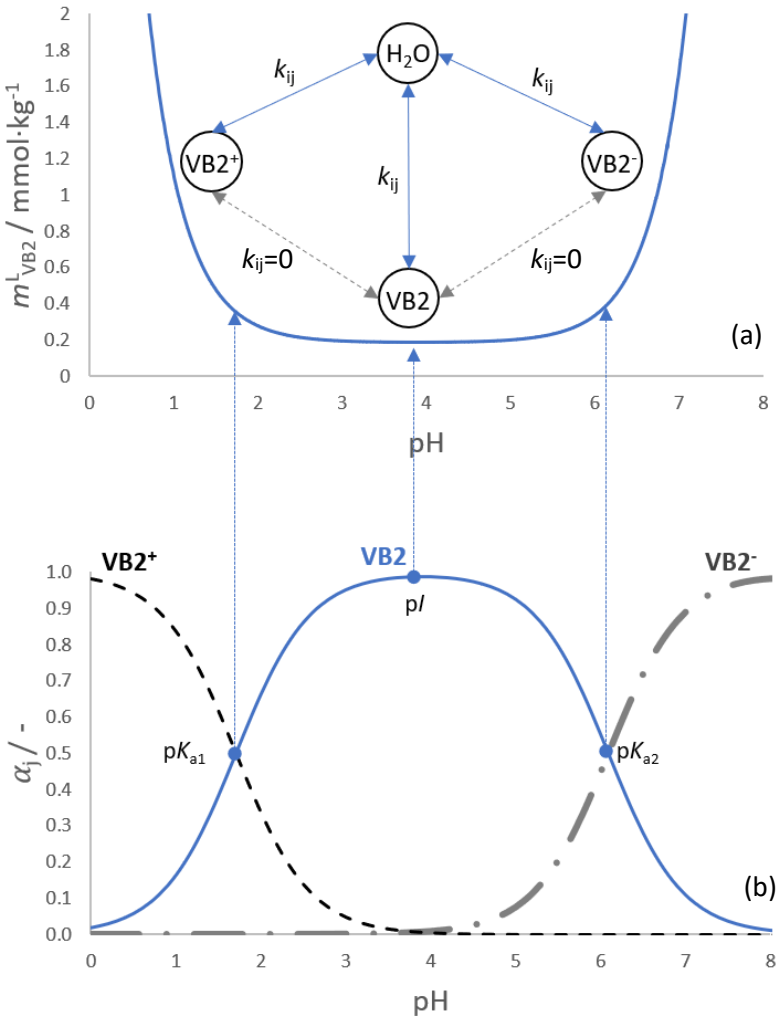

Figure 8.3. Behavior of amphoteric VB2 in aqueous solution: the pH-solubility profile (a) and the pH-dependent species distribution α_j (b). The species *j* presented in the figure are neutral VB2, positively charged VB2$^+$, and negatively charged VB2$^-$. This scheme presents an ideal system. The pK_a is taken from table 2.1. At pH = 1.7: $\alpha_{VB2} = \alpha_{VB2^+} = 0.5$, at pH = 6.1: $\alpha_{VB2} = \alpha_{VB2^-} = 0.5$. At pH < 1.7 VB2+ (dashed line in figure b) are in majority in a solution, while at pH > 6.1 mostly VB2$^-$ (dash-dot in figure b) are present. At isoelectric point (pI) VB2 is neutral. The non-ideality of a mixture of water and VB2 species is predicted with ePC-SAFT pure-component parameters and binary interaction parameter k_{ij} (solid arrows in figure a). The k_{ij} between the species was not considered (dotted arrows in figure a). At a certain pH, the salt is going to be formed. The pH ranges at which salt formation can occur where not considered in this work, however, the solubility product can be calculated as explained in section 2.2.1.

Figure 8.2 shows the behavior of acidic DNP-leucine in water caused by pH change, and their influence on solubility. At pH<pK_a value of DNP-leucine (table 2.1, pK_a=2.8), there will be neutral molecules prevalent, while at pH > pK_a value the negatively charged DNP-leucine$^-$ will be in majority present in the solution. This difference in species distribution influences the solubility in a way that a change in the pH of a solution of only one pH unit,

e.g. from pH=3 to pH=4, leads already to the 4-fold increase of solubility. This is according to experimental data (Appendix, A6) and has been already discussed in section 5.1. Based on pK_a value from table 2.1, at pH=5 the species fraction of negatively charged DNP-leucine$^-$ $\alpha_{DNP-leucine^-}$ equals 0.994. This means that at this pH, interactions mostly between negatively charged species and water may contribute to the observed solubility behavior of a component. Thus, binary interaction parameter k_{ij} values that help describng not only the non-ideality of neutral DNP-leucine and water mixtrues, but also in this case, negatively charged DNP-leucine$^-$ with water were crucial for solubility predictions.

Figure 8.3 shows the behavior of VB2 in water caused by pH change, and their influence on solubility. For simplification, it presents the behavior of VB2 only at pH≤8. Since VB2 is an amphoteric component, the isoelectric point pI = 3.9 (calculated based on data from table 2.1) corresponds to the pH at which VB2 has minimum solubility in water. Above this point occurs the formation of negatively charged species of VB2, below the point – the opposite – i.e. positively charged species of VB2. The presence of charged species relates also to the increase of solubility if comparing to solubility observed if just neutral species are present. VB2 is present in majority as charged species at pH below its pK_{a1} value, as well as above its pK_{a2} (according to table 2.1, pK_{a1} = 1.7, pK_{a2} = 6.1). Thus, k_{ij} values are used in ePC-SAFT to characterize the non-ideal behavior of different species, i.e. neutral or positively and negatively charged, in aqueous solution. This non-ideality can be caused by different interactions of these species with water. Having these k_{ij} values is the key to the accurate predictions of VB2 solubility, especially at the pH of a solution at which besides neutral molecules, also the charged ones are present.

Predicting the covitamin influence on vitamin solubility

The aqueous solubility $m_i^{L,pred}$ of poorly soluble vitamins VB2, VB9, and VB12, under the influence of covitamins VC, VB3^{acid}, and VB3^{amide}, was predicted at T=298.15 K and p=1 bar. The strategy relied on predicting activity coefficients γ_j^L of vitamin species (in a mixture with covitamins) with ePC-SAFT and introducing them to the respective solubility equations from section 2.3.1. The predictions of activity coefficients of the species γ_j^L were done using ePC-SAFT pure-component and binary interaction parameters from table 4.1 and table 4.2. The activity coefficients γ_j^L of neutral molecules

(in the mixture with covitamins) were used to predict the intrinsic solubility values $m_{0,i}^{L,pred}$ (analogously to figure 8.1). The dissociation constants $K_{a,th}$ were taken from table 4.5. In the end, the values of $m_{0,i}^{L,pred}$, γ_j^L, and p$K_{a,th}$ could be introduced to solubility equations (2.58) – for VB12, (2.63) – for VB2, or (2.69) – for VB9, leading to the vitamin solubility prediction (in a mixture with covitamin) as a function of pH.

8.2. Prediction Results: Amino Acid Derivatives

This section presents the predictions of aqueous solubility that were obtained with ePC-SAFT for four DNP-AA (DNP-glycine, DNP-alanine, DNP-valine, and DNP-leucine), at T=298.15 K and p=1 bar. The pure-component ePC-SAFT parameters for neutral DNP-AA were included in table 4.1. They were estimated with designed in this work Joint-Parameter Method (J-PM) as described in section 4.1.2. The binary interaction parameters of neutral DNP-AA and water were set to zero. The pure-component parameters for charged DNP-AA$^-$ (q=-1) based on the parameters fitted for neutral species were included in table 4.2. The pure-component and binary interaction parameters for DNP-AA- were estimated according to the procedure included in section 4.1.1. The solubilities predicted with ePC-SAFT were validated by experimental data obtained in this work at T= 298.15 K and p= 1 bar and provided in Appendix (A11).

The present subchapter 8.2 is divided into two sections. Section 8.2.1 evaluates the ePC-SAFT predictions of DNP-AA solubility in pure water at constant temperature T=298.15 K and p=1 bar. Section 8.2.2 presents the ePC-SAFT solubility predictions obtained for DNP-AA as a function of pH. The observations included in sections 8.2.1 and 8.2.2, can be compared with conclusions obtained based on experimental DNP-AA solubility data in sections 5.1.1 and 5.1.2, accordingly. ARD% determined after the comparison of data predicted with ePC-SAFT to experimental solubility data are included in the Appendix (A11).

8.2.1. Intrinsic Aqueous Solubility at Constant Temperature

The intrinsic solubility of DNP-AA was predicted at T=298.15 K and p=1 bar according to equation (2.25) using the parameters from table 4.1 and melting properties from table 4.6. The results of ePC-SAFT predictions of DNP-AA intrinsic solubilities are shown in figure 8.4. Intrinsic solubility that was based on experimental data presented

was previously evaluated in section 5.1.1 (figure 5.1). Figure 8.4 compares these data with the results of ePC-SAFT predictions discussed in this section.

It can be seen in figure 8.4 that ePC-SAFT was able to predict DNP-AA solubility in water accordingly to the trend observed in section 5.1.1.

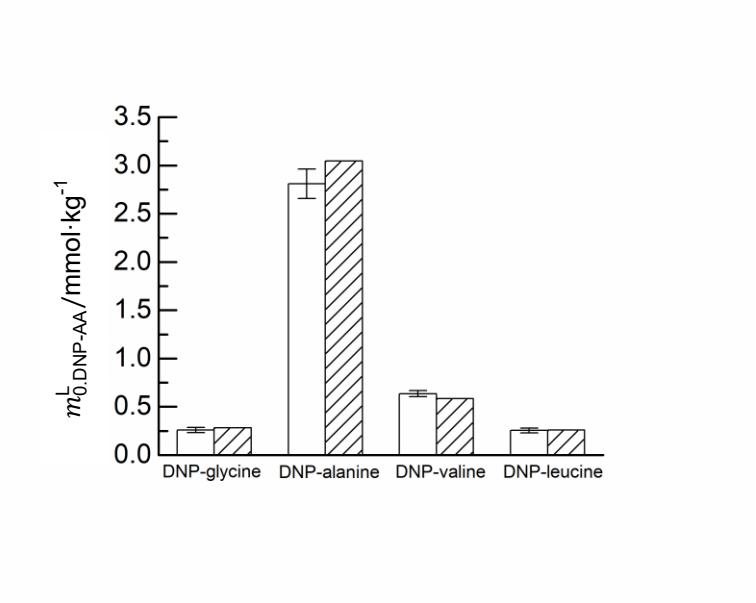

Figure 8.4. Intrinsic aqueous solubility of DNP-AA $m^{L}_{0,DNP-AA}$ at T=298.15 K and p=1 bar. ePC-SAFT solubility $m^{L,pred}_{0,DNP-AA}$predictions (striped bars) were done according to approach described in section 8.1 and compared with intrinsic solubility values $m^{L}_{0,DNP-AA}$ calculated from experimental solubility data (non-patterned bars). Experimental solubility was obtained in this work at pH=3.42 (DNP-glycine), pH=3.09 (DNP-alanine), pH=3.17 (DNP-valine, DNP-leucine) (Appendix, A6). The calculations based on experimental data were performed using experimental solubilities, pK_a values from table 2.1, and solubility equation (2.38), and they were plotted previously in figure 5.1. ARD% of experimental solubility data ≤5.1; ARD% between predictions and experimental-based data ≤ 8.76 (Appendix, A11).

Thus, ePC-SAFT predicts that the solubility trend (assuming the same trend of intrinsic solubility $m^{L,pred}_{0,DNP-AA}$ and total solubility of a component $m^{L,pred}_{DNP-AA}$ at constant pH) for DNP-AA $m^{L,pred}_{DNP-alanine} > m^{L,pred}_{DNP-valine} > m^{L,pred}_{DNP-glycine} > m^{L,pred}_{DNP-leucine}$ is different from the solubility trend of aliphatic AA ($m^{L}_{glycine} < m^{L}_{L-alanine} < m^{L}_{L-valine} < m^{L}_{L-leucine}$) [81, 393, 394]. This agrees with solubility trend obtained based on experimental data. The difference in solubility between $m^{L,pred}_{0,DNP-glycine}$ and $m^{L,pred}_{0,DNP-leucine}$ was ARD%~1. Also, small deviation between experimental $m^{L}_{0,DNP-glycine}$ and $m^{L}_{0,DNP-leucine}$ was observed (ARD%~1). This means that based on solubilities predicted with ePC-SAFT, it is still

difficult to fully ascertain which of the two DNP-AA: DNP-glycine or DNP-leucine, is more soluble. However undoubtedly, DNP-alanine is the most soluble among four studied DNP-AA and the same result was obtained experimentally and predicted with ePC-SAFT.

ePC-SAFT very accurately predicted the solubilities if referring them to intrinsic solubilities obtained based on experimental data. The lowest ARD% between experimental data-based and predicted with ePC-SAFT solubilities was observed for DNP-leucine (ARD% = 2.02), while the highest was found for DNP-glycine (ARD% = 8.76). This is a very good result considering low aqueous solubility of DNP-AA studied in this work (Appendix, A6). Predicting the behavior of DNP-AA in pure water required only ePC-SAFT pure-component parameters of DNP-AA (k_{ij} between neutral species and water were set to zero) that were fitted by joining parameters for associating AA already established as well as applied in several different works [78, 79, 81, 371, 420], with parameters for non-associating DNB (J-PM) (Appendix, A5). Since this modeling method was enough to later accurately predict DNP-AA solubility, developed in this work modeling method (J-PM) and prediction approach, can be considered very advantageous in terms of describing the non-ideal behavior of DNP- AA in water. Thus, ePC-SAFT accordingly predicts the non-ideality caused among others by different interactions (listed in section 2.4) of DNP-AA in aqueous solutions.

8.2.2. Influence of pH on Aqueous Solubility

The pH of aqueous solution influences the charge of DNP-AA and through this also its solubility. According to figure 2.1 presented in section 2.3.2 and figure 8.2 shown in section 8.1, at pH ≤ 5 all considered DNP-AA are present as neutral and negatively charged species. The species fractions can be calculated as explained in section 2.3.2. At pH = 6 DNP-AA are solely present as negatively charged species in a solution. Figure 8.5 shows the solubility of uncharged DNP-AA (intrinsic solubility) and solubility at pH 6.4 of DNP-AA (q=-1). Approximately double increase of solubility was predicted with ePC-SAFT for DNP-glycine, DNP-valine, and DNP-leucine when changing the pH from the pH value of each saturated solution (without an addition of a base) to pH=6.4.

Figure 8.5 compares experimental data-based solubility and solubility predicted with ePC-SAFT (Appendix, A11). Very low deviations between these solubility values were observed proving a great success of the predictive approach designed in this work. The

highest deviation (ARD%) between solubility predicted with ePC-SAFT and experimental data-based values at pH 6.4 was observed for negatively charged DNP-alanine (ARD%=1.1). The difference in non-ideal behavior of the species depends among others on the interactions of DNP-AA with water (k_{ij}). The binary interaction parameters k_{ij} for neutral species were set to zero. For negatively charged DNP-AA k_{ij} were fitted to solubilities measured at pH at which DNP-AA are solely present as negatively charged species (q=-1; $\alpha_{DNP-AA^-} = 1$) accounting simultaneously for the thermodynamic non-ideality towards activity coefficients (γ_j^L) and thermodynamic dissociation constants ($K_{a,th}$). The latter was done according to Lange *et al.* [381]. The solubility can change due to intermolecular hydrogen bond formation and factors like the polarity of a molecule, namely according to the principle that solutes dissolve better in alike solvents [57].

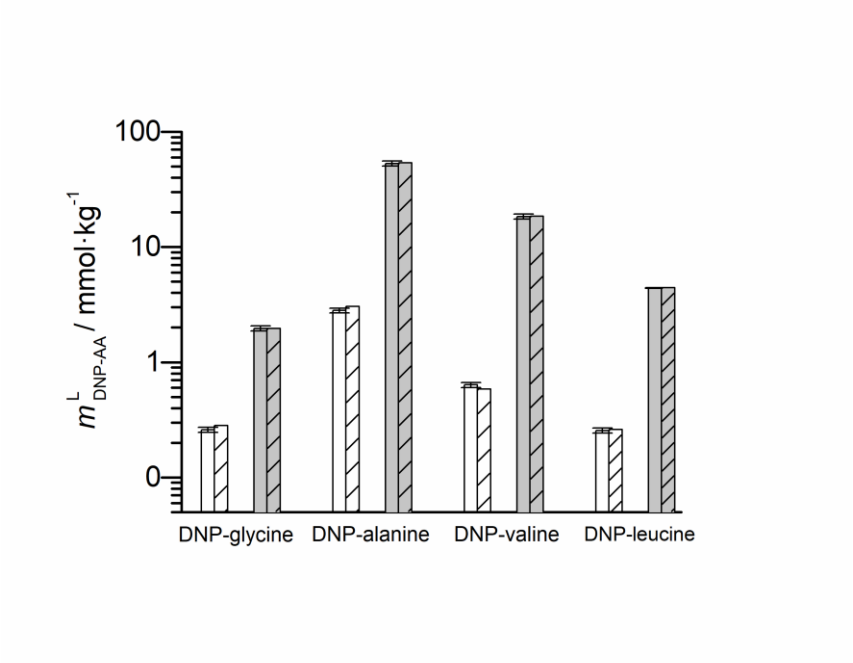

Figure 8.5. Intrinsic aqueous solubility of DNP-AA ($\alpha_{DNP-AA} = 1$) at pH=3.42 (DNP-glycine), pH=3.09 (DNP-alanine), pH=3.17 (DNP-valine, DNP-leucine) (white bars) and solubility of DNP-AA at pH = 6.4 at which $\alpha_{DNP-AA^-} = 1$ (gray bars), experimental data-based (non-patterned bars) and predicted (patterned bars) solubility, m^L_{DNP-AA}, at T=298.15 K and p=1 bar (Appendix, A11). ARD%≤2.92.

Due to low solubility of DNP-AA, it was not possible to evaluate the deviations from non-ideality in DNP-AA aqueous systems based on experimental osmotic coefficients ϕ. The concentrations of DNP-AA were too low to reach detection limits of the apparatus to perform the measurements of ϕ (section 3.2.4). Thus, the non-ideality of these solutions could be evaluated using activity coefficients γ_j^L obtained with ePC-SAFT. Based on the

results of the predictions, DNP-AA solutions deviate from ideality, thus, activity coefficients of the species γ_j^L obtained with ePC-SAFT were different than unity. The values of $\gamma_j^L > 1$ imply that DNP-AA exhibit positive deviation from Raoult`s law since the activity of DNP-AA (species) is higher than its (species) mole fraction. Thus, strong repulsive forces may dominate in aqueous solutions containing low soluble DNP-AA (according to European Pharmacopoeia terms – very slightly soluble [57]). The deviations from non-ideality were observed in figure 4.2(c) (experimental osmotic coefficients ϕ) for another low soluble component, namely VB12, while for more soluble VB3^{acid} and VC – the deviations were negative. Also, the ratios of activity coefficients of neutral DNP-AA species to activity coefficients of charged DNP-AA species γ_j^L were found to be higher than unity. The increase of DNP-AA solubility was observed when increasing the pH through an addition of basic agent ($m_{NaOH} \leq 0.035$ mol·kg^{-1}).

Since aqueous solubility values predicted by ePC-SAFT were very accurate (if comparing them to experimental data-based intrinsic solubility values), it proves that ePC-SAFT accounts on the non-ideality caused among others by different interactions (described in section 2.4) that occur in these aqueous DNP-AA systems and that rule the solubility of DNP-AA in water. For this reason, the approach designed in this work to predict the solubility at different pH can help to understand the behavior of DNP-AA in water in the presence of acidity or basicity agents.

8.3. Prediction Results: Water-Soluble Vitamins

In this work, solubilities in water of vitamins: VC, VB2, VB3^{acid}, VB9, and VB12, at T=298.15 K and p=1 bar were predicted with ePC-SAFT. The parameters used for these predictions were fitted according to the description provided already in subchapter 4.1. The pure-component and binary interaction ePC-SAFT parameters for neutral vitamin species can be found in table 4.1, while the parameters for charged vitamin species were included in table 4.2. Aqueous solubilities predicted with ePC-SAFT were validated by new experimental solubility data at T= 298.15 K and p= 1 bar given in this thesis in Appendix (A7) and discussed in subchapter 5.2.

The present subchapter is divided into four sections. Section 8.3.1 shows the evaluation of ePC-SAFT predictions of vitamin solubility in pure water at constant temperature T = 298.15 K (for all vitamins considered in this work). Knowing the pH-

solubility profiles of vitamins is fundamental for understanding and controlling their behavior in aqueous solutions. Thus, section 8.3.2 presents a discussion on pH-solubility profiles predicted with ePC-SAFT for low soluble VB2 and VB9, at T = 298.15 K and p = 1 bar. These results were compared to the pH-solubility profiles obtained with idealized H-H-based equations. The solubility of vitamins can be influenced by temperature, thus, ePC-SAFT predictions have been performed also in wider range of temperatures, namely T = 283.59 K – 332.01 K ($VB3^{acid}$) and T = 293 K – 323 K (VC). Temperature effect was evaluated in section 8.3.3 and validated with experimental data taken from the literature [149, 150]. In the end of this subchapter, also ePC-SAFT predictions of solubility enhancement of poorly soluble VB2, VB9, and VB12, upon addition of covitamins VC, $VB3^{acid}$, and $VB3^{amide}$, are addressed (section 8.3.4). ARD% values determined after the comparison of data predicted with ePC-SAFT to experimental solubility data were included in the Appendix (A12).

8.3.1. Intrinsic Aqueous Solubility at Constant Temperature

The intrinsic aqueous solubilities of acidic (VC) and amphoteric (VB2, $VB3^{acid}$, VB9, VB12) vitamins were predicted with ePC-SAFT using equation (2.25) at T = 298.15 K and p = 1 bar. The activity coefficients γ_j^L required in this equation were predicted using the parameters for neutral species included in table 4.1. Melting properties needed for these predictions were taken from table 4.6. The results of ePC-SAFT predictions, accompanied with experimental data, are given in Appendix (A12) and are presented in figure 8.6.

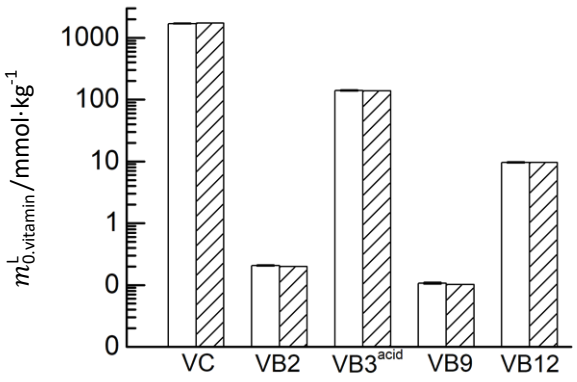

Figure 8.6. Intrinsic solubility of vitamins $m^L_{0,vitamin}$ at T=298.15 K and p=1 bar. ePC-SAFT predictions (patterned bars) were performed according to description from section 8.1 and compared with intrinsic solubility determined based on experimental data (non-patterned bars, presented previously in figure 5.4). Experimental data measured at pH of saturated vitamin solutions in pure water: pH=1.94 (VC), pH=5.68 (VB2), pH=3.42 (VB3^{acid}), pH=4.28 (VB9), pH=5.55 (VB12) (Appendix, table A7.1). Intrinsic solubility was predicted with ePC-SAFT using equation (2.25) and melting properties from table 4.1. ARD% between predictions and experimental-based data ≤ 4.56 (Appendix, A12).

The trend of vitamin solubility $m^L_{VC} > m^L_{VB3acid} > m^L_{VB12} > m^L_{VB2} > m^L_{VB9}$ (assuming the same trend of $m^L_{0,vitamin}$ and $m^L_{vitamin}$ at constant pH) was already discussed in detail in experimental section 5.2.1. For all vitamins considered in this study, ePC-SAFT allowed quantitative predictions of their aqueous solubilities at T = 298.15 K and p=1 bar. The highest deviation between measured and predicted solubility (ARD% = 4.13) was observed for the least soluble vitamin (VB9). However, this ARD% value is still very small and leads to the conclusion that ePC-SAFT can excellently predict the solubilities of even such complex components at T= 298.15 K. This is a very good result for such complex vitamin molecules, especially since solubility data have not been used for ePC-SAFT parameter estimations. Overall, the approaches designed in this work for ePC-SAFT parameter estimation (MM, section 4.1.1) and for predicting the intrinsic solubility of vitamins in water can accurately characterize the non-ideality caused among others by different interactions (listed in section 2.4) that occur in these vitamin systems.

8.3.2. Influence of pH on Aqueous Solubility

Depending on the pH, also charged vitamin species can be present in aqueous solutions in addition to the neutral species. To describe the non-ideality that is caused among others by molecular interactions, according to the pH (and thus according to the vitamin's charge), ePC-SAFT was applied in this work. The ePC-SAFT parameters for different ionic species of the two low soluble vitamins VB2 and VB9 have been determined (table 4.2). VB12 was not included in this step since the solubility of VB12 is not expected to be pH-dependent in the range 4 < pH < 12 (based on figure 5.5).The ePC-SAFT parameters for the charged vitamin species were determined as explained in section 4.1.1. The predicted pH-solubility profiles of VB2 and VB9 are presented in figure 8.7.

The pH change was experimentally induced upon adding HCl or NaOH. This might not only cause the desired pH change, but it also might influence the electrostatic interactions involving the vitamin. However, only very low concentration of NaOH or HCl was used [in the range of several millimoles per kilogram water: VB12: $m_{NaOH} \leq 0.41$ mmol·kg^{-1} (at pH =7.81); VB2: $m_{NaOH} \leq 0.02$ mmol·kg^{-1} (at pH = 6.87)]. This concentration does only marginally influence the ePC-SAFT predictions, while pH is changed dramatically. This in turn causes species change of the vitamin, which ultimately induces formation of non-neutral vitamin species and thus causes strong electrostatic interactions. The species distribution affects aqueous solubility of vitamin as shown in an example for VB2 in figure 8.3. In this work, the presence of added H^+ or Na^+ ions was not considered in the ePC-SAFT predictions shown in figure 8.7. The vitamin solubilities at different pH values were calculated according to the description presented in subchapter 8.1 using equations (2.63) and (2.69). Intrinsic solubility values required in these equations were calculated with equation (2.25). Based on the results presented in figure 8.7, the ion-specific ePC-SAFT parameters for the charged vitamin species allow accurately matching the experimental data as well as the idealized H−H-based lines for VB2 and VB9. Thus, the ePC-SAFT parameters of the vitamin species are validated.

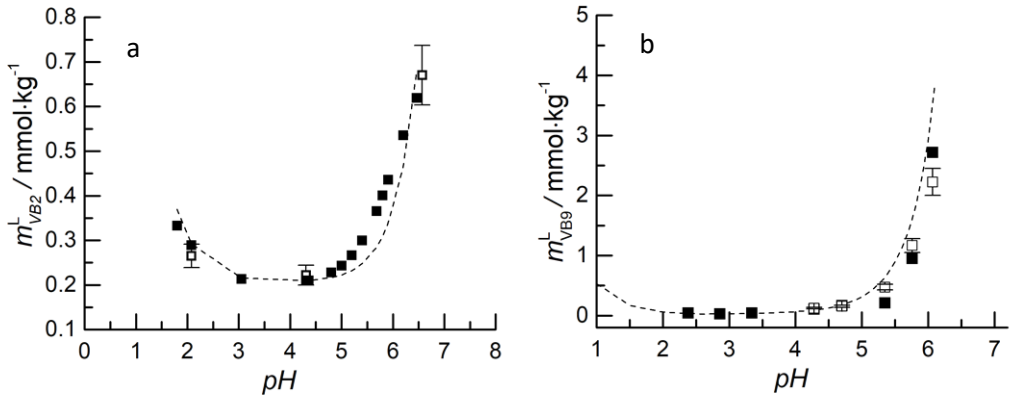

Figure 8.7. ePC-SAFT predictions of pH-solubility ($m^L_{vitamin}$) profiles for VB2 (a) and VB9 (b) at T=298.15 K and p=1 bar (■) and experimental solubility data measured in this work (□) (Appendix, A7). The vitamin solubilities at different pH values were predicted using equations (2.63) and (2.69). The dashed lines represent the calculations using the idealized H-H-based equations (2.62) and (2.68).

8.3.3. Influence of Temperature on Aqueous Solubility

Both pH and temperature can change the solubility of the vitamin. ePC-SAFT predictions allowed separating the pH and temperature effects on vitamin solubility. Thus, in this section, the temperature effect could be evaluated independent of the pH (in contrast to the experimental section 5.2.3 in which combined pH and temperature effect must be considered). The temperature dependence on the solubility of the two most soluble vitamins considered in this work has been studied. ePC-SAFT predictions were performed at T = 283.59 K – 332.01 K for VB3^{acid} and T = 293 K – 323 K for VC. Experimental data for validation of the predictions were taken from the literature [149, 150].

According to figure 8.8, and as expected, the solubility of VC and VB3^{acid} increases with increasing temperature. ePC-SAFT allows accurately predicting the solubility of VB3^{acid} within the range of T = 283.59 K – 332.09 K (ARD% = 2.82). VB3^{acid} is one of the most stable molecules against air, light, acids and alkalis, among other water-soluble vitamins[135]. VC is a very unstable compound concerning air and light, and thus thermo-induced degradation could occur at higher temperatures during solubility experiments. For VC, ePC-SAFT over predicted experimental solubility at temperatures higher than T=298.15 K. This might be caused by decomposition and questionable solubility data which cannot be described by the model (e.g. decomposition) [392] or by the need of temperature-dependent binary interaction parameters. Although an effective method, use of the latter is not within the scope of this work. In sum, these deviations might be due to model inaccuracies or due to the use of harmful experimental conditions (nonharmful: pH~pH of uncharged vitamins, stable around room temperature, protection from light, protection from air by using well-sealed vials).

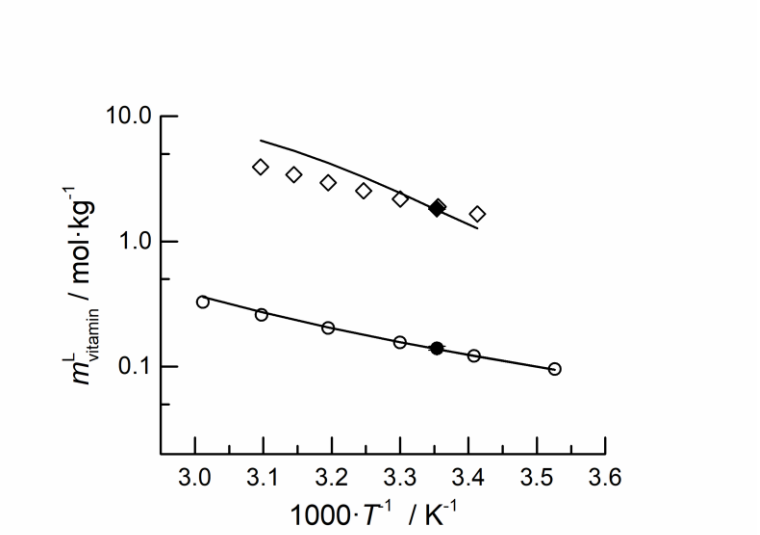

Figure 8.8. Temperature influence on aqueous vitamin solubility $m^L_{vitamin}$. ePC-SAFT predictions are represented by lines, experimental validation are symbols. Black symbols – (◆) VC and (●) VB3^{acid}: this work (Appendix, A7), open symbols – (◇) VC and (○) VB3^{acid}: literature [149, 150]).

Most probably, deviations between predicted and experimental solubilities have been caused by pH effects, which were not considered by ePC-SAFT while predicting the VC solubility at different temperatures. Unfortunately, further evaluation using ePC-SAFT could not be carried out since the pH values were not provided in the work from which experimental data was withdrawn [149]. Nevertheless, the reasoning presented in the

following may explain why the pH effect can be considered the most likely factor causing these deviations. The pH influence on solubility of different natural components (acidic, basic, amphoteric) has been discussed in section 2.3.1 and in the literature[60]. The pH of VC solutions is expected to decrease for higher solubility, which forces the total solubility of VC to decrease. It can be seen in figure 8.8 that the deviation between measured and predicted solubilities of VC increases gradually with increasing solubility. To include this effect into the ePC-SAFT predictions, dissociation equilibria are required. Unfortunately, the pH values of equilibrated solutions are not known, which does not allow fully unravelling the reasons of VC solubility deviations of PC-SAFT predictions. Nevertheless, this example proves that the knowledge on the pH influence of vitamin solutions on solubility data is of high importance, and this has been addressed in the previous section 8.3.2.

8.3.4. Influence of Covitamin on Aqueous Solubility

The aqueous solubilities of poorly water-soluble vitamins (VB2, VB9, and VB12) at T = 298.15 K and p = 1 bar upon addition of better-soluble covitamins (VC, $VB3^{acid}$, $VB3^{amide}$) were predicted with ePC-SAFT following the methodology presented in section 8.1. The pure-component parameters and binary interaction parameters of vitamins required for the predictions were listed in table 4.1 and table 4.2. Melting properties were taken from table 4.6. The ePC-SAFT predictions are presented in the following. The results are divided into two parts: the first part deals with solubility upon addition of vitamins that change pH without modifying the species distribution dramatically, while the second part deals with solubility upon addition of covitamins that change the pH strongly so that the species distribution is dramatically modified. The solubility predictions upon addition of covitamins were validated against experimental solubility data (Appendix, A7).

To evaluate if a given concentration of covitamin will cause minor or major species change, the pH value of water – vitamin - covitamin solution must be known. The species distribution can be calculated based on examples shown in section 2.3.2. Since the formation of different species has an influence on aqueous solubility, thus, solubility data can be used for the comparison of the effect caused by species distribution change.

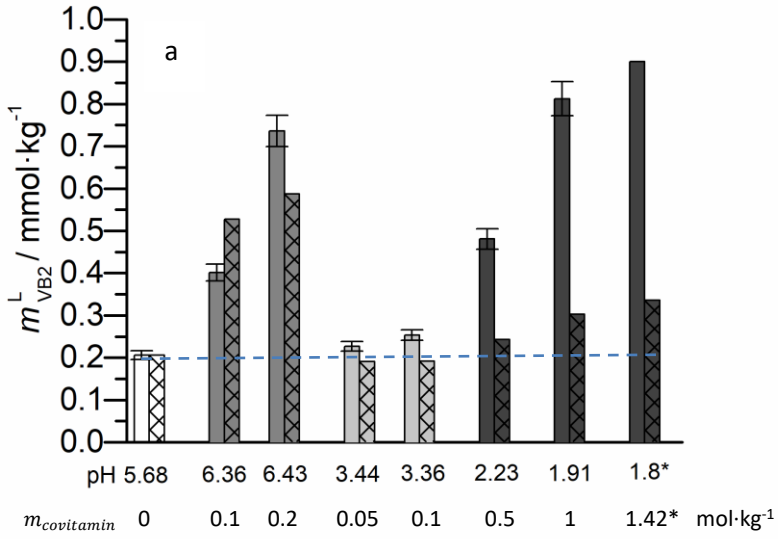

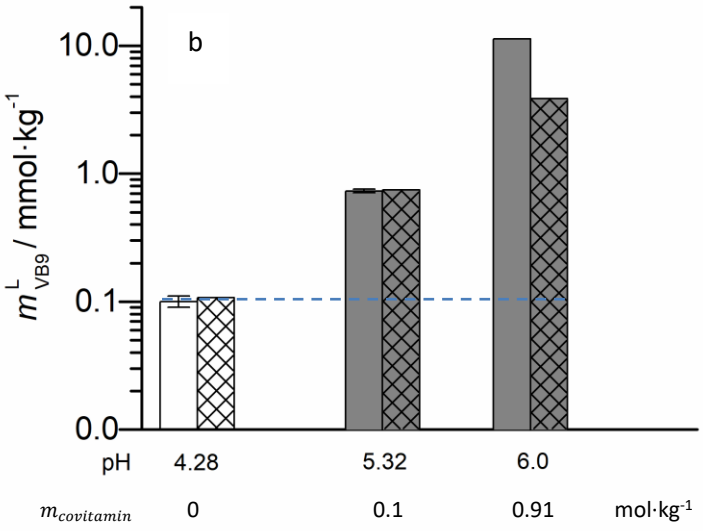

(Figure 8.9, continued on next page)

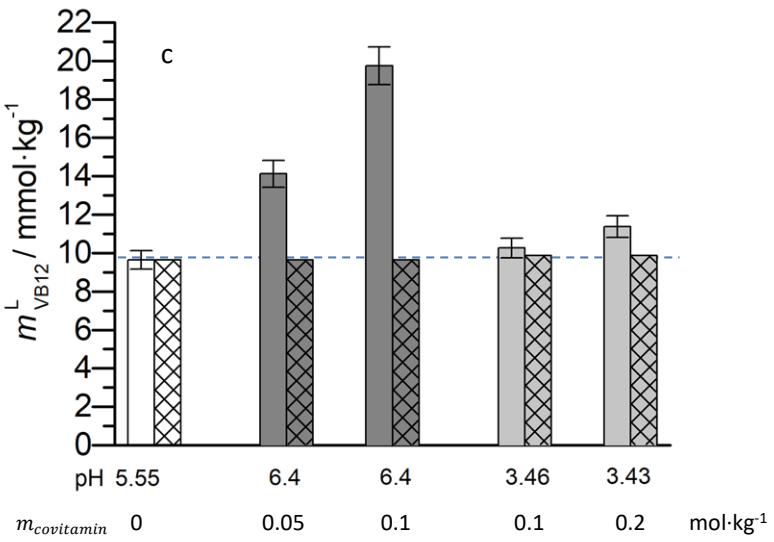

Figure 8.9. The effect of pH (species distribution) and interactions on solubility $m^{L}_{vitamin}$ of VB2 (a), VB9 (b), and VB12 (c). Nonpatterned bars: experimental data obtained in pure water (white) and in the presence of covitamins VC (black bars), VB3^{acid} (light gray), VB3^{amide} (dark gray), at T=298.15 K and p=1 bar. Data from this work (Appendix, A7) or (*) from the literature [177]. Below the graphs the pH of saturated solutions and concentration of covitamin $m_{covitamin}$ are given. Patterned bars: solubility calculated at the pH corresponding to saturated solutions of water-vitamin-covitamin solutions with the H-H-based eq. (2.62) for VB2, (2.68) for VB9, (2.57) for VB12; data calculated at the pH of saturated solutions of water-vitamin-covitamin. Dashed lines were added to guide the eye.

Figure 8.9(a-c) presents the evaluation of calculated (patterned bars) and experimental (nonpatterned bars) aqueous solubility of three low soluble vitamins VB2, VB9, and VB12, in the presence of covitamins VC, VB3^{acid}, and VB3^{amide}. At first, the solubility of a vitamin at the pH corresponding to the solution containing vitamin and covitamin was calculated using idealized H-H-based solubility equations (2.62) for VB2, (2.68) - VB9, and (2.57) - VB12. These equations do account only on the pH effect, so they can be used to estimate the pH influence in water-vitamin-covitamin solutions. Afterwards, the so-calculated value (patterned bars in figure 8.9) was compared with the intrinsic solubility of a vitamin (white bars in figure 8.9) and experimental solubility (nonpatterned bars in figure 8.9).

If the solubility of a vitamin calculated with the H-H-based solubility equation at a given pH was comparable with the intrinsic solubility of a vitamin (ARD%<5), then the minor species change was assumed as described in the following "Addition of Covitamin Causing Only Minor Species Change". In this case, the pH effect has no significant influence on the solubility of vitamin, and an idealized H-H-based equation would be unsuccessful in estimating experimental solubility (nonpatterned bars in figure 8.9). If the solubility of a vitamin calculated with the H-H-based solubility equation (patterned bars in figure 8.9) equals intrinsic solubility (white bars in figure 8.9), but it is different than the experimental value (nonpatterned bar in figure 8.9), then it can be assumed that interactions are a deciding factor influencing the solubility. The solubility is accessible with ePC-SAFT that accounts for interactions. Thus, equation (2.25) postulated by Prausnitz [316] can be used. Based on figure 8.9, it is expected that this situation (solubility influenced by minor species change) applies to VB2 mixed with $VB3^{acid}$ ($m_{VB3acid}$=0.05 – 0.1 mol·kg^{-1}; light gray bars), as well as to VB12 in the presence of covitamins $VB3^{acid}$ ($m_{VB3acid}$ = 0.05 – 0.1 mol·kg^{-1}; light gray bars) and $VB3^{amide}$ ($m_{VB3amide}$ = 0.1 – 0.2 mol·kg^{-1}; dark gray bars).

If the solubility of a vitamin calculated with the H-H-based solubility equation at a given pH was significantly higher than the intrinsic solubility of this vitamin (ARD%>5), then the second case can apply as described in the following "Addition of a Covitamin Causing Major Species Change". Further, if the solubility of a vitamin calculated with the H-H-based solubility equation (patterned bars in figure 8.9) is different than intrinsic solubility (white bars in figure 8.9), but it equals the experimental value (nonpatterned bar in figure 8.9), then it can be assumed that the pH effect is a deciding factor influencing the solubility. Based on figure 8.9, this situation was observed only for VB9 in the presence of lower concentration of $VB3^{amide}$ ($m_{VB3amide}$ = 0.1 mol·kg^{-1}; dark gray bars). The solubility obtained with the H-H-based equation can lead to a similar result like the experimental value. However, the so-calculated solubility is an idealized value, thus, using ePC-SAFT that accounts for non-ideality could be more relevant. This means using equation (2.25) and a respective solubility equation that accounts on the pH, namely (2.63) for VB2, (2.69) – VB9, or (2.58) – VB12. A more detailed explanation is provided in subchapter 8.1.

If the solubility of a vitamin calculated with the H-H-based solubility equation (patterned bars in figure 8.9) differs from intrinsic solubility of a vitamin (white bars in figure 8.9), as well as from the experimental solubility value (nonpatterned bars in figure 8.9), the combined effect of interactions and the pH must be considered. It can be observed from figure 8.9 that this case applies to the mixtures of VB2 with VB3amide ($m_{VB3amide}$ = 0.1 – 0.2 mol·kg^{-1}; dark gray bars) and VC (m_{VC} = 0.5 –1.42 mol·kg^{-1}; black bars), as well as of VB9 with a higher concentration of VB3^{amide} ($m_{VB3amide}$ = 0.2 mol·kg^{-1}; dark gray bars). In this case, the idealized H-H-based equation would be unsuccessful in estimating the solubility, thus, the solubility is accessible with ePC-SAFT. Equation (2.25), $K_{a,th}$ and a respective solubility equation, namely (2.63) for VB2, (2.69) – VB9, or (2.58) – VB12, allow accounting on interactions and the pH. A more detailed explanation is provided in section 8.1.

Addition of Covitamin Causing Only Minor Species Change

This part presents and discusses solubilities of poorly water-soluble vitamins upon addition of covitamin, which causes pH changes of equilibrated vitamin solutions. The experimental and ePC-SAFT prediction results of VB2 and VB12 aqueous solubility upon addition of covitamins VB^{acid} and VB3^{amide} are shown in figure 8.10. However, these pH changes do only slightly modify species distribution as shown with gray areas in figure 8.10(b,d), and pH effects on solubility are not expected. Thus, solubility changes are mainly governed by molecular interactions. Figure 8.10 shows experimental solubilities of VB2 (figure a-b) and of VB12 (figure c-d) upon addition of VB3^{acid} or VB3^{amide} to the respective aqueous vitamin solutions.

Based on the solubility data presented in figure 8.10, it can be observed that the covitamin VB3^{amide} strongly enhances the solubility of VB2 and VB12. Using ePC-SAFT pure-component and binary interactions parameters listed in table 4.1 allowed accurate solubility predictions for several water + vitamin + covitamin systems. Prediction means that no additional binary parameters between the vitamin and the covitamin were introduced to obtain results shown in figure 8.10. ePC-SAFT allows reasonably predicting solubilities of VB12 in the presence of both covitamins, VB3^{acid} (ARD% = 6.89) and VB3^{amide} (ARD% = 3.76), in the range of covitamin concentrations considered in this study. Moreover, an excellent result is observed for the solubility prediction of VB2 upon addition of covitamin VB3^{acid} (0 <$m_{VB3acid}$< 0.1 mol·kg^{-1}; ARD% = 2.04). That is, ePC-SAFT

predictively describes the non-ideality caused by different interactions between the covitamin and the saturated vitamin in the aqueous solutions. The prerequisite for this excellent result is the fact that the addition of covitamin does not change the pH in a way that the new species distribution would lead to a significant solubility impact.

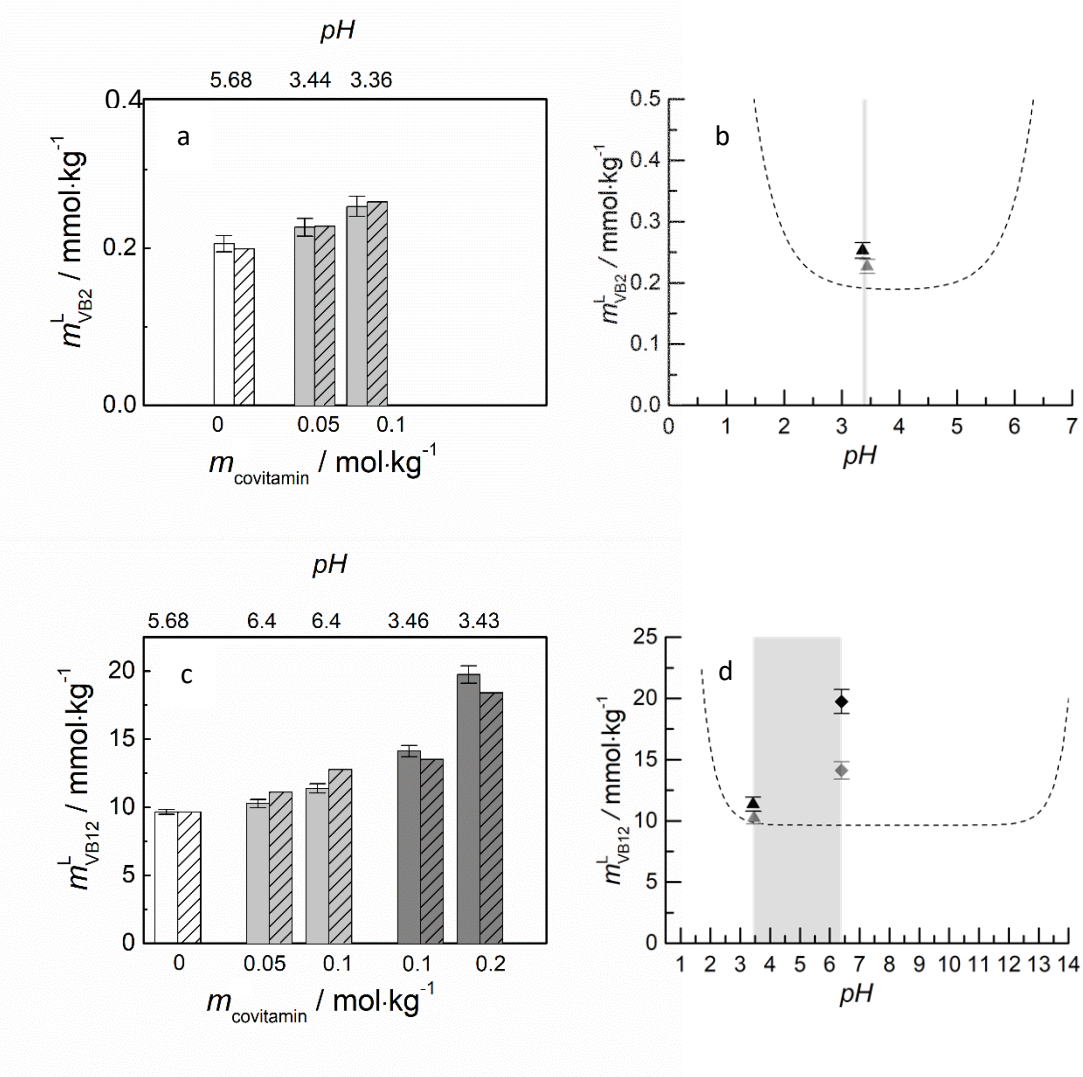

Figure 8.10. ePC-SAFT solubility $m^L_{vitamin}$ predictions (patterned bars) and experimental aqueous vitamin solubility (nonpatterned bars) of VB2 (a-b) and VB12 (c-d), at T=298.15 K, p=1 bar, measured in pure water (white bars), upon addition of VB3^{acid} (light gray bars) or VB3^{amide} (dark gray bars) (Appendix, A7 and A12). The numbers above figures (a) and (c) are pH values of the saturated solutions. Figures (b) and (d) show experimental aqueous solubility upon addition of VB3^{acid} (▲: $m_{VB3acid}$=0.05 mol·kg^{-1} and ▲: $m_{VB3acid}$=0.1 mol·kg^{-1}), and VB3amide (◆: $m_{VB3amide}$=0.1 mol·kg^{-1} and ◆: $m_{VB3amide}$=0.2 mol·kg^{-1}) as a function of pH. Dashed lines: theoretical solubility calculated with idealized H-H-based equations (2.57) and (2.62).

It can be observed for VB2 and VB12 in the pH-solubility profiles (figure 8.10) that the pH has no significant influence on vitamin solubility in the pH range studied (3.43 < pH < 6.4 for VB12 and 3.36 < pH < 5.68 for VB2). According to these pH-solubility profiles, mainly

the neutral vitamin species are present in the considered pH ranges. This demonstrates that the pH change does not cause the observed solubility increase shown in figure 8.10(a, c). Moreover, it can be concluded that in this case, the addition of the covitamin solubilizers relies on hydrotropic solubilization mechanism instead of pH-induced solubility increase.

Addition of a Covitamin Causing Major Species Change

This part presents and discusses solubilities of poorly water-soluble vitamins upon addition of covitamins that modify pH of saturated vitamin solutions. These pH changes significantly modify species distribution, and thus, pH effects on solubility are expected on top of the possible solubilizing effects that are based on molecular interactions. As shown in the previous part (addition of covitamin causing only minor species change), ePC-SAFT allows predicting the non-ideality caused among others by molecular interactions induced by the addition of covitamin at a specific pH. Further, based on the ion-specific parameters of the vitamin species (table 4.1 and table 4.2), ePC-SAFT allows capturing the pH-dependent interactions between vitamin species and water correctly. This finally allows predicting the vitamin solubility upon addition of covitamins that modify the species distribution significantly by pH changes.

The pH-change-induced species distribution also causes modification of molecular interactions between vitamin and covitamin, as the vitamin will not be present as the same species upon pH change. ePC-SAFT pure-component and binary interaction parameters used for predictions are listed in table 4.1 and table 4.2 for different vitamin species. No additional binary parameters between the two vitamins were introduced. The predictions were validated by experimental solubility data of VB2 upon addition of VC and $VB3^{amide}$, as well as the solubility data of VB9 in mixture with $VB3^{amide}$. These data are provided in Appendix (A7). The influence of two different covitamins, VC and $VB3^{amide}$, on the solubility of VB2 is shown in figure 8.11.

It can be observed from figure 8.11(a) that $VB3^{amide}$ increases VB2 solubility more than VC. Figure 8.11(b) illustrates that covitamins $VB3^{amide}$ and VC cause a pH change (gray area) that causes formation of different species. Thus, the observed solubility increase upon addition of the covitamins is a function of pH and of molecular interactions. Figure 8.11 proves that the methodology applied for these predictions (section 8.1) allows

reasonably accurate VB2 solubility predictions upon addition of covitamin VC (ARD% = 14.5). To obtain such results, ePC-SAFT parameters were assigned to different vitamin species (table 4.1 and table 4.2).

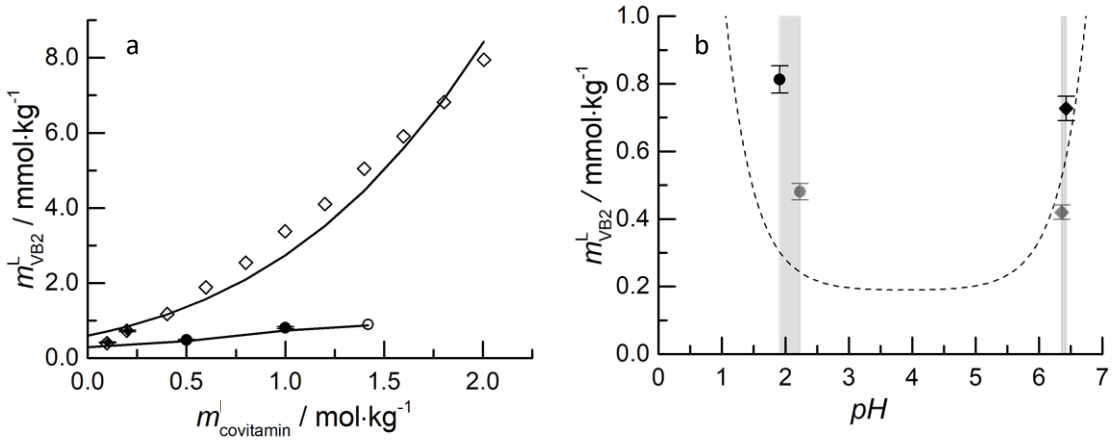

Figure 8.11. ePC-SAFT predictions (solid lines) and experimental validation (symbols) of aqueous VB2 solubility m^L_{VB2} upon addition of covitamins $m_{covitamin}$, at T = 298.15 K and p = 1 bar. Figure (a): black symbols ◆ and ● – this work (Appendix, A7), white symbols ◇ and ○ – literature[153, 177]; ◆ and ◇ - addition of covitamin VB3^{amide}, ● and ○ – addition of covitamin VC; the pH according to experimental data (Appendix, A7); pH = 5.68 if $m_{VC} = 0$ mol·kg^{-1}; predictions using the ePC-SAFT parameters from table 4.1 and table 4.2. Figure (b): experimental (Appendix, A7); ◆: $m_{VB3amide}$= 0.1 mol·kg^{-1} or ◆: $m_{VB3amide}$= 0.2 mol·kg^{-1}; ●: m_{VC}= 0.5 mol·kg^{-1} or ●: m_{VC}= 1 mol·kg^{-1}; dashed line was calculated with idealized H-H-based equation (2.62). Note that data from ref. [153] reported at T=303.15 K and these cause only slight deviaton to the solubility at T=298.15 K[5].

The values of aqueous solubility shown in figure 8.11 were predicted with ePC-SAFT at pH adequate to the value that was measured in equilibrated solutions (with or without a covitamin). These pH values of equilibrated solutions with the corresponding vitamin solubilities are provided in Appendix (A7). To study the interplay of different factors influencing VB2 solubility upon addition of VB3^{amide}, solubility data of VB2 measured in a wide range of covitamin concentration (0 <$m_{VB3amide}$< 1.8 mol·kg^{-1}) have been taken from the literature [153] and presented in figure 8.11(a). The solubility values from the literature were obtained at a slightly different temperature (5 K difference) compared to that in this work. This difference was neglected as it causes only a slight deviation in solubility of VB2[5]. Unfortunately, the authors of the literature data have not

reported the pH values of the saturated solutions. Rather, pH 6.4 was assumed in that work for all samples. Considering the pH-solubility profile of VB2 (figure 5.5 and scheme presented in figure 8.3), only a slight deviation from pH 6.4 might cause a significant solubility change. Nevertheless, ePC-SAFT was used to predict the solubility upon addition of VB3^{amide} assuming pH 6.4. The predictions were successful with reasonable accuracy (ARD% =9.35) by using the methodology described in section 8.1, i.e. by using the parameters for different vitamin species listed in table 4.1 and table 4.2. The composition of the total VB2 content at pH 6.4 can be calculated as explained in section 2.3.2. In the future, more precise reports on the pH values are desirable to further decrease the ARD% values. ePC-SAFT overpredicted VB2 solubilities at very low VB3^{amide} molality (figure 8.11). The reason behind is that experimental measurements of VB2 solubility at low VB3^{amide} molality have been performed at pH≠6.4 (namely, pH 5.68), while ePC-SAFT was used to predict the solubility of VB2 at pH 6.4.

Further, the influence of the covitamin VB3^{amide} on the solubility of VB9 has been investigated. Figure 8.12 illustrates that the addition of VB3^{amide} changes pH values of saturated VB9 solutions significantly (sharp solubility increase region).

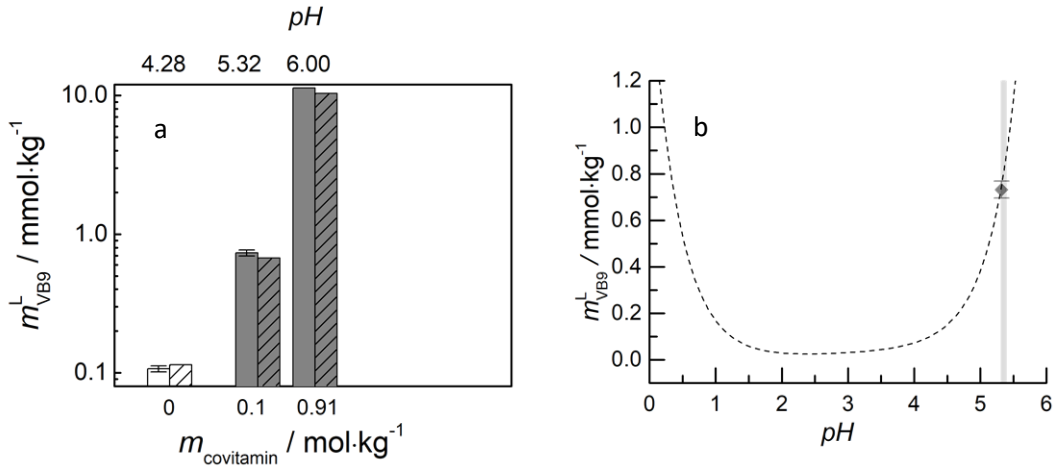

Figure 8.12. ePC-SAFT solubility predictions m^L_{VB9} (patterned bars) and experimental aqueous solubility (nonpatterned bars) of VB9, at T = 298.15 K, p = 1 bar. (a): measured in pure water (white bars) or upon addition of VB3^{amide} (gray bars); solubility of VB9 in pure water and in the presence of covitamin $m_{VB3amide}$= 0.1 mol·kg^{-1} (Appendix, A7) and $m_{VB3amide}$=0.91 mol·kg^{-1} [42]. (b): VB9 solubility measured upon addition of $m_{VB3amide}$=0.1 mol·kg^{-1} (◆), dashed lines were calculated with idealized H-H-based solubility equation (2.68).

The pH of the resulting solutions (pH shift from 2.86 to 5.4) unambiguously indicates that a significant pH-induced solubility increase in this pH range is expected. VB9 solubility upon addition of $VB3^{amide}$ in the specific range of covitamin concentration ($m_{VB3amide}$=0−0.91mol·kg^{-1}) was predicted with reasonable accuracy (ARD% =4.23) using the methodology explained in section 8.1.

The main observation based on the results provided in this part confirms the fact that the pH effect cannot be neglected when the phenomena which rule the vitamin solubilization are studied. The so-called "hydrotropes" [59] might cause pH changes that strongly influence (i) molecular interactions, (ii) species distribution, or (iii)even both. Different covitamins ($VB3^{amide}$ and VC) are considered as solubilizers for VB2 or VB9, and the predominating factor influencing the solubility is related to the concentration of covitamin. At low $VB3^{amide}$ concentrations, solubilities of VB2 and VB9 follow the pH-solubility curves calculated with idealized H−H-based equations (2.62) and (2.68). This means that at low $VB3^{amide}$ concentration, a similar effect on VB2 and VB9 solubility is expected as when adding sodium hydroxide to the vitamin solution. Clearly, NaOH is not considered as a hydrotrope, and the solubilizing effect induced by the addition of a low concentration of $VB3^{amide}$ is just a pH-induced solubility increase. Examples presented in this section prove that at low covitamin concentrations, pH effect is a deciding factor for solubility enhancement. Above a certain covitamin concentration, namely, minimum hydrotrope concentration, the interactions become successively more important and finally dominate the observed solubility increase. This does not mean that pH effects are becoming negligible at high covitamin concentrations. It was shown that this fact can be accessed by ePC-SAFT solubility predictions. ePC-SAFT considers many interactions which probably occur in the aqueous vitamin system at different covitamin concentration. However, it was not possible to accurately predict solubilities of vitamins upon addition of covitamins mentioned in this part, without accounting for the pH. Moreover, the concentration at which the interactions are predominant is different for each covitamin. The solubility enhancement levels also vary, and they can be very different for each vitamin. Thus, the same concentration of $VB3^{amide}$ ($m_{VB3amide}$= 0.91 mol·kg^{-1}) leads to about 100-fold solubility enhancement of VB9, while for VB2, a 15-fold increase observed.

8.4. Conclusion

In this chapter, the results of aqueous solubility predictions of four DNP-AA, namely DNP-glycine, DNP-alanine, DNP-valine, and DNP-leucine, as well as five vitamins VC, VB2, VB3^{acid}, VB9, VB12, carried out using thermodynamic model ePC-SAFT were presented and discussed. Designed in this work ePC-SAFT strategies allowed predicting the intrinsic solubility ($m_{0,i}^{L,pred}$), as well as solubility at different pH and upon addition of covitamins ($m_i^{L,pred}$). The intrinsic solubility of DNP-AA and vitamins was predicted with ePC-SAFT at T = 298.15 K and p = 1 bar. For some vitamins, namely VC and VB3^{acid}, the values of $m_{0,i}^{L,pred}$ have been predicted also in a wider temperature range, namely T = 293 – 323 K (VC) and T = 283.59 – 332.09 K (VB3^{acid}). Solubility values at different pH of a solution and upon addition of covitamins $m_i^{L,pred}$ were predicted at T = 298.15 K and p=1 bar. ePC-SAFT pure-component and binary interaction parameters k_{ij} (only one k_{ij} between water and each solute, i.e. DNP-AA or vitamin) estimated with approaches applied in this work, namely Joint-Parameter Method and Molecular Method, were used to predict the activity coefficients required for ePC-SAFT solubility predictions. These parameters, together with melting properties, as well as dissociation constants p$K_{a,th}$, were already provided in chapter 4.

It has been observed that ePC-SAFT allows quantitative intrinsic solubility prediction of DNP-AA and vitamin solubilities in water at T = 298.15 K and p=1 bar with parameters fitted previously for neutral species to solubility-independent data. ePC-SAFT accurately described the solubility trend of DNP-AA $m_{DNP-alanine}^{L,pred} > m_{DNP-valine}^{L,pred} > m_{DNP-glycine}^{L,pred} > m_{DNP-leucine}^{L,pred}$ that is different than experimental solubility trend observed for aliphatic AA $m_{glycine}^{L} < m_{L-alanine}^{L} < m_{L-valine}^{L} < m_{L-leucine}^{L}$ [81, 393, 394]. Also, the solubility trend obtained for vitamins $m_{VC}^{L} > m_{VB3acid}^{L} > m_{VB12}^{L} > m_{VB2}^{L} > m_{VB9}^{L}$ (assuming the same trend of $m_{0,vitamin}^{L}$ and $m_{vitamin}^{L}$ at constant pH) fully agrees with experimental data from section 5.2. Overall, the approaches applied in this work for ePC-SAFT parameter estimation and for predicting the intrinsic solubility of DNP-AA and vitamins in water can accurately characterize the non-ideality. Such behavior can be caused by different interactions that occur in these aqueous systems and involve neutral molecules (noncharged) of DNP-AA or vitamins.

Depending on the pH, DNP-AA and vitamins can be present in aqueous solutions also as charged species. Since the solubility in water strongly depends on pH-dependent species distribution, ePC-SAFT predictions of the pH-solubility profiles of four DNP-AA, as well as of the two low soluble vitamins VB2 and VB9, at T = 298.15 K and p = 1 bar, have been done and the results were presented and discussed in this chapter. Prior to the predictions, previously estimated ePC-SAFT parameters for charged species (chapter 4) were required. Thermodynamic dissociation constants p$K_{a,th}$ were estimated according to Lange *et al.* [381] simultaneously with ePC-SAFT activity coefficients of the species γ_j^L, using the intrinsic solubility and one experimental solubility data point measured for each solute. This allowed to obtain quantitative predictions of whole pH-solubility profiles of DNP-AA, namely DNP-glycine, DNP-alanine, DNP-valine, DNP-leucine, as well as vitamins VB2 and VB9. The success of ePC-SAFT lays in a fact that in contrast to the mass-balance-based Henderson–Hasselbalch equations, ePC-SAFT explicitly accounts for the interactions involving vitamin species at a certain pH.

Both factors the pH and the temperature may influence the solubility of a vitamin. ePC-SAFT predictions allowed separating the pH and temperature effects on vitamin solubility. Thus, the temperature dependence on the solubility of the two vitamins VB3^{acid} and VC was predicted with ePC-SAFT and discussed. It was found that ePC-SAFT can predict the temperature influence on VB3^{acid} solubility, between T = 283.59 K and T = 332.09 K, with high accuracy if comparing predicted results to experimental VB3^{acid} solubility data. Besides this success, the deviations were observed between ePC-SAFT and experimental VC solubility at increased temperatures (T = 293 K – 323 K). Among all vitamins studied in this work, VC is the least stable against air and light and it is the most acidic vitamin. Thus, the observed deviations might be caused by different effects that are not included in the model (e.g., decomposition, pH effect).

The modeling and prediction strategies designed in this work allow also to predict vitamin solubility in the presence of covitamins at any desired pH. The influence of covitamins VB3^{acid}, VB3^{amide}, or VC, on solubility of vitamins VB2, VB9, or VB12, was predicted with ePC-SAFT at T = 298.15 K and p = 1 bar. The predictions were in accurate agreement to the experimental data, and they were classified into systems with minor and major species distribution change caused upon adding covitamin. In both considered system classes, predictions were found to be in accurate agreement with experimental

data without a need of introducing any additional parameter (minor species change: VB12 + $VB3^{amide}$, VB12 + $VB3^{acid}$, and VB2 + $VB3^{acid}$; major species change: VB2 + VC, VB2 + $VB3^{amide}$, VB9 + $VB3^{amide}$). This work revealed adding covitamins at low concentration mainly has an impact on solubility by a pH change. At a certain covitamin concentration (specific for each vitamin + covitamin system), the molecular interactions become more important than the pH. Thus, predicting the solubility in a wide range of concentrations requires considering both molecular interactions and pH effects. This also raises some issues about the definition of "hydrotropes", which are considered in literature to be solubility enhancers for many components. Based on the results obtained in this work, it is recommended to not assign hydrotropic effects to components that increase solubility by changing mainly the pH of a solution in a sense that also NaOH would be denoted a hydrotrope according to this definition.

9. Predicting Phase Equilibrium of ATPS

This chapter presents the predictions of phase equilibria for different ATPS formed by PEG and biodegradable salts. The predictions were performed using ePC-SAFT that allows an accurate description of non-ideality caused by molecular interactions between the phase forming components. The results were compared with experimental data and presented in terms of the accuracy obtained for ATPS composed by PEG of different average molar mass and salt type. The results presented in this chapter are an essential component for further applications, e.g. for ePC-SAFT predictions on the partitioning of different solutes in ATPS. They were obtained using an approach that was designed to describe the interactions between ATPS phase formers and considered homosegmented PEG chain and spherical ions constitution.

9.1. Approach

ATPS considered in the present work were formed by PEG (M_{PEG} = 4000 - 8000 g·mol^{-1}) and biodegradable salts, namely Na_3Citrate, K_3Citrate, Na_2Tartrate, or KNaTartrate. According to a description provided in section 2.3.2, at the pH of ATPS from this study (pH~8), all considered salts are fully dissociated. Thus, the presence of cations Na^+ and K^+, as well as anions $Citrate^{3-}$, $Tartrate^{2-}$, in ATPS is expected. Predicting phase equilibria of ATPS containing PEG and biodegradable salts have been carried out in this work with ePC-SAFT thorough an accurate description of molecular interactions between the phase forming components, at T = 298.15 K and p = 1 bar. The predictions were performed on a theoretical basis of isoactivity criteria presented already in section 2.2.2. Experimental basis for the modeling and validation of the predictions was included in Appendix (A8). The interactions in ATPS that have been considered by the model are presented in figure 9.1. The non-ideality caused among others by these interactions was characterized with activity coefficients predicted using ePC-SAFT pure-component parameters and binary interaction k_{ij} parameter.

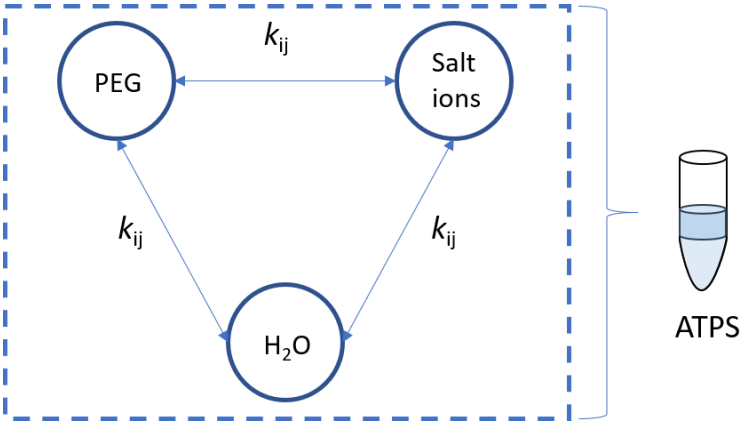

Figure 9.1. Interactions between components present in ATPS considered by ePC-SAFT in this work. Binary interaction parameter k_{ij} was used to help describing the non-ideality caused by these interactions, among others.

In this work, the conventional approach has been followed and a homo-segmented PEG chain and spherical salt species of fully dissociated salt were considered [303]. Although ePC-SAFT copolymer approach proposed in the literature by Reschke *et. al.* [280] was successful in modeling phase equilibria of PEG – organic salt ATPS, it was also very complex. The complexity of this copolymer modeling strategy was related to splitting PEG into two segment types and then accounting for their molecular interactions with salt

and water. This means that many sets of parameters, i.e. the pure-component as well as k_{ij} parameters, were required for the modeling using a copolymer approach (one set for each segment of PEG and for every salt species). A very high computational effort related to ePC-SAFT copolymer approach from the literature [280] was also the factor that has limited further application of this approach to predicting the partitioning of complex molecules, such as DNP-AA and vitamins that dissociate into different ionic species in ATPS. Since predicting the partitioning of DNP-AA and vitamins was one of the main objectives of this work, the conventional approach that uses just single set of pure-component parameters and one k_{ij} with water for PEG and for each salt ion (in this case Na^+, K^+, $Citrate^{3-}$, $Tartrate^{2-}$) was applied. Thus, to model ATPS composed by PEG and salt required only three sets of pure-component parameters and k_{ij} with water (one for PEG, one for cation, and one for anion). Using more conventional strategy simplified the modeling and allowed the predictions (i.e. LLE and further - partition coefficients) with reasonable calculation time and numerical stability. The pure-component parameters and k_{ij} with water for PEG were included in table 4.1 (PEG) and table 4.2 (salt ions). They were taken from the literature [303, 338, 373-375] or fitted in this work to density and osmotic coefficients (section 4.1.1) [7]. The binary interaction parameters between phase formers (water, PEG, salt ions) were given in table 4.3. These parameters were either found in the literature [375] or adjusted in this study according to a description from section 4.1.1[7, 8].

Worth to note is that these results only aimed at determining the interaction parameters between phase formers in ATPS as listed in table 4.3. The ePC-SAFT predicted equilibrium compositions were not used as input for further prediction of the partition coefficients, and rather the experimental equilibrium compositions were applied for this purpose.

9.2. Prediction Results: ATPS Diagrams

Different PEG´s molar mass and salt type are the factors that can influence phase equilibria of ATPS. These effects were already discussed in section 6.1 and the conclusions were drawn based on experimental data (Appendix, A8). The purpose of this section (9.2) is to evaluate the capability of ePC-SAFT to predict phase diagrams of PEG – organic salt (Na_3Citrate, K_3Citrate, or KNaTartrate) ATPS, at T = 298.15 K and p = 1 bar. The following

sections present exemplary figures that show the results obtained with ePC-SAFT for ATPS composed by PEG of different molar mass (9.2.1) and salt type (9.2.2).

Accuracy of the predictions was evaluated based on average absolute deviation (AAD) calculated according to equation (4.15). Experimental data used in this validation are included in Appendix (A8). AAD for different compositions of all ATPS considered in this study are listed in table 9.1. The average value of all AAD values calculated for both phases of different ATPS was equal to 0.025 which is a common result for predicting LLE in literature [98, 280].

Table 9.1. ePC-SAFT predictions of ATPS equilibrium compositions – average absolute deviation (AAD) for all ATPS considered in this work (T = 298.15 K, p = 1 bar) [7]. AAD between predicted and experimental values were calculated according to equation (4.15) from tie-line composition given in mass fraction (Appendix, A8).

Salt	*PEG*	*Np**	*AAD (upper phase)*	*AAD (lower phase)*	*AAD (both phases)*
$Na_3Citrate$	PEG 4000	12	0.0303	0.0007	0.0155
$Na_3Citrate$	PEG 6000	12	0.0336	0.0246	0.0292
$Na_3Citrate$	PEG 8000	6	0.0447	0.0494	0.0471
$Na_2Tartrate$	PEG 4000	12	0.0218	0.0323	0.0271
$Na_2Tartrate$	PEG 6000	12	0.0169	0.0359	0.0264
$K_3Citrate$	PEG 4000	6	0.0220	0.0087	0.0154
$K_3Citrate$	PEG 6000	6	0.0059	0.0161	0.0110
$K_3Citrate$	PEG 8000	6	0.0418	0.0106	0.0262
KNaTartrate	PEG 4000	6	0.0262	0.0221	0.0241
KNaTartrate	PEG 6000	6	0.0357	0.0241	0.0299
KNaTartrate	PEG 8000	6	0.0338	0.0178	0.0258

**Np* – number of experimental data points used for validation of the predictions

9.2.1. PEG Influence on ATPS

Table 9.1 has shown already that ePC-SAFT can predict equilibrium compositions of ATPS formed by different PEG molar mass (M_{PEG} = 4000-8000 g·mol^{-1}) with reasonable accuracy. One example of prediction results for ATPS PEG – $Na_3Citrate$ for two different PEG molar mass (M_{PEG} = 4000-6000 g·mol^{-1}) is presented also in figure 9.2 that illustrates reasonable prediction results compared to experimental data. Conclusions resulting from experimental data (including data plotted in figure 9.2) on PEG influence on ATPS have

been already drawn in section 6.1.1. Based on table 9.1 the deviations (AAD) calculated for both phases of ATPS are higher for ATPS composed with PEG 6000 - $Na_3Citrate$ (AAD = 0.0292) than for ATPS formed by PEG 4000 - $Na_3Citrate$ (AAD = 0.0155). The same trend was observed for PEG (M_{PEG} = 4000 - 6000 g·mol^{-1}) and KNaTartrate. However, all these AAD values are similar to the ones found in literature (copolymer approach) for LLE predictions of PEG – organic salt ATPS [280]. This means that ePC-SAFT conventional approach used in this work for predicting the non-ideality caused by interactions in ATPS composed by PEG of different molar mass and a salt is enough accurate to be a background for further applications (e.g. predicting the partitioning).

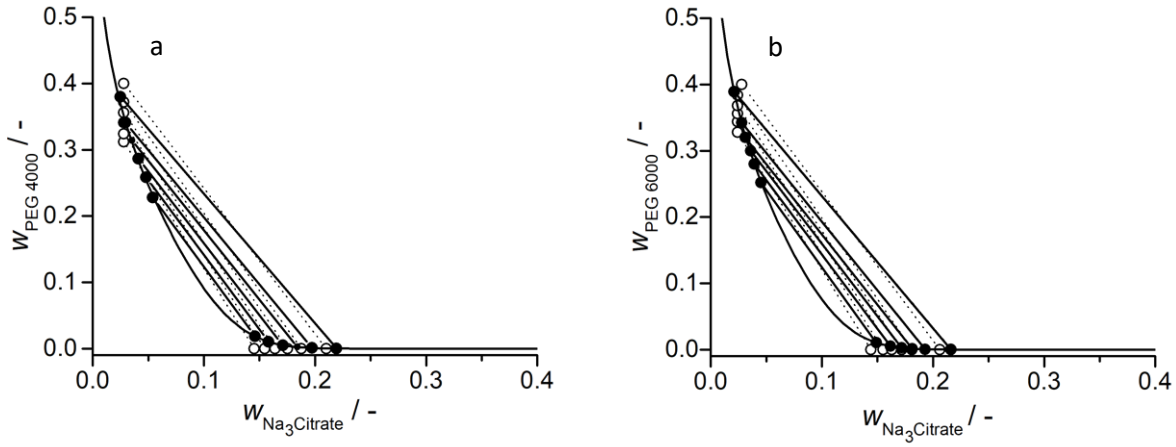

Figure 9.2. ATPS containing PEG of M_{PEG} = 4000 g·mol^{-1} (a) or M_{PEG} = 6000 g·mol^{-1} (b) and $Na_3Citrate$ at T=298.15 K, p=1 bar (concentration given in mass fraction, w). The equilibrium compositions were presented as symbols: ○ ePC-SAFT; ● experimental (Appendix, A8). Dotted lines: tie-lines predicted with ePC-SAFT. Solid lines (binodals, tie-lines): experimental (Appendix, A8).

9.2.2. Salt Influence on ATPS

According to AAD values presented in table 9.1, ePC-SAFT was able to predict LLE for ATPS formed by PEG and different salts with similar accuracy. Figure 9.3 and figure 9.4 present the equilibrium concentration of PEG plotted against the equilibrium concentration of the salt (figures a) or salt ions (figures b). These two figures were used to evaluate ePC-SAFT predictions, while the conclusions based on the involved experimental data were already drawn in section 6.1.2. Figure 9.3 illustrates predictions of cation influence on phase-forming ability in ATPS. At first general conclusions can be

made based on figure 9.3a on which mass fractions of PEG 6000 and salt $Na_3Citrate$ and $K_3Citrate$ are plotted, i.e. ePC-SAFT can capture the effect caused by changing the salt cation and keeping the salt anion constant. The AAD values from table 9.1 have already shown that among the two systems considered (PEG 6000 - $Na_3Citrate$ and PEG 6000 - $K_3Citrate$), better accuracy of the predictions was achieved for ATPS formed by PEG and $K_3Citrate$. However, in both cases, ePC-SAFT predicted the LLE according to the trend observed in the evaluation of experimental data (section 6.1.2). Thus, the higher biphasic area was predicted for PEG 6000 - $Na_3Citrate$ ATPS.

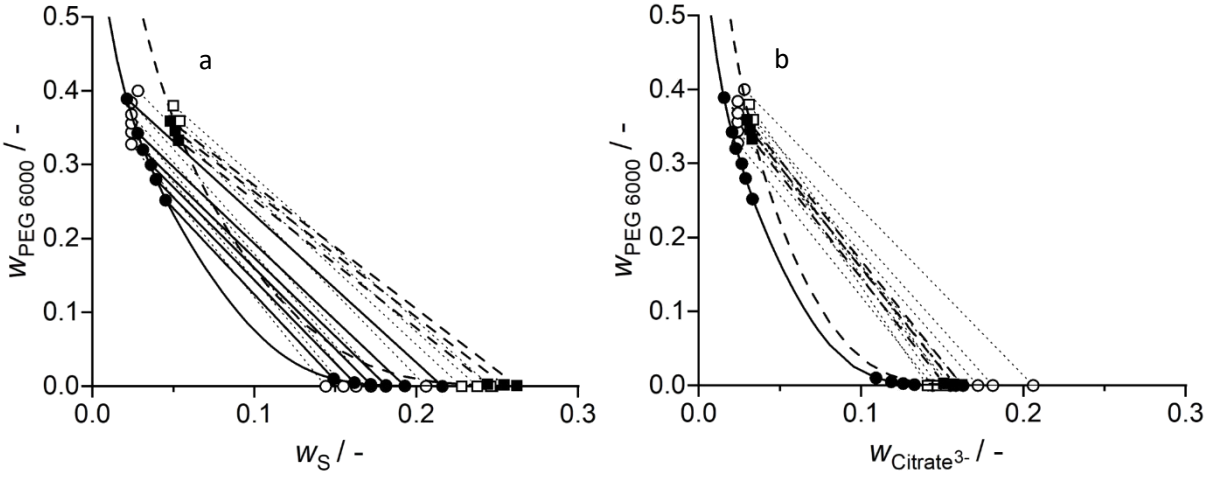

Figure 9.3. ATPS containing PEG and citrate salts, at T=298.15 K and p=1 bar. Concentration in figures a-b is given in mass fractions w of: PEG to salt (a) and PEG over the salt anion (b); The equilibrium compositions of PEG 6000 – citrate salt ATPS are presented as symbols: ePC-SAFT predictions ○ ($Na_3Citrate$) □ ($K_3Citrate$), experimental data (Appendix, A8): ● ($Na_3Citrate$), ■ ($K_3Citrate$); PEG 6000 - $Na_3Citrate$: experimental binodal and tie-lines (solid lines), predicted tie-lines (dotted lines); PEG 6000 - $K_3Citrate$: experimental binodal and tie-lines (dashed lines), predicted tie-lines (dotted lines). For better visibility figure (b) does not present experimental tie-lines for PEG 6000 - $Na_3Citrate$ since they would overlap the predicted lines.

Since figure 9.3a allows only to compare "a total" salt effect, figure 9.3b was presented for the comparison of the cation influence on phase formation of ATPS. Consequently, figure 9.3b shows the equilibrium concentration of PEG against the equilibrium concentration of $Citrate^{3-}$. Since ePC-SAFT successfully predicted the effects caused by the presence of different salts in ATPS, also the cation effect could be captured. Figure 9.3(a-b) shows a decrease in the two-phase area when only the cation effect is evaluated (figure 9.3b). This might result from the cation molar mass, as mentioned already in a discussion included in section 6.1.2. Smaller ion Na^+ (compared to K^+) of a salt, leads to a higher size of the

two-phase region. From the application perspective, using a salt of smaller size cation would be favorable since then less of salt is required to form the two-phases. Thus, the success of ePC-SAFT in predicting this behavior is especially important if this model was applied for selecting phase forming compounds.

ePC-SAFT predictions were evaluated also in terms of salt influence constituted of different anion and same cation. The observations could be made based on the results shown in figure 9.4 for ATPS formed by PEG 6000 and salts Na_3Citrate and Na_2Tartrate.

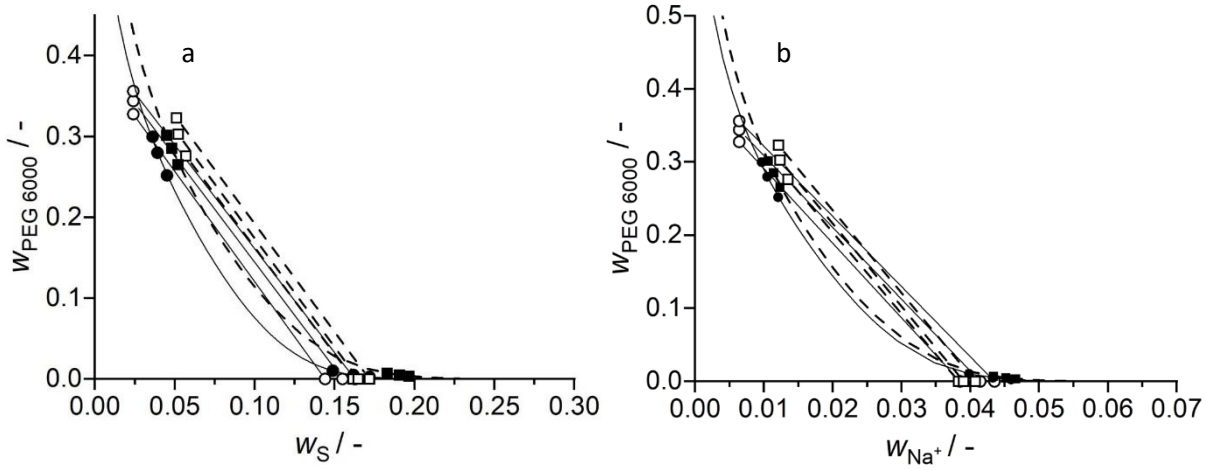

Figure 9.4. ATPS containing PEG and sodium salts, at T=298.15 K and p=1 bar. Concentration in figures a-b is given in mass fractions w of: PEG to salt (a) and PEG over the salt cation (b); The equilibrium compositions of PEG 6000 – citrate salt ATPS are presented as symbols: ePC-SAFT predictions ○ (Na_3Citrate) □ (Na_2Tartrate), experimental data (Appendix, A8): ● (Na_3Citrate), ■ (Na_2Tartrate); PEG 6000 - Na_3Citrate: predicted tie-lines and experimental binodals (solid lines), PEG 6000 – Na_2Tartrate: predicted tie-lines and experimental binodals (dashed lines). For better visibility figures do not present experimental tie-lines since these data would overlap the predicted lines.

Similar to the previous example (figure 9.3) the equilibrium concentration of PEG is plotted against the equilibrium concentration of "a total" salt in figure 9.4a. Figure 9.4b that shows the equilibrium concentration of PEG against the equilibrium concentration of Na^+ was introduced to allow studying the anion effect. ePC-SAFT was able to capture the difference in the size of the biphasic area for both systems. ePC-SAFT predictions were in agreement to experimental data (discussed in experimental section 6.1.2) and showed that ATPS formed by PEG 6000 and Na_3Citrate has a larger two-phase area. The effect observed on figure 9.4 and almost quantitative ePC-SAFT predictions of LLE may relate to the accurate description of electrostatic interactions by ePC-SAFT. In this case, $Tartrate^{2-}$

can bind only two ions Na^+, while $Citrate^{3-}$ can connect with three Na^+. This was accounted for by the model.

The prediction results presented in this section prove that ePC-SAFT through an accurate description of the non-ideality caused by interactions in ATPS (schematically shown in figure 9.1) can capture the effects related to the presence of different salt in the system. It is important to note that the success of ePC-SAFT depends on the pure-component parameters (water, PEG, salt ions) and binary interaction parameters k_{ij} with water (water ↔ PEG, water ↔ salt ions) which were not fitted to LLE data prior to the predictions. These parameters were either available in the literature or they were estimated based on LLE-independent properties of binary aqueous systems (i.e. liquid density or osmotic coefficient) and can be used for predicting other physicochemical properties (e.g. solubility). The binary interaction parameters between phase forming components of ATPS (salt ions ↔ PEG; salt ions: Na^+, K^+, $Citrate^{3-}$, $Tartrate^{2-}$) were taken from the literature or fitted only to a single experimental LLE data of ATPS formed by PEG 4000 and salt i.e. $Na_3Citrate$, $K_3Citrate$, $Na_2Tartrate$ (in detail elaborated in section 4.1).

9.3. Conclusion

In this chapter, ePC-SAFT predictions of phase equilibria at T=298.15 K and p=1 bar in ATPS formed by PEG of different molar mass M_{PEG} = 4000 - 8000 $g \cdot mol^{-1}$ and biodegradable salts, namely $Na_3Citrate$, $K_3Citrate$, $Na_2Tartrate$, or KNaTartrate were evaluated. These results only aimed at determining the interaction parameters between phase formers in ATPS. The predictions were done on a theoretical basis of isoactivity criteria using the ePC-SAFT approach that accounts for a homo-segmented PEG chain and spherical species of fully dissociated salts. It required ePC-SAFT pure-component and binary interaction parameters k_{ij} with water that were either available from the literature or were previously fitted in this work to LLE-independent properties of aqueous binary solutions, e.g. density and osmotic coefficients. The non-ideality caused by interactions between phase forming components (salt ions ↔ PEG) was expressed with help of k_{ij} fitted as described in chapter 4 only to a single experimental LLE data point from three ATPS (PEG 4000 - $Na_3Citrate$, PEG 4000 - $K_3Citrate$, and PEG 4000 – $Na_2Tartrate$).

The results of ePC-SAFT predictions have been compared to experimental data and the absolute average deviations AAD were calculated. Based on AAD values, ePC-SAFT

was capable to accurately predict the LLE of ATPS under study. The overall AAD obtained from the comparison of predicted and experimental equilibrium mass fractions of ATPS components in all considered ATPS (both phases, different tie-lines) was equal to 0.025 (2.5 wt%) which is a common result for predicting LLE in literature. The predictions were also evaluated in terms of the ability of ePC-SAFT to capture the effects on phase equilibria resulting from selecting PEG of different molar mass and type of cation and anion of a salt. ePC-SAFT successfully predicted the effects on the size of the two-phase area caused by the presence of PEG of different molar mass, different salts in ATPS, and related to this cation and anion effect. Almost quantitative ePC-SAFT predictions of LLE may relate to the accurate description of different molecular interactions considered by ePC-SAFT, e.g. electrostatic interactions that are very important when predicting the behavior of ionic species in ATPS. The ePC-SAFT approach proposed in this work for predicting the LLE of ATPS was accurate enoough to be a background for further applications (e.g. predicting the partitioning).

10. Predicting the Partitioning of Biomolecules in ATPS

This chapter shows the results on partition coefficients predicted with ePC-SAFT for DNP-AA and water-soluble vitamins in PEG – biodegradable salt ATPS. Thermodynamic models able to accurately predict influences of system properties that control the partitioning in ATPS can reduce time-consuming and cost-intensive experiments to a minimum extent. Characterization presented in the previous chapters that involve DNP-AA, water-soluble vitamins, as well as ATPS physicochemical properties, was considered background for the application addressed in the present chapter, that consists of predicting the partitioning of these solutes in ATPS. The capability of ePC-SAFT to predict the influence of solute properties, as well as phase formers, with designed in this work ePC-SAFT approach have been evaluated by comparing partition coefficients predicted with the model to experimental data.

10.1. Approach

The number of experiments can be reduced by predicting accurately the partition coefficient. However, even having an extensive database of experimental partition coefficients (*K*), it is not possible to unravel the phenomena that are behind the partitioning with only *K* values. In this work, ePC-SAFT was capable to predict *K* qualitatively, but also by separating different effects that rule the separation it helped in evaluating which effects dominate in the partitioning of different solutes. This was done using activity coefficients γ_i^{∞} that were predicted with ePC-SAFT for different components, separated in the two phases of ATPS. Partition coefficients $K_i^{pred,\infty}$ of DNP-AA (DNP-glycine, DNP-alanine, DNP-valine, DNP-leucine) and water-soluble vitamins (VB2, VB3^{acid}, VB3^{amide}, VB9, VB12) were predicted with ePC-SAFT in ATPS formed by PEG (M_{PEG} = 4000 – 8000 g·mol^{-1}) and biodegradable salt (Na_3Citrate, K_3Citrate, Na_2Tartrate, KNaTartrate), at T = 298.15 K and p = 1 bar. The theoretical background for the ePC-SAFT partitioning approach designed in this work was provided in section 2.2.2.

DNP-AA and water-soluble vitamins in aqueous solutions of pH~8 (pH of ATPS) can be present as species with different charge states, and additionally, these species can have different partition coefficients in ATPS. Since DNP-AA and water-soluble vitamins are usually present at very small concentrations, the ePC-SAFT partitioning approach was based on predicting the infinite dilution activity coefficient γ_j^{∞} of DNP-AA or vitamin species in the two phases of ATPS. Introducing γ_j^{∞} to equation (2.29) allows calculating the partition coefficient of the species *j* ($K_j^{pred,\infty}$). As mentioned in section 2.2.2 experimental partition coefficient of component *i* (DNP-AA or vitamin) K_i^{exp} corresponds to the total partition coefficient $K_i^{pred,\infty}$ that involves all the DNP-AA or vitamin species present in ATPS. Thus, $K_i^{pred,\infty}$ may differ from the ePC-SAFT predicted $K_j^{pred,\infty}$ if pH^{I} ≠ pH^{II} (*I* – top phase and *II* – bottom phase of ATPS). Conversion between $K_i^{pred,\infty}$ and $K_j^{pred,\infty}$ was provided with equation (2.30) and requires the species distributions. The species fraction calculations were presented in section 2.3.2.

ePC-SAFT pure-component and binary interaction k_{ij} parameters with water used for predicting the partitioning have been included in table 4.1 and table 4.2. They were obtained either from the literature [65, 303, 338, 373-375] or estimated in this work

based on physicochemical properties, i.e. density and osmotic coefficients (the modeling procedures were explained in subchapter 4.1). Their fitting did not involve experimental partitioning data. The applicability of ePC-SAFT parameters listed in table 4.1 and table 4.2 was already evaluated in terms of predicting the aqueous solubility of DNP-AA and vitamins, as well as the LLE in PEG – biodegradable salt ATPS (chapters 8 and 9). It showed good accuracy if comparing to experimental data. Thus, the results presented in the following part of this work validate the relevance of using these parameters also for predicting the partitioning in ATPS.

Predicting the partitioning of DNP-AA and water-soluble vitamins in PEG – salt ATPS with ePC-SAFT requires a description of non-ideality caused by interactions between the components present in ATPS. The binary interaction parameters k_{ij} between ATPS forming components (PEG, water, salt ions) included in table 4.3 were already applied in this work for predicting the LLE of PEG – biodegradable salt ATPS (chapter 9). These k_{ij} were either taken from the literature [375] or fitted in this work according to the procedure provided in section 4.1.1. The k_{ij} values between the solutes (DNP-AA, vitamins) and ATPS phase formers were estimated prior to predicting the partitioning and listed in table 4.3. The fitting of these parameters was explained in section 4.1.1.

The following sections 10.1.1 and 10.1.2 explain further ePC-SAFT partitioning approach by focusing on predicting the partitioning of specific neutral or charged components, i.e. DNP- AA and water-soluble vitamins, in ATPS of pH∼8. Thus, section 10.1.1 is centered on predicting the partitioning of amino acid derivatives – DNP-AA, while section 10.1.2 on predicting the partition coefficients of water-soluble vitamins.

10.1.1. Amino Acid Derivatives

DNP-AA (DNP-glycine, DNP-alanine, DNP-valine, DNP-leucine) tend to partition to the top PEG-rich phase of PEG (M_{PEG} = 4000 – 8000 g·mol^{-1}) – biodegradable salt (Na_3Citrate, K_3Citrate, KNaTartrate) ATPS. To accordingly predict the partitioning of DNP-AA in ATPS with ePC-SAFT, the dissociation equilibrium of these molecules in aqueous solutions must be known. Thus, the evaluation of equilibrium expressions for ionizable components is required. Since this is an essential background also for the previously showed calculations (e.g. solubility), the description of dissociation equilibrium of DNP-AA has been already included in this document (section 2.3.1). Based on figure 4.5, at the

pH~8 DNP-AA are solely present as negatively charged species (DNP-AA$^-$) in aqueous solution (charge q=- 1). The species fraction calculations for DNP-AA species (neutral DNP-AA and charged DNP-AA$^-$) were shown in section 2.3.2.

ePC-SAFT binary interaction parameters from table 4.3 that were needed to describe the non-ideality caused by interactions in ATPS, have been assigned according to figure 10.1. The pure-component parameters of charged DNP-AA (DNP-AA$^-$) are given in table 4.2. The predictions of partition coefficients were evaluated based on experimental data provided in Appendix (A9).

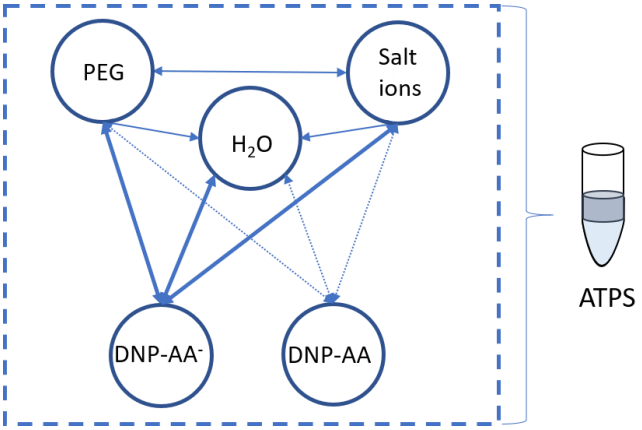

Figure 10.1. Interactions between components present in ATPS (ATPS phase formers PEG, H_2O, salt species; DNP-AA species). Fractions of DNP-AA and salt species are pH-dependent. Lines represent the interactions that can occur in ATPS (solid lines: the interactions considered in ePC-SAFT modeling within this work; dotted lines: theoretically possible interactions if neutral DNP-AA are present in ATPS – not considered in ePC-SAFT modeling carried in this work).

10.1.2. Water-Soluble Vitamins

In this work, vitamins (VB2, VB3^{acid}, VB3^{amide}, VB9, VB12) are mostly partitioned to the top PEG-rich phase of PEG (M_{PEG} = 4000 – 6000 g·mol^{-1}) – biodegradable salt (Na_3Citrate, Na_2Tartrate) ATPS. To accordingly predict the partitioning of vitamins in ATPS with ePC-SAFT, at first the dissociation equilibrium of vitamins in aqueous solutions must be known. Thus, the analysis of equilibrium expressions for ionizable components in their water solutions is needed. This is an essential background required also for the previously shown calculations (e.g. solubility). The description of dissociation equilibrium of vitamins VB2, VB3^{acid}, VB9, VB12 partitioned in ATPS has been already included in this document (section 2.3.1) or provided in the literature (VB3^{amide})[381].

Based on figure 4.5, at pH~8 of ATPS vitamins considered in this work are present as neutral ($VB3^{amide}$, VB12) or negatively charged species ($VB2^{-}$, $VB3^{acid-}$, $VB9^{2-}$, $VB9^{3-}$).

The binary interaction parameters from table 4.3 (needed additionally besides ePC-SAFT pure-component parameters) helped describing the non-ideality caused among others by different interactions in ATPS and were assigned according to figure 10.2. The pure component parameters of water-soluble vitamins partitioned in ATPS are given in table 4.1 and table 4.2. The predictions of partition coefficients were evaluated based on experimental data provided in Appendix (A9).

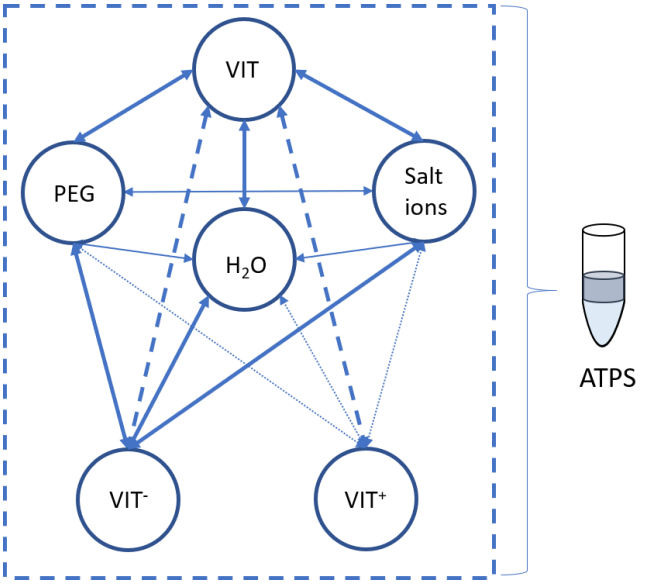

Figure 10.2. Interactions between components present in vitamin partitioning in the ATPS considered in this work (ATPS phase formers PEG, H_2O, salt species; vitamin species). Fractions of vitamin and salt depend on pH. Solid lines: the interactions considered in this work for ePC-SAFT modeling; dashed lines: theoretically possible interactions between different vitamins species (neutral, negatively, or positively charged) present in aqueous solution – for simplification not considered in ePC-SAFT modeling; dotted lines: interactions which could be considered by ePC-SAFT if positively charged species were present in solution.

10.2. Prediction Results: Amino Acid Derivatives

The predictions of partition coefficient $K_{DNP-AA}^{pred,\infty}$ of DNP-AA (DNP-glycine, DNP- alanine, DNP-valine, DNP-leucine) in ATPS: PEG (M_{PEG} = 4000 – 8000 g·mol^{-1}) – biodegradable salt (Na_3Citrate, K_3Citrate, KNaTartrate) were performed using ePC-SAFT,

at T = 298.15 K and p = 1 bar. The pure-component and binary interaction k_{ij} parameters required for ePC-SAFT were given in table 4.1, table 4.2, and table 4.3.

The accuracy of the predictions was evaluated based on experimental data measured in this work and included in Appendix (A13). ARD% between experimental and predicted partition coefficients were calculated using equation (4.14) and are listed in table 10.1. It shows that ePC-SAFT allows predicting $K_{DNP-AA}^{pred,\infty}$ of DNP-AA with reasonable accuracy. In overall, ePC-SAFT the most precisely predicts partition coefficients for DNP-leucine (ARD% in average = 1.85) and for ATPS composed by PEG and Na_3Citrate (ARD% values on average = 6.48). The highest ARD% values were observed for DNP-glycine (ARD% on average = 6.93) and for ATPS composed by PEG and K_3Citrate (ARD% on average = 11.16).

Table 10.1. ePC-SAFT prediction accuracies for partition coefficients $K_{DNP-AA}^{pred,\infty}$ of DNP-AA in ATPS considered in this work (T=298.15 K, p=1 bar). Average relative deviations ARD% between predicted and experimental values were calculated according to equation (4.14) from experimental partition coefficients K_{DNP-AA}^{exp} (Appendix) at different TLL.

DNP-AA	*ARD%*								
	Na_3Citrate +			*K_3Citrate +*			*KNaTartrate +*		
	PEG 4000	*PEG 6000*	*PEG 8000*	*PEG 4000*	*PEG 6000*	*PEG 8000*	*PEG 4000*	*PEG 6000*	*PEG 8000*
DNP-alanine	6.49	4.88	3.62	7.78	6.08	3.86	10.48	14.41	15.17
DNP-glycine	5.54	7.73	6.22	25.50	22.42	20.41	4.45	7.27	12.83
DNP-valine	7.25	3.29	13.96	13.48	5.37	8.10	3.80	4.69	4.46
DNP-leucine	7.86	4.06	6.89	9.51	6.76	4.67	4.38	8.01	11.02

The success of ePC-SAFT (average of all ARD% values = 8.68) relies on a good description of non-ideality caused by different interactions present in ATPS. The partitioning of DNP-AA can be influenced by 1) electrostatic interactions resulting from partitioning of charged components in ATPS, 2) molecular size of DNP-AA, 3) other interactions of DNP-AA with phase formers (e.g. hydrogen bonding, hydrophobic interactions). These factors are dependent among others on PEG molar mass, salt type, ATPS composition expressed as tie-line length (*TLL*) that has been defined with equation (3.3). The non-ideality caused by different interactions is described by ePC-SAFT with help of the binary interaction parameters (k_{ij}).

Since in ATPS of pH~8 DNP-AA is present solely as negatively charged DNP-AA$^-$ species, only the interactions between the charged form of DNP-AA (i.e. DNP-AA$^-$) and ATPS phase formers were considered in the modeling and partitioning predictions. The k_{ij} between charged DNP-AA$^-$ and ATPS phase forming compounds were estimated in this work (table 4.1: water, table 4.3: salt ions, PEG). The procedure used for the k_{ij} estimation was explained in section 4.1.1.

10.2.1. Solute Influence on Partition Coefficient

Figure 10.3 shows the results of ePC-SAFT predictions obtained for different DNP-AA in ATPS formed by PEG of M_{PEG} = 6000 g·mol^{-1} and Na_3Citrate, at T = 298.15 K and p = 1 bar. The accuracy of partitioning predictions in this ATPS, as well as in the systems formed by PEG of different molar mass (M_{PEG} = 4000 g·mol^{-1} and M_{PEG} = 8000 g·mol^{-1}) and other organic salts (K_3Citrate, KNaTartrate), was evaluated based on experimental data measured in this work (Appendix, A9) and can be read from table 10.1. DNP-AA partitioned in the systems considered in this work (pH $\sim$ 8) are fully present as negatively charged DNP-AA$^-$ species. For this reason, ePC-SAFT predictions were performed using the pure-component and binary interaction k_{ij} parameters for ionic species of DNP-AA, i.e. DNP-AA$^-$, from table 4.2 and table 4.3, and were assigned according to figure 10.1.

ePC-SAFT allows not just qualitative, but also the quantitative prediction of $K_{DNP-AA}^{pred,\infty}$ for DNP-glycine, DNP-alanine, DNP-valine and DNP-leucine. DNP-leucine of higher molar mass than DNP-glycine has higher affinity to the top PEG phase than DNP-glycine. This trend can be accordingly predicted with ePC-SAFT. It can be seen that the partitioning order of DNP-AA in ATPS considered: $K_{DNP-leucine}^{pred,\infty} > K_{DNP-valine}^{pred,\infty} > K_{DNP-alanine}^{pred,\infty} > K_{DNP-glycine}^{pred,\infty}$ do not match the trend of DNP-AA (DNP-AA$^-$) solubility in water $m_{DNP-alanine}^{L} > m_{DNP-valine}^{L} > m_{DNP-leucine}^{L}$ and $m_{DNP-glycine}^{L}$ (according to sections 7.1.1 and 8.2.1). This means that different interactions rule the solubility of DNP-AA in water and partitioning of DNP-AA between the two phases of ATPS. The behavior of DNP-AA during the partitioning confirms the relationship found in the discussion coupled to experimental results in section 7.1.1. Thus, the highest $K_{DNP-AA}^{pred,\infty}$ was observed for DNP-leucine of the lowest molar mass among all considered in this work ($M_{DNP-leucine} >$

$M_{DNP-valine} > M_{DNP-alanine} > M_{DNP-glycine}$). This effect could be captured by ePC-SAFT accordingly.

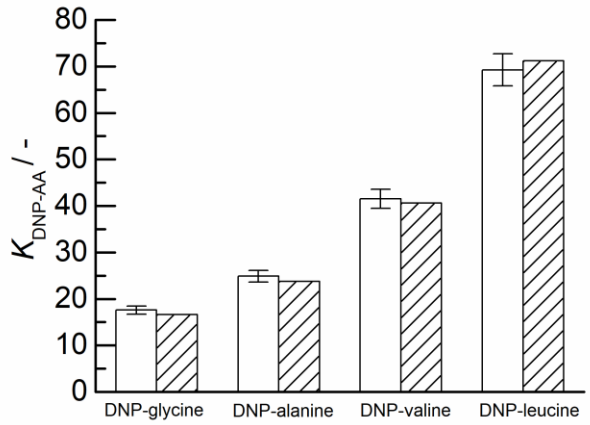

Figure 10.3. Partitioning of different DNP-AA in PEG 6000 – Na_3Citrate ATPS (TLL = 0.427; w_P = 0.18 and w_S = 0.126; Appendix A8) at T = 298.15 K and p = 1 bar. Patterned bars are ePC-SAFT predictions of partition coefficient $K_{DNP-AA}^{pred,\infty}$ (in ATPS of pH~8: total partition coefficient $K_{DNP-AA}^{pred,\infty}$ = partition coefficient of species DNP-AA$^-$ $K_{DNP-AA^-}^{pred,\infty}$). Non-patterned bars represent experimental data K_{DNP-AA}^{exp} (Appendix, A9).

One of the most decisive factors for the partitioning trend of $K_{DNP-AA}^{pred,\infty}$ can be DNP-AA hydrophobicity that in this case may vary with the number of methylene groups $n(CH_2)$ present in the molecule. The effect of $n(CH_2)$ on the hydrophobicity has been already evaluated in the experimental section 7.1.1 presented in this document. Figure 10.4 presents partitioning data predicted with ePC-SAFT in terms of $n(CH_2)$ estimated by Zaslavsky [88]. It shows a reasonable accuracy (table 10.1) of ePC-SAFT predictions in comparison to experimental data. ePC-SAFT was capable to predict that the highest partition coefficient can be obtained for DNP-leucine of the highest $n(CH_2)$ among the four DNP-AA studied, while the lowest partition coefficient was predicted for DNP-glycine of the lowest $n(CH_2)$. It also proves the ability to capture the effect on $n(CH_2)$ on partitioning by showing the highest values of $K_{DNP-AA}^{pred,\infty}$ for a system composed by PEG and Na_3Citrate and the lowest $K_{DNP-AA}^{pred,\infty}$ for ATPS formed by PEG and KNaTartrate. This is in agreement with the observations provided based on experimental data in section 7.1.1.

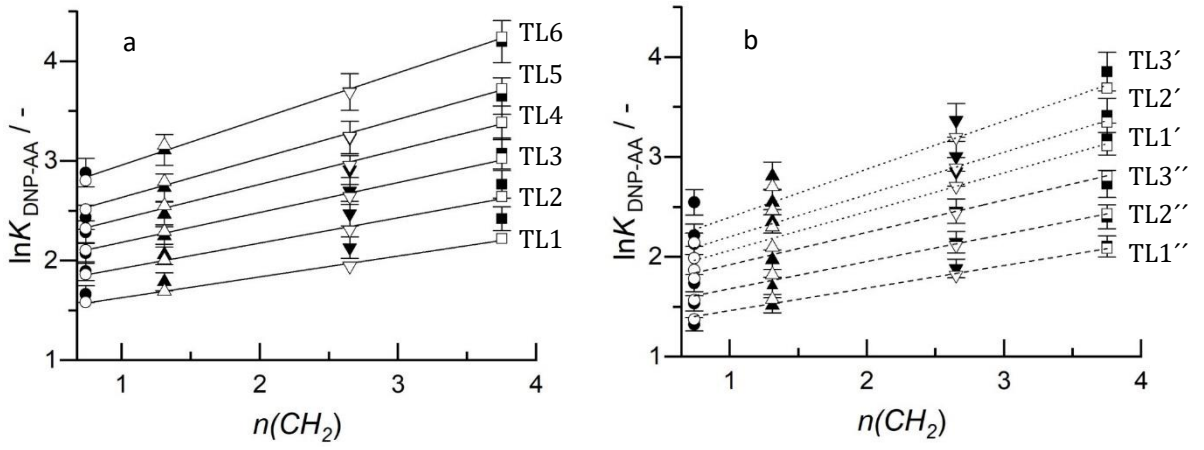

Figure 10.4. Logarithm of partition coefficients of DNP-AA: DNP-glycine (●,○), DNP-alanine (▲, △), DNP-valine (▼,▽), DNP-leucine (■,□) at T=298.15 K and p=1 bar, plotted against average number of $n(CH_2)$ [88] in ATPS formed by PEG 4000 and biodegradable salt (a - Na_3Citrate: solid line; b - K_3Citrate: dotted line, KNaTartrate: dashed line). The open points represent predicted with ePC-SAFT $\ln K_{DNP-AA}^{pred,\infty}$. The lines that connect $\ln K_{DNP-AA}^{pred,\infty}$ are applied just to guide the eye and distinguish the trends caused by selecting different salt. Closed points present experimental data measured in this work. The feed and equilibrium composition for a given TL are provided in Appendix (A8).

The interactions of DNP-AA with ATPS phases depend on the system composition, thus plotting data against TLL is very common. As presented in figure 10.5 the partition coefficient of all DNP-AA increases when the TLL increases. The diagram shows only TLL regions where it was possible to measure the partitioning with reasonable accuracy, as well as to validate the predictions. The lines in figure 10.5 were included just to show the trend of predicted data and to guide the eye. The low regions of TLL might also not be of interest for industrial applications as already mentioned in experimental section 7.1.1. Only an accurate description of non-ideality caused by interactions between a solute i.e. DNP-AA (in this case negatively charged species DNP-AA^-) and phase formers (water, PEG, Na^+, K^+, $Citrate^{3-}$, $Tartrate^{2-}$) with k_{ij} parameter allows predicting the $K_{DNP-AA}^{pred,\infty}$ (at pH ~ 8: $K_{DNP-AA}^{pred,\infty} = K_{DNP-AA^-}^{pred,\infty}$).

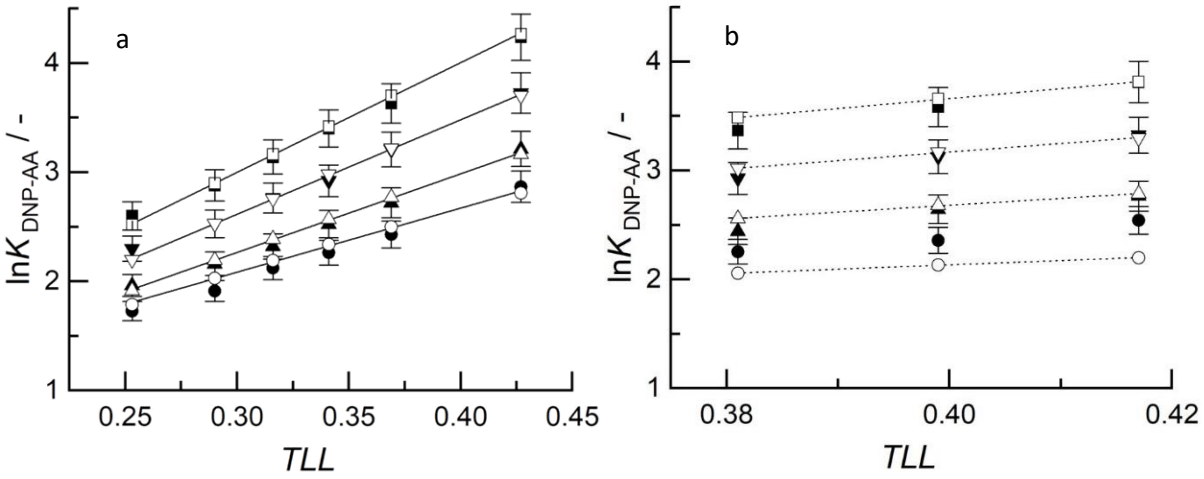

Figure 10.5. Logarithm of partition coefficients of DNP-AA (closed points: experimental $\ln K^{exp}_{DNP-AA}$, open points: $\ln K^{pred,\infty}_{DNP-AA}$ predicted with ePC-SAFT): DNP-glycine(●,○), DNP-alanine (▲, △), DNP-valine (▼,▽), DNP-leucine (■,□) at T=298.15 K and p=1 bar, plotted against TLL of ATPS formed by PEG 6000 and biodegradable salt - Na_3Citrate (a): solid line, K_3Citrate (b): dotted line. The lines that connect $\ln K^{pred,\infty}_{DNP-AA}$ were applied just to guide the eye and improve the readability. The feed and equilibrium composition for a given TL are provided in Appendix (A8)..

Figure 10.6 presents activity coefficients γ^{∞}_{DNP-AA} of four studied DNP-AA predicted with ePC-SAFT in both ATPS phases, in the top phase (figure 10.6a) and in the bottom phase (figure 10.6b). Each phase was considered in this evaluation as a separate aqueous solution – PEG or salt-rich, and the trends of γ^{∞}_{DNP-AA} in PEG (M_{PEG} = 6000 g·mol^{-1}) - Na_3Citrate ATPS were compared among the four DNP-AA studied.

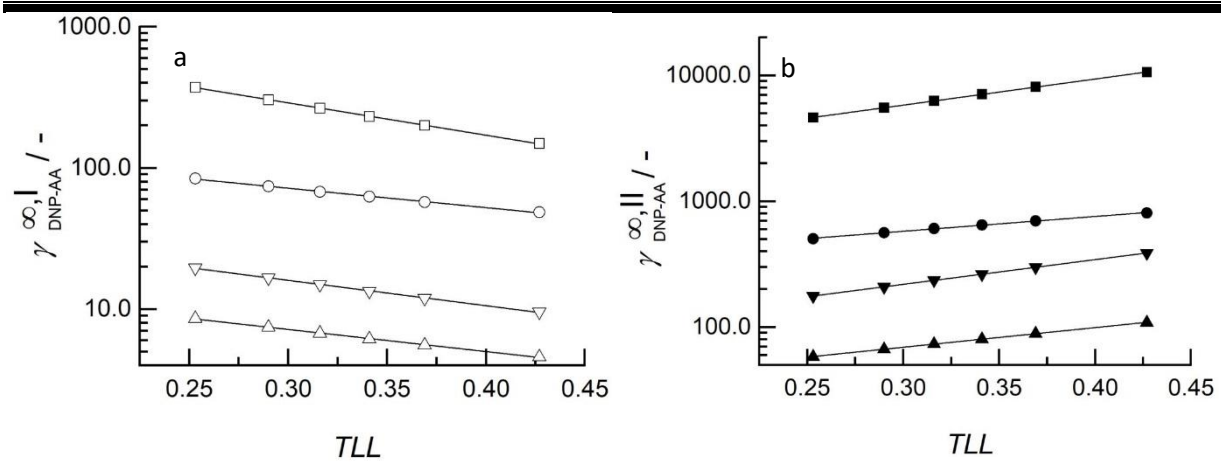

Figure 10.6. Activity coefficient of DNP-AA: $\gamma^{\infty,I}_{DNP-AA}$ in top phase (a) and $\gamma^{\infty,II}_{DNP-AA}$ bottom phase (figure b) of ATPS predicted with ePC-SAFT for DNP-glycine(●,○), DNP-alanine (▲, △), DNP-valine (▼,▽), DNP-leucine (■,□) at T = 298.15 K and p = 1 bar, plotted against TLL of ATPS formed by PEG 6000 and biodegradable salt - $Na_3Citrate$. Open points: top phase, closed points: bottom phase. The species fraction $\alpha_{DNP-AA^-} \approx 1$ at pH ~ 8, thus $\gamma^{\infty}_{DNP-AA} = \gamma^{\infty}_{DNP-AA^-}$). The lines that connect γ^{∞}_{DNP-AA} were applied just to guide the eye and improve the readability. The feed and equilibrium composition for a given TL are provided in Appendix (A8). The diagram shows only TLL regions at which the predictions were carried out.

Figure 10.6a and figure 10.6b show that in each ATPS phase the highest γ^{∞}_{DNP-AA} were found for DNP-leucine, while the lowest γ^{∞}_{DNP-AA} were predicted for DNP-alanine. The trend of $\gamma^{\infty}_{DNP-alanine} < \gamma^{\infty}_{DNP-valine} < \gamma^{\infty}_{DNP-glycine} < \gamma^{\infty}_{DNP-leucine}$ that represents the non-ideality of DNP-AA in considered ATPS can be compared with non-ideality behavior of DNP-AA in water. This impacts e.g. solubility, discussed already in subchapters 5.1 and 8.2 ($m^{L}_{DNP-alanine} > m^{L}_{DNP-valine} > m^{L}_{DNP-glycine}$ and $m^{L}_{DNP-leucine}$). Aqueous solubility of a component is inversely proportional to its activity coefficient in water at saturation γ^{L}_{i} (theoretical background, subchapter 2.2). Even though, DNP-AA partitioned in ATPS are present only at small concentrations ($m_{\text{DNP-AA}} \leq 0.008$ g·mol^{-1}), the trend of γ^{∞}_{DNP-AA} still follows the above-mentioned relation. Also, the water fraction in ATPS is high (at TL studied in this work for PEG 6000 – $Na_3Citrate$ ATPS: $w_{H_2O} \geq 0.69$), thus, it is expected that the interactions between a solute and water have a strong contribution to the value of γ^{∞}_{DNP-AA}. Likely the trend of γ^{∞}_{DNP-AA} for different DNP-AA, obtained separately in each ATPS phase for DNP-AA, depends strongly on DNP-AA interactions with water.

However, if comparing $\gamma^{\infty,\text{I}}_{DNP-AA}$ with $\gamma^{\infty,\text{II}}_{DNP-AA}$, although the bottom (*II*) phase contains higher water fraction than the top phase (*I*) in all ATPS studied in this work, the values of $\gamma^{\infty,\text{II}}_{DNP-AA}$ are much higher than of $\gamma^{\infty,\text{I}}_{DNP-AA}$. This means that even though the

interactions of DNP-AA in water may have a very strong influence on DNP-AA behavior in aqueous solution, the partitioning in ATPS cannot be explained using the solubility in water. A difference of DNP-AA solubility in the two phases ($m_{DNP-AA}^{L,I} \approx m_{DNP-AA}^{L,II}$, as the $\Delta pH_{phases} \leq 0.25$ in ATPS from this study is relatively small) does not correspond to K_{DNP-AA}. Thus, the interactions DNP-AA ↔ PEG and DNP-AA ↔ salt must be considered as factors ruling the separation of DNP-AA between the two phases. In this case, the ratio between $\gamma_{DNP-AA}^{\infty,\mathrm{II}}$ and $\gamma_{DNP-AA}^{\infty,\mathrm{I}}$ is useful for the evaluation of partitioning (equation (2.29)). Higher $\gamma_{DNP-AA}^{\infty,\mathrm{II}}$ observed in figure 10.6b than $\gamma_{DNP-AA}^{\infty,\mathrm{II}}$ in figure 10.6a, obtained for the same DNP-AA, can mean that the repulsive interactions of negatively charged species of DNP-AA$^-$ with Citrate^{3-} have a very strong effect on the partitioning. These interactions depend on the concentration of salt and are stronger if there is a higher salt concentration in the bottom phase (achieved by increasing TLL in this work). Hence, it was found that for all four DNP-AA partitioned in considered ATPS of different TLL, the increase of TLL leads to an increased values of $\gamma_{DNP-AA}^{\infty,II}$ in the (*II*) bottom phase (repulsion from Citrate^{3-}) and decreased values of $\gamma_{DNP-AA}^{\infty,I}$ in the (*I*) top phase (attraction to PEG). However, figure 10.7 is more relevant to compare these effects.

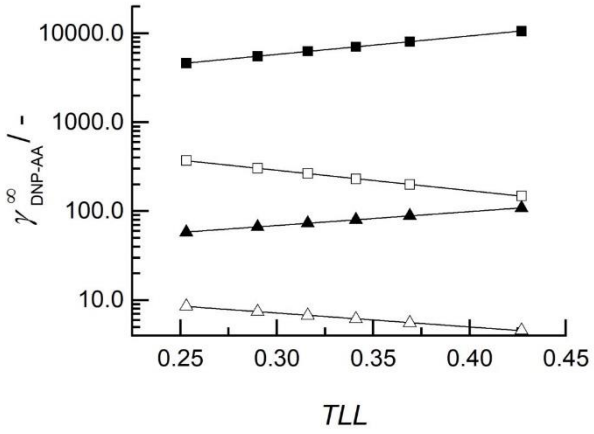

Figure 10.7. Activity coefficient of DNP-AA $\gamma_{DNP-AA}^{\infty,\mathrm{I}}$ in top phase (open symbols) and $\gamma_{DNP-AA}^{\infty,II}$ bottom phase (closed symbols) of ATPS predicted with ePC-SAFT for DNP-alanine (▲, △) and DNP-leucine (■,□) at T=298.15 K and p=1 bar, plotted against TLL of ATPS formed by PEG 6000 and biodegradable salt - $Na_3Citrate$. The species fraction $\alpha_{DNP-AA^-} \approx 1$ at pH ~ 8, thus $\gamma_{DNP-AA}^{\infty} = \gamma_{DNP-AA^-}^{\infty}$. The lines that connect γ_{DNP-AA}^{∞} were applied just to guide the eye and improve the readability. The feed and equilibrium composition for a given TL are provided in Appendix (A8). Logarithmic scale was introduced for better data comparison.

Figure 10.7 shows the trend for DNP-alanine and DNP-leucine partitioned in ATPS formed by PEG 6000 and $Na_3Citrate$ (for a better comparison, in the same ATPS as in the previous figure 10.6); however, it is also valid for the other two DNP-AA considered in this work, namely DNP-glycine and DNP-valine. Based on this diagram the repulsive interactions of DNP-AA with components in the bottom (salt-rich) phase are much decisive than the interactions causing the attraction of DNP-AA to the upper (PEG-rich) phase. Thus, it can be observed from figure 10.7 that with a change of TLL toward higher values, the increase of $\gamma_{DNP-AA}^{\infty,II}$ is much more significant (steeper) than the decrease of $\gamma_{DNP-AA}^{\infty,I}$ (a lot smaller change in γ_{DNP-AA}^{∞} is observed in the top phase than in the bottom). This means that mostly repulsive interactions DNP-AA – $Citrate^{3-}$ in the bottom phase might be dominating in increasing the value of $K_{DNP-AA}^{pred,\infty}$ in the range of TLL studied in this work for different ATPS.

Figure 10.6 and figure 10.7 were shown in this section mostly to allow finding a reason for the affinity of DNP-AA to the top phase and to point out the importance of studying the solute interactions with PEG and salt in partitioning. The two following sections 10.2.2 and 10.2.3 were introduced to present ePC-SAFT predictions of DNP-AA partitioning, as well as to evaluate the effects related also to the usage of different salt and PEG molar mass in ATPS in which these components were separated.

10.2.2. Salt Influence on Partition Coefficient

The results of ePC-SAFT predictions of DNP-AA partitioning in ATPS formed by PEG (M_{PEG} = 4000 g·mol^{-1}) and biodegradable salt ($Na_3Citrate$, $K_3Citrate$, KNaTartrate) are presented in figure 10.6. The accuracy of prediction results obtained for partitioning in these ATPS, as well as in the systems formed by PEG of different molar mass (M_{PEG} = 6000 g·mol^{-1} and M_{PEG} = 8000 g·mol^{-1}) and organic salts ($Na_3Citrate$, $K_3Citrate$, KNaTartrate) can be read from table 10.1. DNP-AA partitioned in the systems considered in this work (pH $\sim$ 8) are fully present as negatively charged DNP-AA$^-$ species. For this reason, ePC-SAFT predictions were performed using the pure-component and binary interaction k_{ij} parameters for ionic species of DNP-AA, i.e. DNP-AA$^-$, from table 4.2 and table 4.3.

The relation of partition coefficient of DNP-AA to different tie-line compositions (TLL) can be accurately predicted with ePC-SAFT, thus, the values of partition coefficients of DNP-AA predicted with ePC-SAFT $K_{DNP-AA}^{pred,\infty}$ were similar (ARD%: table 10.1) to

experimental partition coefficients K_{DNP-AA}^{exp}. Based on figure 10.8, the model was capable to capture an increase of partition coefficient caused by the usage of salts composed by $Citrate^{3-}$ and Na^{+} (more advantageous over K^{+}, $Tartrate^{2-}$) as ATPS formers. It predicted the increase of $K_{DNP-AA}^{pred,\infty}$ values caused by the increase of the salt concentration related to the changes in ionic strength.

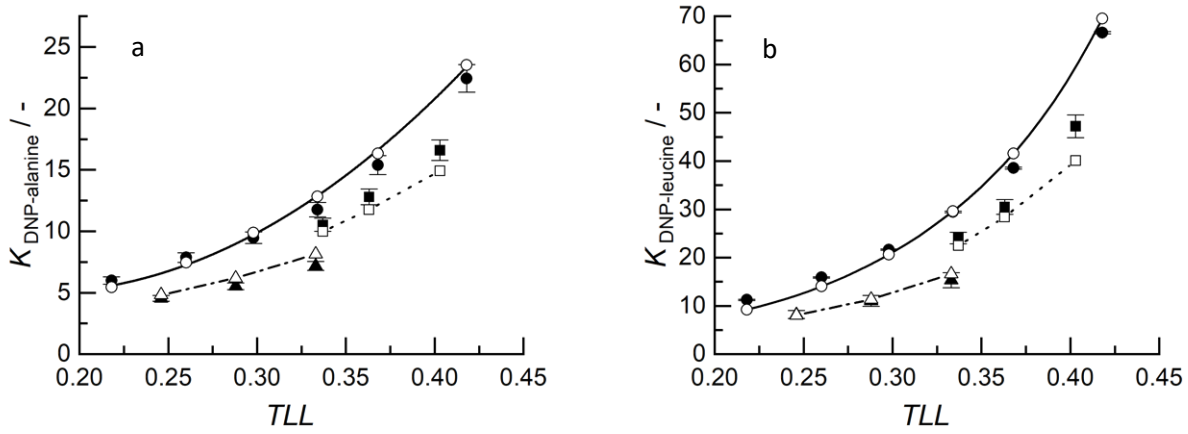

Figure 10.8. Salt influence on the partitioning of DNP-alanine (a) and DNP-leucine (b), in different PEG 4000 – biodegradable salt ($Na_3Citrate$ - ●,○; $K_3Citrate$ - ■, □; KNaTartrate - ▲, △) ATPS compositions (TLL), at T=298.15 K and p=1 bar. The open symbols represent ePC-SAFT predictions of $K_{DNP-AA}^{pred,\infty}$ (at certain TLL values), the closed symbols are experimental data K_{DNP-AA}^{exp} measured in this work (Appendix, A9). In ATPS of pH∼8: total partition coefficient $K_{DNP-AA}^{pred,\infty}$ is equal to $K_{DNP-AA^-}^{pred,\infty}$. The lines connecting the open points were applied only to guide the eye and to better distinguish the trends of the points predicted in different ATPS: PEG 4000 - $Na_3Citrate$ – solid line, PEG 4000 - $K_3Citrate$ – dotted line , PEG 4000 - KNaTartrate – dash-dotted line.

The results that have been shown in figure 10.8 for PEG (M_{PEG} = 4000 g·mol^{-1}) – KNaTartrate ATPS are even more remarkable knowing that no k_{ij} was fitted to experimental data obtained in any PEG - KNaTartrate system. Even though, ePC-SAFT was capable to almost quantitatively predict $K_{DNP-AA}^{pred,\infty}$. The positive k_{ij} between $DNP\text{-}AA^-$ and salt cation (according to table 4.3: k_{ij} between $DNP\text{-}AA^-$ and Na^+ = 0.15; k_{ij} between $DNP\text{-}AA^-$ and K^+ = 0.4) has pointed out that to describe well the behavior of $DNP\text{-}AA^-$ in ATPS, the attractive forces of negatively charged $DNP\text{-}AA^-$ with positively charged salt cation (Na^+, K^+) must be considered in the modeling. Additionally, the more positive k_{ij} for $DNP\text{-}AA^-$ and Na^+ may result from stronger repulsion between $DNP\text{-}AA^-$ and Na^+ if

comparing to DNP-AA$^-$ and K$^+$. This might explain the better affinity of DNP-AA$^-$ to the upper PEG phase in ATPS composed of sodium salt (figure 10.8).

Figure 10.9 helps to understand the interactions that rule the partitioning in ATPS formed by PEG and different salt (Na_3Citrate, K_3Citrate, KNaTartrate). This evaluation is based on activity coefficient γ_{DNP-AA}^{∞} predicted with ePC-SAFT in the two ATPS phases. It can be seen that higher values of $\gamma_{DNP-AA}^{\infty,II}$ in the bottom phase of ATPS were found in systems composed by PEG and Na_3Citrate than in the ones formed by PEG and KNaTartrate. Also, increasing the TLL leads to an increase of $\gamma_{DNP-AA}^{\infty,II}$. This behavior can reflect in higher values of $K_{DNP-AA}^{pred,\infty}$ that were obtained in the system in which Na_3Citrate is present. It might be related to stronger repulsive interactions of Citrate^{3-} toward DNP-AA$^-$ species (in comparison to Tartrate^{2-}). The reverse was observed for $\gamma_{DNP-AA}^{\infty,I}$ in the top phase, in which $\gamma_{DNP-AA}^{\infty,I}$ decreases together with an increase of TLL. Smaller $\gamma_{DNP-AA}^{\infty,I}$ (if comparing it to $\gamma_{DNP-AA}^{\infty,II}$) can indicate the preference of DNP-AA$^-$ to partition into the top phase and the attractive interactions of DNP-AA with PEG.

Very small difference in trends of $\gamma_{DNP-AA}^{\infty,I}$ observed in figure 10.9 for ATPS composed of PEG and biodegradable salt - Na_3Citrate, K_3Citrate, or KNaTartrate, might allow a conclusion that concentration of salt in the top phase is too low to show the difference in $\gamma_{DNP-AA}^{\infty,I}$ obtained for ATPS formed by different salt. Thus, in this case, only $\gamma_{DNP-AA}^{\infty,II}$can be partially used as a non-ideality factor for salt selection. Figure 10.9 allows an observation that $\gamma_{DNP-AA}^{\infty,II}$ in ATPS formed by PEG and Na_3Citrate were higher than in the system composed by PEG and K_3Citrate. Based on k_{ij} between DNP-AA$^-$ and salt cations, Na$^+$ and K$^+$, the attractive interactions DNP-AA$^-$ ↔ K$^+$ might be stronger than DNP-AA$^-$ ↔ Na$^+$. However, the electrostatic interactions are not the only driving force in the partitioning of molecules in ATPS that should be considered. In many cases, other influences may dominate e.g. molecular size, as well as different interactions of DNP-AA with phase formers, e.g. association, hydrogen bonding. ePC-SAFT by accounting on all these interactions was capable to predict partitioning with reasonable accuracy.

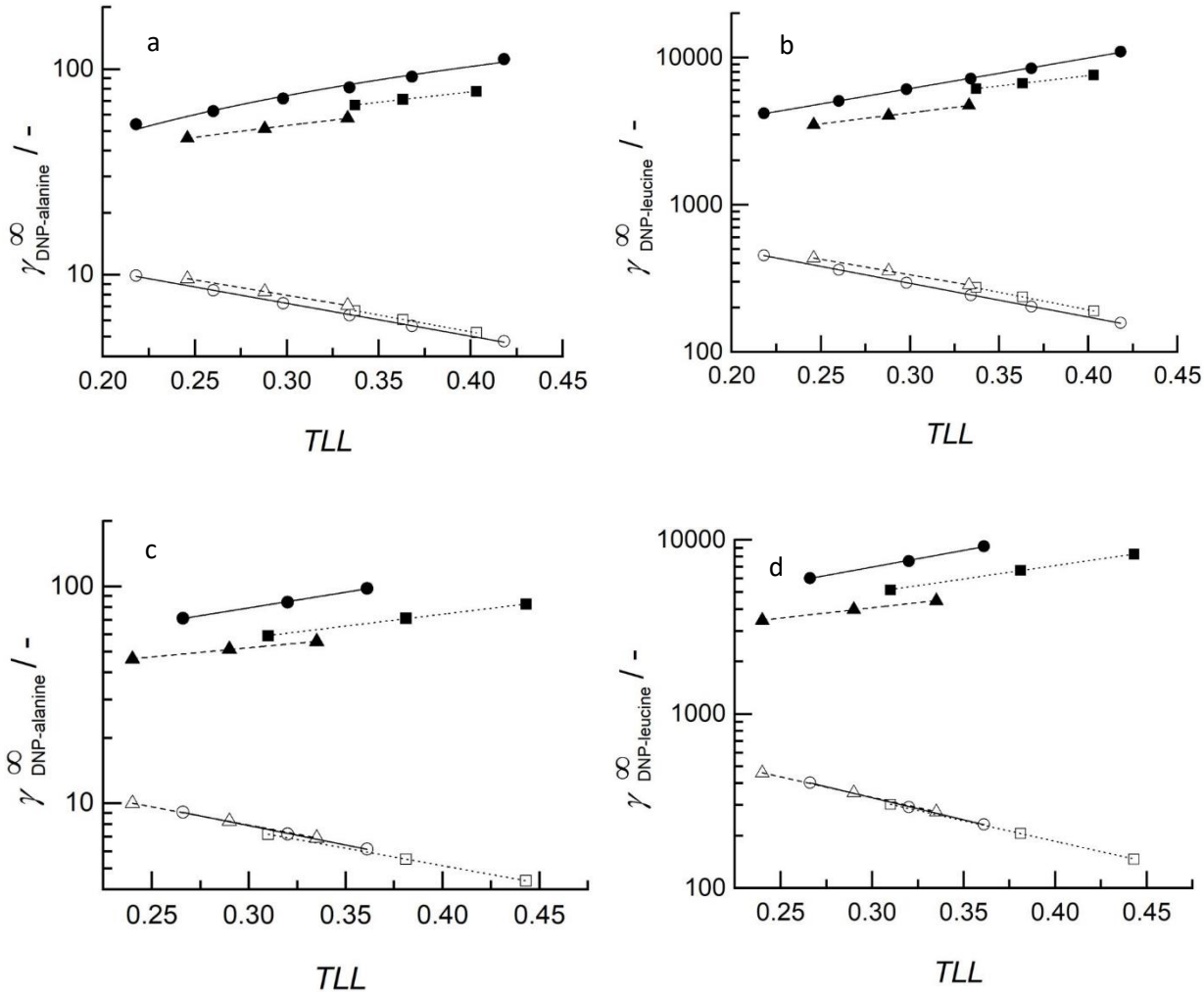

Figure 10.9. Activity coefficient of DNP-alanine (figures a, c) and DNP-leucine (figures b, d) in the top phase $\gamma^{\infty,I}_{DNP-AA}$ (open symbols) and in the bottom phase $\gamma^{\infty,II}_{DNP-AA}$ (closed symbols). Predictions were done at T = 298.15 K and p = 1 bar with ePC-SAFT in ATPS formed by PEG 4000 (figures a-b) or PEG 8000 (figures c-d) and biodegradable salt: Na_3Citrate (●,○ and solid lines), K_3Citrate (■,□ and dotted lines), or KNaTartrate (▲, △ and dashed lines), plotted against different tie-line compositions TLL. The species fraction α_{DNP-AA^-}≈1 at pH ~ 8, thus $\gamma^{\infty}_{DNP-AA} = \gamma^{\infty}_{DNP-AA^-}$. The lines that connect γ^{∞}_{DNP-AA} were applied just to guide the eye and improve the readability. The feed and equilibrium composition for a given TL are provided in Appendix (A8). Logarithmic scale was introduced for better data comparison.

10.2.3. PEG Influence on Partition Coefficient

A higher affinity to the upper PEG-phase was predicted with ePC-SAFT for all DNP-AA considered. The results of ePC-SAFT predictions of DNP-AA partitioning in ATPS formed by biodegradable salt (Na_3Citrate) and PEG (M_{PEG} = 4000 and 6000 g·mol^{-1}), at T = 298.15 K and p = 1 bar, are presented in figure 10.10. Due to the fact that only insignificant

differences in $K_{DNP-AA}^{pred,\infty}$ related to using PEG of different molar mass were expected (based on experimental data from section 7.1.3), figure 10.10 was introduced only to show the capability of ePC-SAFT to predict how strong are the effects caused by different PEG´s molar mass. The intention was to evaluate if ePC-SAFT can compare the influence on partitioning caused either by selecting PEG of different molar mass or type of salt according to experimental data. Although these were only the expectations, the values predicted with the model matched well data obtained through the measurements (Appendix, A9). ePC-SAFT accurately predicted small change of $K_{DNP-AA}^{pred,\infty}$ caused by the decrease of PEG molar mass. The accuracy of the predictions obtained in these ATPS are shown in table 10.1.

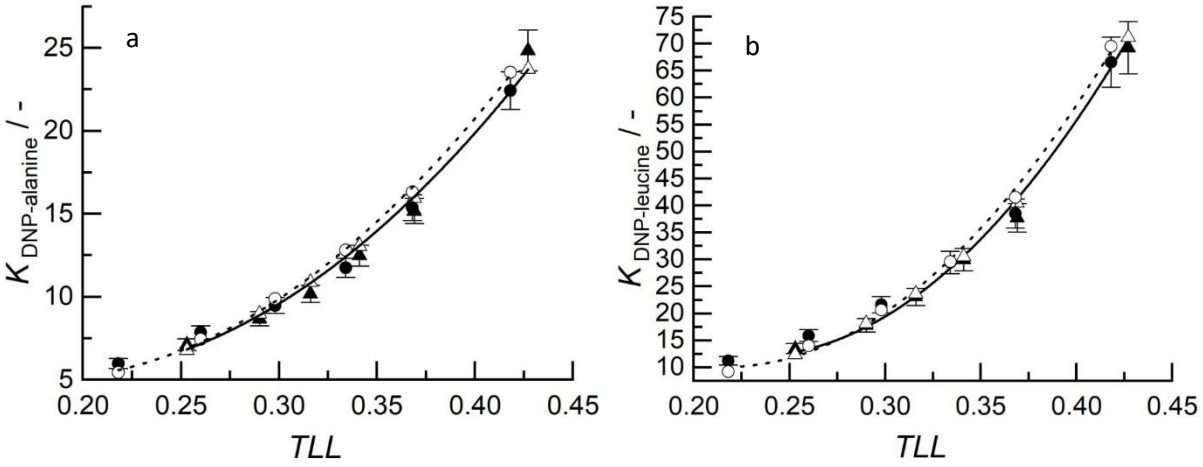

Figure 10.10. PEG molar mass influence on the partitioning of DNP-alanine (a) and DNP-leucine (b) at different ATPS compositions (TLL), at T=298.15 K and p=1 bar. ATPS formed by PEG 4000 or 6000 (PEG 4000 of M_{PEG} = 4000 g·mol^{-1} - dotted line and symbols ●,○; PEG 6000 of M_{PEG} = 6000 g·mol^{-1} – solid line and symbols ▲, △) and $Na_3Citrate$. Lines and open points: ePC-SAFT predictions $K_{DNP-alanine}^{pred,\infty}$(in ATPS of pH~8: total partition coefficient $K_{DNP-alanine}^{pred,\infty}$ = partition coefficient of species DNP-AA$^-$ $K_{DNP-alanine}^{pred,\infty}$–). The lines connecting the open points were applied only to guide the eye and to better distinguish the trends. Closed points: experimental data $K_{DNP-alanine}^{exp}$ measured in this work (Appendix, A9).

DNP-AA at pH ~ 8 of ATPS are only present as negatively charged DNP-AA$^-$ species. Thus, ePC-SAFT predictions were performed using the pure-component and binary interaction k_{ij} parameters for ionic species of DNP-AA, i.e. DNP-AA$^-$, from table 4.2 and table 4.3. The accurate description of high DNP-AA$^-$ affinity to the PEG phase required introducing negative k_{ij} values for most of the DNP-AA$^-$ (DNP-alanine$^-$, DNP-valine$^-$, DNP-

leucine$^-$). The more negative k_{ij} can be related to strong attractive forces between DNP-AA$^-$ and PEG, however, none of the k_{ij} values fitted in this work involves solely the effects related to electrostatic interactions. The ability of binding solutes by PEG can be also related to the formation of hydrogen bonding interactions. However, it was found that $\gamma_{DNP-AA}^{\infty,I}$ in the top PEG-rich phase are only slightly higher and $\gamma_{DNP-AA}^{\infty,II}$ are not significantly lower when DNP-AA$^-$ is partitioned in ATPS formed by PEG of M_{PEG} = 8000 g·mol^{-1} (the range of molar mass for comparison M_{PEG} = 4000 - 8000 g·mol^{-1}). Also, the influence on γ_{DNP-AA}^{∞} of DNP-AA partitioned in ATPS formed by PEG of M_{PEG} = 4000 g·mol^{-1} and M_{PEG} = 8000 g·mol^{-1} was insignificant (ARD% < 5). The difference in values of $\gamma_{DNP-AA}^{\infty,I}$ and $\gamma_{DNP-AA}^{\infty,II}$ when using PEG´s molar mass of M_{PEG} = 4000 g·mol^{-1} or M_{PEG} = 6000 g·mol^{-1} was even lower for $\gamma_{DNP-AA}^{\infty,II}$ and almost unnoticeable for $\gamma_{DNP-AA}^{\infty,I}$. Therefore, the $\gamma_{DNP-AA}^{\infty,I}$ and $\gamma_{DNP-AA}^{\infty,II}$ that confirm the above observations were presented in Appendix (A13), instead of using the figures on which data obtained for ATPS formed by different M_{PEG} of PEG could be difficult to distinguish.

10.3. Prediction Results: Water-Soluble Vitamins

Different non-ideality character in the behavior of vitamins in their aqueous solutions that was shown in 4.1.1 (e.g. in liquid density data), reflects also in expected partition coefficient divergences among the vitamins. In this work, the partition coefficients $K_{vitamin}^{pred,\infty}$ of water-soluble vitamins VB2, VB3^{acid}, VB3^{amide}, VB9, VB12 in ATPS composed by PEG (M_{PEG} = 4000 – 6000 g·mol^{-1}) and biodegradable salt (Na_3Citrate or Na_2Tartarte) were predicted using ePC-SAFT. The partitioning was studied at T = 298.15 K and p = 1 bar and since ATPS at pH~8 were considered, it involved neutral (VB3^{amide}, VB12) or negatively charged vitamin species (VB2$^-$, VB3^{acid-}, VB9^{2-}, VB9^{3-}).

The procedure that has been applied for ePC-SAFT parameter estimation was provided in section 4.1.1. ePC-SAFT pure-component parameters and the binary interaction parameters k_{ij} required for the predictions were given in table 4.1, table 4.2, and table 4.3. Overall, using these parameters enabled to predict the partition coefficients with reasonable accuracy. The deviations expressed as ARD% were calculated with equation (4.14) and provided in table 10.2. They were based on predicted $K_{vitamin}^{pred,\infty}$ and experimental $K_{vitamin}^{exp}$ (Appendix, A10) of vitamins considered in this work, in different ATPS. Among the vitamins partitioned in ATPS studied, ePC-SAFT the most precisely

predicted partitioning of the charged form of $VB3^{acid}$ ($VB3^{acid-}$). ARD% obtained for $VB3^{acid-}$ in all ATPS considered in this study equals on average 4.1. A very reasonable value was determined also for $VB3^{amide}$ (ARD% = 5.8 on average in all ATPS). Moreover, the best accuracy of ePC-SAFT predictions was found for ATPS formed by PEG 6000 and $Na_3Citrate$ (on average for all vitamins ARD% = 4.28). ARD% calculated for VB12 in all ATPS was on average = 12.1 and this is the highest value among all vitamins. It is still a very good result if considering the structural complexity of VB12 and the number of possible interactions. Similar ARD% was observed for partitioning in PEG 4000 – $Na_2Tartrate$ ATPS and the average value determined for all vitamins is ARD% = 12.86. It is also acceptable because the highest ARD% was calculated for the partitioning of very complex molecules, like VB12 or the charged form of VB2 ($VB2^-$).

Table 10.2. ePC-SAFT prediction accuracies of partition coefficients $K_{vitamin}^{pred,\infty}$ of five water-soluble vitamins in each ATPS considered in this work (T = 298.15 K, p = 1 bar). Average relative deviations ARD% between predicted and experimental values were calculated according to equation (4.14) from experimental partition coefficients $K_{vitamin}^{exp}$ (Appendix, A10) and predicted $K_{vitamin}^{pred,\infty}$ at different TLL.

Vitamin	ARD%			
	PEG 6000 + $Na_3Citrate$	*PEG 4000 + $Na_3Citrate$*	*PEG 6000 + $Na_2Tartrate$*	*PEG 4000 + $Na_2Tartrate$*
$VB3^{amide}$	5.92	2.44	9.89	5.16
VB12	5.94	16.01	4.79	21.61
$VB3^{acid-}$	2.77	1.84	4.40	7.38
$VB2^-$	2.82	4.38	5.66	22.79
$VB9^{2-}$	3.48	7.15	4.41	10.89
$VB9^{3-}$	4.80	9.96	8.60	9.33

The number of ePC-SAFT binary interaction parameters (≤4) between species and ATPS phase formers used for the prediction of $K_{vitamin}^{pred,\infty}$ is lower than the number of parameters used only for data correlation, e.g. with Extended Chen-NRTL (6 interaction parameters)[421]. Also, high deviations of Extended Chen-NRTL of ≈ 30% between the experimental and correlated data have been much reduced with ePC-SAFT (table 10.2). This is a very important advance as using these parameters, ePC-SAFT can also purely predict the partitioning behavior in similar systems with reasonable accuracy.

Partitioning behavior of vitamins can be influenced by many factors affecting the separation in ATPS, i.e. temperature, vitamin interactions originating from its charge at pH of ATPS or molecular structure, and physicochemical properties of the vitamin. It may depend on vitamin size, shape, and be affected by the presence of different functional groups, specific bonding sites, surface hydrophobicity, among others [88, 422]. According to literature, the mechanisms ruling the partitioning of biomolecules in ATPS might be related to the interactions, e.g. the van der Waals, hydrophobic, hydrogen bond, and ionic forces [423]. In general, the interactions of vitamin with phase formers can be impacted by ATPS composition, salt type, or PEG molar mass [1-4, 424]. Therefore, the effects on the partition coefficient of vitamins at T = 298.15 K and p = 1 bar considered in the following sections 10.3.1, 10.3.2, 10.3.3, were grouped into the solute, salt, and PEG influences on vitamin partitioning, respectively.

10.3.1. Solute Influence on Partition Coefficient

The partitioning of the water-soluble vitamin in ATPS can be influenced by its different properties, e.g. the charge and molecular structure. Different interactions which are occurring in ATPS between vitamin and ATPS phase forming components determine vitamin affinity to each phase. The latter depends on ATPS composition that in this section is expressed with tie-line length (TLL). In this section, the effects that may dominate in the partitioning of each water-soluble vitamin considered in this work are discussed. The evaluation was done based on ePC-SAFT partitioning predictions carried at T=298.15 K and p=1 bar.

The molecular structure and charge of water-soluble vitamin

Figure 10.11 shows the results of ePC-SAFT predictions obtained for different vitamins VB2, VB3^{acid}, VB3^{amide}, VB9, and VB12, in ATPS formed by PEG of M_{PEG} = 6000 g·mol^{-1} and Na_3Citrate (figure 10.11a) or Na_2Tartrate (figure 10.11b), at T = 298.15 K and p = 1 bar. The accuracy of partitioning predictions in these ATPS, as well as in the systems formed by PEG of M_{PEG} = 4000 g·mol^{-1} and biodegradable salt (Na_3Citrate or Na_2Tartrate) was evaluated based on experimental data measured in this work (Appendix, A10) and included in table 10.2.

Based on the results presented in figure 10.11 and included in table 10.2, ePC-SAFT was very successful in predicting the partitioning of different vitamins in ATPS formed by

PEG and biodegradable salt, i.e. Na_3Citrate and K_2Tartrate. The trend $K_{VB12}^{pred,\infty} > K_{VB9}^{pred,\infty} > K_{VB3amide}^{pred,\infty} > K_{VB3acid}^{pred,\infty} > K_{VB2}^{pred,\infty}$ was matching the experimental data. This outcome is even more remarkable knowing that the properties of each vitamin considered in this evaluation differ a lot and their classification to B-complex class is also not based on molecular structure (more attention to the classification of vitamins was given in subchapter 3.1).

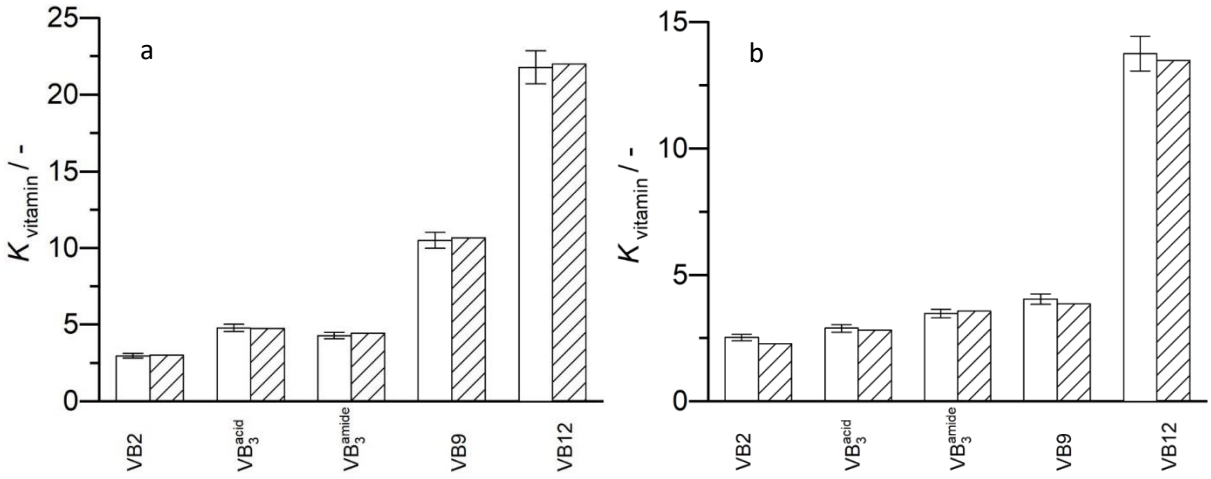

Figure 10.11. Partitioning of different vitamins in PEG 6000 – Na_3Citrate ATPS – figure a (TLL = 0.369; w_P = 0.163 and w_S = 0.114; Appendix, A8) and in PEG 6000 – Na_2Tartrate – figure b (TLL = 0.375; w_P = 0.195 and w_S = 0.110; Appendix, A8) at T = 298.15 K and p = 1 bar. Patterned bars are ePC-SAFT predictions of partition coefficient $K_{vitamin}^{pred,\infty}$. Non-patterned bars represent experimental data $K_{vitamin}^{exp}$ (Appendix, A10).

The pH of ATPS can influence the charge of vitamin (table 2.1). Therefore, the results shown in figure 10.11 relied on the accurate partitioning predictions of different vitamin species: negatively charged ($VB2^-$, $VB3^{acid\ -}$, $VB9^{2-}$, $VB9^{3-}$) or neutral ($VB3^{amide}$, VB12), present in the ATPS considered in this work (pH ~ 8). The influence of dissociation on vitamin partitioning behavior in ATPS has been discussed in more detail in experimental section 7.2.1. However, it is important to remind that at these conditions VB2 and $VB3^{acid}$ exist solely as single-negatively charged (-1) species. Others, $VB3^{amide}$ and VB12 are present exclusively as neutral species. In contrast, VB9 can be present as the two species, $VB9^{2-}$ and $VB9^{3-}$. Therefore, ePC-SAFT partitioning predictions for $VB3^{amide}$ and VB12 required pure-component, and k_{ij} with water parameters for neutral species of vitamins from table 4.1, while for VB2, $VB3^{acid}$, and VB9, the pure-component and k_{ij} with water parameters of the species $VB2^-$, $VB3^{acid\ -}$, $VB9^{2-}$, $VB9^{3-}$ from table 4.2 were applied.

For vitamins VB2, VB3^{acid} that are charged at pH ~ 8 of ATPS, the total partition coefficient of the component ($K_{vitamin}^{pred,\infty}$) was predicted with ePC-SAFT using the partition coefficient of the respective species, $K_{VB2}^{pred,\infty} = K_{VB2^-}^{pred,\infty}$ and $K_{VB3acid}^{pred,\infty} = K_{VB3acid^-}^{pred,\infty}$. This strategy could be applied as the species fractions $\alpha_{VB2^-} \approx 1$ and $\alpha_{VB3acid^-} \approx 1$. In contrast, to obtain $K_{VB9}^{pred,\infty}$ in ATPS formed by PEG and Na_3Citrate the predictions of $K_{VB9^{2-}}^{pred,\infty}$ and $K_{VB9^{3-}}^{pred,\infty}$ were required. They were carried out separately for each species. This procedure was used for the two reasons: at pH ~ 8 VB9 can be present as $VB9^{2-}$ and $VB9^{3-}$ and the difference in pH of the phases (in this work: PEG – citrate salts: $\Delta pH_{phases} \leq 0.25$; PEG – tartrate salt: $\Delta pH_{phases} \leq 0.05$) can change the values of $VB9^{2-}$ and $VB9^{3-}$ distribution in aqueous solution (each phase of ATPS). Therefore, these species can be differently distributed between the phases. To predict $K_{VB9}^{pred,\infty}$, the value of $K_{VB9^{2-}}^{pred,\infty}$ or $K_{VB9^{3-}}^{pred,\infty}$ was introduced into equation (2.30). This equation required the species distribution of VB9 in the two phases of ATPS (Appendix, A2) calculated according to the description provided in section 2.3.2.

The importance of introducing the above procedure can be explained using figure 10.12. This diagram presents activity coefficients of vitamins $\gamma_{vitamin}^{\infty}$ in ATPS. For a better comparison with figure 10.11, data shown in figure 10.12 was obtained in the same ATPS as $K_{vitamin}^{pred,\infty}$ values shown in figure 10.11. It is very important to mention that figure 10.12 presents the results of $\gamma_{vitamin}^{\infty}$ predicted at pH~ 8 of ATPS. The pH does not change the properties of the pure component itself but has an influence on its charge state – and therefore also on the interactions of this component in ATPS. This can be confirmed when comparing ePC-SAFT parameters included in table 4.1 and table 4.2. Thus, the description given under figure 10.12 for most of the vitamins studied (VB2, VB3^{acid}, VB3^{amide}, VB12) refers only to the general nomenclature of vitamins used in this work and does not indicate the name of the ionic species. This is valid if the vitamin at pH~ 8 is fully present as only one type of species. Another proceeding was required for VB9 in this evaluation. The study of partitioning that has been carried out for VB9 involved the partitioning of the two VB9 species $VB9^{2-}$ and $VB9^{3-}$. Since these two species define all the interactions (in total) of VB9 in an aqueous solution of pH~8, it was more reasonable to treat them separately in terms of activity coefficients predictions (as $\gamma_{VB9^{2-}}^{\infty}$ and $\gamma_{VB9^{3-}}^{\infty}$). According to table 4.1 and table 4.2, the pure-component ePC-SAFT parameters of VB9, $VB9^{2-}$, $VB9^{3-}$

are the same. The difference lays in the values of binary interaction parameter k_{ij} estimated for each species. Therefore, both $VB9^{2-}$ and $VB9^{3-}$ contribute to unraveling the partitioning behavior of VB9 for which comparing $\gamma^{\infty}_{VB9^{2-}}$ and $\gamma^{\infty}_{VB9^{3-}}$ plays a key role.

The results of $\gamma^{\infty}_{vitamin}$ predicted with ePC-SAFT and shown in figure 10.12 can be compared with the partitioning predictions of vitamins of VB2, $VB3^{acid}$, $VB3^{amide}$, and VB12 shown in figure 10.11. According to equation (2.29), the $K^{pred,\infty}_{vitamin}$ is expressed as the ratio between $\gamma^{\infty,II}_{vitamin}$ (represented by gray bars) and $\gamma^{\infty,I}_{vitamin}$ (white bars). The highest $\gamma^{\infty,II}_{vitamin}$ to $\gamma^{\infty,I}_{vitamin}$ ratios were observed for VB12 while the lowest for VB2 (figure 10.12). This also explains the highest $K^{pred,\infty}_{VB12}$ and the lowest $K^{pred,\infty}_{VB2}$ values in figure 10.11. Also, these ratios were smaller for vitamins partitioned in ATPS formed by PEG 6000 and Na_2Tartrate, if comparing it to ATPS composed by PEG 6000 and Na_3Citrate. This has an influence on higher $K^{pred,\infty}_{vitamin}$ obtained in PEG 6000 and Na_3Citrate ATPS. Equation (2.29) is enough to predict the partitioning of most of the vitamins studied in this work (VB2, $VB3^{acid}$, $VB3^{amide}$, and VB12). For VB9 additional contribution must be considered. Since $VB9^{2-}$ and $VB9^{3-}$ are differently distributed between the phases and their partitioning strongly depends on the species distribution in each phase, the values of $\gamma^{\infty}_{VB9^{2-}}$ and $\gamma^{\infty}_{VB9^{3-}}$ are also different. Thus, in case of VB9, equation (2.30) corrects the fraction of activity coefficients with the ratio of species distribution calculated for $VB9^{2-}$ ($\alpha^{II}_{VB9^{2-}}$ and $\alpha^{I}_{VB9^{2-}}$) or for $VB9^{3-}$ ($\alpha^{II}_{VB9^{3-}}$ and $\alpha^{I}_{VB9^{3-}}$). It can be observed from figure 10.12 that the species of VB9 in the system formed by PEG 6000 and Na_3Citrate differ each other more than in ATPS formed by PEG 6000 and Na_2Tartrate. This result can be explained with electrostatic interactions (PEG – citrate salts: $\Delta pH_{phases} \leq 0.25$; PEG – tartrate salt: $\Delta pH_{phases} \leq 0.05$) of each VB9 ion with salt ions (Na^+, $Citrate^{3-}$, $Tartrate^{2-}$) present in ATPS. Therefore, higher $K^{pred,\infty}_{VB9}$ were obtained in ATPS formed by PEG 6000 and Na_3Citrate (figure 10.11).

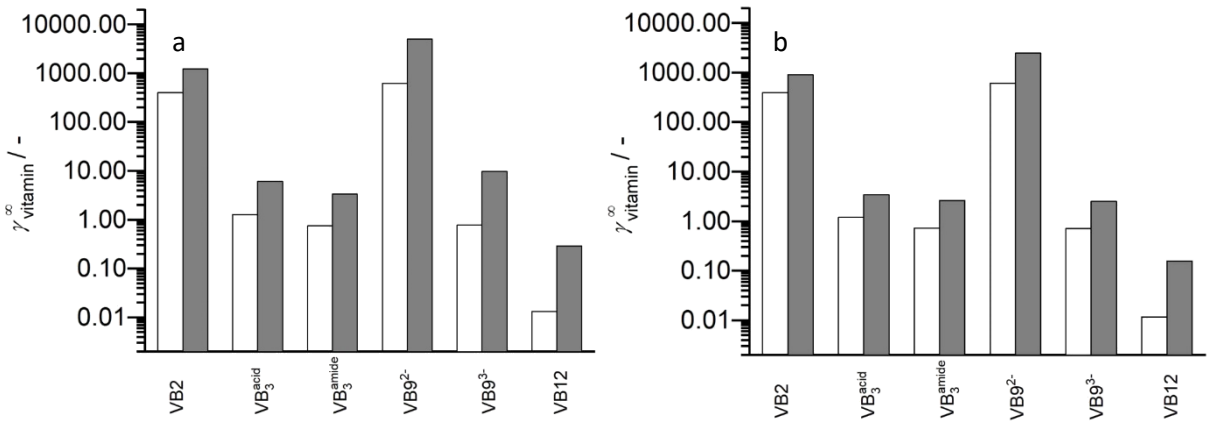

Figure 10.12. Activity coefficient of vitamins VB2 ($\gamma^{\infty}_{\mathrm{VB2}}$–), VB3$^{\mathrm{acid}}$ ($\gamma^{\infty}_{\mathrm{VB3acid}}$–), VB3$^{\mathrm{amide}}$ ($\gamma^{\infty}_{\mathrm{VB3amide}}$), VB9 ($\gamma^{\infty}_{VB9^{2-}}$ and $\gamma^{\infty}_{VB9^{3-}}$), and VB12 ($\gamma^{\infty}_{\mathrm{VB12}}$) in top phase (white bars) and bottom phase (gray bars) of ATPS PEG 6000 – Na_3Citrate ATPS – figure a (TLL = 0.369; w_P = 0.163 and w_S = 0.114; Appendix, A8) and PEG 6000 – Na_2Tartrate – figure b (TLL = 0.375; w_P = 0.195 and w_S = 0.110; Appendix, A8), predicted with ePC-SAFT at T = 298.15 K and p = 1 bar (pH ~ 8, Appendix, A4). The feed and equilibrium composition for a given TL are provided in Appendix, A8. Logarithmic scale was introduced for better data comparison.

Combined effects: the charge of vitamin and ATPS composition

The behavior of VB9 in PEG 6000 and Na_3Citrate is presented in figure 10.13 and was introduced to compare the partitioning of VB9 species at different TLL of ATPS (Appendix, A10). Similar diagram for the partitioning of VB9 species in PEG and Na_2Tartrate ATPS is not presented (data points were overlapping) since the pH difference observed for ATPS composed by PEG and Na_2Tartrate ($\Delta pH_{phases} \leq 0.05$) did not lead to a significant species distribution change (ARD% between the species distribution of $VB9^{2-}$ and $VB9^{3-}$ < 5 %). Based on the results presented already in figure 10.12, it was expected that the pH difference between the phases of PEG and Na_3Citrate influences more the partitioning of VB9 than does in PEG – Na_2Tartrate ATPS. The interactions of vitamins with ATPS phases depend on the system composition, thus plotting data against TLL like it is shown in figure 10.13 is very common. Figure 10.13 shows only TLL regions where it was possible to measure the partitioning with reasonable accuracy and validate the predictions. The lines were included just to show the trend of predicted data and to guide the eye. The low regions of TLL might also not be of interest to industrial applications as already mentioned in experimental section 7.1.1.

As presented in figure 10.13 the partition coefficient of VB9 increases when the TLL increases. Only an accurate description of non-ideality caused by interactions between a solute i.e. vitamin (in this case negatively charged species $VB9^{2-}$ and $VB9^{3-}$) and phase formers (water, PEG, Na^+, K^+, $Citrate^{3-}$, $Tartrate^{2-}$) with help of k_{ij} parameter allows predicting the $K_{VB9}^{pred,\infty}$ (at pH ~ 8: $K_{VB9^{2-}}^{pred,\infty}$ and $K_{VB9^{3-}}^{pred,\infty}$). The procedure used for predicting the partitioning of VB9 was accurate enough (according to table 10.2) to predict partition coefficients very well over a wide range of TLL as shown in figure 10.13. The ARD% values presented in table 10.2 prove that ePC-SAFT can very accurately predict the partitioning of VB9 species in PEG 6000 – $Na_3Citrate$ (ARD% ≤ 4.8). Reasonable predictions with ARD% values ≤ 10.89 are observed for VB9 partitioning in all other systems considered in this work.

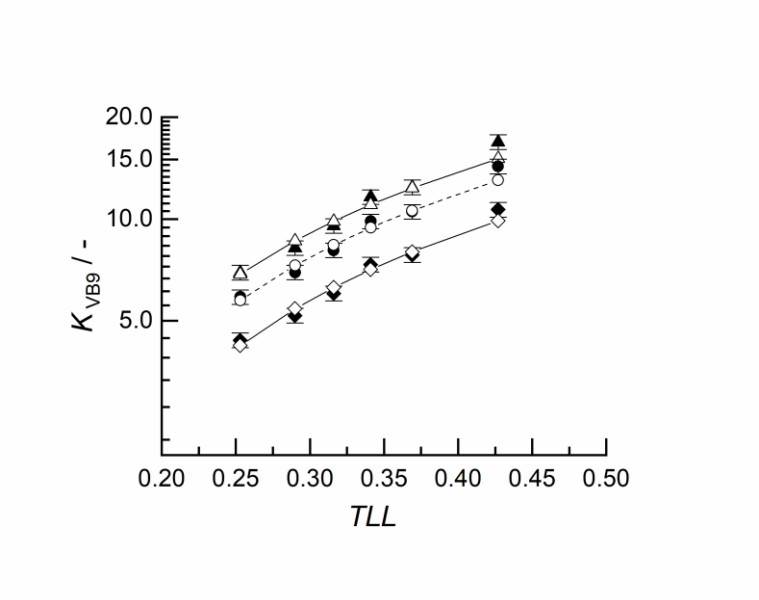

Figure 10.13. Partitioning of VB9 species in ATPS PEG 6000 – $Na_3Citrate$ at different TL compositions, at T = 298.15 K and p = 1 bar. VB9 species: K_{VB9} (●,○), $K_{VB9^{2-}}$ (◇,◆), $K_{VB9^{3-}}$ (△,▲). Closed symbols: experimental data K_{VB9}^{exp} and calculated $K_{VB9^{2-}}^{exp}$ and $K_{VB9^{3-}}^{exp}$ with equation (3.11) (Appendix, A10); open symbols: ePC-SAFT predictions of $K_{VB9^{2-}}^{pred,\infty}$ and $K_{VB9^{3-}}^{pred,\infty}$ and calculated $K_{VB9}^{pred,\infty}$ with equation (2.30); Open symbols (ePC-SAFT) were connected using trend lines only to guide the eye (dashed lines - $K_{VB9}^{pred,\infty}$, solid lines - $K_{VB9^{2-}}^{pred,\infty}$ and $K_{VB9^{3-}}^{pred,\infty}$). Logarithmic scale was introduced for better data comparison.

According to a description provided in section 7.2.1, the $K_{VB9^{2-}}^{exp}$ and $K_{VB9^{3-}}^{exp}$ were calculated with equation (3.11) from experimental K_{VB9}^{exp} and VB9 species distribution at pH of ATPS phases (section 2.3.2). The $K_{VB9^{2-}}^{pred,\infty}$ and $K_{VB9^{3-}}^{pred,\infty}$ were predicted with ePC-SAFT using pure-

component and binary interaction parameters k_{ij} with water from table 4.2 and k_{ij} between ATPS phase forming components from table 4.3. All these parameters were fitted as explained in section 4.1.1. The non-ideality caused by interactions between negatively charged species ($VB9^{2-}$ and $VB9^{3-}$) and phase-forming components was predicted by ePC-SAFT using k_{ij} (besides ePC-SAFT pure-component parameters). These k_{ij} were fitted to one partitioning data point for each species ($K_{VB9^{2-}}^{exp}$, $K_{VB9^{3-}}^{exp}$). One data point means one tie-line data point in the ATPS. In total only the two experimental points were required: K_{VB9}^{exp} measured in PEG 6000 - $Na_3Citrate$ and K_{VB9}^{exp} in PEG 6000 - $Na_2Tartrate$, in order to predict the partitioning of VB9 species in ATPS formed by PEG of M_{PEG} = 4000 g·mol^{-1} and M_{PEG} = 6000 g·mol^{-1} and $Na_3Citrate$ or $Na_2Tartrate$, over different TLL. Solely the two VB9 species were considered while describing the interactions of VB9 (species) - PEG and VB9 (species) - salt ions, since just $VB9^{2-}$ and $VB9^{3-}$ are expected in ATPS of pH~8. The $K_{VB9}^{pred,\infty}$ were obtained by introducing $K_{VB9^{2-}}^{pred,\infty}$ and $K_{VB9^{3-}}^{pred,\infty}$ into equation (2.30). Based on the literature, more negatively charged molecules tend to partition into the more basic phase (in this case – PEG) [85]. It is then expected that $VB9^{3-}$ will have higher K than $VB9^{2-}$ in ATPS considered in the present study ($K_{VB9^{3-}} > K_{VB9^{3-}}$). This behavior was observed in this work, and it corresponds to the very big k_{ij} value between the multi-valent VB9 species and organic anions (table 4.3).

The non-ideality and thus also some interactions that rule the partitioning of VB9 can be evaluated toward activity coefficients of VB9 species ($\gamma_{VB9^{2-}}^{\infty}$ and $\gamma_{VB9^{3-}}^{\infty}$) predicted in PEG 6000 and $Na_3Citrate$ ATPS (figure 10.14). The increasing trend of $\gamma_{VB9^{2-}}^{\infty}$ and $\gamma_{VB9^{3-}}^{\infty}$ in the bottom phase over different TLL can be related to the repulsive interactions of negatively charged species of VB9 with salt anion ($Citrate^{3-}$). The values of $\gamma_{VB9^{2-}}^{\infty,I}$ and $\gamma_{VB9^{2-}}^{\infty,II}$ in the two phases are significantly higher than of $\gamma_{VB9^{3-}}^{\infty,I}$ and $\gamma_{VB9^{3-}}^{\infty,II}$. Also, it is visible that the difference between activity coefficients in the top and bottom phases is higher for VB3-. Lower values of $\gamma_{VB9^{3-}}^{\infty,I}$ than $\gamma_{VB9^{2-}}^{\infty,I}$ may explain the higher affinity of $VB9^{3-}$ to the top phase (if comparing to $VB9^{2-}$).

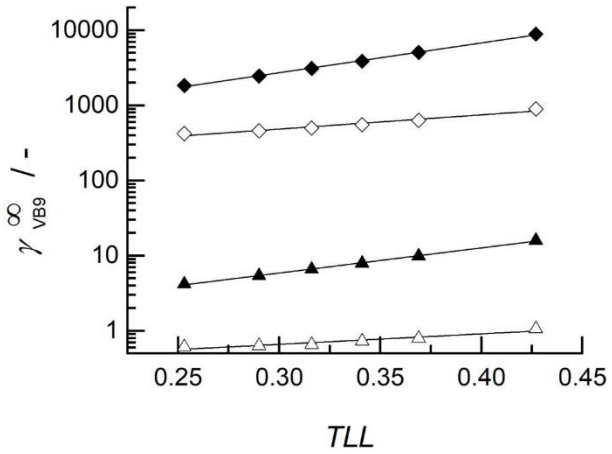

Figure 10.14. Activity coefficient of VB9 species $\gamma^{\infty}_{VB9^{2-}}$ (◇,◆) and $\gamma^{\infty}_{VB9^{3-}}$ (△,▲) in top phase (open symbols) and bottom phase (closed symbols) of ATPS predicted with ePC-SAFT at T = 298.15 K and p = 1 bar, plotted against TLL of ATPS formed by PEG 6000 and biodegradable salt - $Na_3Citrate$ (pH ~ 8, Appendix, A4). The lines that connect different values of $\gamma^{\infty}_{VB9^{2-}}$, as well as $\gamma^{\infty}_{VB9^{3-}}$, were applied just to guide the eye and improve the readability. The feed and equilibrium composition for a given TL are provided in Appendix (A8). Logarithmic scale was introduced for better data comparison.

Combined effects: the molecular structure and charge of vitamin and ATPS composition

The partition coefficients of vitamins do not only depend on charge (on their species distribution), and thus not only on electrostatic interactions. The strong pH-dependency of the partition coefficients shown previously in figure 10.13 is caused by the presence of different VB9 species. However, the pH and thus electrostatic interactions are not dominating vitamin partitioning for those vitamins that are exclusively present at one species in the ATPS [419]. This can be seen in figure 10.15, as the monovalent $VB3^{acid\ -}$ has just slightly higher K values than the neutral $VB3^{amide}$. Different effects have been already discussed in detail section 7.2.1, i.e. molecular structure of water-soluble vitamin and combined effects related to the molecular structure of vitamin and ATPS composition. Similar observations could be found based on ePC-SAFT predictions. However, towards the activity coefficient predictions, it is possible to compare the non-ideality caused by different effects ruling the partitioning.

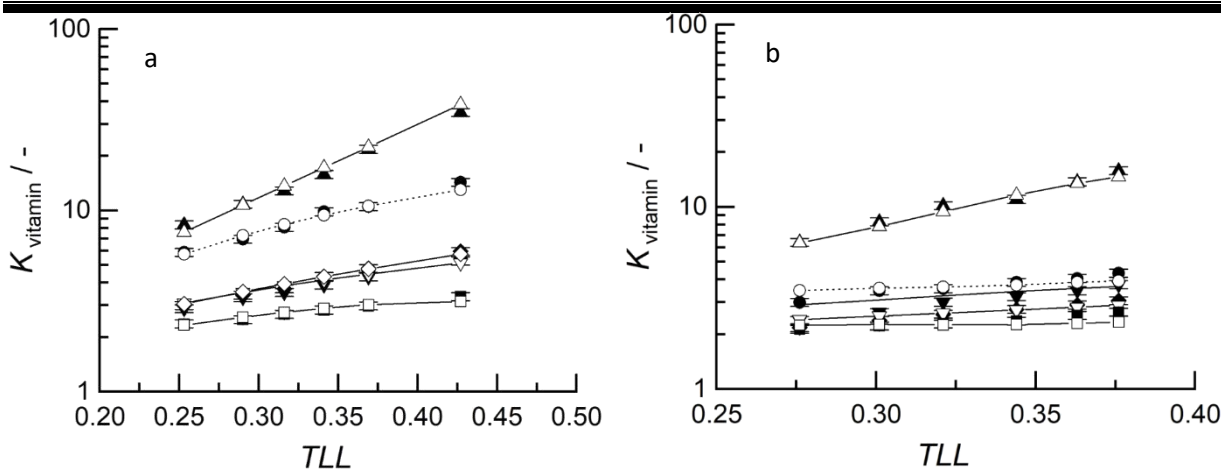

Figure 10.15. The partitioning of vitamins VB2 (●,○), VB3^{acid} (■,□), VB3^{amide} (▼,▽), VB9 (◇,◆), VB12 (△,▲), in ATPS PEG 6000 – biodegradable salt (figure a: $Na_3Citrate$, figure b: $Na_2Tartrate$), at T = 298.15 K and p = 1 bar, at different TL compositions (Appendix, A8). Closed symbols: experimental data (Appendix, A10), open symbols: ePC-SAFT predictions. VB9: $K_{VB9^{2-}}^{exp}$ and $K_{VB9^{3-}}^{exp}$ calculated with equation (3.11). Open symbols were connected using trend lines only to guide the eye: solid lines – showing trends of ePC-SAFT predictions; dotted lines – trends of $K_{VB9}^{pred,\infty}$ calculated with equation (2.30) using ePC-SAFT predictions of $K_{VB9^{2-}}^{pred,\infty}$ and $K_{VB9^{3-}}^{pred,\infty}$. Logarithmic scale was introduced for better data comparison.

Based on activity coefficients $\gamma_{vitamin}^{\infty}$ predicted with ePC-SAFT for each vitamin in the two phases of ATPS and shown in figure 10.16, it is possible to evaluate the non-ideality caused by the effects dominating the partitioning. For a better overview, these data are also included in Appendix (A14). In general, the three situations were observed when predicting the partitioning of vitamins at different TLL. The most observed in this work (since this one was already found for DNP-AA) was the increase of activity coefficient in the bottom phase and decrease in the top phase. This trend is observed in figure 10.16(a-b) for VB3^{acid} and VB3^{amide}. The possible reason for that might be the repulsive interactions of vitamin and salt ions and the attractive interactions of vitamin to PEG. Increasing the concentration of both PEG and salt over TLL leads to an increase of $K_{vitamin}^{pred,\infty}$ (figure 10.15).

Other behavior in ATPS present VB2 (figure 10.16c) and VB9 (figure 10.14). Therefore, it was found that in both the top and bottom phases of ATPS considered in this work, the values of $\gamma_{vitamin}^{\infty}$ increase together with an increase of TLL. The common property of both VB2 and VB9 is that these solutes pose the lowest solubility of all studied

in this work. Their molecules have structures (subcomponents) that may define the interactions of ATPS phase forming components with vitamin.

In the case of VB2 this is dimethyl isoalloxazine ring and ribitol, while for VB9 this is aromatic pteridine ring, para-aminobenzoic acid, and glutamate (section 2.3). The increasing trend of $\gamma_{vitamin}^{\infty}$in both phases can mean that in both phases different interactions are competing. However, in the end the repulsive interactions from the bottom phase are enough strong to lead to the $K_{VB2}^{pred,\infty}$> 2.24 and $K_{VB9}^{pred,\infty}$> 5.32 in the range of TLL studied in this work (Appendix, A8).

The last case was observed for VB12 (figure 10.16d) and shows a decrease of γ_{VB12}^{∞} over increasing TLL in both ATPS phases. The results of ePC-SAFT predictions shown in figure 10.16d confirmed that the assumption used in the literature when correlating *K* of proteins in ATPS with Wilson model wrongly states that the partitioning can be explained solely in terms of electrical effects [425]. The high values of *K* can be related to the fact that large molecules possess larger areas of interactions with the components forming the ATPS[85, 87]. Thus, such large molecules e.g. proteins or VB12, might just have more interactions with PEG due to their size and presence of many functional groups [87, 419]. In ATPS considered in this work, VB12 is present solely as neutral species. Therefore, electrostatic interactions of VB12 and ATPS phase forming components are not significant in predicting the partitioning. A high affinity of VB12 to the PEG-rich phase can result from hydrophobic interactions to PEG or hydrogen-bonding effects between PEG and VB12 [87, 419]. All these effects are considered explicitly in ePC-SAFT predictions.

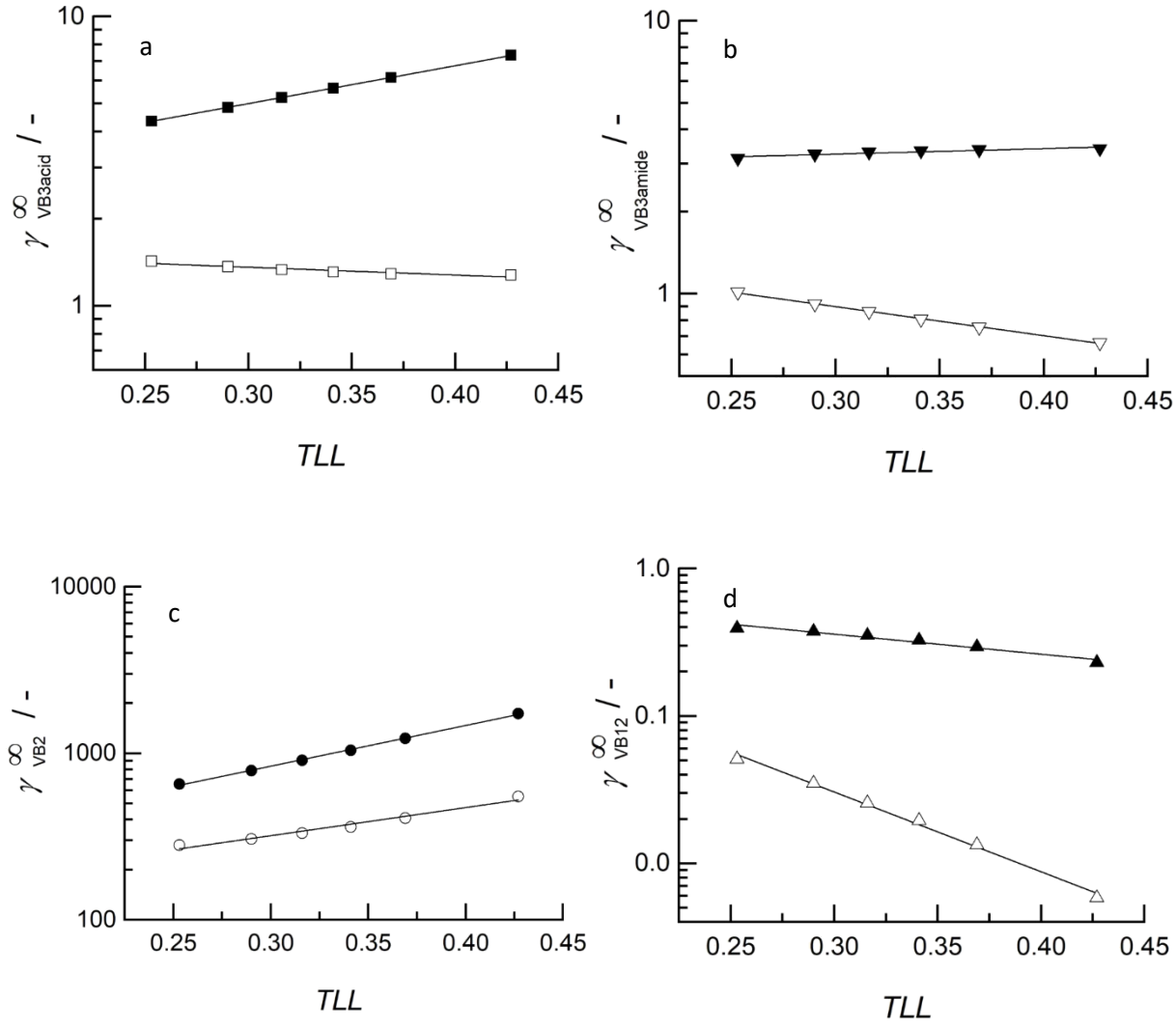

Figure 10.16. Activity coefficient of vitamins VB3^{acid} (figure a: $\gamma^{\infty}_{VB3acid^-}$), VB3^{amide} (figure b: $\gamma^{\infty}_{VB3amide}$), VB2 (figure c: $\gamma^{\infty}_{VB2^-}$), and VB12 (figure d: γ^{∞}_{VB12}) in top phase (open symbols) and bottom phase (closed symbols) of ATPS predicted with ePC-SAFT at T = 298.15 K and p = 1 bar, plotted against TLL of ATPS formed by PEG 6000 and biodegradable salt - $Na_3Citrate$ (pH ~ 8, Appendix, A4). The lines were applied just to guide the eye and improve the readability. The feed and equilibrium composition for a given TL are provided in Appendix (A8). Logarithmic scale was introduced for better data comparison.

Changing PEG and salt concentrations influences the partitioning of vitamins in ATPS in a way that higher K are expected with increasing TLL (figure 10.12). Increasing the salt concentration impacts the ionic strength and can lead to K improvement [95, 415]. Altering PEG concentration might also influence K through hydrophobic PEG – vitamin interactions [95] or increased cross-association forces. The ATPS composition influence expressed as TLL on the partitioning of different vitamins was accurately predicted with ePC-SAFT. The salt and PEG influence in terms of different salt type and PEG molar mass,

as well as the concentration of both, are discussed in the following sections 10.3.2 and 10.3.3, respectively.

10.3.2. Salt Influence on Partition Coefficient

The results of ePC-SAFT predictions of water-soluble vitamin partitioning in ATPS formed by PEG (M_{PEG} = 6000 g·mol^{-1}) and biodegradable salt (Na_3Citrate and Na_2Tartrate) are presented in figure 10.17. The accuracy of prediction results obtained for the partitioning of VB2, VB3^{acid}, VB3^{amide}, VB9, and VB12 in these ATPS, as well as in the systems formed by PEG of M_{PEG} = 4000 g·mol^{-1} and organic salts (Na_3Citrate and Na_2Tartrate) can be seen in table 10.2. Vitamins considered in this work (pH ~ 8) and separated in ATPS under study were present as neutral (VB3^{amide}, VB12) or negatively charged vitamin species (VB2^{-}, VB3^{acid-}, VB9^{2-}, VB9^{3-}). For this reason, ePC-SAFT predictions shown in this section were obtained with the pure-component and binary interaction k_{ij} parameters for neutral and ionic species from table 4.1, table 4.2, table 4.3.

The partition coefficient of vitamins at different tie-line compositions (*TLL*) can be accurately predicted with ePC-SAFT, thus, the $K_{vitamins}^{pred,\infty}$ predicted with ePC-SAFT were similar (ARD%: table 10.2) to experimental $K_{vitamins}^{exp}$. Based on figure 10.17, ePC-SAFT was capable to capture an increase of the partition coefficient caused by the usage of salts composed by Na_3Citrate as ATPS formers. Therefore, the higher $K_{vitamins}^{pred,\infty}$ were observed for vitamins partitioned in ATPS containing Citrate^{3-} and Na^{+}. On the contrary, ATPS formed by a salt of PEG and Na_2Tartrate did allow only lower $K_{vitamins}^{pred,\infty}$ values if compared to ATPS formed by PEG and Na_3Citrate. ePC-SAFT predicted the increase of $K_{DNP-AA}^{pred,\infty}$ caused by the increase of the salt concentration related to the changes in ionic strength. Similar observations were found previously for DNP-AA (section 10.2.2). One of many possible reasons for this partitioning behavior might be related to the fact that the citrate-based salts cause higher repulsion to the vitamin species than the tartrate-based salts due to the presence of higher valency in citrate (-3) over tartrate (-2).

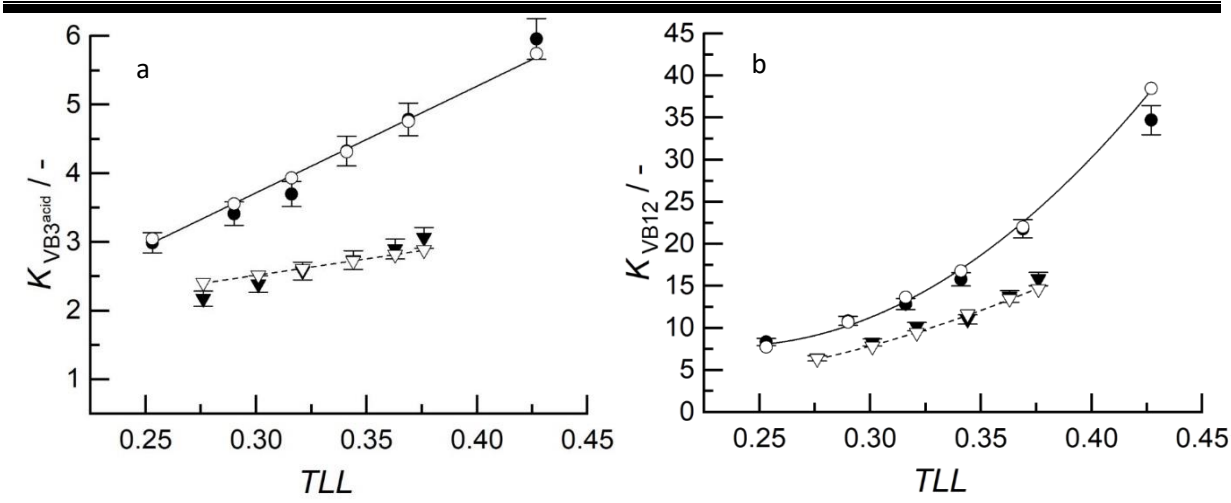

Figure 10.17. Salt influence on the partitioning of VB3^{acid} (a) and VB12 (b), in different PEG 6000 – biodegradable salt ($Na_3Citrate$ - ●,○; $Na_2Tartrate$ - ▼,▽) ATPS compositions (TLL), at T=298.15 K and p=1 bar. The open symbols represent ePC-SAFT predictions of $K_{vitamin}^{pred,\infty}$ (at certain TLL values), the closed symbols are experimental data $K_{vitamin}^{exp}$ measured in this work (Appendix, A10). The lines connecting the open points were applied only to guide the eye and to better distinguish the trends of the points predicted in different ATPS: PEG 6000 - $Na_3Citrate$ – solid line, PEG 6000 – $Na_2Tartrate$ – dashed line.

A comparison of the results of ePC-SAFT predictions obtained for VB9 in ATPS formed by PEG and $Na_3Citrate$ or $Na_2Tartrate$ is presented in figure 10.18. Data $K_{VB9}^{pred,\infty}$ plotted in this figure calculated with equation (2.30) based on ePC-SAFT predictions of $K_{VB9^{2-}}^{pred,\infty}$ and $K_{VB9^{3-}}^{pred,\infty}$ and species distribution ($\alpha_{VB9^{2-}}$, $\alpha_{VB9^{3-}}$ in each phase) showed a good match to experimentally obtained values in this work (Appendix, A10). According to data presented in table 10.2, this procedure allowed ARD% ≤ 8.6 in ATPS considered in figure 10.18. The values of $K_{VB9}^{pred,\infty}$ were higher in ATPS formed by PEG and $Na_3Citrate$ what agrees with a trend observed experimentally.

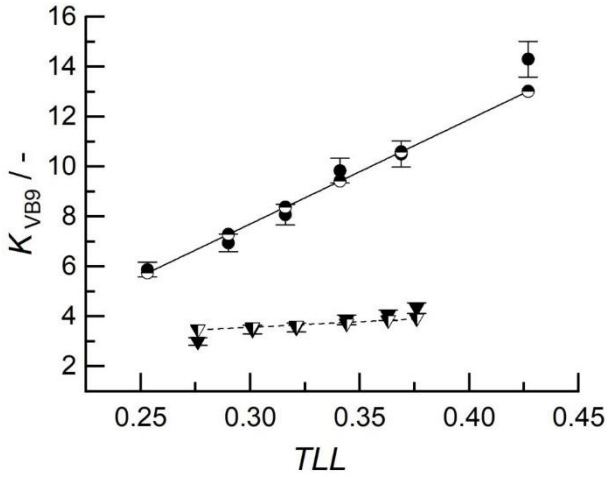

Figure 10.18. Salt influence on the partitioning of VB9 in different PEG 6000 – biodegradable salt ($Na_3Citrate$ - ●,◓; $Na_2Tartrate$ - ▼,∇) ATPS compositions (TLL), at T = 298.15 K and p = 1 bar. The half-open symbols represent the values $K_{VB9}^{pred,\infty}$ calculated based on ePC-SAFT predictions of $K_{VB9^{2-}}^{pred,\infty}$ and $K_{VB9^{3-}}^{pred,\infty}$ (at certain TLL values), the closed symbols are experimental data K_{VB9}^{exp} measured in this work (Appendix, A10). The lines connecting the half-open points were applied only to guide the eye and to better distinguish the trends of the points predicted in different ATPS: PEG 6000 - $Na_3Citrate$ – solid line, PEG 6000 – $Na_2Tartrate$ – dashed line.

The values of k_{ij} found in this work for negatively charged and neutral vitamins can have the following importance in studying their partitioning behavior in ATPS. For negatively charged vitamins one rather very positive k_{ij} was required between each pair vitamin – anion (independent of M_{PEG}), and a slightly positive k_{ij} was applied to a pair vitamin – PEG (independent of M_{PEG}). Obviously, strong repulsion occurs between charged vitamin and the species (especially the organic anions) present in the salt phase. For neutral vitamins one k_{ij} was required between each pair vitamin – salt ion (while no parameter was required for vitamin – PEG). For $VB3^{amide}$ just one binary interaction parameter was introduced (vitamin – $Tartrate^{2-}$). This means that solely with parameters available in literature it was possible to predict $K_{VB3amide}^{pred,\infty}$ of $VB3^{amide}$ in ATPS composed by PEG (M_{PEG} = 4000 – 6000 g·mol^{-1}) and biodegradable salt $Na_3Citrate$ with deviations ARD% ≤ 5.92 or $Na_2Tartrate$ with deviations ARD% ≤ 9.89. This is a very good result in the meaning that ePC-SAFT could quantitatively predict $K_{VB3amide}^{pred,\infty}$ of $VB3^{amide}$ in ATPS formed by different salt (and PEG) without introducing any additional binary parameters.

Figure 10.19 helps to understand the non-ideality in ATPS and thus also to estimate the interactions that may dominate in vitamin partitioning in ATPS formed by PEG and

biodegradable salt (Na_3Citrate, Na_2Tartrate). This evaluation is based on activity coefficient $\gamma_{vitamin}^{\infty}$ predicted with ePC-SAFT in the two ATPS phases. Figure 10.19, independently of the salt used (Na_3Citrate, Na_2Tartrate) leads to similar general observations on the $\gamma_{vitamin}^{\infty}$ trends over TLL as provided in the discussions that concerned figure 10.14 and figure 10.16 given in the previous section 10.3.2. Therefore, also the reasons for this behavior provided in the previous evaluation can apply. The lines that connect $\gamma_{vitamin}^{\infty}$ predicted with ePC-SAFT in the two ATPS: PEG 6000 – Na_3Citrate and PEG 6000 – Na_2Tartrate were used only to guide the eye and improve the readability. Thus, it is visible that the general trends obtained in these two ATPS are similar. The difference in $\gamma_{vitamin}^{\infty}$ lays in the lower values of $\gamma_{vitamin}^{\infty,\mathrm{I}}$ and $\gamma_{vitamin}^{\infty,\mathrm{II}}$ in systems formed by PEG 6000 - Na_2Tartrate than in PEG 6000 – Na_3Citrate.

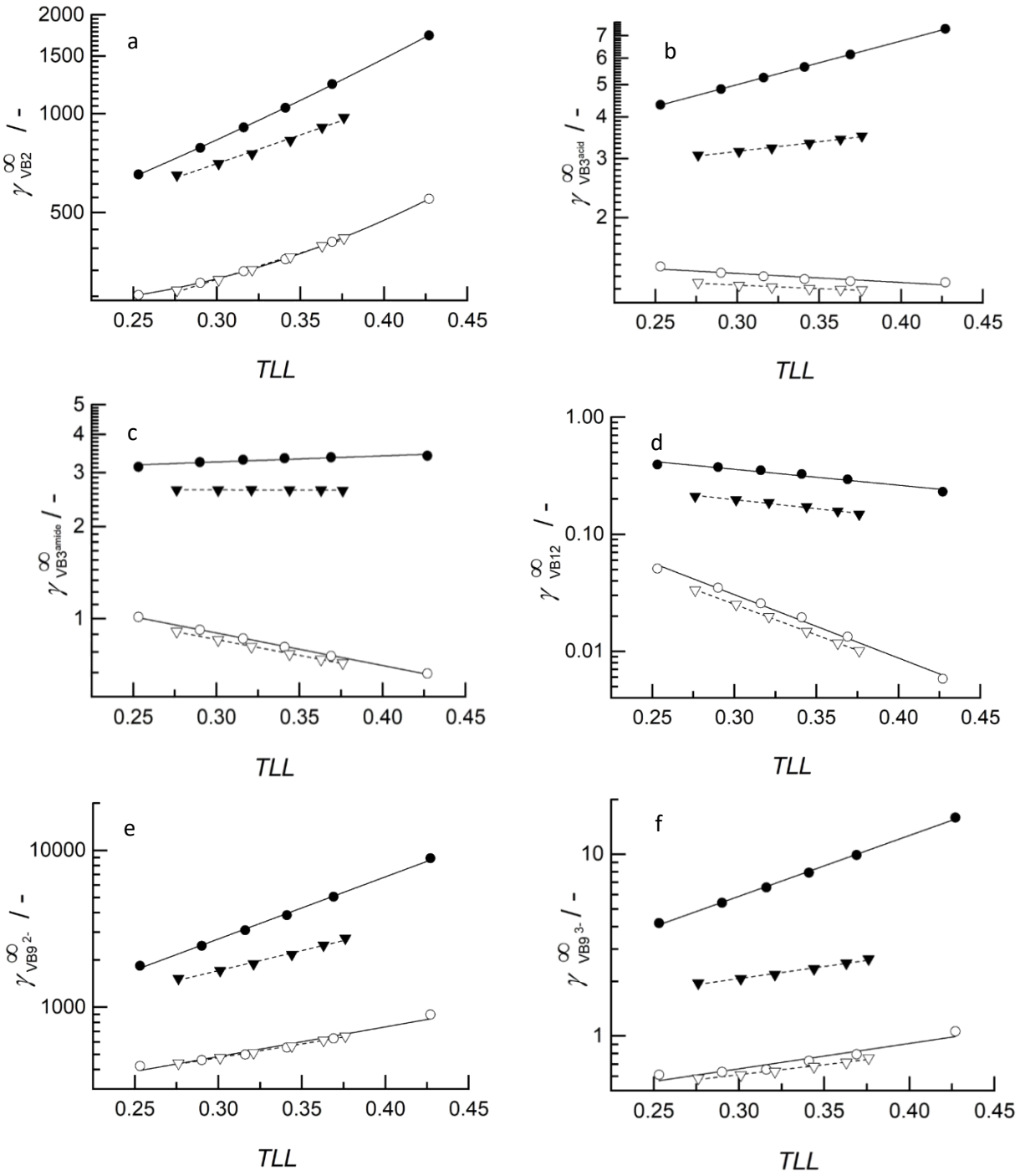

Figure 10.19. Activity coefficient of vitamins VB2 (figure a: $\gamma^{\infty}_{\mathrm{VB2}^-}$), VB3$^{\mathrm{acid}}$ (figure b: $\gamma^{\infty}_{\mathrm{VB3}^{acid}-}$), VB3$^{\mathrm{amide}}$ (figure c: $\gamma^{\infty}_{\mathrm{VB3amide}}$), VB12 (figure d: $\gamma^{\infty}_{\mathrm{VB12}}$), and VB9 (figure e: $\gamma^{\infty}_{VB9^{2-}}$, figure f: $\gamma^{\infty}_{VB9^{3-}}$) in top phase (open symbols) and bottom phase (closed symbols) of ATPS predicted with ePC-SAFT at T = 298.15 K and p = 1 bar, plotted against TLL of ATPS formed by PEG 6000 and biodegradable salt - Na_3Citrate - ●,○ or Na_2Tartrate - ▼,▽ (pH ~ 8, Appendix, A4). The lines were applied just to guide the eye and improve the readability - PEG 6000 - Na_3Citrate – solid line, PEG 6000 – Na_2Tartrate – dashed line. The feed and equilibrium composition for a given TL are provided in Appendix (A8). Logarithmic scale was introduced for better data comparison.

10.3.3. PEG Influence on Partition Coefficient

PEG molar mass (4000 g·mol^{-1} or 6000 g·mol^{-1}) influences K values. A higher affinity to the upper PEG-phase was predicted with ePC-SAFT for all vitamins considered in this evaluation, i.e. VB2, VB3^{acid}, VB3^{amide}, VB9, and VB12. ePC-SAFT parameters from table 4.1, table 4.2 and table 4.3 were used in this evaluation. The results of ePC-SAFT predictions of vitamin partitioning in ATPS formed by biodegradable salt (Na_3Citrate) and PEG (M_{PEG} = 4000 and 6000 g·mol^{-1}), at T = 298.15 K and p = 1 bar, are presented in figure 10.20.

Due to the fact that only small differences in $K_{vitamin}^{pred,\infty}$ related to using PEG of different molar mass were expected (based on experimental data from section 7.2.3), figure 10.20 was introduced only to show the ability of ePC-SAFT to predict the strength of influences caused by selecting different PEG´s molar mass. The intention of presenting figure 10.20 was similar to the one given already in section 10.2.3 (DNP-AA) and relied on evaluating if ePC-SAFT can capture the differences resulting from introducing PEG of different molar mass to ATPS according to experimental data (although these differences are expected to be very low). Though these were only the expectations, the values predicted with the model matched reasonably well data obtained through the experiments (Appendix, A10).

The accuracy of the predictions obtained in these ATPS was shown in table 10.2. Similar to the previous section 10.2.3, the difference in activity coefficients $\gamma_{vitamin}^{\infty}$ in each phase was very low, therefore to avoid overlapping partitioning data points obtained in ATPS of different molar mass, the values of $\gamma_{vitamin}^{\infty}$ were included in Appendix (A14) - instead of using the figures. These data confirm that for most vitamins considered in this study, the values of $\gamma_{vitamin}^{\infty}$ predicted in ATPS of M_{PEG} = 4000 and 6000 g·mol^{-1} were difficult to distinguish. It means that selecting PEG in this range of M_{PEG} leads to an insignificant effect on water-soluble vitamin partitioning in ATPS and $\gamma_{vitamin}^{\infty}$ (comparable non-ideality).

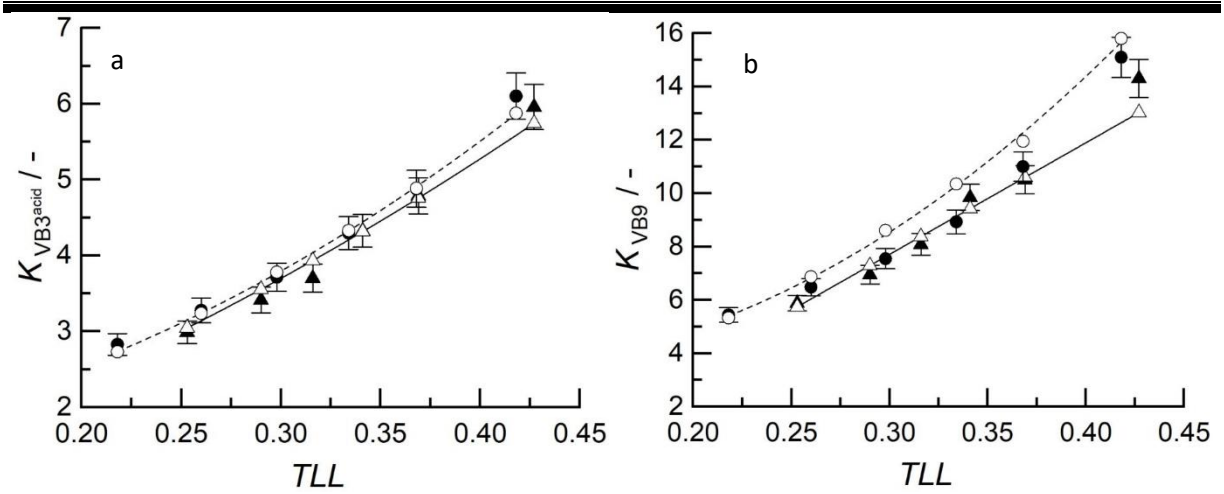

Figure 10.20. PEG molar mass influence on the partitioning of VB3^{acid} (a) and VB9 (b) at different ATPS compositions (TLL), at T=298.15 K and p=1 bar. ATPS formed by PEG 4000 or 6000 (PEG 4000 of M_{PEG} = 4000 g·mol^{-1} - dotted line and symbols ●,○; PEG 6000 of M_{PEG} = 6000 g·mol^{-1} – solid line and symbols ▲, △) and $Na_3Citrate$. Lines and open points: ePC-SAFT predictions $K_{vitamin}^{pred,\infty}$. The lines connecting the open points were applied only to guide the eye and to better distinguish the trends – PEG 6000 – $Na_3Citrate$ – solid lines, PEG 4000 – $Na_3Citrate$ – dashed lines. Closed points: experimental data $K_{vitamin}^{exp}$ measured in this work (Appendix, A10).

10.4. Conclusion

This chapter presented the results of partitioning predictions of four DNP-AA (DNP-glycine, DNP-alanine, DNP-valine, and DNP-leucine), as well as five water-soluble vitamins (VC, VB2, VB3^{acid}, VB9, VB12) in PEG – biodegradable salt ATPS. The predictions were carried out using thermodynamic model ePC-SAFT and concerned the partitioning in ATPS composed by PEG (M_{PEG} = 4000 – 8000 g·mol^{-1}) and $Na_3Citrate$, $K_3Citrate$, or KNaTartrate (for DNP-AA), as well as PEG (M_{PEG} = 4000 – 6000 g·mol^{-1}) and $Na_3Citrate$ or $Na_2Tartrate$ (for vitamins), at T= 298.15 K and p= 1 bar. The results obtained with ePC-SAFT showed good accuracy if comparing to experimental data. It was predicted that all solutes under study have a higher affinity to the upper PEG phase of ATPS considered. This agrees with the observations that were previously found based on experimental data.

ePC-SAFT predictions presented in this chapter confirmed that the number of experiments can be reduced if the partitioning approach designed in this work is applied. In this work, ePC-SAFT was capable to predict K qualitatively, but also by separating different effects that rule the separation it helped in evaluating which effects dominate in

the partitioning of different solutes. This is an outstanding result for practical ATPS application, since even having an extensive database of experimental partition coefficients (K) values is not enough to unravel the phenomena that are behind the partitioning. The success of the present study was achieved based on non-ideality evaluation, toward activity coefficients γ_i^{∞} that were predicted with ePC-SAFT for different solutes, separated in the two phases of ATPS.

The initial base for studying the partitioning in ATPS was a good description of dissociation equilibrium. The solutes considered in this work, i.e. DNP-AA and water-soluble vitamins, in aqueous solutions of pH~8 (pH of ATPS) can be present as species with different charge states, and additionally, these species can have different partition coefficients in ATPS. At pH~8 of ATPS the solutes considered in this work are present as neutral ($VB3^{amide}$, VB12) or negatively charged species (DNP-glycine$^-$, DNP-alanine$^-$, DNP-valine$^-$, DNP-leucine$^-$, VB2$^-$, $VB3^{acid-}$, $VB9^{2-}$, $VB9^{3-}$). Since DNP-AA and water-soluble vitamins are usually present at very small concentrations, the ePC-SAFT partitioning approach was based on predicting the infinite dilution activity coefficient γ_j^{∞} of DNP-AA or vitamin species in the two phases of ATPS.

Predicting the partitioning of DNP-AA and water-soluble vitamins in PEG – salt ATPS with ePC-SAFT requires a description of interactions between all components in ATPS. The interactions lead to non-ideality that is described by ePC-SAFT with help of the binary interaction parameters (k_{ij}). The interactions between a solute (neutral or charged) and water, as well as between ATPS phase formers were described using partitioning-independent data, e.g. liquid density, osmotic coefficients, or solubility. The k_{ij} between DNP-AA or vitamin species and ATPS phase formers were fitted to one experimental K data point. Estimating the binary interactions parameter k_{ij} required for each DNP-AA only three experimental data points K_{DNP-AA}^{exp}, while for each vitamin just two experimental $K_{vitamins}^{exp}$ values were needed.

Using ePC-SAFT pure-component and binary interaction k_{ij} parameters allowed predicting the following partitioning trends $K_{DNP-leucine}^{pred,\infty} > K_{DNP-valine}^{pred,\infty} > K_{DNP-alanine}^{pred,\infty} > K_{DNP-glycine}^{pred,\infty}$ and $K_{VB12}^{pred,\infty} > K_{VB9}^{pred,\infty} > K_{VB3amide}^{pred,\infty} > K_{VB3acid}^{pred,\infty} > K_{VB2}^{pred,\infty}$ that matched the previous observations found based on experimental data. The partitioning can be influenced by 1) electrostatic interactions resulting from partitioning of charged

components in ATPS, 2) molecular size of DNP-AA or vitamin, 3) other interactions of DNP-AA or vitamin with phase formers (e.g. hydrogen bonding, hydrophobic interactions). These factors are dependent among others on PEG molar mass, salt type, ATPS composition expressed as tie-line length (*TLL*) that has been defined with equation (3.3). ePC-SAFT was able to accurately predict the partitioning of DNP-AA or vitamin in ATPS containing PEG of different molar mass and type of a salt. It showed that the highest partition coefficient can be obtained in ATPS formed by PEG of lower molar mass (in this work, M_{PEG} = 4000 kg·mol^{-1}) and salt with ions Na^+ and $Citrate^{3-}$ over K^+ and $Tartrate^{2-}$. The same observation was found based on experimental data.

One of the decisive factors for the partitioning trend of $K_{DNP-AA}^{pred,\infty}$ can be DNP-AA hydrophobicity that in this case vary with the number of methylene groups $n(CH_2)$ present in the molecule. ePC-SAFT predicted that the highest partition coefficient can be obtained for DNP-leucine of the highest $n(CH_2)$ among the four DNP-AA studied, while the lowest partition coefficient was predicted for DNP-glycine of the lowest $n(CH_2)$. It also proved the ability to capture the effect on $n(CH_2)$ on partitioning by showing the highest values of $K_{DNP-AA}^{pred,\infty}$ for a system composed by PEG and $Na_3Citrate$ and the lowest $K_{DNP-AA}^{pred,\infty}$ for ATPS formed by PEG and KNaTartrate. Studying the effects that rule the partitioning of vitamins was much more complex.

Based on ePC-SAFT predictions the three different effects on activity coefficients γ_i^∞ of DNP-AA or vitamin could be found. The most common trend observed in this work was the increase of activity coefficient in the bottom phase and decrease in the top phase. This behavior was observed for all considered DNP-AA, $VB3^{acid}$ and $VB3^{amide}$. The possible reason for such non-ideality might be the repulsive interactions of vitamin and salt ions and the attractive interactions of vitamin to PEG. Increasing the concentration of both PEG and salt over TLL, leads to the increase of $K_i^{pred,\infty}$. Other behavior in ATPS was seen for VB2 and VB9. Therefore, it was found that in both top and bottom phase of ATPS considered in this work, the values of $\gamma_{vitamin}^\infty$ increase together with an increase of TLL. These molecules have structures (subcomponents) that may define the interactions of ATPS phase forming components with vitamin and thus contribute to the non-ideal behavior of a solute in ATPS. Increasing trend of $\gamma_{vitamin}^\infty$ in both phases can mean that in both phases different interactions are competing. The last case was observed for VB12 (figure 10.16d) and shows a decrease of γ_{VB12}^∞ over increasing TLL in both ATPS phases.

This effect might be related with the effects related to the molar mass of VB12 and the presence of many functional groups in a molecule. In ATPS considered in this work, VB12 is present solely as neutral species. Therefore, electrostatic interactions of VB12 and ATPS phase forming components are not significant in predicting the partitioning. A high affinity of VB12 to PEG-rich phase can result from hydrophobic interactions to PEG or hydrogen-bonding effects between PEG and VB12. All these effects are considered explicitly in ePC-SAFT predictions.

11. Summary and Outlook

The intention of this work was to decrease the great lack of understanding of partitioning in ATPS, thus, to break the biggest limitation that disables the implementation of ATPS at industrial scale. This chapter provides the answers to the needs and questions of the current research. It presents new knowledge acquired based on the experimental and thermodynamic studies carried out in this work. This concerns physicochemical properties of aqueous solutions containing biomolecules, i.e., DNP-AA and water-soluble vitamins, and selecting biodegradable aqueous two-phase systems (ATPS). It summarizes the attempts done in this work and shows the new contribution into understanding the behavior of DNP-AA and vitamins in aqueous solutions.

This thesis was focused on studying the behavior of biomolecules in aqueous solutions. It was important from the perspective of science and could contribute to decreasing the lack of understanding of the phenomena that rule the biomolecule solubility in water and its partitioning in biodegradable PEG – organic salt ATPS. The biomolecules considered in this work were DNP-AA: DNP-glycine, DNP-alanine, DNP-valine, and DNP-leucine, and water-soluble vitamins: ascorbic acid (VC), riboflavin (VB2), nicotinic acid ($VB3^{acid}$), nicotinamide ($VB3^{amide}$), folic acid (VB9), and cyanocobalamin (VB12). It was also the intention of the present study to add value to the research by introducing several thermodynamic modeling approaches designed specifically for predicting aqueous solubility, as well as phase separation and solute partitioning in ATPS. This was done to allow decreasing the number of experiments required in future studies.

The main objectives involved studying 1) the solubility of DNP-AA and vitamins in pure water, at different pH, and in the presence of additives (covitamins), 2) the phase equilibrium of ATPS formed of PEG and organic salt at T = 298.15 K and p = 1 bar, and 3) the partitioning of DNP-AA and vitamins in PEG – organic salt ATPS at T = 298.15 K and p = 1 bar. The solubility of DNP-AA and water-soluble vitamins in pure water, at different pH and in the presence of additives were evaluated at T = 298.15 K, p = 1 bar. However, just to provide an idea of the importance of pH effect and additive contribution into the solubility enhancement, the two additional aqueous solubility data points for each DNP-AA were measured in this work: at T = 308.15±0.1 K, p=1 bar and T = 318.15±0.1 K, p=1 bar (only in pure water, without additives). The temperature influence on solubility was evaluated also for vitamins, namely for $VB3^{acid}$ at T = 283.59 K – 332.01 K and for VC at T = 293 K – 323 K, and VB2 at T = 310.15 K, based on data found in literature.

Experimental measurements were carried out using different methods found in the literature and adjusted to the purpose of this work. Therefore, aqueous solubility was determined with the shake-flask method and spectrophotometry UV-VIS. The phase diagrams involving binodals and tie-line compositions were obtained with the cloud point method (binodals) and the procedures from the literature that involved conductivity measurements and freeze-drying (equilibrium concentrations). Experimental methodologies for studying the partitioning in ATPS were adopted from previous publications, but the concentrations of DNP-AA and vitamins in the two-phases have been acquired with UV-VIS and fluorescence spectrophotometry based on the preliminary

studies performed in this work. Density and osmotic coefficients were obtained with the oscillating U-tube density meter and freezing point depression osmometer only for the thermodynamic modeling purpose.

Electrolyte PC-SAFT (ePC-SAFT) with Debye-Hückel electrostatic contribution was chosen for modeling and predictions of different physicochemical properties of DNP-AA and vitamins and their partitioning in ATPS. This involved liquid-liquid and solid-liquid equilibria calculations. ePC-SAFT pure-component and binary interaction parameters of DNP-AA and water-soluble vitamins were estimated with different modeling strategies and used to accurately characterize the pure components and the non-ideality of their mixtures caused by interactions in aqueous solutions. The modeling methods: Molecular Method (MM) and Joint-Parameter Method (J-PM) were designed in this work specifically for the modeling of DNP-AA and water-soluble vitamins.

Molecules selected in this work DNP-AA, water-soluble vitamins, organic salts forming ATPS, may partially dissociate in aqueous solutions leading to the formation of different species of which presence depends on pH. For this reason, the study of the pH influence on the speciation was required. The charge of the components had to be considered while discussing experimental results and for the modeling and predicting the properties with ePC-SAFT. The pH change can influence the solubility of DNP-AA and vitamins. Thus, knowing the pH-solubility profiles is fundamental for understanding and controlling the behavior of these compounds in aqueous solutions. Dissociation constants K_a obtained from literature and intrinsic solubility data measured in this work were introduced to the Henderson-Hasselbalch-based solubility equations to obtain pH-solubility profiles. Similar equations but accounting for the non-ideality (deviations from Raoult´s Law) and involving fitted in this work thermodynamic dissociation constants $K_{a,th}$, were derived to estimate the solubility with ePC-SAFT. A comparison of $K_{a,th}$ and K_a allowed the conclusion that aqueous solutions containing DNP-AA and vitamins deviate from ideality, which is directly related to the fact that the activity-coefficient ratio between the species present in these systems is not unity.

The results of ePC-SAFT solubility predictions were in line with experimental data determined in this study. In regard to the solubility of DNP-AA, the trend observed was $m^L_{DNP-alanine} > m^L_{DNP-valine} > m^L_{DNP-glycine}$ and $m^L_{DNP-leucine}$. However, it is rather

uncertain which DNP-AA from the two least soluble, i.e. DNP-glycine or DNP-leucine, has higher solubility. The reason for that relates to the insignificant difference in solubility of DNP-glycine or DNP-leucine (within the experimental error). The aqueous solubility trend of DNP-AA (decreasing m^L_{DNP-AA}) follows the reversed trend of melting properties (increasing $T_{m,DNP-AA}$). Based on data from the literature for aliphatic AA, the solubility trends observed for DNP-AA and AA do not match ($m^L_{glycine} < m^L_{L-alanine} < m^L_{L-valine} < m^L_{L-leucine}$). Also, the solubility of each DNP-AA is of lower magnitude than for its parent aliphatic AA. The difference between DNP-AA and aliphatic amino acids is also in the dissociation equilibrium. In contrast to aliphatic amino acids that are amphoteric, DNP-AA are acidic components. Thus, a decrease of the pH leads to a lower DNP-AA solubility, while an increase of the pH enhances the solubility of DNP-AA. Regarding the vitamin solubility in water the following trend was observed $m^L_{VC} > m^L_{VB3acid} > m^L_{VB12} > m^L_{VB2} > m^L_{VB9}$. The melting properties could not be correlated with solubility data of each vitamin since the molecular structures of vitamins are very divergent. The vitamins considered in this thesis were either acidic (VC) or amphoteric (VB2, VB3^{acid}, VB9, and VB12). This means that in all cases, an increase in pH leads to an enhancement of vitamin solubility. Except for VC, the solubility can be improved by decreasing the pH.

The temperature effect on DNP-AA and vitamin solubility was only briefly outlined since the pH effect or the presence of additives have shown to be much more powerful in enhancing the solubility of low soluble DNP-AA and vitamins. However, as expected the solubility of all considered DNP-AA and water-soluble vitamins VC and VB3^{acid} increases together with an increase of the temperature. As an example, only slight DNP-AA solubility increase was observed when changing the temperature of 10 K or 20 K (T = 298.15 K – 318.15 K). In contrast, if the pH of DNP-AA solution increased only of 0.5 units (from pH = 4 to pH = 4.5), then more than a double increase of the DNP-AA solubility was found. Similar conclusions were obtained for vitamins. Thus, the alternative to the temperature moderation was addition of covitamins (VC and VB3) to solutions containing low-soluble vitamins. This phenomenon has been already called in literature as hydrotropic solubilization and involves not only VC and VB3, but also different molecules able to dissolve many poorly soluble compounds, e.g. Active Pharmaceutical Ingredients (API). Studies carried out in this work on the influence of different covitamins VC, VB3^{acid}, and VB3^{amide}, on poorly soluble vitamins VB2, VB9, and VB12, have shown that the

solubility of vitamins is related to the concentration of covitamin introduced to the vitamin solution and to the covitamin and vitamin type itself. Covitamin $VB3^{amide}$ has shown the highest potential over VC and $VB3^{acid}$ in enhancing the solubility of VB2, VB9, and VB12. To increase the solubility of VB2 to the comparable level, about a 5-fold higher concentration of covitamin VC than $VB3^{amide}$ was required. When adding the same concentration of covitamin $VB3^{amide}$ to aqueous solutions of VB2 and VB9, lead to about 100-fold solubility enhancement of VB9, while for VB2, a 15-fold increase was observed. It was found that there can be different covitamin effects ruling the enhancement of vitamin solubility. This possibly is related to the differences in the interplay of different factors, e.g. pH and interactions. Overall, it was proven that the so-called in literature "hydrotropes" can cause pH changes that strongly influence molecular interactions, species distribution, or even both.

ePC-SAFT allowed quantitative solubility prediction of vitamin VB2, VB9, VB12, upon addition of covitamins VC and VB3 ($VB3^{acid}$, $VB3^{amide}$). The predictions were classified into systems with minor and major species distribution change caused upon adding covitamin. In both considered system classes, predictions were in accurate agreement with experimental data without a need of introducing any additional parameter (minor species change: VB12 + $VB3^{amide}$, VB12 + $VB3^{acid}$, and VB2 + $VB3^{acid}$; major species change: VB2 + VC, VB2 + $VB3^{amide}$, VB9 + $VB3^{amide}$). This work revealed that adding covitamins at low concentration mainly has an impact on solubility by a pH change. At a certain covitamin concentration (specific for each vitamin + covitamin system), the molecular interactions can overcome the importance of the pH effect. Thus, predicting the solubility in a wide range of concentrations requires considering both molecular interactions and pH effects. This also raises some issues about the definition of "hydrotropes" given in literature. Based on the results obtained in this work, it is not recommended to assign the term of "hydrotrope" to components, but rather to use the term of "hydrotropic solubilization". Adding the covitamin at certain concentration leads to an increase of solubility by changing mainly the pH of a solution and even NaOH would be denoted a hydrotrope according to this definition.

Once the properties of DNP-AA and water-soluble vitamins were known (based on the experiments and predictions), the partitioning of these compounds in biodegradable PEG – organic salt was considered. Prior to this, the measurements and modeling of

experimental biphasic diagrams was carried out. ATPS under study were composed of PEG (average molar mass M_{PEG}: 4000, 6000, 8000 g·mol^{-1}) and biodegradable salt (N_3Citrate, K_3Citrate, Na_2Tartrate, and KNaTartrate), at T=298.15 K and p=1 bar. Using equations of Merchuk, of Othmer-Tobias, and of Bancroft, it was possible to accurately correlate experimental binodal and tie-line composition data. Experimental data was also used for a validation of ePC-SAFT model predictions. The overall AAD obtained from the comparison of predicted with ePC-SAFT and experimental equilibrium mass fractions of ATPS components in all considered ATPS (both phases, different tie-lines) was equal to 0.025 (2.5 wt%) which is a common result for predicting the LLE in literature. Almost quantitative ePC-SAFT predictions of LLE may relate to the accurate description of non-ideality of mixtures caused by different molecular interactions considered by ePC-SAFT. The largest biphasic regions were observed for ATPS formed by PEG 8000 and Na_3Citrate. This is an important finding in terms of the efficiency of phase separation in ATPS, since for ATPS of smaller biphasic area (e.g. PEG - K_3Citrate) more salt is needed to form ATPS. However, the solutions containing PEG 8000 are more viscous and this can be a drawback for industrial application. Salt selected to form ATPS has a stronger effect on phase separation and this influence relies not only on the kind of cation but also on the number of cations present in a molecule. However, the evaluation presented in this work has proven that ATPS phase forming compounds should be chosen based on a compromise between both the consumption of chemicals and partitioning efficiency, thus the practical industrial application insight.

The last part of this work involved partitioning of DNP-AA (DNP-glycine, DNP-alanine, DNP-valine, DNP-leucine) and water-soluble vitamins (VB2, VB3^{acid}, VB3^{amide}, VB9, VB12), at T = 298.15 K and p = 1 bar, in ATPS. Since the measurements were not only carried out in PEG (M_{PEG}: 4000, 6000, 8000 g·mol^{-1}) – organic salt (N_3Citrate, K_3Citrate, Na_2Tartrate, and KNaTartrate) ATPS, but also in PEG (M_{PEG}: 8000 g·mol^{-1}) – inorganic salt (Na_2Sulfate, MgSulfate) ATPS, data shown in this work could prove the merit of replacing inorganic salts to organic biodegradable alternatives. The partition coefficients of DNP-AA measured in PEG 8000 – Na_2Sulfate ATPS were very similar to data determined in PEG 8000 – Na_3Citrate ATPS. The highest partition coefficients K_i^{exp} values were obtained in systems formed by PEG of lower molar mass, namely PEG 4000, and of Na_3Citrate. A linear correlation between $\ln K_i^{exp}$ and TLL for all DNP-AA and vitamins partitioned in ATPS was

observed. Thus, K_i^{exp} depends on the concentration of all ATPS components. Experimental K_i^{exp} determined in this work follow the trends: $K_{DNP-leucine}^{exp} > K_{DNP-valine}^{exp} > K_{DNP-alanine}^{exp} > K_{DNP-glycine}^{exp}$ for DNP-AA and $K_{VB12}^{exp} > K_{VB9}^{exp} > K_{VB3}^{exp} > K_{VB2}^{exp}$ for vitamins. Partitioning trends for DNP-AA and vitamins do not follow the solubility trends: $m_{DNP-alanine}^{L} > m_{DNP-valine}^{L} > m_{DNP-glycine}^{L}$ and $m_{DNP-leucine}^{L}$ (for DNP-AA) and $m_{VB3amide}^{L} > m_{VB3acid}^{L} > m_{VB12}^{L} > m_{VB2}^{L} > m_{VB9}^{L}$ (for vitamins). This means that different phenomena rule the solubilization and partitioning of DNP-AA and vitamins in aqueous systems, thus, distinct types of interactions may dominate in controlling both properties.

ePC-SAFT predictions presented in this work confirmed that the number of experiments can be reduced if the partitioning approach designed in this work is applied. ePC-SAFT could accurately predict both solubility and partitioning in ATPS, although it is expected that different factors rule these behaviors. The quantitative predictions of DNP-AA and water-soluble vitamin partitioning in PEG – biodegradable salt ATPS were obtained after considering all interactions through introducing k_{ij} between DNP-AA and phase formers (water, Na^+, K^+, PEG) that describes the non-ideality of the mixtures. In this work, ePC-SAFT was capable to predict the partition coefficients qualitatively. By separating different effects that rule the separation it helped in evaluating which effects may dominate in the partitioning of different solutes. This is an outstanding result for practical ATPS application, since even having an extensive database of experimental partition coefficients values is not enough to unravel the phenomena that are behind the partitioning. The success of the present study was achieved based on non-ideality evaluation, towards activity coefficients γ_i^{∞} that were predicted with ePC-SAFT for different solutes, separated in the two phases of ATPS.

The partitioning of DNP-AA and water-soluble vitamins can be influenced by 1) electrostatic interactions resulting from partitioning of charged components in ATPS, 2) molecular size of DNP-AA or vitamin, 3) other interactions of DNP-AA or vitamin with phase formers (e.g. hydrogen bonding, hydrophobic interactions). These factors are dependent among others on PEG molar mass, salt type, ATPS composition expressed as tie-line length (*TLL*). The partitioning of DNP-AA and water-soluble vitamins depends on pH in a way, that in aqueous solutions of pH~8 (pH of ATPS) can be present as species with different charge states, and additionally, these species can have different partition coefficients in ATPS. At pH~8 of ATPS the solutes considered in this work are present as

neutral ($VB3^{amide}$, VB12) or negatively charged species (DNP-$glycine^-$, DNP-$alanine^-$, DNP-$valine^-$, DNP-$leucine^-$, $VB2^-$, $VB3^{acid-}$, $VB9^{2-}$, $VB9^{3-}$). Since DNP-AA and water-soluble vitamins are usually present at very small concentrations, the ePC-SAFT partitioning approach was based on predicting the infinite dilution activity coefficient γ_j^{∞} of DNP-AA or vitamin species in the two phases of ATPS. The present work also confirms that the side chains of amino acids, namely the number of methylene groups and related to this hydrophobicity, mainly determine the partitioning of DNP-AA (the highest – DNP-leucine, the lowest – DNP-glycine). The partition coefficients that were accurately predicted with ePC-SAFT followed the reversed order of aliphatic amino acid solubility (the highest – glycine, the lowest – leucine), rather than the sequence of DNP-AA solubility (the highest – DNP-alanine).

Based on ePC-SAFT predictions the three different effects on activity coefficients γ_i^{∞} of DNP-AA or vitamin could be found. The most common trend observed in this work was the increase of activity coefficient in the bottom phase and decrease in the top phase (all considered DNP-AA, $VB3^{acid}$ and $VB3^{amide}$). The possible reason for such non-ideality might be the repulsive interactions of vitamin and salt ions and the attractive interactions of vitamin to PEG. Other behavior in ATPS was seen for VB2 and VB9. Therefore, it was found that in both top and bottom phase of ATPS considered in this work, the values of $\gamma_{vitamin}^{\infty}$ increase together with an increase of TLL. Some molecular structure features might be the reason of such behavior. Increasing trend of $\gamma_{vitamin}^{\infty}$ in both phases can mean that in both phases different contributions are competing. The non-ideality trend observed for VB12 is different from the two previous behaviors. It shows a decrease of γ_{VB12}^{∞} over increasing TLL in both ATPS phases. This effect might be related with the effects related to the size of VB12 and the presence of many functional groups in a molecule. In ATPS considered in this work, VB12 is present solely as neutral species. Therefore, electrostatic interactions of VB12 and ATPS phase forming components might not be significant in predicting the partitioning. A high affinity of VB12 to PEG-rich phase can result from hydrophobic interactions to PEG or hydrogen-bonding effects between PEG and VB12. All these effects are considered explicitly in ePC-SAFT predictions.

This elaboration, although being significant contribution to the understanding the solubilization of DNP-AA and water-soluble vitamins and their partitioning in ATPS, opens at least several research lines to new possible topics that could finally allow

implementing ATPS in industry. This could be among others the application or design of different methods able to unravel the solubility and partitioning behavior at the molecular level. Such a deep understanding of solubility and partitioning would allow better screening for the possible solubilizers or separation systems. It could be also beneficial from the perspective of designing and optimizing novel ATPS. However, the screening for new systems could be done as well using approaches for ePC-SAFT modeling and predictions provided in this work. These approaches might be further applied for predicting the solubility and partitioning in different ATPS. A very important issue that should also be considered in future research is the recovery of partitioned solutes from the ATPS phases. Since the present thesis provides already theoretical, experimental, and modeling background, it can contribute to the scale-up of the partitioning in ATPS. This could be done by performing further experiments on a Mixer-Settler. Another aspect that should catch the attention of scientific research is related to gaining a better understanding and improvement of the dynamics of partitioning (the present work provides just a “stationary” approach to partitioning). This could be done through performing the simulations of separation and by building or applying the tools which could be beneficial in the design and optimization of a process.

References

1. Wysoczanska, K., et al., *Cation effect on the (PEG 8000+ sodium sulfate) and (PEG 8000+ magnesium sulfate) aqueous two-phase system: Relative hydrophobicity of the equilibrium phases.* The Journal of Chemical Thermodynamics, 2015. **91**: p. 321-326.
2. Wysoczanska, K. and E.n.A. Macedo, *Influence of the molecular weight of peg on the polymer/salt phase diagrams of aqueous two-phase systems.* Journal of Chemical & Engineering Data, 2016. **61**(12): p. 4229-4235.
3. Wysoczanska, K. and E.A. Macedo, *Effect of molecular weight of polyethylene glycol on the partitioning of DNP-amino acids: PEG (4000, 6000) with sodium citrate at 298.15 K.* Fluid Phase Equilibria, 2016. **428**: p. 84-91.
4. Wysoczanska, K., et al., *Effect of different organic salts on amino acids partition behaviour in PEG-salt ATPS.* Fluid Phase Equilibria, 2018. **456**: p. 84-91.
5. Wysoczanska, K., et al., *Toward Thermodynamic Predictions of Aqueous Vitamin Solubility: An Activity Coefficient-Based Approach.* Industrial & Engineering Chemistry Research, 2019. **58**(17): p. 7362-7369.
6. Wysoczanska, K., et al., *Solubility enhancement of vitamins in water in the presence of covitamins: measurements and ePC-SAFT predictions.* Industrial & Engineering Chemistry Research, 2019.
7. Wysoczanska, K., et al., *Partitioning of water-soluble vitamins in biodegradable ATPS: ePC-SAFT predictions and experimental validation.* American Institute of Chemical Engineers, 2020 (accepted).
8. Wysoczanska, K., et al., *Predicting the solubility of DNP-amino acids and their partitioning in biodegradable ATPS: experimental and ePC-SAFT modeling.* American Institute of Chemical Engineers, 2020 (submitted).
9. Ribeiro, S.S., et al., *The synergic effect of water and biomolecules in intracellular phase separation.* Nature Reviews Chemistry, 2019. **3**(9): p. 552-561.
10. Hayashi, T., *Statistical Thermodynamics on the Binding of Biomolecules*, in *The Role of Water in ATP Hydrolysis Energy Transduction by Protein Machinery*. 2018, Springer. p. 203-227.
11. Español, E.S. and M.M. Villamil, *Calixarenes: generalities and their role in improving the solubility, biocompatibility, stability, bioavailability, detection, and transport of biomolecules.* Biomolecules, 2019. **9**(3): p. 90.
12. Mizera, M., et al., *Computer-Aided Design of Cefuroxime Axetil/Cyclodextrin System with Enhanced Solubility and Antimicrobial Activity.* Biomolecules, 2020. **10**(1): p. 24.
13. Jhala, D., H. Rather, and R. Vasita, *Nano-delivery of Food-Derived Biomolecules: An Overview*, in *Functional Food and Human Health*. 2018, Springer. p. 447-470.
14. Soppimath, K.S., et al., *Multifunctional Core/Shell Nanoparticles Self-Assembled from pH-Induced Thermosensitive Polymers for Targeted Intracellular Anticancer Drug Delivery.* Advanced Functional Materials, 2007. **17**(3): p. 355-362.
15. Khosravian, P., et al., *Mesoporous silica nanoparticles functionalized with folic acid/methionine for active targeted delivery of docetaxel.* OncoTargets and therapy, 2016. **9**: p. 7315.
16. Poschlad, K. and S. Enders, *Thermodynamics of aqueous solutions containing poly (N-isopropylacrylamide) and vitamin C.* Fluid Phase Equilibria, 2011. **302**(1): p. 153-160.
17. Lane, M. and D.K. Gardner, *Amino acids and vitamins prevent culture-induced metabolic perturbations and associated loss of viability of mouse blastocysts.* Human reproduction (Oxford, England), 1998. **13**(4): p. 991-997.

18. Shi, X.-Y. and T.-W. Tan, *Preparation of chitosan/ethylcellulose complex microcapsule and its application in controlled release of Vitamin D2.* Biomaterials, 2002. **23**(23): p. 4469-4473.
19. Pardeike, J., et al., *Nanosuspensions as advanced printing ink for accurate dosing of poorly soluble drugs in personalized medicines.* International Journal of Pharmaceutics, 2011. **420**(1): p. 93-100.
20. Zhao, P., et al., *Paclitaxel loaded folic acid targeted nanoparticles of mixed lipid-shell and polymer-core: In vitro and in vivo evaluation.* European Journal of Pharmaceutics and Biopharmaceutics, 2012. **81**(2): p. 248-256.
21. Zhang, R. and W. Chen, *Nitrogen-doped carbon quantum dots: Facile synthesis and application as a "turn-off" fluorescent probe for detection of Hg2+ ions.* Biosensors and Bioelectronics, 2014. **55**: p. 83-90.
22. Nayaka, G.P., et al., *Dissolution of cathode active material of spent Li-ion batteries using tartaric acid and ascorbic acid mixture to recover Co.* Hydrometallurgy, 2016. **161**: p. 54-57.
23. Li, L., et al., *Ascorbic-acid-assisted recovery of cobalt and lithium from spent Li-ion batteries.* Journal of Power Sources, 2012. **218**: p. 21-27.
24. Zuo, P., et al., *Ascorbic acid-assisted solvothermal synthesis of LiMn0.9Fe0.1PO4/C nanoplatelets with enhanced electrochemical performance for lithium ion batteries.* Journal of Power Sources, 2013. **243**: p. 872-879.
25. Chaudhari, N.K., et al., *Hematite (α-Fe2O3) nanoparticles on vulcan carbon as an ultrahigh capacity anode material in lithium ion battery.* Electrochimica Acta, 2013. **114**: p. 60-67.
26. Wu, S., et al., *Amino Acid-Assisted Hydrothermal Synthesis and Photocatalysis of SnO2 Nanocrystals.* The Journal of Physical Chemistry C, 2009. **113**(41): p. 17893-17898.
27. Jia, D., et al., *Dual Passivation of CsPbI3 Perovskite Nanocrystals with Amino Acid Ligands for Efficient Quantum Dot Solar Cells.* Small. **n/a**(n/a): p. 2001772.
28. Kango, N., *Textbook of microbiology*. 2010: IK International Pvt Ltd.
29. Holmberg, K., *Novel surfactants: preparation applications and biodegradability, revised and expanded*. Vol. 114. 2003: Crc Press.
30. Tripathy, D.B., et al., *Synthesis, chemistry, physicochemical properties and industrial applications of amino acid surfactants: A review.* Comptes Rendus Chimie, 2018. **21**(2): p. 112-130.
31. Molina, G., et al., *Bioprocessing for Biomolecules Production*. 2019: Wiley Online Library.
32. Tarento, T.D., et al., *A potential biotechnological process for the sustainable production of vitamin K1.* Critical reviews in biotechnology, 2019. **39**(1): p. 1-19.
33. Khezeli, T., et al., *Chapter 9 - Deep eutectic solvent in separation and preconcentration of organic and inorganic species*, in *New Generation Green Solvents for Separation and Preconcentration of Organic and Inorganic Species*, M. Soylak and E. Yilmaz, Editors. 2020, Elsevier. p. 381-423.
34. Ferreira, A.M., et al., *An integrated process for enzymatic catalysis allowing product recovery and enzyme reuse by applying thermoreversible aqueous biphasic systems.* Green chemistry, 2018. **20**(6): p. 1218-1223.
35. Hanefeld, U., L. Cao, and E. Magner, *Enzyme immobilisation: fundamentals and application.* Chemical Society Reviews, 2013. **42**(15): p. 6211-6212.
36. Wang, L., et al., *Green separation of bromelain in food sample with high retention of enzyme activity using recyclable aqueous two-phase system containing a new synthesized thermo-responsive copolymer and salt.* Food Chemistry, 2019. **282**: p. 48-57.
37. Cunha, E.V. and M.n. Aznar, *Liquid– liquid equilibrium in aqueous two-phase (water+ PEG 8000+ salt): Experimental determination and thermodynamic modeling.* Journal of Chemical & Engineering Data, 2009. **54**(12): p. 3242-3246.
38. Mousavi Khaneghah, A., et al., *8 - Water-soluble vitamins ☆*, in *Innovative Thermal and Non-Thermal Processing, Bioaccessibility and Bioavailability of Nutrients and Bioactive Compounds*, F.J. Barba, et al., Editors. 2019, Woodhead Publishing. p. 241-266.

39. Randaccio, L., et al., *Vitamin B12: unique metalorganic compounds and the most complex vitamins.* Molecules, 2010. **15**(5): p. 3228-3259.
40. Ahmad, I., et al., *Effect of ascorbic acid on the degradation of cyanocobalamin and hydroxocobalamin in aqueous solution: A kinetic study.* AAPS PharmSciTech, 2014. **15**(5): p. 1324-1333.
41. Juzeniene, A. and Z. Nizauskaite, *Photodegradation of cobalamins in aqueous solutions and in human blood.* Journal of Photochemistry and Photobiology B: Biology, 2013. **122**: p. 7-14.
42. Taub, A. and H. Lieberman, *Stability of vitamin B12—Folic acid parenteral solutions.* Journal of the American Pharmaceutical Association, 1953. **42**(4): p. 183-186.
43. Ferreira, L., et al., *Effect of salt additives on protein partition in polyethylene glycol–sodium sulfate aqueous two-phase systems.* Biochimica et Biophysica Acta (BBA) - Proteins and Proteomics, 2013. **1834**(12): p. 2859-2866.
44. Gulyaeva, N., et al., *pH dependence of the relative hydrophobicity and lipophilicity of amino acids and peptides measured by aqueous two-phase and octanol–buffer partitioning.* The Journal of peptide research, 2003. **61**(2): p. 71-79.
45. Madeira, P.P., et al., *Analysis of amino acid–water interactions by partitioning in aqueous two-phase systems. I—Amino acids with non-polar side-chains.* Journal of Chromatography A, 2013. **1274**: p. 82-86.
46. Zaslavsky, B.Y., et al., *Measurement of relative hydrophobicity of amino acid side-chains by partition in an aqueous two-phase polymeric system: Hydrophobicity scale for non-polar and ionogenic side-chains.* Journal of Chromatography A, 1982. **240**(1): p. 21-28.
47. Zaslavsky, B.Y., et al., *Phase separation in aqueous poly (ethylene glycol)-(NH4) 2SO4 systems and some physicochemical properties of the phases.* Journal of colloid and interface science, 1990. **137**(1): p. 147-156.
48. da Silva, N.R., et al., *Effects of sodium chloride and sodium perchlorate on properties and partition behavior of solutes in aqueous dextran-polyethylene glycol and polyethylene glycol-sodium sulfate two-phase systems.* Journal of Chromatography A, 2019. **1583**: p. 28-38.
49. Madeira, P.P., et al., *Cooperativity between various types of polar solute–solvent interactions in aqueous media.* Journal of Chromatography A, 2015. **1408**: p. 108-117.
50. Dewick, P.M., *Essentials of organic chemistry: for students of pharmacy, medicinal chemistry and biological chemistry*. 2006: John Wiley & Sons.
51. Avdeef, A., et al., *Equilibrium solubility measurement of ionizable drugs–consensus recommendations for improving data quality.* ADMET and DMPK, 2016. **4**(2): p. 117-178.
52. Kim, J.Y., et al., *Hydrotropic Solubilization of Poorly Water-Soluble Drugs.* Journal of Pharmaceutical Sciences, 2010. **99**(9): p. 3953-3965.
53. Shimizu, S. and N. Matubayasi, *Hydrotropy: Monomer–Micelle equilibrium and minimum hydrotrope concentration.* The Journal of Physical Chemistry B, 2014. **118**(35): p. 10515-10524.
54. Shimizu, S. and N. Matubayasi, *The origin of cooperative solubilisation by hydrotropes.* Physical Chemistry Chemical Physics, 2016. **18**(36): p. 25621-25628.
55. Booth, J.J., et al., *Hydrotrope accumulation around the drug: the driving force for solubilization and minimum hydrotrope concentration for nicotinamide and urea.* Physical Chemistry Chemical Physics, 2015. **17**(12): p. 8028-8037.
56. Stegemann, S., et al., *When poor solubility becomes an issue: From early stage to proof of concept.* European Journal of Pharmaceutical Sciences, 2007. **31**(5): p. 249-261.
57. Aulton, M.E. and K.M. Taylor, *Aulton's Pharmaceutics E-Book: The Design and Manufacture of Medicines*. 2017: Elsevier Health Sciences.
58. Kumar, V.S., C. Raja, and C. Jayakumar, *A review on solubility enhancement using hydrotropic phenomena.* Int. J. Pharm. Pharm. Sci, 2014. **6**(6): p. 1-7.
59. Neuberg, C., *Hydrotropic phenomena.* Biochem. Z, 1916. **76**(107): p. 107-176.
60. Avdeef, A., *Solubility of sparingly-soluble ionizable drugs.* Advanced Drug Delivery Reviews, 2007. **59**(7): p. 568-590.

61. Serajuddin, A.T., *Salt formation to improve drug solubility.* Advanced drug delivery reviews, 2007. **59**(7): p. 603-616.
62. Mota, F.L., et al., *Solubility of drug-like molecules in pure organic solvents with the CPA EoS.* Fluid Phase Equilibria, 2011. **303**(1): p. 62-70.
63. Moodley, K., J. Rarey, and D. Ramjugernath, *Model evaluation for the prediction of solubility of active pharmaceutical ingredients (APIs) to guide solid–liquid separator design.* Asian Journal of Pharmaceutical Sciences, 2018. **13**(3): p. 265-278.
64. Schröder, B., et al., *Prediction of aqueous solubilities of solid carboxylic acids with COSMO-RS.* Fluid Phase Equilibria, 2010. **289**(2): p. 140-147.
65. Laube, F., T. Klein, and G. Sadowski, *Partition Coefficients of Pharmaceuticals as Functions of Temperature and pH.* Industrial & Engineering Chemistry Research, 2015. **54**(15): p. 3968-3975.
66. Lange, L., K. Lehmkemper, and G. Sadowski, *Predicting the aqueous solubility of pharmaceutical cocrystals as a function of pH and temperature.* Crystal Growth & Design, 2016. **16**(5): p. 2726-2740.
67. Jeffrey, G.A. and W. Saenger, *Hydrogen bonding in biological structures*. 2012: Springer Science & Business Media.
68. Lund, M. and B. Jönsson, *Charge regulation in biomolecular solution.* Quarterly reviews of biophysics, 2013. **46**(3): p. 265-281.
69. Chen, C.-C., et al., *Local composition model for excess Gibbs energy of electrolyte systems. Part I: Single solvent, single completely dissociated electrolyte systems.* AIChE Journal, 1982. **28**(4): p. 588-596.
70. Fredenslund, A., R.L. Jones, and J.M. Prausnitz, *Group-contribution estimation of activity coefficients in nonideal liquid mixtures.* AIChE Journal, 1975. **21**(6): p. 1086-1099.
71. Klamt, A. and G. Schüürmann, *COSMO: a new approach to dielectric screening in solvents with explicit expressions for the screening energy and its gradient.* Journal of the Chemical Society, Perkin Transactions 2, 1993(5): p. 799-805.
72. Kontogeorgis, G.M., et al., *An Equation of State for Associating Fluids.* Industrial & Engineering Chemistry Research, 1996. **35**(11): p. 4310-4318.
73. Chapman, W.G., et al., *SAFT: Equation-of-state solution model for associating fluids.* Fluid Phase Equilibria, 1989. **52**: p. 31-38.
74. Cameretti, L.F., G. Sadowski, and J.M. Mollerup, *Modeling of aqueous electrolyte solutions with perturbed-chain statistical associated fluid theory.* Industrial & Engineering Chemistry Research, 2005. **44**(9): p. 3355-3362.
75. Gross, J. and G. Sadowski, *Perturbed-chain SAFT: An equation of state based on a perturbation theory for chain molecules.* Industrial & engineering chemistry research, 2001. **40**(4): p. 1244-1260.
76. Gross, J. and G. Sadowski, *Application of the perturbed-chain SAFT equation of state to associating systems.* Industrial & engineering chemistry research, 2002. **41**(22): p. 5510-5515.
77. Choscz, C., et al., *Measurement and Modeling of Lactose Solubility in Aqueous Electrolyte Solutions.* Industrial & Engineering Chemistry Research, 2019. **58**(45): p. 20797-20805.
78. Grosse Daldrup, J.-B., et al., *Measurement and modeling solubility of aqueous multisolute amino-acid solutions.* Industrial & engineering chemistry research, 2010. **49**(3): p. 1395-1401.
79. Held, C., L.F. Cameretti, and G. Sadowski, *Measuring and modeling activity coefficients in aqueous amino-acid solutions.* Industrial & Engineering Chemistry Research, 2010. **50**(1): p. 131-141.
80. Held, C., *Measuring and Modeling Thermodynamic Properties of Biological Solutions*. 2011: Verlag Dr. Hut.
81. Held, C., et al., *Measuring and modeling aqueous electrolyte/amino-acid solutions with ePC-SAFT.* The Journal of Chemical Thermodynamics, 2014. **68**: p. 1-12.

82. Rose, H.B., et al., *Mutual Influence of Furfural and Furancarboxylic Acids on Their Solubility in Aqueous Solutions: Experiments and Perturbed-Chain Statistical Associating Fluid Theory (PC-SAFT) Predictions.* Journal of Chemical & Engineering Data, 2018. **63**(5): p. 1460-1470.
83. Held, C. and G. Sadowski, *Thermodynamics of bioreactions.* Annual review of chemical and biomolecular engineering, 2016. **7**: p. 395-414.
84. Mohammad, S., et al., *Influence of Salts on the Partitioning of 5-Hydroxymethylfurfural in Water/MIBK.* The Journal of Physical Chemistry B, 2016. **120**(16): p. 3797-3808.
85. Albertsson, P., *Aqueous polymer-phase systems.* Partition of Cell Particles and Macromolecules: Separation and Purification of Biomolecules, Cell Organelles, Membranes, and Cells in Aqueous Polymer Two-Phase Systems and Their Use in Biochemical Analysis and Biotechnology, 1986.
86. Walter, H., *Partitioning in aqueous two–phase system: theory, methods, uses, and applications to biotechnology*. 2012: Elsevier.
87. Walter, H., D.E. Brooks, and D. Fisher, *Partitioning in aqueous two-phase systems*. 1985, Elsevier.
88. Zaslavsky, B.Y., *Aqueous two-phase partitioning: physical chemistry and bioanalytical applications*. 1994: CRC press.
89. Phong, W.N., et al., *Recovery of biotechnological products using aqueous two phase systems.* Journal of Bioscience and Bioengineering, 2018. **126**(3): p. 273-281.
90. Dutra Molino, J., et al., *Biomolecules extracted by ATPS: practical examples.* 2014.
91. Azevedo, A.M., et al., *Chromatography-free recovery of biopharmaceuticals through aqueous two-phase processing.* Trends in Biotechnology, 2009. **27**(4): p. 240-247.
92. Atefi, E., et al., *Interfacial tension effect on cell partition in aqueous two-phase systems.* ACS applied materials & interfaces, 2015. **7**(38): p. 21305-21314.
93. Ferreira, G.B., et al., *Partitioning optimization of proteins from Zea mays malt in ATPS PEG 6000/CaCl2.* Brazilian Archives of Biology and Technology, 2007. **50**(3): p. 557-564.
94. Madadi, B., G. Pazuki, and B. Nasernejad, *Partitioning of cefazolin in biocompatible aqueous biphasic systems based on surfactant.* Journal of Chemical & Engineering Data, 2013. **58**(10): p. 2785-2792.
95. Raja, S., et al., *Aqueous two phase systems for the recovery of biomolecules–a review.* Sci Technol, 2011. **1**(1): p. 7-16.
96. Cleland, J.L., C. Hedgepeth, and D. Wang, *Polyethylene glycol enhanced refolding of bovine carbonic anhydrase B. Reaction stoichiometry and refolding model.* Journal of Biological Chemistry, 1992. **267**(19): p. 13327-13334.
97. Silvério, S.C., et al., *Gibbs free energy of transfer of a methylene group on {UCON+(sodium or potassium) phosphate salts} aqueous two-phase systems: Hydrophobicity effects.* The Journal of Chemical Thermodynamics, 2010. **42**(8): p. 1063-1069.
98. Perez, B., et al., *Experimental determination and thermodynamic modeling of phase equilibrium and protein partitioning in aqueous two-phase systems containing biodegradable salts.* The Journal of Chemical Thermodynamics, 2013. **56**: p. 136-143.
99. Boaglio, A., et al., *Features of the milk whey protein partitioning in polyethyleneglycol-sodium citrate aqueous two-phase systems with the goal of isolating human alpha-1 antitrypsin expressed in bovine milk.* Journal of Chromatography B, 2006. **837**(1-2): p. 18-23.
100. Kalaivani, S. and I. Regupathi, *Partitioning studies of α-lactalbumin in environmental friendly poly (ethylene glycol)—citrate salt aqueous two phase systems.* Bioprocess and biosystems engineering, 2013. **36**(10): p. 1475-1483.
101. Nascimento, S.S., et al., *Assessment of the purification of phycobiliproteins in cyanobacteria through aqueous two-phase systems with different proportions of PEG/salt.* Food and Bioproducts Processing, 2020. **119**: p. 345-349.
102. Marcos, J., et al., *Variation of penicillin acylase partition coefficient with phase volume ratio in poly (ethylene glycol)–sodium citrate aqueous two-phase systems.* Journal of Chromatography B: Biomedical Sciences and Applications, 1998. **711**(1-2): p. 295-299.

103. Junior, J.A., et al., *Sequential degradation of raw vinasse by a laccase enzyme producing fungus Pleurotus sajor-caju and its ATPS purification.* Biotechnology Reports, 2020. **25**: p. e00411.
104. Malpiedi, L.P., et al., *Role of polymer–protein interaction on partitioning pattern of bovine pancreatic trypsinogen and alpha-chymotrypsinogen in polyethyleneglycol/sodium tartrate aqueous two-phase systems.* Journal of Chromatography B, 2010. **878**(21): p. 1831-1836.
105. Shahriari, S., S.G. Doozandeh, and G. Pazuki, *Partitioning of cephalexin in aqueous two-phase systems containing poly (ethylene glycol) and sodium citrate salt at different temperatures.* Journal of Chemical & Engineering Data, 2012. **57**(2): p. 256-262.
106. Ghaffari, S., et al., *Partitioning of cefazolin in aqueous two-phase systems containing poly (ethylene glycol) and sodium salts (citrate, tartrate, and sulphate).* Fluid Phase Equilibria, 2019. **488**: p. 54-61.
107. Li, Y., et al., *Partition behavior of spiramycin in an aqueous two-phase system based on polyethylene glycol and sulfates.* Separation Science and Technology, 2018. **53**(3): p. 496-502.
108. Vobecká, L., et al., *Enzyme synthesis of cephalexin in continuous-flow microfluidic device in ATPS environment.* Chemical Engineering Journal, 2020. **396**: p. 125236.
109. Ramakrishnan, V., et al., *Extraction and purification of lipase from Enterococcus faecium MTCC5695 by PEG/phosphate aqueous-two phase system (ATPS) and its biochemical characterization.* Biocatalysis and Agricultural Biotechnology, 2016. **6**: p. 19-27.
110. Nascimento, C.O., et al., *Purification of a lectin from Cratylia mollis crude extract seed by a single step PEG/phosphate aqueous two-phase system.* Preparative Biochemistry & Biotechnology, 2020: p. 1-9.
111. Sun, T., et al., *Recovery of vanadium using an aqueous two-phase system consisting of poly (ethylene glycol) 2000 and sodium sulfate.* Hydrometallurgy, 2019. **189**: p. 105135.
112. Rodrigues Barreto, C.u.L., et al., *Liquid–Liquid Equilibrium Data and Thermodynamic Modeling for Aqueous Two-Phase System Peg 1500+ Sodium Sulfate+ Water at Different Temperatures.* Journal of Chemical & Engineering Data, 2019. **64**(2): p. 810-816.
113. Gonzalez-Amado, M., et al., *The effect of temperature on polyethylene glycol (4000 or 8000)–(sodium or ammonium) sulfate Aqueous Two Phase Systems.* Fluid Phase Equilibria, 2016. **428**: p. 95-101.
114. de Araujo Sampaio, D., et al., *Aqueous two-phase (polyethylene glycol+sodium sulfate) system for caffeine extraction: Equilibrium diagrams and partitioning study.* The Journal of Chemical Thermodynamics, 2016. **98**: p. 86-94.
115. Ananthapadmanabhan, K. and E. Goddard, *Aqueous biphase formation in polyethylene oxide-inorganic salt systems.* Langmuir, 1987. **3**(1): p. 25-31.
116. Snyder, S.M., K.D. Cole, and D.C. Szlag, *Phase compositions, viscosities, and densities for aqueous two-phase systems composed of polyethylene glycol and various salts at 25. degree. C.* Journal of Chemical and Engineering Data, 1992. **37**(2): p. 268-274.
117. Huddleston, J.G., H.D. Willauer, and R.D. Rogers, *Phase diagram data for several PEG+ salt aqueous biphasic systems at 25 C.* Journal of Chemical & Engineering Data, 2003. **48**(5): p. 1230-1236.
118. McNaughton, L.R., et al., *Buffering agents: Sodium Bicarbonate, Sodium Citrate, and Sodium Phosphate, In Hoffman, J.(Ed.) Dietary Supplementation in Sport and Exercise: Evidence, Safety, and Ergogenic Benefits.* 2018.
119. Additives, E.P.o.F., et al., *Re-evaluation of l (+)-tartaric acid (E 334), sodium tartrates (E 335), potassium tartrates (E 336), potassium sodium tartrate (E 337) and calcium tartrate (E 354) as food additives.* EFSA Journal, 2020. **18**(3): p. e06030.
120. Fletcher, C., A. Lowther, and W. Reith, *Studies on the determination of the sequence of amino acids in peptides and proteins. 2. The separation of the methyl esters of N-2: 4-dinitrophenyl derivatives of amino acids by adsorption chromatography and the free amino groups of insulin.* Biochemical Journal, 1954. **56**(1): p. 106.

121. Sanger, F. and E. Thompson, *The amino-acid sequence in the glycyl chain of insulin. 1. The identification of lower peptides from partial hydrolysates.* Biochemical Journal, 1953. **53**(3): p. 353.
122. Lockhart, I. and E. Abraham, *The amino acid sequence in bacitracin A.* Biochemical Journal, 1954. **58**(4): p. 633.
123. Warner, C.M., et al., *The immune response of allophenic mice to 2, 4-dinitrophenyl (DNP)-bovine gamma globulin. I. Allotype analysis of anti-DNP antibody.* The Journal of experimental medicine, 1978. **147**(6): p. 1849-1853.
124. Feldmann, M. and A. Basten, *Cell interactions in the immune response in vitro. I. Metabolic activities of T cells in a collaborative antibody response.* European journal of immunology, 1972. **2**(3): p. 213-224.
125. Thanzeel, F.Y. and C. Wolf, *Substrate-specific amino acid sensing using a molecular D/L-cysteine probe for comprehensive stereochemical analysis in aqueous solution.* Angewandte Chemie International Edition, 2017. **56**(25): p. 7276-7281.
126. Kim, I.-W., et al., *9-O-(Phenylcarbamoyl) quinine-bonded carbon-clad zirconia for chiral separation of racemic 2, 4-dinitrophenyl amino acids in RPLC.* Bulletin of the Korean Chemical Society, 2006. **27**(4): p. 589-592.
127. Rao, K.R. and H.A. Sober, *Preparation and properties of 2, 4-dinitrophenyl-L-amino acids.* Journal of the American Chemical Society, 1954. **76**(5): p. 1328-1331.
128. Abderhalden, E. and P. Blumberg, *Derivate von Aminosäuren.* Hoppe-Seyler´ s Zeitschrift für physiologische Chemie, 1910. **65**(4): p. 318-322.
129. Rice, H. and F. Sowden, *X-ray Diffraction Patterns of Dinitrophenyl Derivatives of Amino Compounds.* Canadian Journal of Chemistry, 1952. **30**(8): p. 575-580.
130. Ramachandran, L. and L. Sastry, *Spectrometric evaluation of the approximate pK of the carboxyl group in 2, 4-dinitrophenyl-amino acids.* Biochemistry, 1962. **1**(1): p. 75-78.
131. Reynolds, E., et al., *Anticonvulsant therapy, folic acid and vitamin B12 metabolism and mental symptoms.* Epilepsia, 1966. **7**(4): p. 261-270.
132. Huskisson, E., S. Maggini, and M. Ruf, *The role of vitamins and minerals in energy metabolism and well-being.* Journal of international medical research, 2007. **35**(3): p. 277-289.
133. Yoshii, K., et al., *Metabolism of dietary and microbial vitamin B family in the regulation of host immunity.* Frontiers in nutrition, 2019. **6**: p. 48.
134. Balasubramaniam, S., J. Christodoulou, and S. Rahman, *Disorders of riboflavin metabolism.* Journal of inherited metabolic disease, 2019. **42**(4): p. 608-619.
135. Combs Jr, G.F., *The vitamins: fundamental aspects in nutrition and health*. 2007: Academic press.
136. Drouin, G., J.-R. Godin, and B. Pagé, *The genetics of vitamin C loss in vertebrates.* Current genomics, 2011. **12**(5): p. 371-378.
137. Eitenmiller, R.R., W. Landen Jr, and L. Ye, *Vitamin analysis for the health and food sciences*. 2016: CRC press.
138. Kennedy, R. and A. Abd-Elsayed, *Vitamins and Supplements*, in *Pain*. 2019, Springer. p. 329-333.
139. Ströhle, A., et al., *The Revised D-A-CH-Reference Values for the Intake of Vitamin B12: Prevention of Deficiency and Beyond.* Molecular nutrition & food research, 2019. **63**(6): p. 1801178.
140. Maiorova, L.A., et al., *Encapsulation of vitamin B12 into nanoengineered capsules and soft matter nanosystems for targeted delivery.* Colloids and Surfaces B: Biointerfaces, 2019. **182**: p. 110366.
141. Mazzocato, M.C., M. Thomazini, and C.S. Favaro-Trindade, *Improving stability of vitamin B12 (Cyanocobalamin) using microencapsulation by spray chilling technique.* Food Research International, 2019. **126**: p. 108663.
142. Rehman, A., et al., *Pectin polymers as wall materials for the nano-encapsulation of bioactive compounds.* Trends in Food Science & Technology, 2019.

143. Alavijeh, M.A., M.N. Sarvi, and Z.R. Afarani, *Modified montmorillonite nanolayers for nano-encapsulation of biomolecules.* Heliyon, 2019. **5**(3): p. e01379.
144. Descombes, E., A.B. Hanck, and G. Fellay, *Water soluble vitamins in chronic hemodialysis patients and need for supplementation.* Kidney International, 1993. **43**(6): p. 1319-1328.
145. Lucock, M., *Folic Acid: Nutritional Biochemistry, Molecular Biology, and Role in Disease Processes.* Molecular Genetics and Metabolism, 2000. **71**(1): p. 121-138.
146. Nayak, S., et al., *Folate-Mediated Cell Targeting and Cytotoxicity Using Thermoresponsive Microgels.* Journal of the American Chemical Society, 2004. **126**(33): p. 10258-10259.
147. Preedy, V.R., *B vitamins and folate: chemistry, analysis, function and effects*. 2012: Royal Society of Chemistry.
148. Yalkowsky, S.H., Y. He, and P. Jain, *Handbook of aqueous solubility data*. 2016: CRC press.
149. Shalmashi, A. and A. Eliassi, *Solubility of L-(+)-ascorbic acid in water, ethanol, methanol, propan-2-ol, acetone, acetonitrile, ethyl acetate, and tetrahydrofuran from (293 to 323) K.* Journal of Chemical & Engineering Data, 2008. **53**(6): p. 1332-1334.
150. Gonçalves, E.M. and M.E. Minas da Piedade, *Solubility of nicotinic acid in water, ethanol, acetone, diethyl ether, acetonitrile, and dimethyl sulfoxide.* The Journal of Chemical Thermodynamics, 2012. **47**: p. 362-371.
151. Ottaway, P.B., *Stability of vitamins in food*, in *The technology of vitamins in food*. 1993, Springer. p. 90-113.
152. Ball, G.F., *Vitamins in foods: analysis, bioavailability, and stability*. 2005: CRC Press.
153. Coffman, R.E. and D.O. Kildsig, *Effect of nicotinamide and urea on the solubility of riboflavin in various solvents.* Journal of Pharmaceutical Sciences, 1996. **85**(9): p. 951-954.
154. El-Khawas, F. and N. El-Gindy, *Solubility and dissolution enhancement of riboflavin by solid dispersion technique. Part II: Riboflavin-urea and nicotinamide systems.* Pharm Ind, 1977. **39**: p. 1019-1022.
155. Wu, Z., et al., *Solubility of Folic Acid in Water at pH Values between 0 and 7 at Temperatures (298.15, 303.15, and 313.15) K.* Journal of Chemical & Engineering Data, 2010. **55**(9): p. 3958-3961.
156. Deritter, E., *Vitamins in pharmaceutical formulations.* Journal of Pharmaceutical Sciences, 1982. **71**(10): p. 1073-1096.
157. Nixon, J. and B. Chawla, *Solubilization and rheology of the system ascorbic acid-water-polysorbate 80: temperature effects.* Journal of Pharmacy and Pharmacology, 1969. **21**(2): p. 79-84.
158. Apelblat, A. and E. Manzurola, *Solubility of ascorbic, 2-furancarboxylic, glutaric, pimelic, salicylic, and o-phthalic acids in water from 279.15 to 342.15 K, and apparent molar volumes of ascorbic, glutaric, and pimelic acids in water at 298.15 K.* The Journal of Chemical Thermodynamics, 1989. **21**(9): p. 1005-1008.
159. Dawson, R.M.C., et al., *Data for biochemical research*. Vol. 3. 2002: Clarendon Press.
160. Pathare, B., V. Tambe, and V. Patil, *A review on various analytical methods used in determination of dissociation constant.* Int. J. Pharm. Pharm. Sci, 2014. **6**(8): p. 26-34.
161. Szakács, Z. and B. Noszál, *Determination of dissociation constants of folic acid, methotrexate, and other photolabile pteridines by pressure-assisted capillary electrophoresis.* Electrophoresis, 2006. **27**(17): p. 3399-3409.
162. Poole, S.K., et al., *Determination of acid dissociation constants by capillary electrophoresis.* Journal of Chromatography A, 2004. **1037**(1-2): p. 445-454.
163. Babić, S., et al., *Determination of pKa values of active pharmaceutical ingredients.* TrAC Trends in Analytical Chemistry, 2007. **26**(11): p. 1043-1061.
164. Stuart, M. and K. Box, *Chasing Equilibrium: Measuring the Intrinsic Solubility of Weak Acids and Bases.* Analytical Chemistry, 2005. **77**(4): p. 983-990.
165. Brittain, H.G., *Profiles of drug substances, excipients and related methodology: critical compilation of pKa values for pharmaceutical substances*. Vol. 33. 2007: Elsevier.
166. Klingsberg, E., *Pyridine and its Derivatives*. Vol. 32. 2009: John Wiley & Sons.
167. Rivlin, R., *Riboflavin*. 2012: Springer Science & Business Media.

168. Michaelis, L., M.P. Schubert, and C. Smythe, *Potentiometric study of the flavins.* Journal of Biological Chemistry, 1936. **116**: p. 587-607.
169. Kuhn, R. and G. Moruzzi, *Über das Reduktions-Oxydations-Potential des Lacto-flavins und seiner Derivate.* Berichte der deutschen chemischen Gesellschaft (A and B Series), 1934. **67**(7): p. 1220-1223.
170. Suelter, C.H., *Mechanism of oxidation of reduced pyridine nucleotide analogs by riboflavin.* 1959.
171. Hofsäss, M.A., et al., *Biowaiver monographs for immediate-release solid oral dosage forms: folic acid.* Journal of pharmaceutical sciences, 2017. **106**(12): p. 3421-3430.
172. Sköld, C., et al., *Presentation of a structurally diverse and commercially available drug data set for correlation and benchmarking studies.* Journal of medicinal chemistry, 2006. **49**(23): p. 6660-6671.
173. Chemicalize, *Calculation module developed by ChemAxon*, in *https://chemicalize.com*. 2019, Calculation module developed by ChemAxon.
174. Sanghvi, R., D. Evans, and S.H. Yalkowsky, *Stacking complexation by nicotinamide: A useful way of enhancing drug solubility.* International Journal of Pharmaceutics, 2007. **336**(1): p. 35-41.
175. Coffman, R.E. and D.O. Kildsig, *Hydrotropic solubilization—mechanistic studies.* Pharmaceutical research, 1996. **13**(10): p. 1460-1463.
176. Evstigneev, M.P., et al., *Effect of a mixture of caffeine and nicotinamide on the solubility of vitamin (B2) in aqueous solution.* European Journal of Pharmaceutical Sciences, 2006. **28**(1): p. 59-66.
177. Hüttenrauch, R., *The hydrotropic effects of ascorbic acid on riboflavin. 8. Galenics of vitamins.* Die Pharmazie, 1965. **20**(4): p. 243.
178. Guttman, D.E. and M.Y. Athalye, *Solubilization of riboflavin by complex formation with caffeine, theophylline, and dimethyluracil.* Journal of the American Pharmaceutical Association, 1960. **49**(11): p. 687-691.
179. Cui, Y., *Parallel stacking of caffeine with riboflavin in aqueous solutions: The potential mechanism for hydrotropic solubilization of riboflavin.* International Journal of Pharmaceutics, 2010. **397**(1): p. 36-43.
180. Banipal, T.S., et al., *Volumetric and viscometric studies on L-ascorbic acid, nicotinic acid, thiamine hydrochloride and pyridoxine hydrochloride in water at temperatures (288.15–318.15)K and at atmospheric pressure.* Thermochimica Acta, 2013. **553**: p. 31-39.
181. Seng, C., M. Shamim, and M. Baki, *Conductance and cryoscopic measurements in aqueous l-ascorbic acid solutions.* Pertanika, 1987. **10**: p. 311-313.
182. Joseph, A., C.E.S. Bernardes, and M.E. Minas da Piedade, *Heat capacity and thermodynamics of solid and liquid pyridine-3-carboxylic acid (nicotinic acid) over the temperature range 296K to 531K.* The Journal of Chemical Thermodynamics, 2012. **55**: p. 23-28.
183. Lide, D.R., *CRC Handbook of chemistry and physics. B&T*. 2007, Oxford.
184. Jean-Claude, B., W. Antony, and L. Andrew, *Jean-Claude Bradley Open Melting Point Dataset*. 2014.
185. Orbey, H. and S.I. Sandler, *On the combination of equation of state and excess free energy models.* Fluid Phase Equilibria, 1995. **111**(1): p. 53-70.
186. Mathias, P.M. and H.C. Klotz, *Take a closer look at thermodynamic property models.* Chemical Engineering Progress;(United States), 1994. **90**(6).
187. Renon, H. and J.M. Prausnitz, *Local compositions in thermodynamic excess functions for liquid mixtures.* AIChE Journal, 1968. **14**(1): p. 135-144.
188. Abrams, D.S. and J.M. Prausnitz, *Statistical thermodynamics of liquid mixtures: A new expression for the excess Gibbs energy of partly or completely miscible systems.* AIChE Journal, 1975. **21**(1): p. 116-128.
189. Maurer, G. and J.M. Prausnitz, *On the derivation and extension of the uniquac equation.* Fluid Phase Equilibria, 1978. **2**(2): p. 91-99.
190. Kikic, I., et al., *On the combinatorial part of the UNIFAC and UNIQUAC models.* The Canadian Journal of Chemical Engineering, 1980. **58**(2): p. 253-258.

191. Tessier, S.R., J.F. Brennecke, and M.A. Stadtherr, *Reliable phase stability analysis for excess Gibbs energy models.* Chemical Engineering Science, 2000. **55**(10): p. 1785-1796.
192. Coutinho, J.A.P., *Predictive local composition models: NRTL and UNIQUAC and their application to model solid–liquid equilibrium of n-alkanes.* Fluid Phase Equilibria, 1999. **158**: p. 447-457.
193. Juliá, J.A., et al., *On the application of the NRTL method to ternary (liquid+ liquid) equilibria.* The Journal of Chemical Thermodynamics, 2005. **37**(5): p. 437-443.
194. Díaz, I., et al., *A simple and reliable procedure to accurately estimate NRTL interaction parameters from liquid-liquid equilibrium data.* Chemical Engineering Science, 2019. **193**: p. 370-378.
195. Dong, Y., et al., *UNIFAC Model for Ionic Liquids. 2. Revision and Extension.* Industrial & Engineering Chemistry Research, 2020.
196. Pereira, E., et al., *Prediction of the melting behavior of edible fats using UNIFAC and UNIQUAC models.* Fluid Phase Equilibria, 2019. **493**: p. 58-66.
197. Kontogeorgis, G.M., et al., *Equations of state in three centuries. Are we closer to arriving to a single model for all applications?* Chemical Engineering Science: X, 2020. **7**: p. 100060.
198. Michelsen, M.L. and E.M. Hendriks, *Physical properties from association models.* Fluid phase equilibria, 2001. **180**(1-2): p. 165-174.
199. Voutsas, E.C., et al., *Water/hydrocarbon phase equilibria using the thermodynamic perturbation theory.* Industrial & engineering chemistry research, 2000. **39**(3): p. 797-804.
200. Wu, J. and J.M. Prausnitz, *Phase equilibria for systems containing hydrocarbons, water, and salt: An extended Peng− Robinson equation of state.* Industrial & Engineering Chemistry Research, 1998. **37**(5): p. 1634-1643.
201. Kontogeorgis, G.M., et al., *Ten Years with the CPA (Cubic-Plus-Association) Equation of State. Part 1. Pure Compounds and Self-Associating Systems.* Industrial & Engineering Chemistry Research, 2006. **45**(14): p. 4855-4868.
202. Tumakaka, F., J. Gross, and G. Sadowski, *Thermodynamic modeling of complex systems using PC-SAFT.* Fluid Phase Equilibria, 2005. **228-229**: p. 89-98.
203. Wertheim, M.S., *Fluids with highly directional attractive forces. I. Statistical thermodynamics.* Journal of Statistical Physics, 1984. **35**(1): p. 19-34.
204. Wertheim, M.S., *Fluids with highly directional attractive forces. II. Thermodynamic perturbation theory and integral equations.* Journal of Statistical Physics, 1984. **35**(1): p. 35-47.
205. Wertheim, M.S., *Fluids with highly directional attractive forces. III. Multiple attraction sites.* Journal of Statistical Physics, 1986. **42**(3): p. 459-476.
206. Wertheim, M.S., *Fluids with highly directional attractive forces. IV. Equilibrium polymerization.* Journal of Statistical Physics, 1986. **42**(3): p. 477-492.
207. Chapman, W.G., G. Jackson, and K.E. Gubbins, *Phase equilibria of associating fluids: chain molecules with multiple bonding sites.* Molecular Physics, 1988. **65**(5): p. 1057-1079.
208. Chapman, W.G., et al., *New reference equation of state for associating liquids.* Industrial & Engineering Chemistry Research, 1990. **29**(8): p. 1709-1721.
209. Huang, S.H. and M. Radosz, *Equation of state for small, large, polydisperse, and associating molecules.* Industrial & Engineering Chemistry Research, 1990. **29**(11): p. 2284-2294.
210. Huang, S.H. and M. Radosz, *Equation of state for small, large, polydisperse, and associating molecules: extension to fluid mixtures.* Industrial & Engineering Chemistry Research, 1991. **30**(8): p. 1994-2005.
211. Chen, S.S. and A. Kreglewski, *Applications of the Augmented van der Waals Theory of Fluids.: I. Pure Fluids.* Berichte der Bunsengesellschaft für physikalische Chemie, 1977. **81**(10): p. 1048-1052.
212. De Villiers, A., et al., *Evaluation of the PC-SAFT, SAFT and CPA equations of state in predicting derivative properties of selected non-polar and hydrogen-bonding compounds.* Fluid Phase Equilibria, 2013. **338**: p. 1-15.

213. Knierbein, M., C. Held, and G. Sadowski, *The role of molecular interactions on Michaelis constants of α-chymotrypsin catalyzed peptide hydrolyses.* The Journal of Chemical Thermodynamics, 2020. **148**: p. 106142.
214. Dohrn, S., et al., *Phase behavior of pharmaceutically relevant polymer/solvent mixtures.* International Journal of Pharmaceutics, 2020. **577**: p. 119065.
215. Veith, H., et al., *Hydrate formation in polymer-based pharmaceutical formulations.* Fluid Phase Equilibria, 2020: p. 112677.
216. Brinkmann, J., et al., *Solubility of Pharmaceutical Ingredients in Natural Edible Oils.* Molecular Pharmaceutics, 2020.
217. Andzelm, J., C. Kölmel, and A. Klamt, *Incorporation of solvent effects into density functional calculations of molecular energies and geometries.* The Journal of chemical physics, 1995. **103**(21): p. 9312-9320.
218. Klamt, A., et al., *Refinement and parametrization of COSMO-RS.* The Journal of Physical Chemistry A, 1998. **102**(26): p. 5074-5085.
219. Mu, T., J. Rarey, and J. Gmehling, *Performance of COSMO-RS with Sigma Profiles from Different Model Chemistries.* Industrial & Engineering Chemistry Research, 2007. **46**(20): p. 6612-6629.
220. Chemat, F. and J. Strube, *Green extraction of natural products: theory and practice*. 2015: John Wiley & Sons.
221. Chen, C.C., et al., *Extension and application of the pitzer equation for vapor-liquid equilibrium of aqueous electrolyte systems with molecular solutes.* AIChE Journal, 1979. **25**(5): p. 820-831.
222. Chen, C.C. and L.B. Evans, *A local composition model for the excess Gibbs energy of aqueous electrolyte systems.* AIChE Journal, 1986. **32**(3): p. 444-454.
223. Thomsen, K., P. Rasmussen, and R. Gani, *Correlation and prediction of thermal properties and phase behaviour for a class of aqueous electrolyte systems.* Chemical Engineering Science, 1996. **51**(14): p. 3675-3683.
224. Thomsen, K. and P. Rasmussen, *Modeling of vapor–liquid–solid equilibrium in gas–aqueous electrolyte systems.* Chemical Engineering Science, 1999. **54**(12): p. 1787-1802.
225. Gmehling, J., J. Li, and M. Schiller, *A modified UNIFAC model. 2. Present parameter matrix and results for different thermodynamic properties.* Industrial & Engineering Chemistry Research, 1993. **32**(1): p. 178-193.
226. Weidlich, U. and J. Gmehling, *A modified UNIFAC model. 1. Prediction of VLE, hE, and. gamma.. infin.* Industrial & engineering chemistry research, 1987. **26**(7): p. 1372-1381.
227. Inchekel, R., J.-C. de Hemptinne, and W. Fürst, *The simultaneous representation of dielectric constant, volume and activity coefficients using an electrolyte equation of state.* Fluid Phase Equilibria, 2008. **271**(1): p. 19-27.
228. Robinson, R. and R. Stokes, *Electrolyte Solutions*. 1970, London: Butterworths.
229. Kaj, T., *Modeling electrolyte solutions with the extended universal quasichemical (UNIQUAC) model.* Pure and Applied Chemistry, 2005. **77**(3): p. 531-542.
230. Soto, A., et al., *Measurements and modelling of the solubility of a mixture of two amino acids in aqueous solutions.* Fluid Phase Equilibria, 1999. **158-160**: p. 893-901.
231. Chen, C.-C., Y. Zhu, and L.B. Evans, *Phase Partitioning of Biomolecules: Solubilities of Amino Acids.* Biotechnology Progress, 1989. **5**(3): p. 111-118.
232. Khoshkbarchi, M.K. and J.H. Vera, *A simplified perturbed hard-sphere model for the activity coefficients of amino acids and peptides in aqueous solutions.* Industrial & engineering chemistry research, 1996. **35**(11): p. 4319-4327.
233. Peres, A.M. and E.A. Macedo, *Representation of solubilities of amino acids using the UNIQUAC model for electrolytes.* Chemical engineering science, 1994. **49**(22): p. 3803-3812.
234. Held, C., et al., *Modeling thermodynamic properties of aqueous single-solute and multi-solute sugar solutions with PC-SAFT.* AIChE Journal, 2013. **59**(12): p. 4794-4805.
235. Cassens, J., et al., *Solubility of Pharmaceuticals and Their Salts As a Function of pH.* Industrial & Engineering Chemistry Research, 2013. **52**(7): p. 2721-2731.

236. Albertsson, P.-Å., *Partition of proteins in liquid polymer–polymer two-phase systems.* Nature, 1958. **182**(4637): p. 709-711.
237. Molino, J.V.D., et al., *Different types of aqueous two-phase systems for biomolecule and bioparticle extraction and purification.* Biotechnology Progress, 2013. **29**(6): p. 1343-1353.
238. Ruiz-Ruiz, F., et al., *Aqueous two-phase affinity partitioning systems: Current applications and trends.* Journal of Chromatography A, 2012. **1244**: p. 1-13.
239. Hatti-Kaul, R., *Aqueous two-phase systems.* Molecular Biotechnology, 2001. **19**(3): p. 269-277.
240. Diamond, A.D. and J.T. Hsu, *Aqueous two-phase systems for biomolecule separation*, in *Bioseparation*, G.T. Tsao, Editor. 1992, Springer Berlin Heidelberg: Berlin, Heidelberg. p. 89-135.
241. Pereira, J.F.B., M.G. Freire, and J.A.P. Coutinho, *Aqueous two-phase systems: Towards novel and more disruptive applications.* Fluid Phase Equilibria, 2020. **505**: p. 112341.
242. Iqbal, M., et al., *Aqueous two-phase system (ATPS): an overview and advances in its applications.* Biological procedures online, 2016. **18**(1): p. 18.
243. Srivastava, P.K. and M. Kapoor, *Extracellular endo-mannanase from Bacillus sp. CFR1601: Economical production using response surface methodology and downstream processing using aqueous two phase system.* Food and Bioproducts Processing, 2013. **91**(4): p. 672-681.
244. Li, Z., et al., *Ionic liquid-based aqueous two-phase systems and their applications in green separation processes.* TrAC Trends in Analytical Chemistry, 2010. **29**(11): p. 1336-1346.
245. Desai, R.K., et al., *Extraction and stability of selected proteins in ionic liquid based aqueous two phase systems.* Green Chemistry, 2014. **16**(5): p. 2670-2679.
246. Yu, C., et al., *Liquid–liquid equilibrium composed of imidazolium tetrafluoroborate ionic liquids+ sodium carbonate aqueous two-phase systems and correlation at (288.15, 298.15, and 308.15) K.* Thermochimica acta, 2011. **523**(1-2): p. 221-226.
247. Passos, H., et al., *Characterization of aqueous biphasic systems composed of ionic liquids and a citrate-based biodegradable salt.* Biochemical Engineering Journal, 2012. **67**: p. 68-76.
248. Hammond, O.S., D.T. Bowron, and K.J. Edler, *The Effect of Water upon Deep Eutectic Solvent Nanostructure: An Unusual Transition from Ionic Mixture to Aqueous Solution.* Angewandte Chemie International Edition, 2017. **56**(33): p. 9782-9785.
249. Meng, X., et al., *Impact of water on the melting temperature of urea + choline chloride deep eutectic solvent.* New Journal of Chemistry, 2016. **40**(5): p. 4492-4499.
250. Govindarajan, R., K. Divya, and M. Perumalsamy, *Phase Behavior and Density for Binary and Ternary Solutions of PEG 4000 + Triammonium Citrate + Water Aqueous Two Phase Systems at Different Temperatures.* Journal of Chemical & Engineering Data, 2013. **58**(2): p. 315-321.
251. Vernau, J. and M.-R. Kula, *Extraction of proteins from biological raw material using aqueous polyethylene glycol-citrate phase systems.* Biotechnology and applied biochemistry, 1990. **12**(4): p. 397-404.
252. Zafarani-Moattar, M.T., R. Sadeghi, and A.A. Hamidi, *Liquid–liquid equilibria of an aqueous two-phase system containing polyethylene glycol and sodium citrate: experiment and correlation.* Fluid Phase Equilibria, 2004. **219**(2): p. 149-155.
253. Kazemi, S., et al., *Measurement and correlation of vapor–liquid equilibria of the aqueous poly(ethylene glycol)+sodium citrate and poly(ethylene glycol)+potassium citrate systems.* Fluid Phase Equilibria, 2007. **262**(1): p. 137-148.
254. Shahriari, S., S.G. Doozandeh, and G. Pazuki, *Partitioning of Cephalexin in Aqueous Two-Phase Systems Containing Poly(ethylene glycol) and Sodium Citrate Salt at Different Temperatures.* Journal of Chemical & Engineering Data, 2012. **57**(2): p. 256-262.
255. Perumalsamy, M. and T. Murugesan, *Liquid–liquid equilibrium of aqueous two-phase system (PEG 2000-Sodium Citrate–Water) using potential difference as a key tool.* Physics and Chemistry of Liquids, 2014. **52**(1): p. 26-36.

256. Carvalho, C.P., et al., *Influence of the temperature and type of salt on the phase equilibrium of peg 1500 + potassium phosphate and peg 1500 + sodium citrate aqueous two-phase systems.* Química Nova, 2008. **31**: p. 209-213.
257. de Souza, E.C., et al., *Measurements and Modeling of Liquid–Liquid Equilibrium of Polyethylene Glycol 400, Sodium Phosphate, or Sodium Citrate Aqueous Two-Phase Systems at (298.2, 308.2, and 318.2) K.* Journal of Chemical & Engineering Data, 2013. **58**(7): p. 2008-2017.
258. Silvério, S.C., et al., *Effect of aqueous two-phase system constituents in different poly (ethylene glycol)–salt phase diagrams.* Journal of Chemical & Engineering Data, 2012. **57**(4): p. 1203-1208.
259. Zafarani-Moattar, M.T. and P. Jafari, *Phase diagrams for liquid–liquid and liquid–solid equilibrium of the ternary polyethylene glycol+di-sodium hydrogen citrate+water system.* Fluid Phase Equilibria, 2013. **337**: p. 224-233.
260. Silvério, S.C., et al., *The Effect of Salts on the Liquid–Liquid Phase Equilibria of PEG600 + Salt Aqueous Two-Phase Systems.* Journal of Chemical & Engineering Data, 2013. **58**(12): p. 3528-3535.
261. Zafarani-Moattar, M.T. and A.A. Hamidi, *Liquid–Liquid Equilibria of Aqueous Two-Phase Poly(ethylene glycol)–Potassium Citrate System.* Journal of Chemical & Engineering Data, 2003. **48**(2): p. 262-265.
262. Iyyaswami, R., et al., *Development and evaluation of PEG-lithium citrate salt based aqueous two phase system and its application in partitioning of proteins from fish industry effluent.* Separation Science and Technology, 2012. **47**(4): p. 591-598.
263. Regupathi, I., C.K. Srikanth, and N. Sindhu, *Liquid–Liquid Equilibrium of Poly(ethylene glycol) 2000 + Diammonium Hydrogen Citrate + Water System at Different Temperatures.* Journal of Chemical & Engineering Data, 2011. **56**(9): p. 3643-3650.
264. Govindarajan, R. and M. Perumalsamy, *Phase Equilibrium of PEG 2000 + Triammonium Citrate + Water System Relating PEG Molecular Weight, Cation, Anion with Effective Excluded Volume, Gibbs Free Energy of Hydration, Size of Cation, and Type of Anion at (298.15, 308.15, and 318.15) K.* Journal of Chemical & Engineering Data, 2013. **58**(11): p. 2952-2958.
265. Zafarani-Moattar, M.T. and S. Hamzehzadeh, *Liquid–liquid equilibria of aqueous two-phase systems containing polyethylene glycol and sodium succinate or sodium formate.* Calphad, 2005. **29**(1): p. 1-6.
266. Raja, S. and V.R. Murty, *Liquid-Liquid Equilibrium of Poly(Ethylene Glycol) 6000 + Sodium Succinate + Water System at Different Temperatures.* The Scientific World Journal, 2013. **2013**: p. 819259.
267. Pirdashti, M., et al., *Phase equilibria of aqueous mixtures of PEG with formate salt: Effects of pH, type of cation, polymer molecular weight and temperature.* Fluid Phase Equilibria, 2019. **485**: p. 158-167.
268. Malpiedi, L.P., et al., *Liquid–Liquid Equilibrium Phase Diagrams of Polyethyleneglycol + Sodium Tartrate + Water Two-Phase Systems.* Journal of Chemical & Engineering Data, 2008. **53**(5): p. 1175-1178.
269. Zafarani-Moattar, M.T., S. Hamzehzadeh, and S. Hosseinzadeh, *Phase diagrams for liquid–liquid equilibrium of ternary poly(ethylene glycol)+di-sodium tartrate aqueous system and vapor–liquid equilibrium of constituting binary aqueous systems at T=(298.15, 308.15, and 318.15)K: Experiment and correlation.* Fluid Phase Equilibria, 2008. **268**(1): p. 142-152.
270. Zafarani-Moattar, M.T. and S. Tolouei, *Liquid–liquid equilibria of aqueous two-phase systems containing polyethylene glycol 4000 and di-potassium tartrate, potassium sodium tartrate, or di-potassium oxalate: Experiment and correlation.* Calphad, 2008. **32**(4): p. 655-660.
271. Othmer, D. and P. Tobias, *Liquid-Liquid Extraction Data - The Line Correlation.* Industrial & Engineering Chemistry, 1942. **34**(6): p. 693-696.
272. González-Tello, P., et al., *Liquid–Liquid Equilibrium in the System Poly(ethylene glycol) + MgSO4 + H2O at 298 K.* Journal of Chemical & Engineering Data, 1996. **41**(6): p. 1333-1336.

273. Hu, M., et al., *Liquid–Liquid and Liquid–Liquid–Solid Equilibrium in PEG + Cs2SO4 + H2O.* Journal of Chemical & Engineering Data, 2004. **49**(5): p. 1440-1443.
274. Tubío, G., et al., *Liquid–Liquid Equilibria of Aqueous Two-Phase Systems Containing Poly(ethylene glycols) of Different Molecular Weight and Sodium Citrate.* Journal of Chemical & Engineering Data, 2006. **51**(1): p. 209-212.
275. Merchuk, J.C., B.A. Andrews, and J.A. Asenjo, *Aqueous two-phase systems for protein separation: Studies on phase inversion.* Journal of Chromatography B: Biomedical Sciences and Applications, 1998. **711**(1): p. 285-293.
276. Perumalsamy, M. and T. Murugesan, *Prediction of liquid–liquid equilibria for PEG 2000–sodium citrate based aqueous two-phase systems.* Fluid Phase Equilibria, 2006. **244**(1): p. 52-61.
277. Zafarani-Moattar, M.T., et al., *The effect of temperature and molar mass on the (liquid+liquid) equilibria of (poly ethylene glycol dimethyl ether+di-sodium hydrogen citrate+water) systems: Experimental and correlation.* The Journal of Chemical Thermodynamics, 2015. **91**: p. 435-444.
278. Ketabi, M., M. Pirdashti, and P. Mobalegholeslam, *Liquid-liquid equilibrium and physical properties of aqueous mixtures of poly (ethylene glycol) 3000 with tri-potassium citrate at different pH: experiment, correlation and thermodynamic modeling.* J. Korean Chem. Soc, 2019. **63**: p. 12-23.
279. Reschke, T., C. Brandenbusch, and G. Sadowski, *Modeling aqueous two-phase systems: II. Inorganic salts and polyether homo- and copolymers as ATPS former.* Fluid Phase Equilibria, 2014. **375**: p. 306-315.
280. Reschke, T., C. Brandenbusch, and G. Sadowski, *Modeling aqueous two-phase systems: III. Polymers and organic salts as ATPS former.* Fluid Phase Equilibria, 2015. **387**: p. 178-189.
281. da Silva, C.A.S., et al., *Partitioning of glycomacropeptide in aqueous two-phase systems.* Process Biochemistry, 2009. **44**(11): p. 1213-1216.
282. Tubío, G., B. Nerli, and G. Picó, *Partitioning features of bovine trypsin and α-chymotrypsin in polyethyleneglycol-sodium citrate aqueous two-phase systems.* Journal of Chromatography B, 2007. **852**(1): p. 244-249.
283. Azevedo, A.M., et al., *Partitioning of human antibodies in polyethylene glycol–sodium citrate aqueous two-phase systems.* Separation and Purification Technology, 2009. **65**(1): p. 14-21.
284. Nascimento, M.B.d., et al., *Equilibrium data and thermodynamic studies of α-amylase partition in aqueous two-phase systems.* Fluid Phase Equilibria, 2018. **463**: p. 69-79.
285. Neves, M.L.C., et al., *Partition and recovery of phytase from Absidia blakesleeana URM5604 using PEG–citrate aqueous two-phase systems.* Fluid Phase Equilibria, 2012. **318**: p. 34-39.
286. Costa, A.R.d., et al., *Partitioning of bovine lactoferrin in aqueous two-phase system containing poly(ethylene glycol) and sodium citrate.* Food and Bioproducts Processing, 2015. **95**: p. 118-124.
287. Xavier, L., et al., *Application of aqueous two phase systems based on polyethylene glycol and sodium citrate for the recovery of phenolic compounds from Eucalyptus wood.* Maderas. Ciencia y tecnología, 2015. **17**(2): p. 345-354.
288. Soares, P.A.G., et al., *Purification of a lectin from Canavalia ensiformis using PEG–citrate aqueous two-phase system.* Journal of Chromatography B, 2011. **879**(5): p. 457-460.
289. de Araújo, R.F.F., et al., *Partitioning of lactate dehydrogenase from bovine heart crude extract by polyethylene glycol–citrate aqueous two-phase systems.* Fluid Phase Equilibria, 2011. **301**(1): p. 46-50.
290. Lu, Y.-M., et al., *Bovine serum albumin partitioning in polyethylene glycol (PEG)/potassium citrate aqueous two-phase systems.* Food and Bioproducts Processing, 2010. **88**(1): p. 40-46.
291. Edrisi, S., H. Bakhshi, and M. Rahimnejad, *Aqueous two-phase systems for cephalexin monohydrate partitioning using poly ethylene glycol and sodium tartrate dihydrate: Experimental and thermodynamic modeling.* Korean Journal of Chemical Engineering, 2019. **36**(5): p. 780-788.

292. Khayati, G. and S. Alizadeh, *Extraction of lipase from Rhodotorula glutinis fermentation culture by aqueous two-phase partitioning.* Fluid Phase Equilibria, 2013. **353**: p. 132-134.
293. Held, C. and G. Sadowski, *Compatible solutes: Thermodynamic properties relevant for effective protection against osmotic stress.* Fluid Phase Equilibria, 2016. **407**: p. 224-235.
294. Carneiro, A.P., et al., *Density of Mixtures Containing Sugars and Ionic Liquids: Experimental Data and PC-SAFT Modeling.* Journal of Chemical & Engineering Data, 2014. **59**(10): p. 2942-2954.
295. Silvério, S.C., et al., *Liquid–Liquid Equilibria of UCON + (Sodium or Potassium) Phosphate Salt Aqueous Two-Phase Systems at 23 °C.* Journal of Chemical & Engineering Data, 2010. **55**(3): p. 1285-1288.
296. Hübner, M., et al., *Measuring and modeling thermodynamic properties of aqueous lysozyme and BSA solutions.* Fluid Phase Equilibria, 2018. **472**: p. 62-74.
297. Sadowski, G., *Thermodynamik der Polymerlösungen, Habilitationsschrift.* Shaker Verlag (Aachen), 2000.
298. Walas, S.M., *Phase equilibria in chemical engineering*. 2013: Butterworth-Heinemann.
299. Thomsen, K., *Electrolyte solutions: Thermodynamics, crystallization, separation methods.* 2009.
300. Luckas, M. and J. Krissmann, *Thermodynamik der Elektrolytlösungen: eine einheitliche Darstellung der Berechnung komplexer Gleichgewichte*. 2013: Springer-Verlag.
301. Dietz, C.H.J.T., et al., *Thermodynamic properties of hydrophobic deep eutectic solvents and solubility of water and HMF in them: Measurements and PC-SAFT modeling.* Fluid Phase Equilibria, 2019. **489**: p. 75-82.
302. Mohammad, S., et al., *Salt influence on MIBK/water liquid–liquid equilibrium: Measuring and modeling with ePC-SAFT and COSMO-RS.* Fluid Phase Equilibria, 2016. **416**: p. 83-93.
303. Held, C., et al., *ePC-SAFT revised.* Chemical Engineering Research and Design, 2014. **92**(12): p. 2884-2897.
304. Fürst, W. and H. Renon, *Representation of excess properties of electrolyte solutions using a new equation of state.* AIChE Journal, 1993. **39**(2): p. 335-343.
305. Myers, J.A., S.I. Sandler, and R.H. Wood, *An equation of state for electrolyte solutions covering wide ranges of temperature, pressure, and composition.* Industrial & engineering chemistry research, 2002. **41**(13): p. 3282-3297.
306. Maribo-Mogensen, B., K. Thomsen, and G.M. Kontogeorgis, *An electrolyte CPA equation of state for mixed solvent electrolytes.* AIChE Journal, 2015. **61**(9): p. 2933-2950.
307. Schlaikjer, A., K. Thomsen, and G.M. Kontogeorgis, *eCPA: An ion-specific approach to parametrization.* Fluid Phase Equilibria, 2018. **470**: p. 176-187.
308. Ingram, T., et al., *Extension of COSMO-RS for monoatomic electrolytes: Modeling of liquid–liquid equilibria in presence of salts.* Fluid Phase Equilibria, 2012. **314**: p. 29-37.
309. Müller, S., et al., *Evaluation and refinement of the novel predictive electrolyte model COSMO-RS-ES based on solid-liquid equilibria of salts and Gibbs free energies of transfer of ions.* Fluid Phase Equilibria, 2019. **483**: p. 165-174.
310. Kiepe, J., O. Noll, and J. Gmehling, *Modified LIQUAC and Modified LIFACA Further Development of Electrolyte Models for the Reliable Prediction of Phase Equilibria with Strong Electrolytes.* Industrial & Engineering Chemistry Research, 2006. **45**(7): p. 2361-2373.
311. Pitzer, K.S., *Thermodynamics of electrolytes. I. Theoretical basis and general equations.* The Journal of Physical Chemistry, 1973. **77**(2): p. 268-277.
312. Mohs, A. and J. Gmehling, *A revised LIQUAC and LIFAC model (LIQUAC*/LIFAC*) for the prediction of properties of electrolyte containing solutions.* Fluid Phase Equilibria, 2013. **337**: p. 311-322.
313. Liu, Y., A.H. Harvey, and J.M. Prausnitz, *THERMODYNAMICS OF CONCENTRATED ELECTROLYTE SOLUTIONS.* Chemical Engineering Communications, 1989. **77**(1): p. 43-66.
314. Li, J., H.-M. Polka, and J. Gmehling, *A gE model for single and mixed solvent electrolyte systems: 1. Model and results for strong electrolytes.* Fluid Phase Equilibria, 1994. **94**: p. 89-114.

315. Yan, W., et al., *Prediction of vapor–liquid equilibria in mixed-solvent electrolyte systems using the group contribution concept.* Fluid Phase Equilibria, 1999. **162**(1): p. 97-113.
316. Prausnitz, J., R. Lichtenthaler, and E. Azevedo, *Molecular thermodynamics of fluid-phase equilibria Prentice Hall.* Inc., Englewood Cliffs, NJ, 1969.
317. Völgyi, G., et al., *Study of pH-dependent solubility of organic bases. Revisit of Henderson-Hasselbalch relationship.* Analytica Chimica Acta, 2010. **673**(1): p. 40-46.
318. Zaworotko, M., et al., *Pharmaceutical salts and co-crystals*. 2011: Royal Society of Chemistry.
319. von Stockar, U. and L.A. van der Wielen, *Biothermodynamics: The role of thermodynamics in biochemical engineering*. 2013: EPFL Press.
320. Bergström, C.A., K. Luthman, and P. Artursson, *Accuracy of calculated pH-dependent aqueous drug solubility.* European Journal of Pharmaceutical Sciences, 2004. **22**(5): p. 387-398.
321. Plummer, L.N., B.F. Jones, and A.H. Truesdell, *WATEQF-a FORTRAN IV version of WATEQ: a computer program for calculating chemical equilibrium of natural waters*. Vol. 76. 1976: Department of the Interior, Geological Survey, Water Resources Division.
322. Truesdell, A.H. and B.F. Jones, *WATEQ, a computer program for calculating chemical equilibria of natural waters.* J. Res. US Geol. Surv, 1974. **2**(2): p. 233-248.
323. Zimmermann, I., *Determination of pKa values from solubility data.* International Journal of Pharmaceutics, 1982. **13**(1): p. 57-65.
324. Thurlkill, R.L., et al., *pKa of Fentanyl Varies With Temperature: Implications for Acid-Base Management During Extremes of Body Temperature.* Journal of Cardiothoracic and Vascular Anesthesia, 2005. **19**(6): p. 759-762.
325. Reijenga, J., et al., *Development of Methods for the Determination of pKa Values.* Analytical chemistry insights, 2013. **8**: p. 53-71.
326. Po, H.N. and N.M. Senozan, *The Henderson-Hasselbalch Equation: Its History and Limitations.* Journal of Chemical Education, 2001. **78**(11): p. 1499.
327. Hasselbalch, K., *The calculation of blood pH via the partition of carbon dioxide in plasma and oxygen binding of the blood as a function of plasma pH.* Biochem Z, 1916. **78**: p. 112-144.
328. Lange, L., *Phase Behavior of Pharmaceutical Cocrystals*. 2017: Verlag Dr. Hut.
329. Reschke, T., C. Brandenbusch, and G. Sadowski, *Modeling aqueous two-phase systems: I. Polyethylene glycol and inorganic salts as ATPS former.* Fluid Phase Equilibria, 2014. **368**: p. 91-103.
330. IUPAC, *Compendium of Chemical Terminology, 2nd ed. (the "Gold Book"). Compiled by A. D. McNaught and A. Wilkinson.* Oxford (1997). Online version (2019-) created by S. J. Chalk. Blackwell Scientific Publications, ISBN 0-9678550-9-8. , 1997. https://doi.org/10.1351/goldbook.
331. Berg, R.W., *Investigation of L (+)-ascorbic acid with Raman spectroscopy in visible and UV light.* Applied Spectroscopy Reviews, 2015. **50**(3): p. 193-239.
332. Hughes, E., H. Jellinek, and B. Ambrose, *Nicotinic Acid. Ultraviolet Absorption Spectrum and Dissociation Constants.* The Journal of Physical Chemistry, 1949. **53**(3): p. 414-423.
333. Mollin, J. and T. Kucerova, *Acid-base properties and isomerism of nicotinic acid.* Chemical Papers, 1979. **33**(1): p. 52-56.
334. Maynard, R., *The Merck Index: 1996.* Occupational and environmental medicine, 1997. **54**(4): p. 288.
335. Smith, J. and L. Hong-Shum, *Food additives data book*. 2011: John Wiley & Sons.
336. Gross, J. and G. Sadowski, *Modeling polymer systems using the perturbed-chain statistical associating fluid theory equation of state.* Industrial & engineering chemistry research, 2002. **41**(5): p. 1084-1093.
337. Ruether, F. and G. Sadowski, *Solubility of complex natural and pharmaceutical Substances.* Industrial Scale Natural Products Extraction, 1st ed.; Bart, H.-J., Pilz, S., Eds, 2011.
338. Held, C., L.F. Cameretti, and G. Sadowski, *Modeling aqueous electrolyte solutions: Part 1. Fully dissociated electrolytes.* Fluid Phase Equilibria, 2008. **270**(1-2): p. 87-96.

339. Held, C. and G. Sadowski, *Modeling aqueous electrolyte solutions. Part 2. Weak electrolytes.* Fluid Phase Equilibria, 2009. **279**(2): p. 141-148.
340. Debye, P. and E. Hückel, *De la theorie des electrolytes. I. abaissement du point de congelation et phenomenes associes.* Physikalische Zeitschrift, 1923. **24**(9): p. 185-206.
341. Berthelot, D., *Sur le mélange des gaz.* Compt. Rendus, 1898. **126**: p. 1703-1706.
342. Lorentz, H.A., *Ueber die Anwendung des Satzes vom Virial in der kinetischen Theorie der Gase.* Annalen der Physik, 1881. **248**(1): p. 127-136.
343. Wolbach, J.P. and S.I. Sandler, *Using Molecular Orbital Calculations To Describe the Phase Behavior of Cross-associating Mixtures.* Industrial & Engineering Chemistry Research, 1998. **37**(8): p. 2917-2928.
344. Madeira, P.P., et al., *Solvatochromic relationship: Prediction of distribution of ionic solutes in aqueous two-phase systems.* Journal of Chromatography A, 2013. **1271**(1): p. 10-16.
345. da Silva, N.R., et al., *Analysis of partitioning of organic compounds and proteins in aqueous polyethylene glycol-sodium sulfate aqueous two-phase systems in terms of solute–solvent interactions.* Journal of Chromatography A, 2015. **1415**: p. 1-10.
346. Reschke, T., *Modeling and Design of Aqueous Two-Phase Systems*. Vol. 11. 2014: Verlag Dr. Hut.
347. Hosemann, R. and W. Schramek, *Statistische methoden zur ermittlung der verteilung der molekülgrössen in hochopolymeren polymolekularen systemen aus experimentalergebnissen der fraktionierten fällung. I. Mitteilung: Mathematische grundlangen.* Journal of Polymer Science, 1962. **59**(167): p. 13-27.
348. Alves, J.G.L.F., et al., *Aqueous Two-Phase Systems of Poly(ethylene glycol) and Sodium Citrate: Experimental Results and Modeling.* Journal of Chemical & Engineering Data, 2008. **53**(7): p. 1587-1594.
349. Lladosa, E., et al., *(Liquid+liquid) equilibria of polymer-salt aqueous two-phase systems for laccase partitioning: UCON 50-HB-5100 with potassium citrate and (sodium or potassium) formate at 23°C.* The Journal of Chemical Thermodynamics, 2012. **55**: p. 166-171.
350. Madeira, P.P., et al., *Correlations between distribution coefficients of various biomolecules in different polymer/polymer aqueous two-phase systems.* Fluid Phase Equilibria, 2008. **267**(2): p. 150-157.
351. Ferreira, L.A., et al., *Responses of proteins to different ionic environment are linearly interrelated.* Journal of Chromatography A, 2015. **1387**: p. 32-41.
352. Sanderson, M. and C. Schorah, *Measurement of ascorbic acid and dehydroascorbic acid in gastric juice by HPLC.* Biomedical Chromatography, 1987. **2**(5): p. 197-202.
353. Maltais, A., G.E. Remondetto, and M. Subirade, *Tabletted soy protein cold-set hydrogels as carriers of nutraceutical substances.* Food Hydrocolloids, 2010. **24**(5): p. 518-524.
354. Chen, P. and W.R. Wolf, *LC/UV/MS-MRM for the simultaneous determination of water-soluble vitamins in multi-vitamin dietary supplements.* Analytical and Bioanalytical Chemistry, 2007. **387**(7): p. 2441-2448.
355. Papadoyannis, I., G. Tsioni, and V. Samanidou, *Simultaneous determination of nine water and fat soluble vitamins after SPE separation and RP-HPLC analysis in pharmaceutical preparations and biological fluids.* Journal of liquid chromatography & related technologies, 1997. **20**(19): p. 3203-3231.
356. Iwase, H., *Determination of folic acid in an elemental diet by high-performance liquid chromatography with UV detection.* Journal of Chromatography A, 1992. **609**(1): p. 399-401.
357. Iwase, H., *Ultramicrodetermination of cyanocobalamin in elemental diet by solid-phase extraction and high-performance liquid chromatography with visible detection.* Journal of Chromatography A, 1992. **590**(2): p. 359-363.
358. Murari, G.F., et al., *Phase diagrams of aqueous two-phase systems formed by polyethylene glycol+ammonium sulfate+water: equilibrium data and thermodynamic modeling.* Fluid Phase Equilibria, 2015. **406**: p. 61-69.

359. Hamta, A., M.R. Dehghani, and M. Gholami, *Novel experimental data on aqueous two–phase system containing PEG–6000 and Na2CO3 at T=(293.15, 303.15 and 313.15) K.* Journal of Molecular Liquids, 2017. **241**: p. 144-149.
360. Regupathi, I., et al., *Liquid–Liquid Equilibrium of Poly(ethylene glycol) 6000 + Triammonium Citrate + Water Systems at Different Temperatures.* Journal of Chemical & Engineering Data, 2009. **54**(3): p. 1094-1097.
361. Silvério, S.C., et al., *ΔG(CH2) in PEG–Salt and Ucon–Salt Aqueous Two-Phase Systems.* Journal of Chemical & Engineering Data, 2008. **53**(7): p. 1622-1625.
362. Silvério, S.C., et al., *Solute partitioning in polymer–salt ATPS: The Collander equation.* Fluid Phase Equilibria, 2010. **296**(2): p. 173-177.
363. Shibata, K., *Simultaneous Measurement of Nicotinic Acid and Its Major Metabolite, Nicotinuric Acid in Blood and Urine by a Reversed-phase High-performance Liquid Chromatography.* Agricultural and Biological Chemistry, 1988. **52**(11): p. 2973-2976.
364. Jegle, U., *Separation of water-soluble vitamins via highperformance capillary electrophoresis.* Journal of Chromatography A, 1993. **652**(2): p. 495-501.
365. Žiak, L.u., et al., *Simultaneous determination of caffeine, caramel and riboflavin in cola-type and energy drinks by synchronous fluorescence technique coupled with partial least squares.* Food Chemistry, 2014. **159**: p. 282-286.
366. Silvério, S.C., et al., *Polyethylene glycol 8000+ citrate salts aqueous two-phase systems: Relative hydrophobicity of the equilibrium phases.* Fluid Phase Equilibria, 2016. **407**: p. 298-303.
367. Silvério, S.C., et al., *Laccase recovery with aqueous two-phase systems: Enzyme partitioning and stability.* Journal of Molecular Catalysis B: Enzymatic, 2013. **87**: p. 37-43.
368. Nagaraja, V.H. and R. Iyyaswami, *Aqueous two phase partitioning of fish proteins: partitioning studies and ATPS evaluation.* Journal of Food Science and Technology, 2015. **52**(6): p. 3539-3548.
369. Lord, R., *Osmosis, osmometry, and osmoregulation.* Postgraduate medical journal, 1999. **75**(880): p. 67-73.
370. Held, C., T. Neuhaus, and G. Sadowski, *Compatible solutes: Thermodynamic properties and biological impact of ectoines and prolines.* Biophysical Chemistry, 2010. **152**(1): p. 28-39.
371. Knierbein, M., et al., *Combined co-solvent and pressure effect on kinetics of a peptide hydrolysis: an activity-based approach.* Physical Chemistry Chemical Physics, 2019. **21**(40): p. 22224-22229.
372. Greinert, T., et al., *Standard Gibbs energy of metabolic reactions: VI. Glyceraldehyde 3-phosphate dehydrogenase reaction.* Fluid Phase Equilibria, 2020: p. 112597.
373. Fuchs, D., et al., *Solubility of amino acids: Influence of the pH value and the addition of alcoholic cosolvents on aqueous solubility.* Industrial & engineering chemistry research, 2006. **45**(19): p. 6578-6584.
374. Stoychev, I., et al., *Modeling the Phase Behavior of PEO–PPO–PEO Surfactants in Carbon Dioxide Using the PC-SAFT Equation of State: Application to Dry Decontamination of Solid Substrates.* Journal of Chemical & Engineering Data, 2009. **54**(5): p. 1551-1559.
375. Wangler, A., et al., *Predicting the high concentration co-solvent influence on the reaction equilibria of the ADH-catalyzed reduction of acetophenone.* The Journal of Chemical Thermodynamics, 2019. **128**: p. 275-282.
376. Kim, S., et al., *PubChem 2019 update: improved access to chemical data.* Nucleic acids research, 2019. **47**(D1): p. D1102-D1109.
377. Zafarani-Moattar, M.T. and S. Hosseinzadeh, *Refractive Index, Viscosity, Density, and Speed of Sound of Aqueous Sodium Tartrate Solutions at Various Temperatures.* Journal of Chemical & Engineering Data, 2006. **51**(4): p. 1190-1193.
378. Sadeghi, R. and F. Ziamajidi, *Vapor–liquid equilibria of binary tri-potassium citrate+water and ternary polypropylene oxide 400+tri-potassium citrate+water systems from isopiestic measurements over a range of temperatures.* Fluid Phase Equilibria, 2007. **255**(1): p. 46-54.

379. Zafarani-Moattar, M.T. and B. Asadzadeh, *Vapor–Liquid Equilibria, Density, Speed of Sound, and Viscosity of Aqueous Dipotassium Tartrate Solutions at T = (298.15, 308.15, and 318.15) K.* Journal of Chemical & Engineering Data, 2008. **53**(4): p. 1000-1006.
380. Sadeghi, R. and F. Ziamajidi, *Thermodynamic properties of tripotassium citrate in water and in aqueous solutions of polypropylene oxide 400 over a range of temperatures.* Journal of Chemical & Engineering Data, 2007. **52**(5): p. 1753-1759.
381. Lange, L., M. Schleinitz, and G. Sadowski, *Predicting the Effect of pH on Stability and Solubility of Polymorphs, Hydrates, and Cocrystals.* Crystal Growth & Design, 2016. **16**(7): p. 4136-4147.
382. Yaws, C.L., *The Yaws handbook of vapor pressure: Antoine coefficients*. The Yaws Handbook of Vapor Pressure. 2015: Gulf Professional Publishing.
383. Jaeger, F.M., *Über die Temperaturabhängigkeit der molekularen freien Oberflächenenergie von Flüssigkeiten im Temperaturbereich von − 80 bis + 1650° C.* Zeitschrift für anorganische und allgemeine Chemie, 1917. **101**(1): p. 1-214.
384. Stanculescu, A., F. Stanculescu, and H. Alexandru, *Melt growth and characterization of pure and doped meta-dinitrobenzene crystals.* Journal of Crystal Growth, 1999. **198-199**: p. 572-577.
385. Acree, W.E., *Thermodynamic properties of organic compounds: enthalpy of fusion and melting point temperature compilation.* Thermochimica Acta, 1991. **189**(1): p. 37-56.
386. Hull, C., *International critical tables of numerical data, physics, chemistry and technology: Index, volumes I-VII*. Vol. 1. 1933: National Academies.
387. bioWORLD. *Cyanocobalamin: specifications*. https://www.bio-world.com 2018.
388. Gilbert, A.S., *Entropy–enthalpy compensation in the fusion of organic molecules: implications for Walden's rule and molecular freedom in the liquid state.* Thermochimica Acta, 1999. **339**(1): p. 131-142.
389. Vora, A., et al., *Thermal Stability Of Folic Acid in the solid-state.* Journal of Thermal Analysis and Calorimetry, 2004. **75**(3): p. 709-717.
390. Boissevain, C., W. Drea, and H. Schultz, *Isolation and determination of riboflavin produced by tubercle bacilli in culture media.* Proceedings of the Society for Experimental Biology and Medicine, 1938. **39**(3): p. 481-483.
391. Schneider, Z. and A. Stroinski, *Comprehensive B12: chemistry, biochemistry, nutrition, ecology, medicine*. 2011: Walter de Gruyter.
392. Huelin, F., et al., *The anaerobic decomposition of ascorbic acid in the pH range of foods and in more acid solutions.* Journal of the Science of Food and Agriculture, 1971. **22**(10): p. 540-542.
393. Carta, R. and G. Tola, *Solubilities of l-Cystine, l-Tyrosine, l-Leucine, and Glycine in Aqueous Solutions at Various pHs and NaCl Concentrations.* Journal of Chemical & Engineering Data, 1996. **41**(3): p. 414-417.
394. Tseng, H.-C., et al., *Solubilities of amino acids in water at various pH values under 298.15K.* Fluid Phase Equilibria, 2009. **285**(1): p. 90-95.
395. Chua, Y.Z., et al., *New experimental melting properties as access for predicting amino-acid solubility.* RSC advances, 2018. **8**(12): p. 6365-6372.
396. Yuldasheva, G.A., et al., *The effect of the amphoteric properties of amino acids in the zwitterionic form on the structure of iodine complex compounds in aqueous solutions.* Journal of Molecular Structure, 2013. **1033**: p. 321-330.
397. Vora, A., et al., *Thermal stability of folic acid.* Thermochimica Acta, 2002. **392-393**: p. 209-220.
398. Arcot, J., A.K. Shrestha, and U. Gusanov, *Enzyme protein binding assay for determining folic acid in fortified cereal foods and stability of folic acid under different extraction conditions.* Food Control, 2002. **13**(4): p. 245-252.
399. Hickman, K., M.W. Kaley, and P.L. Harris, *Covitamin Studies. I. The Sparing Action of Natural Toeopherol Concentrates on Vitamin A.* Journal of Biological Chemistry, 1944. **152**(2): p. 303-11.

400. Harris, P.L., M.W. Kaley, and K. Hickman, *Covitamin Studies. II. The Sparing Action of Natural Toeopherol Concentrates on Carotene.* Journal of Biological Chemistry, 1944. **152**(2): p. 313-20.
401. Fakhari, M.A. and F. Rahimpour, *Measurements and thermodynamic modelling of liquid–liquid equilibrium of PEG 6000–phosphate affinity aqueous two-phase systems at various ligand concentrations and pH.* Physics and Chemistry of Liquids, 2019: p. 1-17.
402. Song, C.P., et al., *Primary and secondary aqueous two-phase systems composed of thermo switchable polymers and bio-derived ionic liquids.* The Journal of Chemical Thermodynamics, 2017. **115**: p. 191-201.
403. Asenjo, J.A. and B.A. Andrews, *Aqueous two-phase systems for protein separation: a perspective.* Journal of Chromatography A, 2011. **1218**(49): p. 8826-8835.
404. Gonzalez-Tello, P., F. Camacho, and G. Blazquez, *Density and viscosity of concentrated aqueous solutions of polyethylene glycol.* Journal of Chemical and Engineering Data, 1994. **39**(3): p. 611-614.
405. Ferreira, G.M.D., et al., *Partitioning of cocaine and its adulterants in aqueous two-phase systems: An alternative drug identification method.* Fluid Phase Equilibria, 2020. **506**: p. 112367.
406. Fu, H., et al., *Salting-out extraction of carboxylic acids.* Separation and Purification Technology, 2015. **139**: p. 36-42.
407. Lebreton, B. and A. Lyddiatt, *Application of aqueous two-phase partition to the production of homogeneous preparations of fluorescently labelled human serum albumin.* Journal of Chromatography B: Biomedical Sciences and Applications, 2000. **743**(1-2): p. 263-269.
408. Saravanan, S., et al., *Aqueous two-phase poly(ethylene glycol)–poly(acrylic acid) system for protein partitioning: Influence of molecular weight, pH and temperature.* Process Biochemistry, 2008. **43**(9): p. 905-911.
409. Rito-Palomares, M. and A.P.J. Middelberg, *Aqueous two-phase systems for the recovery of a recombinant viral coat protein from Escherichia coli.* Journal of Chemical Technology & Biotechnology: International Research in Process, Environmental & Clean Technology, 2002. **77**(9): p. 1025-1029.
410. Von Stockar, U., *Biothermodynamics: The role of thermodynamics in biochemical engineering*. 2013: PPUR Presses polytechniques.
411. Zafarani-Moattar, M.T., H. Shekaari, and P. Jafari, *The Effect of pH on the Liquid-liquid Equilibrium for a System Containing Polyethylene Glycol Di-methyl Ether and Tri-potassium Citrate and its Application for Acetaminophen Separation.* Physical Chemistry Research, 2017. **5**(3): p. 555-567.
412. Rito-Palomares, M. and A. Lyddiatt, *Process integration using aqueous two-phase partition for the recovery of intracellular proteins.* Chemical Engineering Journal, 2002. **87**(3): p. 313-319.
413. da Silva, L.H.M., et al., *Hydrophobic effect on the partitioning of [Fe(CN)5(NO)]2− and [Fe(CN)6]3− anions in aqueous two-phase systems formed by triblock copolymers and phosphate salts.* Separation and Purification Technology, 2008. **60**(1): p. 103-112.
414. Dallora, N.L.P., J.G.D. Klemz, and P.d.A. Pessôa Filho, *Partitioning of model proteins in aqueous two-phase systems containing polyethylene glycol and ammonium carbamate.* Biochemical Engineering Journal, 2007. **34**(1): p. 92-97.
415. Amid, A., *Recombinant Enzymes-From Basic Science to Commercialization*. 2015: Springer.
416. Salabat, A., et al., *Partitioning of l-methionine in aqueous two-phase systems containing poly(propylene glycol) and sodium phosphate salts.* The Journal of Chemical Thermodynamics, 2011. **43**(10): p. 1525-1529.
417. Salabat, A., M.H. Abnosi, and A.R. Bahar, *Amino acids partitioning in aqueous two-phase system of polypropylene glycol and magnesium sulfate.* Journal of Chromatography B, 2007. **858**(1): p. 234-238.
418. van Berlo, M., et al., *Partitioning behavior of amino acids in aqueous two-phase systems with recyclable volatile salts.* Journal of Chromatography B: Biomedical Sciences and Applications, 2000. **743**(1): p. 317-325.

419. Andrews, B., A. Schmidt, and J. Asenjo, *Correlation for the partition behavior of proteins in aqueous two-phase systems: Effect of surface hydrophobicity and charge.* Biotechnology and bioengineering, 2005. **90**(3): p. 380-390.
420. Voges, M., et al., *Thermodynamics of the alanine aminotransferase reaction.* Fluid Phase Equilibria, 2016. **422**: p. 87-98.
421. Jimenez, Y.P., H.R. Galleguillos, and M. Claros, *Liquid-liquid partition of perchlorate ion in the aqueous two-phase system formed by NaNO3 + Poly(ethylene glycol) + H2O.* Fluid Phase Equilibria, 2016. **421**: p. 93-103.
422. Franco, T., A. Andrews, and J. Asenjo, *Use of chemically modified proteins to study the effect of a single protein property on partitioning in aqueous two-phase systems: effect of surface hydrophobicity.* Biotechnology and bioengineering, 1996. **49**(3): p. 300-308.
423. Su, C.-K. and B.H. Chiang, *Partitioning and purification of lysozyme from chicken egg white using aqueous two-phase system.* Process Biochemistry, 2006. **41**(2): p. 257-263.
424. Gündüz, U., *Partitioning of bovine serum albumin in an aqueous two-phase system: optimization of partition coefficient.* Journal of Chromatography B: Biomedical Sciences and Applications, 2000. **743**(1-2): p. 259-262.
425. Madeira, P.P., et al., *Prediction of protein partition in polymer/salt aqueous two-phase systems using the modified Wilson model.* Biochemical Engineering Journal, 2005. **24**(2): p. 147-155.

PXRD measurements were done by Lars Jensen within the internal collaboration at Laboratory of Thermodynamics (TU Dortmund). Part of this work contains measured data evolved from supervised student theses at the Faculty of Engineering University of Porto, Portugal [b], and Laboratory of Thermodynamics, Department of Biochemical and Chemical Engineering, TU Dortmund University, Germany [a, b].

[a] Birte Nierhauve

[b] Hoang Tam Do

Data from student theses [a,b] or obtained together with student [b] used partly as indicated below:

Section 5.1 [a]

Section 6.1 [b]

Section 7.1 [b]

Section 7.2 [b]

Appendix

A1. Species fractions of DNP-AA

Table A1.1 Species fractions of DNP-AA calculated with idealized approach according to a procedure from section 2.3 (T=298.15 K, p=1 bar).

pH	**DNP-alanine**		**DNP-glycine**		**DNP-valine**		**DNP-leucine**	
	q = 0	q = -1	q = 0	q = -1	q = 0	q = -1	q = 0	q = -1
1	0.99	0.01	0.98	0.02	1.00	0.00	0.99	0.01
2	0.93	0.07	0.86	0.14	0.97	0.03	0.93	0.07
3	0.56	0.44	0.39	0.61	0.76	0.24	0.56	0.44
4	0.11	0.89	0.06	0.94	0.24	0.76	0.11	0.89
5	0.01	0.99	0.01	0.99	0.03	0.97	0.01	0.99
6	0.00	1.00	0.00	1.00	0.00	1.00	0.00	1.00
7	0.00	1.00	0.00	1.00	0.00	1.00	0.00	1.00
8	**0.00**	**1.00**	**0.00**	**1.00**	**0.00**	**1.00**	**0.00**	**1.00**
9	0.00	1.00	0.00	1.00	0.00	1.00	0.00	1.00

A2. Species fractions of water-soluble vitamins

Table A2.1 Species fractions of vitamins calculated with idealized approach according to a procedure from section 2.3 (T=298.15 K, p=1 bar).

pH	VC			VB3^{acid}			VB2			
	q = 0	q = -1	q = -2	q = +1	q = 0	q = -1	q = +1	q = 0	q = -1	q = -2
1	1.00	0.00	0.00	0.92	0.08	0.00	0.83	0.17	0.00	0.00
2	0.99	0.01	0.00	0.54	0.46	0.00	0.33	0.67	0.00	0.00
3	0.94	0.06	0.00	0.10	0.88	0.01	0.05	0.95	0.00	0.00
4	0.60	0.40	0.00	0.01	0.86	0.13	0.00	0.99	0.01	0.00
5	0.13	0.87	0.00	0.00	0.39	0.61	0.00	0.92	0.08	0.00
6	0.01	0.99	0.00	0.00	0.06	0.94	0.00	0.55	0.45	0.00
7	0.00	1.00	0.00	0.00	0.01	0.99	0.00	0.11	0.89	0.00
8	**0.00**	**1.00**	**0.00**	**0.00**	**0.00**	**1.00**	**0.00**	**0.01**	**0.98**	**0.01**
9	0.00	1.00	0.00	0.00	0.00	1.00	0.00	0.00	0.94	0.06

pH	VB9					VB12		
	q = +1	q = 0	q = -1	q = -2	q = -3	q = +1	q = *0*	q = -1
1	0.96	0.04	0.00	0.00	0.00	0.00	0.83	0.17
2	0.70	0.29	0.01	0.00	0.00	0.00	0.33	0.67
3	0.14	0.58	0.27	0.01	0.00	0.01	0.05	0.95
4	0.00	0.15	0.70	0.14	0.00	0.13	0.00	0.99
5	0.00	0.01	0.32	0.67	0.00	0.61	0.00	0.92
6	0.00	0.00	0.05	0.95	0.01	0.94	0.00	0.55
7	0.00	0.00	0.00	0.92	0.08	0.99	0.00	0.11
8	**0.00**	**0.00**	**0.00**	**0.54**	**0.46**	**1.00**	**0.00**	**0.01**
9	0.00	0.00	0.00	0.11	0.89	1.00	0.00	0.00

A3. Experimental physicochemical properties (density, osmotic coefficient)

Table A3.1 Experimental densities (ρ^{exp}) of NaOH + DNP-AA aqueous solutions. Data were measured by Student (under the supervision) [a] and included in the publication of Wysoczanska *et al.* [8]. Data were measured according to a description from section 3.2.4. x_i are mole fractions [-].

			$\rho^{exp}_{NaOH+DNP-AA}$ [kg·m^{-3}]		
$x_{NaOH}+x_{DNP-AA}$	x_{NaOH}	x_{DNP-AA}	T=298.15 K	T=308.15 K	T=318.15 K
		DNP-Alanine			
3.26E-06	1.46E-06	1.80E-06	997.1	994.1	990
7.08E-07	4.08E-07	3.00E-07	997.1	994.1	990.3
2.47E-05	2.10E-05	3.70E-06	997.2	994.2	989.8
5.06E-04	3.62E-04	1.44E-04	998.7	995.6	991.8
7.22E-04	5.29E-04	1.93E-04	999.3	996.3	992.4
8.38E-04	6.06E-04	2.32E-04	999.7	996.6	992.8
		DNP-Glycine			
3.59E-05	0.00E+00	3.59E-05	997.3	994.3	990.4
4.83E-04	3.37E-04	1.46E-04	998.6	995.6	991.7
7.31E-04	5.44E-04	1.87E-04	999.3	996.3	992.4
1.01E-03	8.16E-04	1.99E-04	999.7	996.6	992.7
		DNP-Valine			
3.28E-07	0.00E+00	3.28E-07	997.1	994.1	990.3
1.60E-05	1.24E-05	3.58E-06	997.1	994.1	990.3
8.96E-04	6.73E-04	2.24E-04	999.9	996.8	992.9
7.76E-04	5.95E-04	1.80E-04	999.5	996.4	992.6
5.58E-04	4.22E-04	1.37E-04	998.8	995.8	991.9
		DNP-Leucine			
6.96E-04	4.99E-04	1.97E-04	999	995.9	992
7.75E-04	5.62E-04	2.13E-04	999.3	996.3	992.4
8.85E-04	6.07E-04	2.78E-04	999.7	996.6	992.7

uncertainty: ±1.5 kg·m^{-3} (ρ), ±0.1 K (T), ±0.05 bar (p).

Table A3.2 Experimental densities (ρ^{exp}) of aqueous vitamin systems at different mole fractions of vitamins (x_i; [-]); T=298.15 K, p=1 bar. Data were measured according to a description from section 3.2.4.

VC		**VB2**		**VB9**	
x_i	ρ_i^{exp} [kg·m^{-3}]	x_i	ρ_i^{exp} [kg·m^{-3}]	x_i	ρ_i^{exp} [kg·m^{-3}]
8.34E-03	1028.17	5.53E-06	997.06	1.00E-04	999.03
1.52E-02	1051.10	1.08E-05	997.11	1.07E-04	999.03
2.09E-02	1069.90	1.20E-05	997.11	2.60E-04	1000.00
2.62E-02	1086.24	2.04E-05	997.18	2.66E-04	1000.30
				2.76E-04	1000.00
				5.02E-04	1003.37
				7.64E-04	1005.86

VB3		**VB12**	
x_i	ρ_i^{exp} [kg·m^{-3}]	x_i	ρ_i^{exp} [kg·m^{-3}]
5.60E-04	998.27	1.29E-05	997.15
1.06E-03	999.35	4.11E-05	997.82
1.07E-03	999.51	8.68E-05	998.82
1.70E-03	1000.84	8.76E-05	998.87
1.77E-03	1001.05	1.15E-04	999.43
2.48E-03	1002.52	1.16E-04	999.43
2.50E-03	1002.64		

uncertainty: ±1.5 kg·m^{-3} (ρ), ±0.1 K (T), ±0.05 bar (p).

Table A3.3 Experimental osmotic coefficients (ϕ_i^{exp}) of aqueous vitamin systems. Data were measured according to a description from section 3.2.4. x_i are mole fractions [-].

VC				**VB3**			
x_i	ϕ_i^{meas}			x_i	ϕ_i^{meas}		
0.0113	0.876	±	0.008	0.0011	0.978	±	0.012
0.0151	0.864	±	0.007	0.0013	0.963	±	0.012
*0.0032	0.181			0.0014	0.963	±	0.012
				0.0015	0.959	±	0.012
				0.0018	0.941	±	0.011
				0.0021	0.912	±	0.011

VB12			
x_i	ϕ_i^{meas}		
0.0001	1.091	±	0.017
0.0002	1.099	±	0.016
0.0004	1.183	±	0.017

*data point from literature, ref. [181].

A4. Experimental pH of ATPS phases and influence on vitamin species fractions

Table A4.1 Species fractions in PEG – Na_3Citrate of water-soluble vitamins calculated with idealized approach according to a procedure from section 2.3 (T=298.15 K, p=1 bar). pH of the phase was calculated as an average of pH measured at >3 tie-lines of all PEG – Na_3Citrate ATPS under study. The deviation between each measurement was <5%.

top phase pH 8.45

vitamins	**VB3^{amide}**	**VB12**	**VB2**	**VB3^{acid}**	**VB9**
0	1.00	1.00			
-1			0.98	1.00	
-2			0.02		0.31
-3					0.69

bottom phase pH 8.25

vitamins	**VB3^{amide}**	**VB12**	**VB2**	**VB3^{acid}**	**VB9**
0	1.00	1.00	0.01		
-1			0.98	1.00	
-2			0.01		0.41
-3					0.59

Table A4.2 Species fractions in PEG – Na_2Tartrate of water-soluble vitamins calculated with idealized approach according to a procedure from section 2.3 (T=298.15 K, p=1 bar). pH of the phase was calculated as an average of pH measured at >3 tie-lines of all PEG – Na_3Citrate ATPS under study. The deviation between each measurement was <5%.

top phase pH 7.7

vitamins	**VB3^{amide}**	**VB12**	**VB2**	**VB3^{acid}**	**VB9**
0	1.00	1.00	0.02		
-1			0.97	1.00	
-2			0.00		0.71
-3					0.28

bottom phase 7.75

vitamins	**VB3^{amide}**	**VB12**	**VB2**	**VB3^{acid}**	**VB9**
0	1.00	1.00	0.02		
-1			0.97	1.00	
-2			0.00		0.69
-3					0.31

A5. DNB modeling

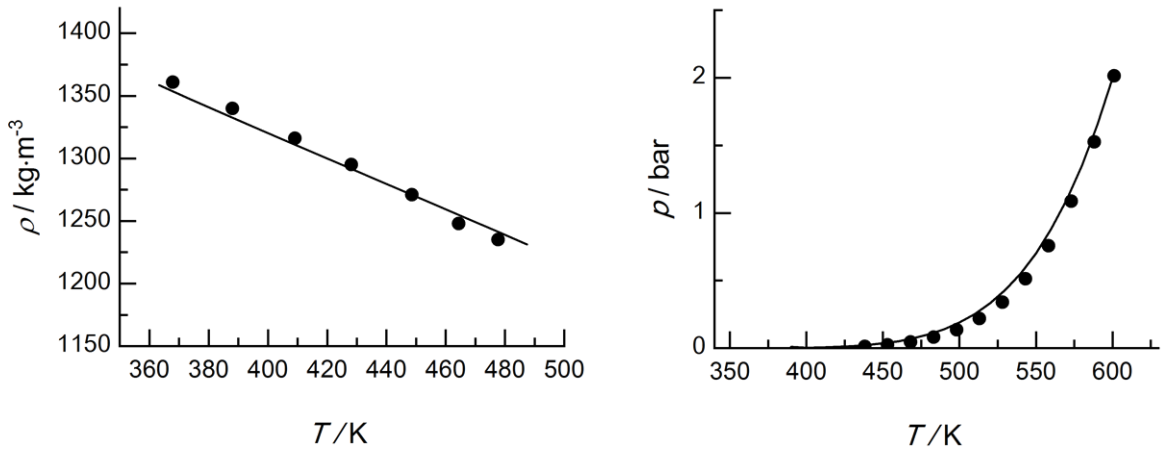

Figure A5.1 ePC-SAFT modeling of dinitrobenzene (DNB); left figure: density of DNB over temperature, ARD% between experimental and predicted data = 0.4; right figure: vapor pressure of DNB over temperature, ARD% between experimental and predicted data = 4.84. Symbols: experimental data from the literature [381,382], Lines: ePC-SAFT modeling. ePC-SAFT parameters are provided in table 4.1.

A6. Experimental solubility of DNP-AA

Table A6.1 Experimental solubility ($m^{L,\,exp}$, mol·kg^{-1}) of DNP-AA in water at T=298.15±0.1 K K and p=1 bar. ARD% calculated with equation (4.14). Data were measured by Student under the supervision of K.Wysoczanska [a] and included in the publication of Wysoczanska *et al.* [8]. Data measured according to a procedure from section 3.2.1.

DNP-alanine			**DNP-glycine**		
pH	$m^{L,exp}$ [mol·kg^{-1}]	ARD%	**pH**	$m^{L,exp}$ [mol·kg^{-1}]	ARD%
3.09	0.002487	4.32	**3.42**	0.00134	3.98
DNP-valine			**DNP-leucine**		
pH	$m^{L,exp}$ [mol·kg^{-1}]	ARD%	**pH**	$m^{L,exp}$ [mol·kg^{-1}]	ARD%
3.17	0.001818	3.87	**3.17**	0.000895	4.32

Table A6.2 The pH-dependent solubility ($m^{L,\,exp}$, mol·kg^{-1}) of DNP-AA measured at T=298.15 K±0.1 K and p=1 bar. ARD% calculated with equation (4.14). Data were measured by Student under the supervision of K.Wysoczanska [a] and included in the publication of Wysoczanska *et al.* [8]. Data measured according to a procedure from section 3.2.1.

DNP-alanine			**DNP-glycine**		
pH	$m^{L,exp}$ [mol·kg^{-1}]	ARD%	**pH**	$m^{L,exp}$ [mol·kg^{-1}]	ARD%
1.87	0.001065	5.1	**2.35**	0.000617	4.78
4.1	0.015196	3.7	**3.97**	0.003607	3.87
6.37	0.053080	4.32	**6.23**	0.019651	3.29
DNP-valine			**DNP-leucine**		
pH	$m^{L,exp}$ [mol·kg^{-1}]	ARD%	**pH**	$m^{L,exp}$ [mol·kg^{-1}]	ARD%
2.23	0.001139	4.37	**2.29**	0.000644	5.01
3.87	0.007155	4.21	**3.95**	0.004124	4.56
6.60	0.018402	3.54	**6.45**	0.004408	4.32

Table A6.3 Temperature influence on experimental solubility ($m^{L,\,exp}$, mol·kg^{-1}) of DNP-AA in water. Data were measured by Student under the supervision of K.Wysoczanska [a] and included in the publication of Wysoczanska *et al.* [8]. ARD% calculated with equation (4.14).

	***T*=308.15 K**			***T*=318.15 K**		
DNP-AA	pH	$m^{L,exp}$ [mol·kg^{-1}]	ARD%	pH	$m^{L,exp}$ [mol·kg^{-1}]	ARD%
DNP-glycine	3.16	0.00182	5.43	3.01	0.0029	4.54
DNP-alanine	2.97	0.00314	3.43	2.75	0.00562	3.45
DNP-valine	3.05	0.00283	5.02	2.87	0.00514	4.89
DNP-leucine	3.08	0.001693	5.23	2.92	0.0029	5.42

uncertainty: ±0.1 K (*T*)

Table A6.4 Intrinsic solubility of DNP-AA (m^{L}, mol·kg^{-1}) at *T*=298.15±0.1 K K and *p*=1 bar calculated using experimental solubilities from table A6.1. Data were calculated according to section 2.3.1.

DNP-AA	m_0^L[mol·kg^{-1}]
DNP-alanine	0.003051
DNP-glycine	0.000259
DNP-valine	0.000635
DNP-leucine	0.000255

A7. Experimental solubility of water-soluble vitamins

Table A7.1 Experimental solubility ($m^{L,\,exp}$, mol·kg^{-1}) of water-solule vitamins in water at T=298.15±0.1 K K and p=1 bar. ARD% calculated with equation (4.14). Data measured according to a procedure from section 3.2.1.

vitamin	pH	$m^{L,exp}$ [mmol·kg^{-1}]	ARD%
VC	1.94	1691.9	0.59
VB3	3.42	140.1	1.2
VB2	5.68	0.2058	1.05
VB9	4.28	0.1069	1.26
VB12	5.55	9.6449	0.95

Table A7.2 The pH-dependent solubility of water-soluble vitamins ($m^{L,\,exp}$, mol·kg^{-1}) measured in this work; T=298.15±0.1 K, p=1 bar. ARD% calculated with equation (4.14). Data measured according to a procedure from section 3.2.1.

VC			**VB2**			**VB3**		
pH	$m^{L,\,exp}$	ARD%	pH	$m^{L,\,exp}$	ARD%	pH	$m^{L,\,exp}$	ARD%
1.94	1.8262	3.56	2.08	0.00027	3.82	3.42	0.1401	2.27
3.64	2.3682	3.54	4.31	0.00022	4.76	3.61	0.1567	2.12
3.98	3.1317	3.98	5.68	0.00021	2.05	4.89	0.3022	2.56
			5.91	0.00025	3.89	5.59	0.7290	2.64
			6.57	0.00067	2.98			
			6.93	0.00126	3.54			

VB9			**VB12**		
pH	$m^{L,\,exp}$	ARD%	pH	$m^{L,\,exp}$	ARD%
4.28	0.00011	4.15	5.55	0.00964	3.95
4.70	0.000168	4.98	6.38	0.00952	4.54
5.35	0.00021	5.03	6.58	0.00957	3.98
5.76	0.00095	4.78	7.81	0.00931	4.23
6.07	0.00272	4.67			

Table A7.3 Experimental aqueous solubilities of poorly-soluble vitamins ($m^{L,exp}_{vitamin(1)}$, mol·kg^{-1}) upon addition of different vitamin additives ($m_{vitamin(2)}$); T=298.15±0.1 K, p=1 bar. Data measured according to a procedure from section 3.2.1. ARD% calculated with equation (4.14).

Vitamin (1)	**Vitamin (2)**	$m_{vitamin(2)}$	pH	$m^{L,exp}_{vitamin(1)}$	ARD%
VB2	-	0	5.68	0.000206	2.05
	VB3^{amide}	0.1	6.36	0.000420	4.98
		0.2	6.43	0.000727	4.23
	VB3^{acid}	0.05	3.44	0.000227	5.08
		0.1	3.36	0.000253	4.27
	VC	0.5	2.23	0.000481	4.23
		1	1.91	0.000813	5.01
VB9	-	0	4.28	0.000107	4.15
	VB3^{amide}	0.1	5.32	0.000732	4.29
VB12	-	0	5.55	0.009645	3.95
	VB3^{amide}	0.1	6.4	0.014123	3.56
		0.2	6.4	0.019749	4.32
	VB3^{acid}	0.05	3.46	0.010263	3.45
		0.1	3.43	0.011379	3.89

A8. ATPS composition (binodals, tie-lines)

Table A8.1 Experimenal binodal data obtained at T=298.15±0.2 K, p=1 bar for PEG – $Na_3Citrate$ and PEG – $K_3Citrate$ ATPS, according to a procedure from section 3.2.2. The values were provided in mass fractions, w [-].

PEG 4000 – $Na_3Citrate$		**PEG 6000 – $Na_3Citrate$**		**PEG 8000 – $Na_3Citrate$***	
w_{PEG}	w_{salt}	w_{PEG}	w_{salt}	w_{PEG}	w_{salt}
0.5675	0.0055	0.4653	0.0123	0.4505	0.0116
0.5393	0.0075	0.4553	0.0139	0.3327	0.0309
0.5098	0.0095	0.4190	0.0173	0.2211	0.0517
0.4394	0.0163	0.3996	0.0198	0.1551	0.0684
0.4215	0.0190	0.3779	0.0227	0.1818	0.0609
0.4023	0.0214	0.3548	0.0264	0.1311	0.0754
0.3626	0.0267	0.3368	0.0287	0.0236	0.1236
0.3496	0.0283	0.3288	0.0298	0.0537	0.1072
0.3422	0.0296	0.3232	0.0312	0.0985	0.0891
0.3242	0.0329	0.3089	0.0343	0.0669	0.1010
0.2934	0.0371	0.2974	0.0361	0.4296	0.0154
0.2819	0.0414	0.2805	0.0393	0.3881	0.0237
0.2421	0.0497	0.2556	0.0440	0.3135	0.0323
0.2215	0.0568	0.2319	0.0488	0.3434	0.0291
0.2019	0.0623	0.2233	0.0512		
0.1672	0.0709	0.2185	0.0520		
0.1443	0.0807	0.2143	0.0538		
0.1375	0.0823	0.1977	0.0588		
0.1310	0.0856	0.1642	0.0682		
0.1238	0.0876	0.1573	0.0717		
0.1068	0.0937	0.1434	0.0757		
0.0769	0.1074	0.1190	0.0843		
0.0613	0.1150	0.0998	0.0899		
0.0344	0.1321	0.0954	0.0919		
0.0216	0.1415	0.0777	0.1003		
0.0109	0.1547	0.0625	0.1065		
0.0065	0.1645	0.0565	0.1101		
		0.0462	0.1160		
		0.0312	0.1230		
		0.0255	0.1279		
		0.0208	0.1318		
		0.0067	0.1490		

PEG 4000 – K_3Citrate		**PEG 6000 – K_3Citrate**		**PEG 8000 – K_3Citrate***	
w_{PEG}	w_{salt}	w_{PEG}	w_{PEG}	w_{salt}	w_{PEG}
0.4494	0.0378	0.4165	0.0416	0.4542	0.0327
0.3670	0.0504	0.3110	0.0591	0.3544	0.0459
0.3308	0.0563	0.2787	0.0659	0.2755	0.0612
0.2548	0.0743	0.2481	0.0722	0.2084	0.0792
0.2396	0.0809	0.2174	0.0818	0.1797	0.0854
0.2006	0.0920	0.1961	0.0873	0.1198	0.1067
0.1905	0.0960	0.1809	0.0922	0.1127	0.1103
0.0282	0.1774	0.1579	0.1013	0.0160	0.1673
0.1291	0.1213	0.0090	0.1911	0.0352	0.1566
0.0737	0.1471	0.0220	0.1727	0.0440	0.1501
0.1522	0.1090	0.0256	0.1672	0.2246	0.0754
0.0061	0.2141	0.0533	0.1482	0.0086	0.1710
		0.0709	0.1408	0.4151	0.0359
		0.0989	0.1257	0.3113	0.0526
		0.1327	0.1107		
		0.1482	0.1037		

*these data were measured only the valiation of binodal curve previously reported by Silverio *et al.* [258]. The standard uncertainties (u) for mass fraction, temperature and pressure are $u(w_i)$=0.002; u(T)=0.2K, u(p)= 0.05 bar.

Table A8.2 Experimenal tie-line data obtained at T=298.15±0.2 K, p=1 bar for PEG – $Na_3Citrate$ and PEG – $K_3Citrate$ ATPS, according to a procedure from section 3.2.2. The values were provided in mass fractions, w [-]. Tie-line length (TLL) was calculated with equation (3.3).

PEG 4000 - $Na_3Citrate$

feed		top phase		bottom phase		
w_{PEG}	w_{salt}	w_{PEG}	w_{salt}	w_{PEG}	w_{salt}	TLL
0.1361	0.0942	0.228	0.054	0.0185	0.146	0.218
0.143	0.0989	0.2585	0.0479	0.0104	0.158	0.260
0.1501	0.1041	0.2864	0.0411	0.0051	0.171	0.298
0.1584	0.1097	0.3143	0.0354	0.0023	0.184	0.334
0.1674	0.1159	0.341	0.0295	0.0009	0.1972	0.368
0.1831	0.1268	0.3801	0.0249	0.0001	0.2193	0.418

PEG 6000 - $Na_3Citrate$

feed		top phase		bottom phase		
w_{PEG}	w_{salt}	w_{PEG}	w_{salt}	w_{PEG}	w_{salt}	TLL
0.1349	0.0946	0.252	0.0451	0.0103	0.1489	0.253
0.1431	0.1005	0.2799	0.0392	0.0049	0.1618	0.290
0.1492	0.1046	0.2998	0.0361	0.0025	0.1718	0.316
0.1558	0.1093	0.3201	0.031	0.0013	0.1813	0.341
0.1631	0.1144	0.3425	0.0279	0.0005	0.1929	0.369
0.1798	0.126	0.3889	0.0212	0.0001	0.2161	0.427

PEG 8000 - $Na_3Citrate$*

feed		top phase		bottom phase		
w_{PEG}	w_{salt}	w_{PEG}	w_{salt}	w_{PEG}	w_{salt}	TLL
0.1091	0.1027	0.193	0.062	0.014	0.15	0.199
0.1201	0.1105	0.242	0.051	0.005	0.17	0.266
0.1305	0.1206	0.286	0.041	0.002	0.188	0.320
0.1397	0.1299	0.319	0.035	0.0005	0.204	0.361
0.1498	0.1382	0.345	0.029	0.0001	0.222	0.395

PEG 4000 - $K_3Citrate$

feed		top phase		bottom phase		
w_{PEG}	w_{salt}	w_{PEG}	w_{salt}	w_{PEG}	w_{salt}	TLL
0.1642	0.1393	0.2959	0.063	0.0049	0.2327	0.337
0.1688	0.1431	0.3167	0.058	0.0033	0.2421	0.363
0.1787	0.152	0.348	0.052	0.0016	0.2576	0.403

PEG 6000 - $K_3Citrate$

feed		top phase		bottom phase		
w_{PEG}	w_{salt}	w_{PEG}	w_{salt}	w_{PEG}	w_{salt}	TLL
0.1754	0.1412	0.3329	0.0531	0.0029	0.2445	0.381
0.1806	0.1453	0.3465	0.0515	0.0019	0.2536	0.399
0.186	0.1496	0.3594	0.0482	0.0012	0.2621	0.417

PEG 8000 - K_3Citrate*

feed		top phase		bottom phase		
w_{PEG}	w_{salt}	w_{PEG}	w_{salt}	w_{PEG}	w_{salt}	TLL
0.1188	0.1255	0.193	0.088	0.013	0.19	0.207
0.1295	0.145	0.28	0.064	0.006	0.21	0.310
0.1404	0.1645	0.334	0.054	0.001	0.239	0.381
0.1502	0.1842	0.384	0.046	0.0002	0.267	0.443
0.1593	0.2036	0.418	0.042	0.0002	0.304	0.493

*literature data that were reported by Silverio *et al.* [258].

The standard uncertainties (u) for mass fraction, temperature and pressure are $u(w_i)$=0.002; u(T)=0.2K, u(p)= 0.05 bar.

Table A8.3 Experimenal binodal data obtained at T=298.15±0.2 K, p=1 bar for PEG – Na_2Tartrate and PEG – KNaTartrate ATPS, according to a procedure from section 3.2.2. The values were provided in mass fractions, w [-]. Data for ATPS composed of PEG and Na_2Tartrate were obtained with Student [b] and included in publication of Wysoczanska *et al.* [7].

PEG 4000 – Na_2Tartrate		**PEG 6000 – Na_2Tartrate**	
w_{PEG}	w_{salt}	w_{PEG}	w_{salt}
0.4257	0.0261	0.0473	0.1355
0.4240	0.0282	0.4085	0.0266
0.3448	0.0413	0.0088	0.1690
0.3082	0.0487	0.0151	0.1617
0.2986	0.0506	0.0216	0.1537
0.2701	0.0571	0.0457	0.1321
0.2251	0.0699	0.0687	0.1245
0.2343	0.0692	0.0043	0.1811
0.2032	0.0768	0.0090	0.1700
0.1944	0.0799	0.4416	0.0233
0.1831	0.0838	0.4296	0.0241
0.1805	0.0848	0.3707	0.0319
0.1565	0.0935	0.3554	0.0348
0.1650	0.0907	0.4361	0.0227
0.1585	0.0930	0.2895	0.0456
0.1549	0.0943	0.2423	0.0580
0.1419	0.0998	0.1814	0.0753

0.1382	0.1017	0.1625	0.0818
0.0156	0.1755	0.1376	0.0917
0.4312	0.0260	0.1180	0.1003
0.0202	0.1685	0.0235	0.1488
0.4515	0.0256	0.0529	0.1308
0.0251	0.1648	0.0619	0.1267
0.0419	0.1521	0.0803	0.1175
0.0493	0.1468	0.0939	0.1110
0.0564	0.1420	0.0074	0.1716
0.0636	0.1398	0.1027	0.1064
0.0637	0.1390	0.1159	0.1010
0.0713	0.1349		
0.0793	0.1306		
0.0855	0.1275		
0.0942	0.1234		
0.1048	0.1175		
0.1056	0.1176		
0.1162	0.1116		
0.1315	0.1058		
0.1349	0.1036		
0.1422	0.1005		
0.1502	0.0973		
0.4270	0.0262		
0.0063	0.1895		
0.0054	0.1986		
0.0054	0.1921		
0.0033	0.2055		
0.0052	0.1945		

PEG 4000 – KNaTartrate		**PEG 6000 – KNaTartrate**		**PEG 8000 – KNaTartrate**	
w_{PEG}	w_{salt}	w_{PEG}	w_{salt}	w_{PEG}	w_{salt}
0.4881	0.0315	0.3409	0.0522	0.3139	0.056
0.4186	0.0399	0.371	0.0475	0.4053	0.0391
0.3795	0.0464	0.3698	0.0477	0.3613	0.0479
0.3402	0.0562	0.2361	0.0799	0.3018	0.0584
0.3164	0.0609	0.2024	0.0913	0.3101	0.058
0.2732	0.0693	0.1157	0.127	0.2213	0.0791
0.2338	0.0829	0.1732	0.1001	0.1821	0.0914
0.2199	0.0879	0.1548	0.11	0.0215	0.1709
0.1938	0.0976	0.0212	0.1875	0.0954	0.1251
0.0349	0.1825	0.0178	0.1855	0.0941	0.1254
0.0656	0.1624	0.108	0.1294	0.1575	0.1001
0.1006	0.1412	0.0806	0.1447	0.1514	0.1022
0.0203	0.1978	0.1479	0.1112	0.0179	0.1739
0.1477	0.1169	0.0325	0.1702	0.3245	0.0532
		0.3605	0.0474	0.0469	0.1526
		0.3052	0.061	0.4094	0.0387
		0.3231	0.0575	0.0684	0.143
		0.0578	0.1572		

The standard uncertainties (u) for mass fraction, temperature and pressure are $u(w_i)$=0.002; $u(T)$=0.2K, $u(p)$= 0.05 bar.

Table A8.4 Experimenal tie-line data obtained at T=298.15±0.2 K, p=1 bar for PEG – Na_2Tartrate and PEG – KNaTartrate ATPS, according to a procedure from section 3.2.2. The values were provided in mass fractions, w [-]. Data for PEG – Na_2Tartrate ATPS were obtained with Student [b] and included in publication of Wysoczanska *et al.* [7]. Tie-line length (TLL) was calculated with equation (3.3).

PEG 4000 - Na_2Tartrate

feed		top phase		bottom phase		
w_{PEG}	w_{salt}	w_{PEG}	w_{salt}	w_{PEG}	w_{salt}	TLL
0.1806	0.0933	0.2396	0.0661	0.0248	0.1696	0.238
0.1866	0.0975	0.2608	0.0607	0.0169	0.1805	0.272
0.1924	0.1018	0.2834	0.0544	0.0127	0.1880	0.302
0.1985	0.1060	0.3030	0.0505	0.0092	0.1957	0.328
0.2044	0.1102	0.3218	0.0467	0.0057	0.2067	0.354
0.2103	0.1144	0.3399	0.0429	0.0041	0.2134	0.377

PEG 6000 - Na_2Tartrate

feed		top phase		bottom phase		
w_{PEG}	w_{salt}	w_{PEG}	w_{salt}	w_{PEG}	w_{salt}	TLL
0.1755	0.0951	0.2654	0.0520	0.0071	0.1830	0.290
0.1802	0.0987	0.2852	0.0481	0.0048	0.1906	0.315
0.1849	0.1021	0.3014	0.0450	0.0035	0.1965	0.334
0.1898	0.1056	0.3199	0.0417	0.0022	0.2046	0.357
0.1951	0.1096	0.3341	0.0394	0.0014	0.2127	0.375
0.1979	0.1126	0.3437	0.0374	0.0009	0.2185	0.388

PEG 4000 - KNaTartrate

feed		top phase		bottom phase		
w_{PEG}	w_{salt}	w_{PEG}	w_{salt}	w_{PEG}	w_{salt}	TLL
0.1618	0.1226	0.2264	0.0849	0.0154	0.2112	0.246
0.1683	0.1268	0.2540	0.0749	0.0097	0.2273	0.288
0.1747	0.1339	0.2856	0.0658	0.0039	0.2430	0.333

PEG 4000 - KNaTartrate

feed		top phase		bottom phase		
w_{PEG}	w_{salt}	w_{PEG}	w_{salt}	w_{PEG}	w_{salt}	TLL
0.1636	0.1165	0.2265	0.0821	0.0123	0.2061	0.248
0.1721	0.1231	0.2643	0.0710	0.0056	0.2248	0.301
0.1781	0.1281	0.2866	0.0641	0.0025	0.2363	0.332

PEG 8000 - KNaTartrate

feed		top phase		bottom phase		
w_{PEG}	w_{salt}	w_{PEG}	w_{salt}	w_{PEG}	w_{salt}	TLL
0.1505	0.1141	0.2159	0.0797	0.0053	0.1942	0.240
0.1587	0.1204	0.2535	0.0693	0.0016	0.2134	0.290
0.1700	0.1295	0.2901	0.0609	0.0008	0.2298	0.335

The standard uncertainties (u) for mass fraction, temperature and pressure are $u(w_i)$=0.002; $u(T)$=0.2K, $u(p)$=0.05 bar.

A9. Partitioning of DNP-AA in ATPS

Table A9.1 Experimenal partition coefficients of DNP-AA $K_{DNP-AA}^{exp,A}$ obtained according to a procedure from section 3.2.3 in ATPS composed by PEG (4000, 6000) and Na_3Citrate, at T=298.15±0.2 K, p=1 bar. Data for PEG 8000 – Na_3Citrate were obtained with Student [b] and included in publication of Wysoczanska *et al.* [4].

	$K_{DNP-AA}^{exp,A}$[-]			
TLL	**DNP-glicyne**	**DNP-alanine**	**DNP-valine**	**DNP-leucine**
	PEG4000 - Na_3Citrate			
0.218	5.278 ± 0.079	5.984 ± 0.104	8.423 ± 0.140	11.252 ± 0.122
0.260	6.641 ± 0.038	7.863 ± 0.042	11.840 ± 0.140	15.903 ± 0.138
0.298	7.984 ± 0.159	9.476 ± 0.112	14.858 ± 0.160	21.656 ± 0.154
0.334	9.844 ± 0.147	11.752 ± 0.154	18.339 ± 0.130	29.456 ± 0.205
0.368	11.402 ± 0.140	15.380 ± 0.065	25.416 ± 0.148	38.548 ± 0.128
0.418	17.875 ± 0.074	22.436 ± 0.244	40.150 ± 0.215	66.591 ± 0.227
	PEG6000 - Na_3Citrate			
0.253	5.623 ± 0.077	7.114 ± 0.104	9.971 ± 0.109	13.470 ± 0.082
0.290	6.769 ± 0.043	8.675 ± 0.079	12.530 ± 0.098	17.800 ± 0.097
0.316	8.349 ± 0.000	10.177 ± 0.127	15.881 ± 0.125	23.080 ± 0.152
0.341	9.611 ± 0.049	12.488 ± 0.120	18.561 ± 0.128	30.000 ± 0.207
0.369	11.347 ± 0.152	15.178 ± 0.154	24.744 ± 0.133	37.738 ± 0.169
0.427	17.576 ± 0.156	24.858 ± 0.143	41.508 ± 0.191	69.258 ± 0.193
	PEG8000 - Na_3Citrate			
0.266	7.25 ± 0.01	8.45 ± 0.04	13.46 ± 0.03	17.36 ± 0.03
0.320	9.87 ± 0.03	12.12 ± 0.08	20.02 ± 0.03	26.86 ± 0.01
0.361	12.76 ± 0.04	15.95 ± 0.08	27.73 ± 0.08	38.39 ± 0.06

The standard uncertainties (u) for mass fraction, temperature and pressure are $u(w_i)$=0.002; u(T)=0.2K, u(p)=0.05 bar.

Table A9.2 Experimenal partition coefficients of DNP-AA $K_{DNP-AA}^{exp,A}$ obtained according to a procedure from section 3.2.3 in ATPS composed by PEG and K_3Citrate, at T=298.15±0.2 K, p=1 bar. Data were obtained with Student [b] and included in publication of Wysoczanska *et al.* [4].

	$K_{DNP-AA}^{exp,A}$[-]			
TLL	**DNP-glycine**	**DNP-alanine**	**DNP-valine**	**DNP-leucine**
	PEG4000 - K_3Citrate			
0.337	8.42 ± 0.01	10.53 ± 0.01	17.35 ± 0.03	24.04 ± 0.02
0.363	9.18 ± 0.01	12.8 ± 0.05	20.21 ± 0.04	30.5 ± 0.04
0.403	12.77 ± 0.03	16.6 ± 0.03	29.01 ± 0.03	47.23 ± 0.13
	PEG6000 - K_3Citrate			
0.381	9.52 ± 0.04	11.49 ± 0.03	18.7 ± 0.05	28.99 ± 0.08
0.399	10.58 ± 0.06	14.07 ± 0.04	22.79 ± 0.01	36.02 ± 0.02
0.417	12.72 ± 0.08	15.88 ± 0.02	27.8 ± 0.17	45.3 ± 0.12
	PEG8000 - K_3Citrate			
0.310	6.39 ± 0.17	8.01 ± 0.01	12.72 ± 0.01	16.52 ± 0.04
0.381	9.75 ± 0.03	13.31 ± 0.04	21.04 ± 0.03	30.57 ± 0.05
0.443	15.35 ± 0.04	19.99 ± 0.08	37.14 ± 0.12	54.02 ± 0.20

The standard uncertainties (u) for mass fraction, temperature and pressure are $u(w_i)$=0.002; u(T)=0.2K, u(p)=0.05 bar.

Table A9.3 Experimenal partition coefficients of DNP-AA $K_{DNP-AA}^{exp,A}$ obtained according to a procedure from section 3.2.3 in ATPS composed by PEG and KNaTartrate, at T=298.15±0.2 K, p=1 bar. Data were obtained with Student [b] and included in publication of Wysoczanska *et al.* [4].

	$K_{DNP-AA}^{exp,A}$[-]			
TLL	**DNP-glicyne**	**DNP-alanine**	**DNP-valine**	**DNP-leucine**
	PEG4000 - K_3Citrate			
0.246	3.76 ± 0.01	4.55 ± 0.01	6.58 ± 0.01	8.21 ± 0.01
0.288	4.64 ± 0.01	5.53 ± 0.01	8.55 ± 0.01	11.04 ± 0.02
0.333	5.68 ± 0.01	7.18 ± 0.01	11.68 ± 0.01	15.33 ± 0.08
	PEG6000 - K_3Citrate			
0.248	3.9 ± 0.02	4.48 ± 0.01	6.49 ± 0.02	8.39 ± 0.01
0.301	4.81 ± 0.01	5.8 ± 0.02	8.87 ± 0.03	11.75 ± 0.01
0.332	5.41 ± 0.01	6.77 ± 0.01	10.52 ± 0.02	14.48 ± 0.01
	PEG8000 - K_3Citrate			
0.240	3.49 ± 0.01	4.23 ± 0.01	5.84 ± 0.01	7.16 ± 0.01
0.290	4.28 ± 0.01	5.07 ± 0.03	7.73 ± 0.01	9.76 ± 0.01
0.335	5.53 ± 0.01	7.09 ± 0.03	10.54 ± 0.01	14.61 ± 0.02

The standard uncertainties for mass fraction, temperature and pressure are $u(w_i)$=0.002; u(T)=0.2K, u(p)=0.05 bar.

Table A9.4 Experimenal partition coefficients of DNP-AA $K_{DNP-AA}^{exp,A}$ obtained according to a procedure from section 3.2.3 in ATPS composed by PEG 8000 and inorganic salt (Na_2Sulfate, MgSulfate), at T=298.15±0.2 K, p=1 bar.

	$K_{DNP-AA}^{exp,A}$[-]			
TLL	**DNP-glicyne**	**DNP-alanine**	**DNP-valine**	**DNP-leucine**
	PEG8000 – Na_2Sulfate			
0.262	6.863 ± 0.098	7.999 ± 0.152	13.354 ± 0.206	17.851 ± 0.254
0.294	8.557 ± 0.074	10.490 ± 0.043	16.946 ± 0.189	24.107 ± 0.265
0.336	11.603 ± 0.220	13.327 ± 0.232	23.575 ± 0.246	34.097 ± 0.320
0.368	14.369 ± 0.243	16.794 ± 0.135	29.398 ± 0.294	45.222 ± 0.445
0.389	18.301 ± 0.193	22.134 ± 0.262	36.345 ± 0.350	61.153 ± 0.599
	PEG8000 - MgSulfate			
0.279	4.161 ± 0.042	4.842 ± 0.066	7.333 ± 0.047	9.272 ± 0.107
0.308	4.852 ± 0.074	5.788 ± 0.058	9.188 ± 0.107	11.952 ± 0.175
0.333	5.971 ± 0.031	7.634 ± 0.031	11.806 ± 0.059	16.475 ± 0.069
0.361	7.518 ± 0.085	9.887 ± 0.082	16.285 ± 0.181	23.010 ± 0.288
0.396	8.937 ± 0.136	11.883 ± 0.136	20.938 ± 0.180	30.613 ± 0.327

The standard uncertainties for mass fraction, temperature and pressure are $u(w_i)$=0.002; u(T)=0.2K, u(p)=0.05 bar.

A10. Partitioning of vitamins in ATPS

Table A10.1 Experimenal partition coefficients $K_{vitamin}^{exp,A}$ obtained according to a procedure from section 3.2.3 in ATPS composed by PEG and Na_3Citrate, at T=298.15±0.2 K, p=1 bar. Data were obtained with Student [b] and included in publication of Wysoczanska *et al.* [7].

	$K_{vitamin}^{exp,A}$ [-]									
TLL	**VB2**		**VB3^{acid}**		**VB3^{amide}**		**VB9**		**VB12**	
					PEG4000 - Na_3Citrate					
0.218	2.205	±0.098	2.828	±0.119	2.710	±0.114	5.438	±0.232	7.013	±0.313
0.260	2.380	±0.109	3.276	±0.140	3.117	±0.135	6.480	±0.277	9.612	±0.437
0.298	2.571	±0.124	3.714	±0.170	3.412	±0.158	7.544	±0.325	13.559	±0.583
0.334	2.843	±0.131	4.296	±0.193	3.927	±0.163	8.926	±0.384	17.179	±0.763
0.368	3.054	±0.135	4.879	±0.214	4.423	±0.185	10.996	±0.477	23.664	±1.073
0.418	3.352	±0.149	6.101	±0.257	5.190	±0.258	15.095	±0.645	39.971	±1.728
					PEG6000 - Na_3Citrate					
0.253	2.367	±0.106	2.989	±0.127	2.878	±0.124	5.877	±0.249	8.339	±0.354
0.29	2.501	±0.111	3.413	±0.154	3.309	±0.138	6.951	±0.308	10.845	±0.484
0.316	2.675	±0.116	3.700	±0.163	3.530	±0.156	8.082	±0.348	12.854	±0.557
0.341	2.825	±0.133	4.325	±0.186	3.882	±0.163	9.841	±0.410	15.804	±0.722
0.369	2.976	±0.131	4.786	±0.210	4.301	±0.194	10.508	±0.456	21.790	±0.978
0.427	3.354	±0.147	5.959	±0.262	5.270	±0.222	14.304	±0.617	34.727	±1.902

The standard uncertainties (u) for mass fraction, temperature and pressure are $u(w_i)$=0.002; u(T)=0.2K, u(p)=0.05 bar.

Table A10.2 Experimenal partition coefficients $K_{vitamin}^{exp,A}$ obtained according to a procedure from section 3.2.3 in ATPS composed by PEG and Na_2Tartrate, at T=298.15±0.2 K, p=1 bar. Data were obtained with Student [b] and included in publication of Wysoczanska *et al.* [7].

	$K_{vitamin}^{exp,A}$ [-]									
TLL	**VB2**		**VB3^{acid}**		**VB3^{amide}**		**VB9**		**VB12**	
PEG4000 - Na_2Tartrate										
0.238	1.886	±0.096	2.025	±0.089	2.124	±0.099	2.695	±0.114	5.978	±0.269
0.272	2.165	±0.105	2.332	±0.100	2.602	±0.122	3.272	±0.241	7.930	±0.343
0.302	2.331	±0.111	2.561	±0.111	2.845	±0.123	3.636	±0.154	10.514	±0.457
0.328	2.463	±0.113	2.819	±0.124	3.218	±0.144	4.043	±0.172	13.165	±0.598
0.354	2.680	±0.130	3.041	±0.130	3.475	±0.148	4.350	±0.183	16.107	±0.746
0.377	2.765	±0.141	3.231	±0.138	3.802	±0.164	4.751	±0.199	19.279	±0.832
PEG6000 - Na_2Tartrate										
0.290	2.028	±0.115	2.175	±0.103	2.380	±0.106	2.996	±0.126	6.402	±0.283
0.314	2.201	±0.108	2.386	±0.110	2.636	±0.132	3.473	±0.147	8.291	±0.354
0.334	2.302	±0.118	2.578	±0.111	3.002	±0.128	3.563	±0.151	10.174	±0.450
0.357	2.384	±0.125	2.738	±0.119	3.224	±0.143	3.861	±0.161	11.021	±0.485
0.375	2.536	±0.111	2.897	±0.136	3.470	±0.291	4.051	±0.169	13.763	±0.585
0.388	2.650	±0.121	3.061	±0.139	3.744	±0.167	4.334	±0.182	15.823	±0.670

The standard uncertainties (u) for mass fraction, temperature and pressure are $u(w_i)$=0.002; u(T)=0.2K, u(p)=0.05 bar.

Table A10.3 Theoretical partition coefficients of VB9 (K_{VB9}) obtained according to sections 2.3.2 and 3.2.3 in ATPS composed by PEG and Na_3Citrate and PEG and Na_2Tartrate, at T=298.15±0.2 K, p=1 bar. The species at pH∼8 of ATPS are $VB9^{2-}$ and $VB9^{3-}$.

PEG 6000 + Na_3Citrate

$K_{vitamin}^{exp,A}$	TLL	K (-2)	K (-3)
5.88	0.253	4.38	6.94
6.95	0.290	5.18	8.21
8.08	0.316	6.02	9.54
9.84	0.341	7.33	11.62
10.51	0.369	7.83	12.41
14.30	0.427	10.66	16.89

PEG 4000 + Na_3Citrate

$K_{vitamin}^{exp,A}$	TLL	K (-2)	K (-3)
5.44	0.218	4.05	6.42
6.48	0.260	4.83	7.65
7.54	0.298	5.62	8.91
8.93	0.334	6.65	10.54
11.00	0.368	8.19	12.98
15.10	0.418	11.25	17.82

PEG 6000 + Na_2Tartrate

$K_{vitamin}^{exp,A}$	TLL	K (-2)	K (-3)
3.00	0.225	3.10	2.76
3.47	0.258	3.59	3.20
3.56	0.289	3.69	3.29
3.86	0.315	3.99	3.56
4.05	0.342	4.19	3.74
4.33	0.365	4.48	4.00

PEG 4000 + Na_2Tartrate

$K_{vitamin}^{exp,A}$	TLL	K (-2)	K (-3)
2.70	0.276	2.79	2.49
3.27	0.301	3.39	3.02
3.64	0.321	3.76	3.35
4.04	0.344	4.18	3.73
4.35	0.363	4.50	4.01
4.75	0.376	4.92	4.38

Table A10.4 Experimental partition coefficients of VC obtained according to section3.2.3 in ATPS composed by PEG and Na_3Citrate and PEG and Na_2Tartrate, at T=298.15±0.2 K, p=1 bar. Data were obtained with Student [b], however they were not further considered.

	$K_{vitamin}^{exp,A}$ [-]	
TLL	**VC**	
PEG 4000 – Na_3Citrate		
0.218	0.645	±0.002
0.260	0.624	±0.009
0.298	0.628	±0.012
0.334	0.611	±0.006
0.368	0.610	±0.015
0.418	0.634	±0.010
PEG 6000 – Na_3Citrate		
0.253	0.649	±0.007
0.29	0.641	±0.011
0.316	0.652	±0.015
0.341	0.638	±0.009
0.369	0.614	±0.012
0.427	0.628	±0.013

	$K_{vitamin}^{exp,A}$ [-]	
TLL	**VC**	
PEG 4000 – Na_2Tartrate		
0.238	0.830	±0.010
0.272	0.792	±0.008
0.302	0.765	±0.008
0.328	0.735	±0.006
0.354	0.728	±0.027
0.377	0.710	±0.020
PEG 6000 – Na_2Tartrate		
0.290	0.857	±0.007
0.314	0.810	±0.021
0.334	0.803	±0.008
0.357	0.819	±0.015
0.375	0.757	±0.024
0.388	0.745	±0.017

The standard uncertainties (u) for mass fraction, temperature and pressure are $u(w_i)$=0.002; u(T)=0.2K, u(p)=0.05 bar.

A11. Reliability of ePC-SAFT solubility and density predictions (DNP-AA)

Table A11.1 ARD% for predicted with ePC-SAFT intrinsic solubility of DNP-AA $m_{0,DNP-AA}^{L,pred}$ at T=298.15 K and p=1 bar. ARD% calculated with equation (4.14).

DNP-AA	ARD%($m_{0,DNP-AA}^{L,pred}$)
DNP-alanine	0.19
DNP-glycine	8.76
DNP-valine	7.76
DNP-leucine	2.02

Table A11.2 ARD% for predicted with ePC-SAFT density of DNP-AA at T=298.15 K, T=308.15K, and 318.15 K, and p=1 bar. ARD% calculated with equation (4.14).

	ARD% ($\rho_{DNP-AA+NaOH}^{pred}$)		
Aqueous system	(T=298.15 K)	(T= 308.15 K)	(T=318.15 K)
water + DNP-glycine + NaOH	0.04	0.04	0.04
water + DNP-alanine + NaOH	0.04	0.04	0.04
water + DNP-valine + NaOH	0.04	0.04	0.05
water + DNP-leucine + NaOH	0.08	0.08	0.08

A12. Reliability of ePC-SAFT solubility predictions and modeling of density and osmolality (vitamins)

Table A12.1 ARD% for predicted with ePC-SAFT intrinsic solubility of vitamins $m_{0,vitamin}^{L,pred}$ at T=298.15 K and p=1 bar. ARD% calculated with equation (4.14).

vitamin	ARD%($m_{0,vitamin}^{L,pred}$)
VC	2.57
VB2	3.28
VB3^{acid}	1.62
VB9	4.56
VB12	0.20

Table A12.2 ARD% for predicted with ePC-SAFT solubility of vitamins $m_{vitamin}^{L,pred}$ at T=298.15 K and p=1 bar. ARD% calculated with equation (4.14).

Vitamin system	$m_{additive}^{max}$	% ARD $m^{L,pred}$
VB2 + VB3^{amide}	2	9.35
VB2 + VB3^{acid}	0.1	2.04
VB2 + VC	1.4	14.50
VB9 + VB3^{amide}	0.2	4.23
VB12 + VB3^{amide}	0.2	3.76
VB12 + VB3^{acid}	0.1	6.89

Table A12.3 ARD% for predicted with ePC-SAFT temperature-dependent solubility of vitamins $m_{vitamin}^{L,pred}$ at T=298.15 K and p=1 bar. ARD% calculated with equation (4.14).

vitamin	ARD%($m_{vitamin}^{L,pred}$)
VC	29.24
VB3^{acid}	2.82

Table A12.3 ARD% for modeled with ePC-SAFT density (T=298.15 K and p=1 bar) and osmotic coefficient of vitamins.

	% ARD	
vitamin	ρ_i	ϕ_i
VC	0.16	0.90
VB2	0.00	n.a.
VB3	0.02	0.99
VB9	0.04	n.a.
VB12	0.01	1.61

A13. Partitioning of DNP-AA predicted with ePC-SAFT (partition coefficient accuracy + activity coefficient)

Table A13.1 Activity coefficients of DNP-AA predicted using ePC-SAFT in two phases of ATPS, γ(I) - top and γ(II) – bottom. ARD% are the values calculated with equation (4.14) based on experimental K_{DNP-AA}^{exp} and predicted partition coefficients K_{DNP-AA}^{pred} (calculated as K_{DNP-AA}^{pred}= γ(II)/ γ(I)).

	DNP-alanine			**DNP-glycine**		
PEG 4000 - Na_3Citrate						
TLL	***γ(I)***	***γ(II)***	***ARD%(K)***	***γ(I)***	***γ(II)***	***ARD%(K)***
0.218	9.91	53.93	9.05	95.80	466.79	7.67
0.26	8.40	62.51	5.34	82.10	529.47	2.90
0.298	7.27	71.90	4.34	72.17	593.19	2.96
0.334	6.36	81.53	9.15	64.05	653.55	3.66
0.368	5.63	91.96	6.11	57.80	714.71	8.46
0.418	4.75	111.85	4.92	49.87	823.57	7.61
PEG 6000 - Na_3Citrate						
TLL	***γ(I)***	***γ(II)***	***ARD%(K)***	***γ(I)***	***γ(II)***	***ARD%(K)***
0.253	8.59	58.30	4.65	84.46	504.29	6.20
0.29	7.45	66.85	3.42	74.16	563.62	12.28
0.316	6.77	73.64	6.95	67.91	607.53	7.16
0.341	6.16	80.46	4.58	62.68	649.63	7.85
0.369	5.57	88.95	5.17	57.36	698.84	7.37
0.427	4.59	108.99	4.50	48.71	808.95	5.51
PEG 8000 - Na_3Citrate						
TLL	***γ(I)***	***γ(II)***	***ARD%(K)***	***γ(I)***	***γ(II)***	***ARD%(K)***
0.266	9.10	71.30	7.23	88.39	589.62	7.99
0.32	7.22	84.53	3.41	71.67	671.21	5.11
0.361	6.15	97.89	0.22	62.11	748.52	5.56
PEG 4000 - K_3Citrate						
TLL	***γ(I)***	***γ(II)***	***ARD%(K)***	***γ(I)***	***γ(II)***	***ARD%(K)***
0.337	6.71	66.93	5.21	60.32	391.64	22.89
0.363	6.05	71.21	8.03	55.39	404.50	20.46
0.403	5.22	77.98	10.09	49.07	418.90	33.15
PEG 6000 - K_3Citrate						
TLL	***γ(I)***	***γ(II)***	***ARD%(K)***	***γ(I)***	***γ(II)***	***ARD%(K)***
0.381	5.57	71.99	12.46	51.97	406.10	17.91
0.399	5.24	76.46	3.66	49.36	416.68	20.22
0.417	4.94	80.18	2.13	47.15	425.01	29.14

PEG 8000 - K_3Citrate

TLL	*γ(I)*	*γ(II)*	*ARD%(K)*	*γ(I)*	*γ(II)*	*ARD%(K)*
0.31	7.20	59.24	2.77	64.45	374.71	9.01
0.381	5.52	71.27	3.04	51.38	409.90	18.18
0.443	4.39	82.76	5.76	42.58	431.15	34.03

PEG 6000 - KNaTartrate

TLL	*γ(I)*	*γ(II)*	*ARD%(K)*	*γ(I)*	*γ(II)*	*ARD%(K)*
0.25	9.57	46.20	6.06	86.45	342.18	5.26
0.29	8.28	51.31	12.00	76.32	366.02	3.36
0.33	7.09	57.74	13.39	66.70	396.75	4.72

PEG 6000 - KNaTartrate

TLL	*γ(I)*	*γ(II)*	*ARD%(K)*	*γ(I)*	*γ(II)*	*ARD%(K)*
0.116	9.51	46.21	8.44	86.47	347.62	3.08
0.123	7.84	52.43	15.32	72.86	377.44	7.71
0.128	7.02	56.78	19.46	66.32	398.39	11.03

PEG 8000 - KNaTartrate

TLL	*γ(I)*	*γ(II)*	*ARD%(K)*	*γ(I)*	*γ(II)*	*ARD%(K)*
0.24	9.99	46.29	9.55	91.30	361.28	13.39
0.29	8.27	51.29	22.38	77.14	382.43	15.83
0.335	6.91	55.67	13.57	65.75	397.31	9.27

	DNP-valine			**DNP-leucine**		

PEG 4000 - Na_3Citrate

TLL	*γ(I)*	*γ(II)*	*ARD%(K)*	*γ(I)*	*γ(II)*	*ARD%(K)*
0.218	23.17	161.95	17.03	454.42	4188.96	18.07
0.26	19.23	193.44	15.05	361.93	5078.79	11.76
0.298	16.31	229.70	5.21	295.42	6106.02	4.56
0.334	13.98	268.75	4.84	243.46	7212.91	0.58
0.368	12.16	312.84	1.27	203.73	8464.95	7.79
0.418	10.00	401.30	0.09	158.01	10987.33	4.42

PEG 6000 - Na_3Citrate

TLL	*γ(I)*	*γ(II)*	*ARD%(K)*	*γ(I)*	*γ(II)*	*ARD%(K)*
0.253	19.62	176.76	9.66	372.38	4620.89	7.88
0.29	16.68	209.14	0.04	304.83	5534.95	2.01
0.316	14.96	235.93	0.69	265.80	6291.90	2.57
0.341	13.41	263.71	5.91	231.66	7078.12	1.85
0.369	11.97	299.64	1.20	200.00	8094.30	7.24
0.427	9.56	388.10	2.24	149.02	10612.21	2.82

PEG 8000 - Na_3Citrate

TLL	*γ(I)*	*γ(II)*	*ARD%(K)*	*γ(I)*	*γ(II)*	*ARD%(K)*
0.266	21.01	227.23	19.64	403.90	6037.23	13.90
0.32	16.15	281.28	13.00	292.34	7567.50	3.63
0.361	13.45	338.57	9.23	232.31	9198.57	3.14

PEG 4000 - K_3Citrate

TLL	*γ(I)*	*γ(II)*	*ARD%(K)*	*γ(I)*	*γ(II)*	*ARD%(K)*
0.337	15.36	229.90	13.71	274.16	6159.27	6.55
0.363	13.85	249.15	11.00	236.08	6709.48	6.82
0.403	11.52	281.60	15.73	190.38	7627.64	15.17

PEG 6000 - K_3Citrate

TLL	*γ(I)*	*γ(II)*	*ARD%(K)*	*γ(I)*	*γ(II)*	*ARD%(K)*
0.381	12.36	252.89	9.38	208.94	6814.89	12.51
0.399	11.53	274.02	4.26	191.06	7415.25	7.75
0.417	10.77	291.97	2.47	174.92	7925.99	0.03

PEG 8000 - K_3Citrate

TLL	*γ(I)*	*γ(II)*	*ARD%(K)*	*γ(I)*	*γ(II)*	*ARD%(K)*
0.31	16.58	194.63	7.69	302.53	5172.77	3.50
0.381	12.25	248.23	3.69	206.53	6696.01	6.06
0.443	9.41	304.44	12.90	146.79	8283.27	4.46

PEG 6000 - KNaTartrate

TLL	*γ(I)*	*γ(II)*	*ARD%(K)*	*γ(I)*	*γ(II)*	*ARD%(K)*
0.25	22.45	138.09	6.50	435.11	3504.41	1.90
0.29	19.02	157.67	3.05	355.39	4039.36	2.95
0.33	15.94	182.70	1.84	285.11	4732.50	8.28

PEG 6000 - KNaTartrate

TLL	*γ(I)*	*γ(II)*	*ARD%(K)*	*γ(I)*	*γ(II)*	*ARD%(K)*
0.116	22.20	137.20	4.79	430.34	3489.96	3.34
0.123	17.83	160.91	1.75	328.52	4140.68	7.27
0.128	15.71	177.76	7.54	280.61	4608.22	13.41

PEG 8000 - KNaTartrate

TLL	*γ(I)*	*γ(II)*	*ARD%(K)*	*γ(I)*	*γ(II)*	*ARD%(K)*
0.24	23.35	135.25	0.79	458.60	3459.44	5.36
0.29	18.84	154.67	6.21	352.56	3987.98	15.90
0.335	15.40	172.65	6.36	273.96	4474.63	11.80

A14. Partitioning of vitamins predicted with ePC-SAFT (partition coefficient accuracy + activity coefficient)

Table A14.1 Activity coefficients of vitamins predicted using ePC-SAFT in two phases of ATPS, γ(I) - top and γ(II) – bottom. ARD% are the values calculated with equation (4.14) based on experimental $K_{vitamin}^{exp}$ and predicted partition coefficients $K_{vitamin}^{pred}$ (calculated as $K_{vitamin}^{pred} = \gamma(\text{II})/\gamma(\text{I})$).

	VB2			VB3^{acid}		
PEG 4000 - Na_3Citrate						
TLL	***γ(I)***	***γ(II)***	***ARD%(K)***	***γ(I)***	***γ(II)***	***ARD%(K)***
0.218	275.86	618.09	1.61	1.51	4.13	3.47
0.260	296.72	738.09	4.52	1.43	4.62	1.15
0.298	322.16	893.06	7.82	1.36	5.16	1.81
0.334	360.82	1079.17	5.20	1.32	5.72	0.76
0.368	410.71	1308.50	4.32	1.30	6.34	0.14
0.418	526.89	1815.32	2.79	1.28	7.52	3.71
PEG 6000 - Na_3Citrate						
TLL	***γ(I)***	***γ(II)***	***ARD%(K)***	***γ(I)***	***γ(II)***	***ARD%(K)***
0.253	280.94	654.08	1.64	1.43	4.35	2.04
0.290	305.88	787.65	2.96	1.37	4.85	3.97
0.316	331.80	909.13	2.43	1.33	5.25	6.28
0.341	361.21	1043.23	2.24	1.31	5.65	0.29
0.369	407.94	1231.70	1.46	1.29	6.15	0.37
0.427	550.83	1733.22	6.19	1.28	7.34	3.67
PEG 4000 - Na_2Tartrate						
TLL	***γ(I)***	***γ(II)***	***ARD%(K)***	***γ(I)***	***γ(II)***	***ARD%(K)***
0.238	282.70	536.95	13.99	1.32	2.73	2.38
0.272	299.79	611.28	15.22	1.28	2.90	2.68
0.302	321.41	668.15	19.62	1.25	3.01	5.92
0.328	349.24	735.45	25.92	1.23	3.14	9.47
0.354	381.73	838.83	26.66	1.22	3.30	10.77
0.377	420.04	908.43	35.31	1.21	3.40	13.05
PEG 6000 - Na_2Tartrate						
TLL	***γ(I)***	***γ(II)***	***ARD%(K)***	***γ(I)***	***γ(II)***	***ARD%(K)***
0.290	290.19	650.83	5.24	1.28	3.08	10.68
0.314	312.66	705.60	1.57	1.25	3.15	5.50
0.334	335.25	755.66	1.32	1.24	3.23	1.24
0.357	366.96	829.76	4.33	1.22	3.33	0.60
0.375	396.32	910.33	9.43	1.22	3.43	2.66
0.388	418.12	974.41	12.04	1.22	3.51	5.72

	VB3^{amide}			VB12		
PEG 4000 - Na_3Citrate						
TLL	***γ(I)***	***γ(II)***	***ARD%(K)***	***γ(I)***	***γ(II)***	***ARD%(K)***
0.218	1.11	2.98	0.61	0.07	0.37	20.39
0.260	0.99	3.14	1.80	0.04	0.36	13.51
0.298	0.90	3.26	5.94	0.03	0.34	16.32
0.334	0.82	3.32	2.80	0.02	0.31	9.14
0.368	0.76	3.37	0.13	0.01	0.28	12.51
0.418	0.68	3.41	3.36	0.01	0.22	15.05
PEG 6000 - Na_3Citrate						
TLL	***γ(I)***	***γ(II)***	***ARD%(K)***	***γ(I)***	***γ(II)***	***ARD%(K)***
0.253	1.01	3.13	7.38	0.05	0.39	7.18
0.290	0.92	3.25	6.64	0.03	0.38	1.11
0.316	0.86	3.31	8.72	0.03	0.35	6.40
0.341	0.81	3.35	6.54	0.02	0.33	6.21
0.369	0.76	3.37	3.72	0.01	0.29	1.04
0.427	0.66	3.41	2.50	0.01	0.23	13.74
PEG 4000 - Na_2Tartrate						
TLL	***γ(I)***	***γ(II)***	***ARD%(K)***	***γ(I)***	***γ(II)***	***ARD%(K)***
0.238	0.98	2.38	14.60	0.04	0.19	18.57
0.272	0.91	2.47	4.12	0.03	0.19	21.37
0.302	0.85	2.50	3.53	0.02	0.18	24.97
0.328	0.80	2.55	1.06	0.02	0.17	22.81
0.354	0.76	2.58	2.07	0.01	0.16	22.70
0.377	0.72	2.58	5.58	0.01	0.15	19.26
PEG 6000 - Na_2Tartrate						
TLL	***γ(I)***	***γ(II)***	***ARD%(K)***	***γ(I)***	***γ(II)***	***ARD%(K)***
0.290	0.91	2.64	21.90	0.03	0.21	0.79
0.314	0.85	2.63	17.10	0.03	0.20	5.67
0.334	0.81	2.64	8.38	0.02	0.19	7.32
0.357	0.77	2.64	6.66	0.01	0.17	5.58
0.375	0.74	2.63	3.01	0.01	0.16	1.95
0.388	0.72	2.62	2.31	0.01	0.15	7.40

	VB9 (2-)			VB9 (3-)		
PEG 4000 - Na_3Citrate						
TLL	***γ(I)***	***γ(II)***	***ARD%(K)***	***γ(I)***	***γ(II)***	***ARD%(K)***
0.218	417.65	1685.80	0.36	0.60	3.70	3.72
0.260	442.55	2227.07	4.25	0.59	4.82	7.75
0.298	479.45	3014.84	11.89	0.61	6.33	16.24
0.334	540.68	4090.93	13.79	0.66	8.22	18.09
0.368	629.17	5604.54	8.74	0.76	10.73	8.53
0.418	825.72	9645.46	3.88	0.90	17.01	5.46
PEG 6000 - Na_3Citrate						
TLL	***γ(I)***	***γ(II)***	***ARD%(K)***	***γ(I)***	***γ(II)***	***ARD%(K)***
0.253	422.11	1837.79	0.55	0.61	4.19	1.45
0.290	459.32	2462.94	3.55	0.63	5.42	4.03
0.316	499.09	3096.85	3.06	0.66	6.58	5.20
0.341	552.90	3866.25	4.62	0.73	7.93	6.50
0.369	632.08	5070.83	2.48	0.79	9.91	0.60
0.427	897.07	8924.71	6.64	1.06	15.94	11.03
PEG 4000 - Na_2Tartrate						
TLL	***γ(I)***	***γ(II)***	***ARD%(K)***	***γ(I)***	***γ(II)***	***ARD%(K)***
0.238	419.72	1161.40	0.76	0.50	1.50	19.42
0.272	443.84	1397.36	7.00	0.51	1.71	10.21
0.302	477.76	1587.74	11.66	0.54	1.86	1.64
0.328	520.69	1823.19	16.29	0.57	2.04	4.00
0.354	572.94	2207.78	14.38	0.61	2.29	5.86
0.377	636.78	2481.95	20.71	0.66	2.45	14.83
PEG 6000 - Na_2Tartrate						
TLL	***γ(I)***	***γ(II)***	***ARD%(K)***	***γ(I)***	***γ(II)***	***ARD%(K)***
0.290	438.98	1524.29	12.02	0.59	1.95	20.61
0.314	474.91	1712.86	0.37	0.61	2.07	5.74
0.334	512.17	1891.53	0.18	0.64	2.18	3.94
0.357	565.10	2168.10	3.96	0.68	2.34	3.00
0.375	614.69	2484.69	3.56	0.72	2.52	5.95
0.388	654.31	2747.97	6.34	0.76	2.65	12.34

Acknowledgments: This work was financed through BD scholarship of Kamila Wysoczanska supported by FCT (PD/BD/114315/2016) and funds of LSRE-LCM financially supported by POCI-01-0145-FEDER-006984, FEDER funds through COMPETE2020, FCT, AlProcMat@N2020-Advanced Industrial Processes and Materials for a Sustainable Northern Region of Portugal 2020; NORTE-01-0145-FEDER-000006 (supported by NORTE 2020), under the Portugal 2020 Partnership Agreement, through ERDF; CRUP A. Integrada 08/17; Associate Laboratory LSRE-LCM UID/EQU/50020/2019, funded by FCT/MCTES (PIDDAC). The collaboration work with TUD K. Wysoczanska did at Laboratory of Thermodynamics supported by RESOLV (EXC 1069); DMA 4200, DAAD; BMBF and Deutsche Forschungsgemeinschaft.

Curriculum Vitae

Personal data

Name	Kamila Wysoczańska
Date and place of birth	09.09.1987 in Krosno, Poland

Professional experience

2017 - 2019 Guest Researcher, Laboratory of Thermodynamics, Faculty of Biochemical and Chemical Engineering, Dortmund Technical University, Germany (research stay and collaboration)

Major tasks:

- Experimental determination of phase equilibria (SLE)
- ePC-SAFT modeling of phase equilibria
- Supervision of M.Sc and B.Sc theses of Students from TU Dortmund

2015 - 2019 Researcher, Laboratory of Separation and Reaction Engineering, Faculty of Engineering, University of Porto, Portugal

Major tasks:

- Experiments on partitioning of biomolecules in biodegradable ATPS
- Characterization of binary mixtures containing polar solvents and ionic liquids
- Supervision of experimental work and discussion sessions for students

2013 - 2015 Business Travel Counselor - Carlson Wagonlit Travel – Global Support Centre, Rzeszow, Poland

2012 - 2013 Researcher, Laboratory of Soft Computing and Image Analysis, Department of Computer Engineering, University of Beira Interior, Covilhã, Portugal

Major tasks:

- Investigation of computer vision and biometry in medical diagnosis systems

2012 Intern, Laboratory of Environmental Electrochemistry, Department of Chemistry, University of Beira Interior, Covilhã, Portugal

Major tasks:

- Investigation of tetracycline degradation
- Tests carried out: COD, TOC, nitrogen fluoride
- Methods used: Conductometry, UV-VIS spectroscopy

2009 Intern, Department of Computational Methods in Chemistry, Rzeszów University of Technology, Poland

Major tasks:

- Machine learning for biochemical reactions
- Use of Chemical Sense Builder program

2008 Intern, Institute of Microbiology and Medical Analytics, Subcarpathian Regional Hospital, Krosno, Poland

Major tasks:

- Biochemical, hematological and coagulation tests
- Immunochemical and microbiological tests

Education

2016 - 2019 Doctoral Studies in Chemical and Biological Engineering, Department of Chemical Engineering. University of Porto, Portugal/TU Dortmund, Germany

- European Doctorate Programme in cooperation with TU Dortmund. Dissertation entitled " Solubility and partitioning of biomolecules. Experimental studies and modeling"

2008 - 2013 Bachelor's Degree in Engineering, Chemistry Faculty, Major in Chemical Technology, Rzeszów University of Technology, Poland

- Thesis entitled "Computer designing for biodegradation of chemical compounds" - Final grade: **17**

2011 - 2012 Erasmus Lifelong Learning Programme, Chemistry Faculty, Major in Industrial Chemistry, University of Beira Interior, Covilhã, Portugal

2010 - 2012 Master of Science Degree in Engineering, Chemistry Faculty, Major in Biotechnology, Rzeszów University of Technology, Poland

- Thesis entitled "Computer simulation of biochemical reactions" Final grade: **19**

2006 - 2010 Bachelor's Degree in Engineering, Chemistry Faculty, Major in Biotechnology, Purification and Analysis of Biotechnological Products, Rzeszów University of Technology, Poland

- Thesis entitled "Use of machine learning for the computer simulation of biochemical reactions"

Projects

2017 - 2019 "Novel functional Aqueous Two-Phase System for Extraction and Stabilization of Biomolecules". University of Porto, Portugal/TU Dortmund, Germany

2012 - 2013 "Early detection of Secondary Raynaud's Phenomenon based on the Biometrical Analysis of Nailfold Capillaroscopy Images". University of Beira Interior, Covilhã, Portugal

Scientific contributions

Full papers

2020 Wysoczanska, K., Sadowski, G., Macedo, E. A., & Held, C. (2020). Solubility of DNP-amino acids and their partitioning in biodegradable ATPS; experimental and ePC-SAFT modeling. Fluid Phase Equilib, 527, 112830.

2020 Wysoczanska, K., Do, H. T., Sadowski, G., Macedo, E. A., & Held, C. (2020). Partitioning of water-soluble vitamins in biodegradable ATPS: ePC-SAFT predictions and experimental validation. AIChE. 10.1002/aic.16984.

2019 Wysoczanska, K., Macedo, E. A., Sadowski, G., & Held, C. (2019). Solubility Enhancement of Vitamins in Water in the Presence of Covitamins: Measurements and ePC-SAFT Predictions. Industrial & Engineering Chemistry Research, 58(47), 21761-21771.

2019 Wysoczanska, K., Sadowski, G., Macedo, E. A., & Held, C. (2019). Toward Thermodynamic Predictions of Aqueous Vitamin Solubility: An Activity Coefficient-Based Approach. Ind. Eng. Chem. Res, 58(17), 7362-7369.

2018 Wysoczanska, K., Do, H. T., Held, C., Sadowski, G., & Macedo, E. A. (2018). Effect of different organic salts on amino acids partition behaviour in PEG-salt ATPS. Fluid Phase Equilib, 456, 84-91.

2016 Wysoczanska, K., & Macedo, E. A. (2016). Influence of the molecular weight of peg on the polymer/salt phase diagrams of aqueous two-phase systems. J. Chem. Eng. Data, 61(12), 4229-4235.

2016 Wysoczanska, K., & Macedo, E. A. (2016). Effect of molecular weight of polyethylene glycol on the partitioning of DNP-amino acids: PEG (4000, 6000) with sodium citrate at 298.15 K. Fluid Phase Equilib, 428, 84-91.

2016 Wysoczanska, K., Calvar, N., & Macedo, E. A. (2016). (Vapor+ liquid) equilibria of alcohol+ 1-methyl-1-propylpiperidinium triflate ionic liquid: VPO measurements and modeling. J. Chem. Thermodyn., 97, 183-190.

2015 Wysoczanska, K., Silvério, S. C., Teixeira, J. A., & Macedo, E. A. (2015). Cation effect on the (PEG8000+ sodium sulfate) and (PEG 8000+ magnesium sulfate) aqueous two-phase system: Relative hydrophobicity of the equilibrium phases. J. Chem. Thermodyn., 91, 321-326

Conference papers

2016 Wysoczanska, K. & Macedo, E. A., (2016). Influence of PEG's Molecular Weight on Different Polymer/Salt ATPS Phase Diagrams. In Book of abstracts PPEPPD 2016-14th International Conference on Properties and Phase Equilibria for Product and Process Design

Communications

2019 Wysoczanska, K., Held, C., Sadowski, G., Macedo, E.A. "PC-SAFT assisted study on thermodynamic behaviour of low-soluble organic compounds in aqueous solution". 15th International Conference on Properties and Phase Equilibria for Products and Process Design, 12-16 May 2019, Vancouver, Canada. Presented as a poster.

2018 Wysoczanska, K., Do, H.T, Held. C., Sadowski, G., Macedo, E.A. "ATPS: Advantages in the extraction of biomolecules". 2nd German-Polish Symposium on Chemical Processes in Liquid Multiphase Systems. 21 September 2018, Dortmund, Germany. Presented as a poster.

2018 Wysoczanska, K., Held, C., Sadowski G., Macedo, E.A. "Thermodynamic properties of aqueous vitamin solutions". FEUP Doctoral Seminar, 21 June 2018, Porto, Portugal. Oral presentation.

2018 Wysoczanska, K., Held, C., Sadowski, G., Macedo, E.A. "Thermodynamic properties of aqueous vitamin solutions: experimental and PC-SAFT

modelling". 30th European Symposium on Applied Thermodynamics, 10-13 June 2018, Prague, Czech Republic. Oral presentation.

2017 Wysoczanska, K., Do, H.T., Held, C., Sadowski, G., Macedo, E.A. "Biodegradable ATPS: Advantages in the extraction of biomolecules". Thermodynamik-Kolloquium 2017, 27-29, September 2017, Dresden, Germany. Presented as a poster.

2017 Wysoczanska, K., Macedo, E.A. "Liquid-liquid extraction of biomolecules in biodegradable ATPS: phase equilibria and partitioning". 2nd Doctoral Congress in Engineering, 8-9 June 2017, Porto, Portugal. Presented as a poster.

2017 Wysoczanska, K., Macedo, E.A. "Purification of biomolecules using PEG and biodegradable salts". 29th European Symposium on Applied Thermodynamics, 18 - 21 May 2017, Bucharest, Romania. Presented as a poster.

2016 Wysoczanska, K., Macedo, E.A. "Influence of the molecular weight of PEG on Polymer/Salt ATPS phase diagrams". 14th International Conference on Properties and Phase Equilibria for Products and Process Design, 22 - 26 May 2016, Porto, Portugal. Presented as a poster.

Additional conferences

2018 Science: Polish perspectives. Polonium Foundation. 12-13 October 2018, Berlin, Germany.

2017 1st German-Polish Symposium on Chemical Processes in Liquid Multiphase Systems. 22-24 September 2017, Lodz, Poland.

Other contribution

2016 1st International Meeting of Researchers and Students of DEQ, July 7, Porto, Portugal (committee member).

2016 14th International Conference on Properties and Phase Equilibria for Product and Process Design, May 22-26, Porto, Portugal (local organizing committee member).

Selected Grants

2016 The Portuguese Foundation for Science and Technology, 4-years term Ph.D. grant (PD/BD/114315/2016)

2015 University of Porto, FEUP, 1-year term scholarship for the research initiation (NORTE-07-0124-FEDER-0000011, RL1_P4 Molecular Engineering and Simulation)

2011 Rzeszow University of Technology: Dean's scholarship for outstanding academic records during Biotechnology course.